Functional dissection of *T. brucei* Protein Tyrosine Phosphatase 1 and investigation of its development as a therapeutic target

Irene Ruberto

Table of Contents

List of Figures

List of Tables

Abstract

Trypanosoma brucei undergoes developmentally regulated morphological and biochemical changes during its life cycle, being transmitted between the mammalian host and the tsetse fly. It is generally recognized that cellular responses to environmental changes are mediated through signalling pathways, but our understanding of trypanosome signal transduction during differentiation is limited.

Protein Tyrosine Phosphatase 1 (*Tb*PTP1) is the one of the few factors identified to be responsible for differentiation from stumpy to procyclic form parasite, whereby *Tb*PTP1 inhibition stimulates transition to insect-form cells (Szoor *et al*., 2006).

In order to characterize the *Tb*PTP1 signalling pathway, a substrate-trapping approach was used, which identified a phosphatase *Tb*PIP39 as substrate of *Tb*PTP1. *Tb*PIP39 interacts with, and is dephosphorylated by *Tb*PTP1 in stumpy form cells. Additionally, it has been shown that upon citrate/cis-aconitate (CCA) treatment, phosphorylated *Tb*PIP39 localizes to the parasite glycosomes, the organelles responsible for bloodstream forms metabolism, thereby promoting cellular differentiation to procyclic forms (Szoor *et al*., 2010). With the aim of further dissecting the *Tb*PTP1 signalling pathway, the substrate-trapping approach was used, which identified one novel *Tb*PTP1 substrate candidate, potentially involved in regulation of differentiation.

In addition, the effect of other differentiation triggers, namely protease treatment or mild acid exposure, on the level of *Tb*PIP39 phosphorylation was analyzed, to determine whether these stimuli operate via the same *Tb*PIP39–dependent pathway as CCA signalling. Specifically, changes in the phosphorylation status of *Tb*PIP39 were visualized and quantitated by the use of antibodies detecting either *Tb*PIP39 or the Y278 phosphorylated form of *Tb*PIP39 generated during CCA-dependent differentiation. Both protease treatment and mild acid exposure generated a different pattern of *Tb*PIP39 phosphorylation, thus suggesting a different mechanism of action than CCA.

Finally, the possibility of using piggyback strategies targeting *Tb*PTP1 was investigated, as a means to decrease the number of the fly-transmissible

stumpy form cells in the bloodstream, thereby controlling parasite transmission. For this purpose, natural and synthetic inhibitors of human PTP1B were tested against the parasite enzyme, since they are being developed by pharmaceutical companies for the treatment of diabetes and obesity. The compounds tested showed a moderate *in vitro* inhibitory activity against recombinant *Tb*PTP1 and mainly a non-competitive type of inhibition, similarly to that observed for human PTP1B. However, none of the compounds showed *in vivo* specificity for *Tb*PTP1, indicating that further studies will be needed to identify more specific inhibitors.

Declaration

I declare that all the work presented in this study is my own, unless otherwise acknowledged, and that this thesis was written entirely by me.

Acknowledgements

There are many people who have made these three years an enriching experience both in and outside the lab. I wish I had the space and time to thank everyone with more than just a few words, and I apologize if I have accidentally missed someone.

Firstly, I would like to thank my supervisor Keith, for having been patient and supportive during these years and for always finding the time for me. I will remember his positive attitude during our meetings, which always had the unique effect of relieving me from the frustration of certain results. I would also like to thank Rachel Clark (Strathclyde University) and her colleagues for their technical assistance with the studies related to the TbPTP1 inhibitors.

A huge thank-you goes to Balazs, for having been a great guide inside the lab and a very caring friend outside. I enjoyed very much discussing results and planning experiments together: it was constructive, inspiring and fun!

In addition, I owe lots of nice words to the rest of the Matthews' lab for the friendly atmosphere they created during these years. Starting with the most senior, a big thank-you to the warm and smiling Debs, who has always been ready to help and to share funny jokes, despite the huge amount of work in the animal house. I will certainly miss her lively presence and delicious carrot cakes! Then, of course, the post Docs of the lab, who have also been very helpful and great people to have around. I will remember Katelyn, for her funny lab meetings and great active presence in the lab; Peg, for her help for the immunoprecipitation experiment and her constructive comments and nice chats in and outside the lab; Adam, for his smart ideas and annoying jokes on Italians, which I unexpectedly enjoyed. Thank you also to the other PhD students (past and present) of the lab, Steph, Paula, Sarah and Ellie, for their friendly chats during tea&cake breaks, and Helen, Athina and Sam for their lively presence. Special words go also to the rest of my office/lab mates, Ahmed, Antoine, Ruth, Clare for having been so friendly and nice with me; thank you also to Sarah, Monica, Ash and Antoine for keeping me company during the quiet weekends in the lab.

Thank you Melanie, friend of many adventures (including lots of westerns and northerns), for having supported me day after day, in and outside the lab, with your great smile and lively presence! Thank you Carol for your contagious happiness, which made me feel always so much better! I will miss sharing successes and frustrations with the two of you, but will keep our special plans in my mind. Thank you Anu, for being a caring friend, a

lovely person, and an excellent cook, I will certainly miss your Singalese recipes! Thank you Silvia and Yvone for the great nights out that made my evenings much more exciting and Yasin and Kate for having been good flatmates and very caring friends.

I would also like to express my gratefulness to all the people that made my days and lunch breaks so relaxing and enjoyable: Carol, Dario, Elaine, Kasia, Laurence, Matt, Melanie, Richard Ennos, Rinku, Ronnie, Roberta Bergero, ... will certainly miss very much our deep discussions and loud laughter! I would also like to thank others in Ashworth, paticularly Toni and Achim for their supervisions, Matt for helping me with the Alamar assay, and Martin for assistance with flow cytometry analyses. Thank you also to Ailie, Laura, Paul Hunt, Richard Carter, Stefano, Roberta Spilotri and Carloni, Jayna, Michelle, Sarah Hall, Magda, Daniel and Bet for having been so friendly with me.

I am also indebted to my previous boss, Lawrence Banks, for his support and to the rest of the Tumour Virology group (ICGEB, Trieste). I owe special thanks particularly to Daniela, Dave, Paola, Nisha and Noor for having been good friends and excellent examples of inspiring and hard working scientists and PhD students. I would also like to thank the rest of my past colleagues and friends from the ICGEB, for the great time spent together during my Master's degree.

Special words of gratitude go to my life-long friends in Italy, particularly Eva, Ingrid, Vale, Alba, Francesca, Elisabetta, Sabina and Silvia for having been in touch through these years and for always welcoming me home so warmly!

There are not enough words to properly thank my boyfriend, Pawan, for his love, great support and positive attitude that kept me going day after day, learning from my mistakes and making the most out of every moment. It has been a pleasure sharing successes and difficulties together, with perseverance and excitement. I also owe special words to Pawan's parents and family, for having accepted and sustained me like a daughter.

I cannot thank enough my parents and sister, for their love, encouragement and especially for the lively and stimulating atmosphere they have always created in the family, which has made me the passionate person that I am now.

List of Abbreviations

aa	Amino acids
AC	Adenylate cyclase
AGC	cAMP-dep., cGMP-dep. and PKC kinases
aPKs	Atypical protein kinases
ATP	Adenosine tri-phosphate
bp	Base pair
BSA	Bovine serum albumin
Bsf	bloodstream form cells
BZ3	PTP1B inhibitor (Calbiochem 539741)
CA	Cis-aconitate
CAM	Calmodulin
cAMP	Cyclic adenosine monophosphate
CCA	Citrate/cis-aconitate
CDC	Cell division cycle
CDK	Cyclin-dependent kinase
CE	Cell extract
CI	Citrate
95% CI	95% confidence interval
Da	Dalton
DAG	Diacylglycerol
DAPI	4',6-diamidino-2-phenylindole
DDP	Drug Discovery Portal (University of Strathclyde)
DIG	Digoxygenin
DMSO	dimethyl sulfoxide
DNA	Deoxyribonucleic Acid
dNTPs	Deoxyribonucleoside Triphosphates
dsDNA	Double Stranded DNA
DSP	Dual specificity phosphatase
DTT	Dithiothreitol
E. coli	*Escherichia coli*
EDTA	Ethylenediaminetetraacetic Acid
EP	Glutamic acid-Prolin (E-P) procyclin
ePKs	Eukaryotic protein kinases
ER	Endoplasmic reticulum
ESAG	Expression site associated genes
EtBr	Ethidium bromide
FACS	Flow cytometry
FCS	Foetal calf serum
g	gravitational force
G418	Geneticin (resistance conferred by the neo gene)
Glu	Glutamic acid
GPI	Glycophosphatidylinositol
GPI-PLC	GPI phospholipase C
GRESAG	Gene related to ESAG

HAT	Human African Trypanosomiasis
HCl	Hydrochloric Acid
H_2-DCFDA	2′, 7′-dichlorofluorescin diacetate
hPTP1B	Human Protein Tyrosine Phosphatase 1B
hsp	Heat shock protein
IC_{50}	Concentration to obtain 50% the maximal enzyme velocity
Ig	Immunoglobulin
IP	Immune-precipitation
IPTG	Isopropyl-β-D-thio-galactose
Kbp	Kilo Base Pair
K_i	Dissociation constant
K_M	Michaelis and Menten costant
KDa	Kilo Daltons
LAR	Leukocyte common antigen related phosphatase
LB	Luria Broth
LD_{50}	Dose lethal to 50% of the cells
LMW-PTP	Low molecular weight PTP
M1-M10	PTP landmark motifs
MAP	Mitogen activated protein
mRNA	Messenger RNA
MS	Mass spectrometry
ntd	Nucleotide
nm	Nano meter
O.D.	Optical density
PBS	Phosphate buffered saline
Pcf	Procyclic form cells
PCR	Polymerase Chain Reaction
PcT1-2	Precatalytic trypanosome-specific motifs
PFR	Paraflagellar rod
PH domain	Plekstrin homology domain (PI pathway)
PI	Phosphatidylinositol
PI3K	Phosphatidylinositol 3-kinase
PIP_2	di-phosphorylated PI
PIP_3	tri-phosphorylated PI
PKA	Protein kinase A
PKC	Protein kinase C
pNPP	phopsho-nitrophenylphosphate
P-loop	Phosphotyrosine-selectivity motif
Pol	Polymerase
pp	Phenyls
p-PIP39	*Tb*PIP39 phosphorylated on Y278
PP1	Protein Phosphatase 1
PP2A	Protein Phosphatase 2 A
Pro	Proline
pTyr	Phosphorylated tyrosine
PTP	Protein tyrosine phosphatase
PTP-loop	Loop containing the catalytic cysteine

Q-loop	Loop containing the catalytic glutamine
RNA	Ribonucleic acid
RNAi	RNA interference
rRNA	Ribosomal RNA
ROS	Reactive Oxygen Species
rpm	rotations per minute
RPTP	Receptor protein tyrosine phosphatase
SDS	Sodium Dodecyl Sulphate
SDS-PAGE	SDS Polyacrylamide gel electrophoresis
Ser	Serine
SH_2	Src kinase homolgy 2 domain
SIF	Stumpy induction factor
STKs	Ser/Thr protein kinases
STPs	Ser/Thr protein phosphatases
T1-T4	Trypanosome-specific motifs
T. brucei	*Trypanosoma brucei*
*Tb*PTP1	*T. brucei* Protein Tyrosine Phosphatase 1
Tet	Tetracycline
Thr	Thr
Tyr	Tyrosine
Tris	tris(hydroxymethyl)aminomethane
UV	Ultra-Violet light
VSG	Variable surface glycoprotein
V_{max}	Maximal velocity
WB	Western blot
WHO	World Health Organization
WPD-loop	Loop containing the catalytic aspartic acid
WT	Wild type
ZFP	Zinc Finger Protein
3-D	Three dimentional
α-His	Anti histidine
α-PIP39	Anti *Tb*PIP39
ε	Extinction coefficient
μg	microgram
μM	micromolar
μl	microliter

Chapter 1

Introduction

1.1. *Trypanosoma brucei sp.* classification and evolution

Trypanosoma brucei is a unicellular eukaryote belonging to the genus *Trypanosoma*, family Trypanosomatidae, order Kinetoplastida and phylum Euglenozoa (**Table 1.1**).

Kingdom	Excavata
Phylum	Euglenozoa
Order	Kinetoplastida
Family	Trypanosomatidae
Genus	*Trypanosoma*
Species	*Trypanosoma brucei*
Sub-species	*T. brucei brucei*

Table 1.1 *Trypanosoma brucei* classification. Schematic diagram showing the scientific classification of *Trypanosoma brucei* spieces.

All the species belonging to the genus *Trypanosoma* are parasites of vertebrate bloodstream and are transmitted by bloodsucking invertebrates, such as tsetse flies, fleas or leeches. Trypanosomes can be divided into two groups, according to their mode of transmission: by inoculation (Salivaria) or by contamination through feces of the insect vector (Stercoraria) (Haag *et al.*, 1998). Salivarian trypanosomes comprise, among others, *T. brucei*, *T. equiperdum*, *T. evansi*, whereas stercorarian trypanosomes include several clades: *T. cruzi* (transmitted by triatomine bugs), the rodent (*T. musculi* and *T. lewisi*, transmitted by fleas), the avian (transmitted by black flies and hippoboscid flies), the amphibian (transmitted by leeches), the reptilian and the fish trypanosomes (Haag *et al.*, 1998; Simpson *et al.*, 2006).

1.2. Burden and epidemiology of African Trypanosomiasis

The *Trypanosoma brucei* (*T. b.*) species include the subspecies of *T. b. brucei*, *T. b. gambiense* and *T.b. rhodesiense*, and are transmitted by different subspecies of tsetse fly (of the *Glossina* genus), which are found only in sub-Saharan Africa, between 14°N and 20°S (from Senegal in the west, to Somalia in the east) (WHO, 1998). *T. b. brucei*, as well as *T. congolense* and *T. vivax*, infect wild and game animals, particularly affecting African cattle with a wasting disease called nagana (or n'gana), which is estimated to cost livestock producers and consumers US $ 340 million/year in Africa (Mulumba, 2003). Such loss of food, manure and transport has a serious impact on the rural poor in Africa, whose income is often based exclusively on livestock.

T. b. gambiense and *T. b. rhodesiense* infect animals and humans, causing Human African Trypanosomiasis (HAT) or sleeping sickness; HAT, together with leishmaniasis, represent the major protozoan infections of sub-Saharan Africa, accounting for 1.5 million of disability-adjusted life years (DALYs)(Hotez *et al.*, 2009), a measure of diseases burden, defined as the loss of the equivalent of one year of full health (Murray, 1994). Sleeping sickness is found in 36 African countries, with more than 250 discrete foci detected, particularly in rural areas. In 2006 an incidence of 50,000-70,000 new cases per year was estimated from detected cases (calculated using a ratio of detected over actual cases of 1:3-4) (WHO, 2006a), but a drop to 10,000 detected new cases, the lowest level in the last 50 years, has been reported in 2010, due to the strengthening of the control and surveillance efforts of the national sleeping sickness programmes (WHO, 2010). Consequently, elimination is nowadays considered a reasonable aim in countries reporting less than 100 cases per year (Welburn *et al.*, 2009).

HAT describes not one but two separate diseases: Gambiense and Rhodesiense HAT, which are characterized by different geographical distribution, epidemiology and clinical features (Fevre *et al.*, 2006a). Gambiense sleeping sickness represents 90% of HAT cases and it is found in west and central Africa, particularly in the war-torn countries of Angola, Central African Republic, Democratic Republic of Congo, southern Sudan

and western part of Uganda, with most of the new cases occurring in DRC (**Figure 1.1**). In contrast, the rest of Uganda and the eastern African states of Kenya, Tanzania, Zambia, Malawi and Mozambique, are afflicted by Rhodesiense HAT (WHO, 2006a).

T. b. gambiense
Countries endemic (> 1500 cases/year)
Angola
DRC
Sudan
Countries reporting 50-1500 cases/year
Central African Republic
Chad
Congo
Coite d'Avoire
Guinea
Uganda

T. b. rhodesiense
Countries reporting 50-1500 cases/year
Malawi
Uganda
Tanzania

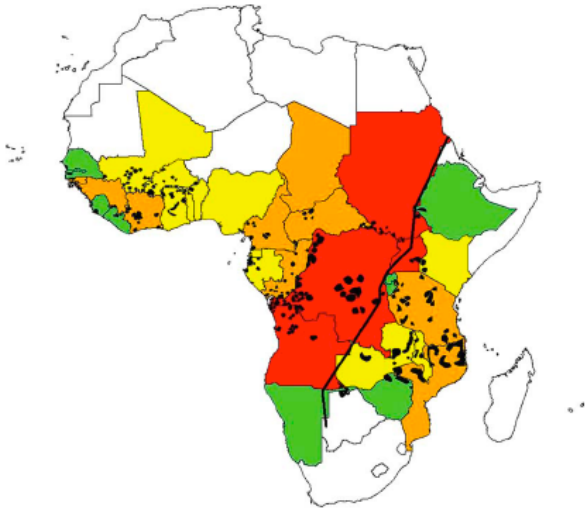

Figure 1.1 Prevalence of HAT. The African countries mainly affected by HAT are listed, according to the data reported (WHO, 2006a); the corresponding map is showing beneath (from Fevre *et al.*, 2006) where red, orange, yellow and green indicate countries with very high, high, low and sporadic HAT frequencies, respectively

1.3. Trypanosomiasis control strategies

Several control strategies exist for the control of African trypanosomiasis: from animal and human-targeted interventions to vector control methods. These different approaches are complementary and their use is dictated by the epidemiology of the disease and by the local ecological and social environment (Torr *et al.*, 2005; Fevre *et al.*, 2006a).

Nowadays, animal-targeted interventions and vector control are the main strategies adopted for the control of Rhodesiense HAT (Welburn *et al.*, 2001). Several drugs, such as diminazene aceturate, homidium bromide and isometamidium chloride, are currently widely employed in Africa for curative or prophylactic animal chemotherapy, but their availability and improper use has caused cases of resistance, which might become a serious issue in the near future (Geerts *et al.*, 2001). For gambiense HAT, human-targeted activities are more important, with active case finding combined with drug treatment of positive cases, being the cornerstone of disease control (Ekwanzala *et al.*, 1996)

1.4. HAT pathology

The clinical signs and symptoms of gambiense and rhodesiense HAT are classified according to the stage of the disease: first or heamatolymphatic stage, when the parasite is found only in the blood, and second or meningoencephalitic stage, when the parasite is found also in the cerebrospinal fluid. Signs and symptoms of the two forms of HAT are generally the same, but *T. b. rhodesiense* form causes an acute infection, developing within days and leading to death after 6-8 months if untreated; by contrast Gambiense HAT is a chronic infection, which can take months or even years before the appearance of any sign or symptoms.

In the first stage of sleeping sickness patients develop mainly common complaints such as fever, muscle ache, headache, joint pain and other signs of inflammation, which only partly correlate to the level of parasiteamia (WHO, 1998).

More specific signs are visible in patients in the second stage of the disease, particularly sleep disturbances caused by the disappearance of the circadian rhythm; alteration of mental state and abnormal reflexes, as well as coordination disorder are also typical of the meningoencephalitic stage. Most organs, but especially the heart and brain show sign of inflammation, which can lead to coma and death if untreated. Although the molecular mechanisms of cerebral damage are not completely understood, studies on infected mice seem to indicate that cytokines play an important role (Lundkvist *et al.*, 2004).

1.5. HAT treatment

1.5.1. Naphthylamine derivatives

The first compound found to be effective against trypanosomes came from the synthetic dyestuff industry, with its most influential protagonist being Paul Ehrlich, the father of modern chemotherapy (Bosch *et al.*, 2008). In 1901 Ehrlich identified a sulphated naphthylamine derivative named Nagana Red, as a dye displaying trypanocidal activity, which was then further modified into Trypan Red and then in Trypan Blue (**Figure 1.2 A**) by others, including the German pharmaceutical company Bayer. Trypan Blue was found to be particularly effective against the parasite but had the limitation of staining the skin of the infected animal, and thus was unusable to treat humans.

Only in 1917, Bayer identified a colourless but effective compound (Bayer 205), named Germanin (Dressel *et al.*, 1961) and later renamed suramin (**Figure 1.2 A**), which is still in use today for the treatment of early stage rhodesiense HAT.

The mode of action of suramin has not been definitely proven. Indeed, although it has been shown to inhibit glycerolphosphate oxidase and other glycolytic enzymes (Fairlamb *et al.*, 1977), it is believed to have additional targets due to its six negative charges, which can easily form strong electrostatic interactions with a variety of enzymes (Fairlamb *et al.*, 1977; Wierenga *et al.*, 1987; Barrett *et al.*, 2007).

1.5.2. Arsenical drugs

In parallel to the development of naphthlylamine derivatives, arsenical drugs were also found to be effective against trypanosomes, particularly Atoxyl® (**Figure 1.2 B**) (Thomas, 1905), which was used in clinical practice in 1905 to treat sleeping sickness; however, the treatment required high doses of the compound and often resulted in blindness due to atrophy of the optic nerve (Bosch *et al.*, 2008). In 1938 the compound melarsen (**Figure 1.2 B**) was synthetized from Atoxyl® by addition of a melamine moiety, which resulted in increased trypanocidal activity but increased and retained toxicity against the optic nerve. In order to limit the severe side effects of melarsen, the drug was combined with dimercaprol, an arsenic antidote developed during World War II to protect against poisoning by arsenic gas (Friedheim, 1949); the resulting product was melarsoprol (**Figure 1.2 B**), the only drug for the treatment of second stage of *T. b. rhodesiense* HAT (**Table 1.2**), which, although lacking melarsen's toxic effect on the optic nerve, results in reactive encephalopathy in 5-10 % of the patients (WHO, 1998).
Melarsoprol has been shown to cause parasite lysis (Meshnick *et al.*, 1978), likely due to inhibition of glycolysis (Van Schaftingen *et al.*, 1987) and to interact with trypanothione (Fairlamb *et al.*, 1989), however how these interaction affect the trypanocidal activity is not clear.

1.5.3. Diamidines

In the 1940s the hypoglycaemic drug synthalin (**Figure 1.2 C**) was found to cure trypanosome infection from mice and rats, and it was believed to do so by lowering the glucose levels in the blood. It was later noticed that the compound had a direct effect on the parasite itself, thus discovering the trypanocidal effect of diamidines (Lourie *et al.*, 1937; Steverding, 2010). Among the different diamidine derivatives, pentamidine (**Figure 1.2 C**) was found to have more limited side effects, and thus employed for the treatment of first stage *T. b. gambiense* and it is nowadays still in use (Soeiro *et al.*, 2005).

Pentamidine enters the cell through the P2 amino-purine transporter, also used by melarsoprol, and the low and high affinity pentamidine transporters (De Koning, 2001). Although the drug preferentially accumulates in the kinetoplast in *Leishmania,* where it interacts electrostatically with the mitochondrial DNA (Basselin *et al.*, 1998), its definite mode of action has not been characterized. However, it has been suggested that pentamidine is likely to exert its effect from inhibition of multiple cellular targets, due to its high positive charge and concentration (Denise *et al.*, 2001).

The trypanocidal activity of pentamidine is high, with an *in vitro* IC_{50} of 1-10 nM (Miezan *et al.*, 1994), however it is not readily absorbed and thus requires intramuscular injections.

Another diamidine derivative was also identified as having good trypanocidal activity (Das *et al.*, 1977) but was not pursued further at that time. More recently, the same compound was synthesized as the prodrug, pafuramidine maleate (or compound DB289) (**Figure 1.2 C**), in order to increase its intestinal absorption, and in 2007 it was the first oral drug for HAT to ever enter clinical trials; however, it then failed phase I studies due to severe kidney toxicity and it was thus abandoned (Midgley *et al.*, 2007).

1.5.4. Nifurtimox

Nifurtimox (**Figure 1.2 D**) was developed in the 1960s by the German company Bayer and was then discovered to be effective for the treatment of Chagas disease (Van den Bossche, 1978), caused by *Trypanosoma cruzi,* by causing oxidative damage to the parasite (Docampo *et al.*, 1986). It was then found to be effective also against *Trypanosoma brucei*, although at high doses, and it has been used for the treatment of melarsoprol-refractory sleeping sickness cases (Pepin *et al.*, 1989).

More recently, oral nifurtimox has been used in combination with eflornithine, resulting in a shorter and easier to administer treatment for second stage *T. b. gambiense* (Priotto *et al.*, 2006; Priotto *et al.*, 2009).

1.5.5. Eflornithine (DFMO)

Eflornitine (α-difluoromethylornithine or DFMO) (**Figure 1.2 E**) is the only drug for the treatment of sleeping sickness that has been registered in the last 50 years (**Table 1.2**). It was initially developed for the treatment of cancer and other hyperproliferative diseases in the 1970s (Bey *et al.*, 1978) and specifically designed to target the amino acid decarboxylase, ornithine decarboxylase (ODC).

In parallel, DFMO was discovered to be effective against *T. b. brucei* (Bacchi *et al.*, 1980) and treat gambiense sleeping sickness (Van Nieuwenhove *et al.*, 1985). DFMO was found not to be effective against *T. b. rhodesiense*, due to an almost 5 fold higher turnover rate of the ODC of this species (Iten *et al.*, 1997). In addition to ODC, DMFO has been reported to target the parasite trypanothione, rendering the cells more susceptible to oxidative stress (Fairlamb *et al.*, 1987). In 1990 eflornithine was registered for the treatment of gambiense sleeping sickness but its expensiveness and lack of market in higher income countries caused its manufacturing to cease in 1995. Five years later, DMFO was relaunched by the pharmaceutical company Bristol-Myers Squibb, as a topical formulation to suppress the growth of facial hair, and a donation of the drug to treat sleeping sickness was agreed with the WHO (TDRnews, 2001).

Although DMFO is less toxic than melarsoprol, its relatively poor *in vitro* activity (IC_{50} of 81-693 μM (Zweygarth *et al.*, 1991)) and pharmacokinetic profile, render it far from ideal for the use in tropical environments (Barrett *et al.*, 2007). However, until a better substitute will be identified, eflornithine is currently the only cure for melarsoprol-refractory HAT cases and used in combination with nifurtimox (NECT: "nifurtimox-eflornithine combination therapy", i.e. 7 days of eflornithine followed by 10 days of oral nifurtimox) has been shown to decrease by half the length of the treatment and to render it cheaper and easier to administer (Priotto *et al.*, 2006; Priotto *et al.*, 2009).

1.5.6. Future directions in drug discovery

In the last ten years several new initiatives for drug discovery for sleeping sickness and other neglected tropical diseases have been established (Barrett *et al.*, 2007), such as the Drug Discovery Unit in Dundee (http://www.drugdiscovery.dundee.ac.uk/) and the Drug for Neglected Diseases Initiative (DNDi) in Geneva (http://www.dndi.org/index.php), which work in partnership with industry and academia to facilitate the identification of new lead compounds.

The first priority set by the DNDi is the development of a safe, effective, cheap and practical stage 2 HAT treatment (for both gambiense and rhodesiense disease) (DNDi *et al.*, 2009). A new drug, fexinidazole, a nitroimidazole compound similar to nifurtimox, which was initially discovered in the 1980s (Raether *et al.*, 1983), is currently undergoing clinical trials (http://www.dndi.org/portfolio/fexinidazole.html).

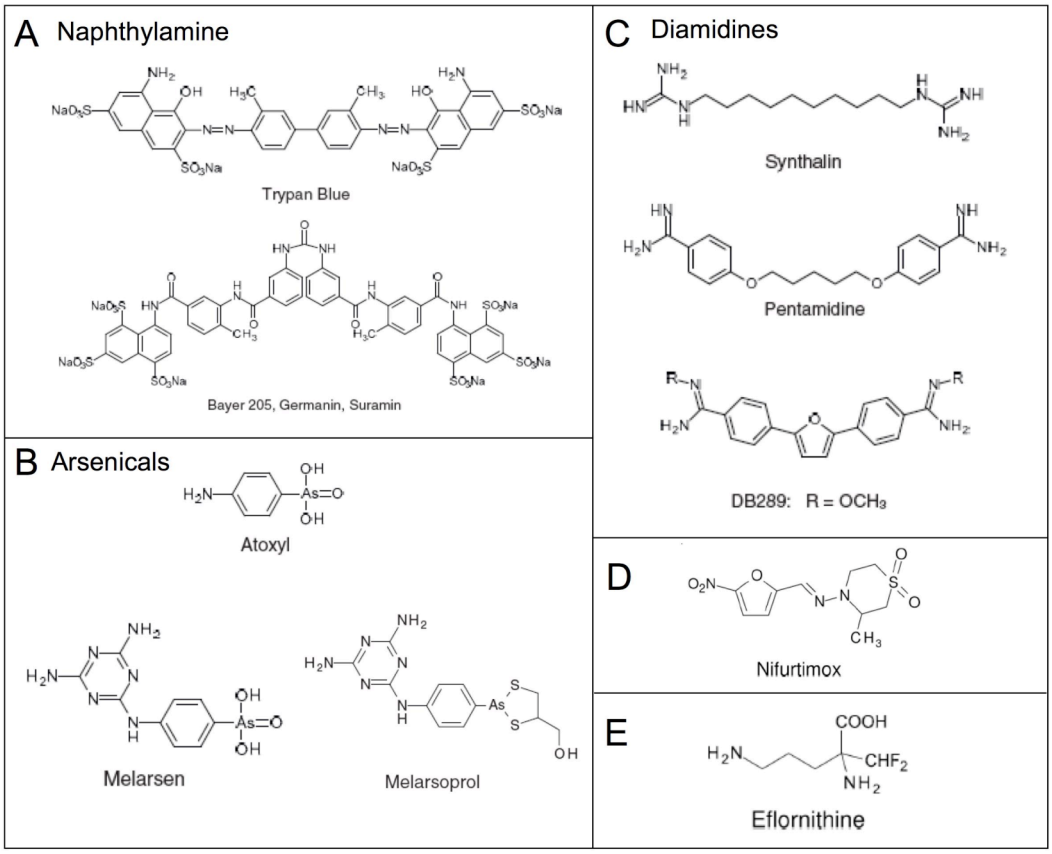

Figure 1.2 Chemical structure of the different drugs effective against HAT (modified from Steverding, 2010). The chemical structures of the main compounds found to be effective against Human African Trypanosomiasis are shown, and the family of compounds are highlighted: Trypan blue, Suramin, together with Nagana Red and Trypan Red (not shown) belong to the sulphated naphthylamine family (A); atoxyl, melarsen and melarsoprol belong to the arsenicals group (B); Synthalin, Pentamidine and DB289 (pafuramidine maleate) are diamidine derivatives (C); Nifurtimox is a nitrofuran (D) and Eflornithine is analogue to the amino acid ornithine (E).

1.6. Trypanosomes cell architecture

1.6.1 The cytoskeleton, flagellum and flagellar pocket

Trypanosomes are unicellular flagellated protozoa about 20 μm long and with a diameter of 2 μm (Cross, 1984). Their shape and form are maintained by the cellular cytoskeleton which is made up of subpellicular microtubules, that are cross linked to each other and to the plasma membrane, forming a corset that extends throughout the cell, with the exception of the flagellar pocket (Hemphill *et al.*, 1991) (**Figure 1.3** number **10**). An important component of the trypanosome structure is the flagellum, which serves as a locomotory organ in bloodstream forms and is essential for parasite attachment to the tsetse fly salivary glands (Sherwin *et al.*, 1989). The flagellum runs in a left-handed spiral from the posterior to the anterior pole along the length of the cell and is attached to the plasma membrane through the flagellum attachment zone (FAZ) (Kohl *et al.*, 1999). Two different types of structure make up the flagellum: the classical 9+2 microtubule structure (axoneme) and the kinetoplastid and euglenoids-specific paraflagellar rod (PFR) (Vaughan *et al.*, 2003).

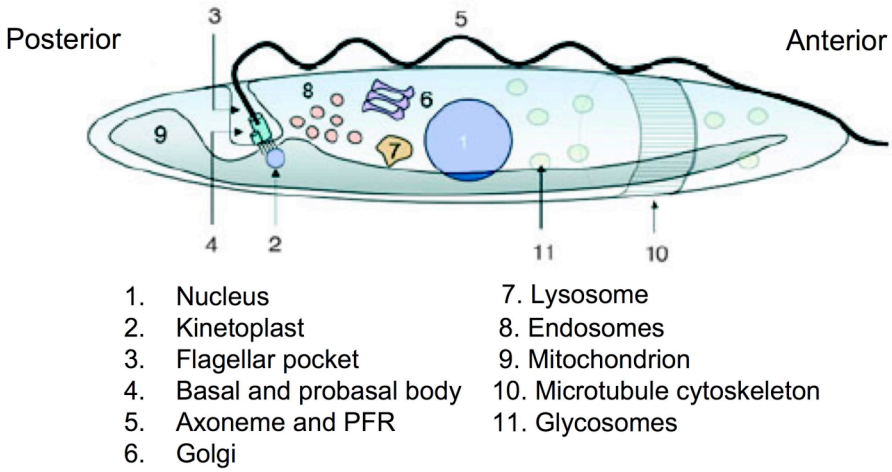

Figure 1.3 The trypanosome cell architecture. Simplified diagram showing a section of the trypanosome cell with the main features highlighted (from Matthews K. R., 2005).

The axoneme is necessary to allow the correct orientation and directionality of the flagellum movements (Branche *et al.*, 2006), similarly the PFR has been shown to play a central role in flagellar and cellular motility (Bastin *et al.*, 1998; Bastin *et al.*, 1999).

The flagellum enters the cytoplasm of the cell in a small invagination of the plasma membrane called the flagellar pocket (FP) (Webster *et al.*, 1993) (**Figure 1.3** number **3**). The FP proximal end is represented by the basal body, the nucleation site of the axoneme microtubules, which is physically linked to the mitochondrial DNA via the tripartite attachment complex (Ogbadoyi *et al.*, 2003); distal to the basal body the collarette can be identified, which is represented by the area where the flagellum enters the FP; distal to the collarette, the neck of the FP, an electron-dense ring structure, is found, which is called flagellar pocket collar (Lacomble *et al.*, 2009).

The flagellar pocket represents the only site of endo and exocytosis, as the subpellicular microtubules are too closely spaced to allow transport vesicles to access the plasma membrane (Overath *et al.*, 2004). Importantly, the variable surface glycoprotein (VSG), that is recognized by the host IgG, is rapidly recycled through the FP and the bound antibodies are concomitantly degraded, thus allowing the parasite to evade the immune system (Ferrante *et al.*, 1983; Engstler *et al.*, 2007). Endocytosis of the VSGs and of other molecules is clathrin-dependent (Allen *et al.*, 2003), as seen in higher eukaryotes, however in trypanosomes this process is particularly fast, with the whole VSG pool being turned over in 15 min (Bangs *et al.*, 1997).

Apart from the FP, the rest of the vesicle trafficking machinery of trypanosomes resemble that of other eukaryotes, comprising of endosomes, lysosomes, the endoplasmic reticulum (ER) and the Golgi complex. However, the secretory and endocytic organelles display a more compact localization compared to higher eukaryotes, being found between the nucleus and the kinetoplast, with the exception of the ER, which is distributed across the cytoplasm (Field *et al.*, 2009).

1.6.2. The mitochondrion and the glycosomes

The biggest and one of the most developmentally regulated intracellular structure found in trypanosomes is the mitochondrion (**Figure 1.3** number **9**). The mitochodrion is a single elongated organelle that runs the entire length of the cell, in contrast to mammalian cells, which contain thousands of them (Vickerman *et al.*, 1988).

In bloodstream form trypanosomes, the mitochondrion is underdeveloped and devoid of cristae, whereas in the insect stage cells this organelle is fully functional and it is used to metabolize amino acids, the main energy source found in the fly (Durieux *et al.*, 1991).

The main energy source of the bloodstream is glucose, which is metabolized in the kinetoplastid-specific organelles called glycosomes (Opperdoes *et al.*, 1977) (**Figure 1.3** number **11**). There are around 65-250 glycosomes per cell in bloodstream forms (Opperdoes *et al.*, 1984) and during parasite development the abundance of most of their glycolytic enzymes decreases (Hart *et al.*, 1987; Parsons, 2004).

In addition to glycolysis, glycosomes also contain enzymes involved in pyrimidine synthesis, purine salvage, ether-lipid biosynthesis and β-oxidation (Michels, 1989).

1.6.3. The metabolism of bloodstream and procyclic forms

The mitochondrion and the glycosomes play different but complementary roles during parasite development (**Figure 1.4**) (Vickerman, 1965; Vickerman *et al.*, 1988). In the bloodstream glucose is found in millimolar concentrations and thus represents the main energy source for the cell, which uses the glycolytic enzymes of the glycosomes to convert glucose into 3-phosphoglycerate. Then 3-phosphoglycerate is converted into pyruvate and ATP in the cytosol, which represents the main location of energy production for bloodstream form trypanosomes (Besteiro *et al.*, 2005). The pyruvate produced from glycolysis is excreted outside the cell (Vickerman, 1965), unlike what happens in mammalian cells, where glucose is metabolized into pyruvate in the cytosol and then further transformed into acetyl CoA in the

mitochondria (**Figure 1.4**) (Alberts *et al.*, 2002). As a consequently of their active metabolism, glycosomes of bloodstream forms appear spherical in shape, in contrast to the less active and rodshaped glycosomes of insect-form parasites (Vickerman, 1985).

The mitochondrion of bloodstream form cells, although lacking the enzymes of Krebs cycle, does possess the nucleus-encoded alternative oxidase (TAO), which is important to maintain the glycosomal and glycolytic redox balance, together with the glycerol-3-phosphate dehydrogenase (GP-DH), which reduces FAD to $FADH_2$ (Clarkson *et al.*, 1989). TAO is the only terminal oxidase of the mitochondrial electron transport chain in bloodstream forms and is considered to be essential in this life cycle form (Chaudhuri *et al.*, 2006). Indeed most of the cytochrome oxidase complex is absent in bloodstream forms, with the exception of the ATP synthase. Interestingly, the ATP synthase of bloodstream forms hydrolyzes ATP, thus working in the opposite manner to procyclic forms, and its function is essential to maintain mitochondrial membrane potential and parasite survival (Schnaufer *et al.*, 2005).

Inside the tsetse fly, glucose found in the bloodmeal disappears within 15 min of ingestion, and in the insect midgut exist mainly amino acids, particularly proline and threonine, which are metabolized in the fully active mitochondrion of procyclic forms (Vickerman, 1985). However, insect-stage cells can adjust their metabolism in response to the prevailing metabolic condition, indeed they still retain some degree of glycosomal activity, with some enzymes being expressed only in procyclic forms, such as the NADH-dependent fumarate reductase, which is responsible for the convertion of phosphoenolpyruvate into succinate (Besteiro *et al.*, 2002).

Moreover, procyclic forms still possess a phosphoglycerate kinase (PGK), the enzyme responsible for one of the last steps of glycolysis, but its localization is mainly cytosolic, compared to the glycosomal form found in bloodstream parasites, thereby creating an additional site of ATP production (Besteiro *et al.*, 2005). In addition, the end product of glycolysis, pyruvate, that was excreted in bloodstream forms, is imported into the mitochondrion in insect-form cells, where it is degraded to acetyl CoA and then to acetate, through the Krebs cycle (Tielens *et al.*, 1998).

In contrast to what happens in mammalian cells, the trypanosomes Krebs cycle does not degrade acetyl CoA or amino acids to CO_2 but to acetate, succinate and alanine. Consequently, the main site of energy generation in procyclic forms is the mitochondrial respiratory chain, which is essential for parasite survival and growth, in a glucose-depleted environment (**Figure 1.4**) (van Weelden *et al.*, 2003). Acetyl CoA is also converted into acetate through a trypanosome-specific cycle comprising an acetate:succinate CoA transferase and a succinyl-CoA synthetase (ASCT cycle), which generates extra ATP (Van Hellemond *et al.*, 1998).

The mitochondrial electron transport chain of procyclic forms is composed of two terminal oxidases, TAO and the cytochrome oxidase complex (COX), although TAO is expressed at lower levels. The presence of both of these enzymes seems to be beneficial to the parasite in order to adjust itself to the different availability of nutrients and oxygen (Chaudhuri *et al.*, 2006). The cytochrome oxidase complex of procyclic forms is similar to the electron transport system of mammalian cells, which generates a proton gradient that is exploited by the ATP synthase to produce ATP (van Weelden *et al.*, 2003). Oxidative phosphorylation is essential for procyclic forms in a glucose-depleted environment; in contrast, in the presence of glucose, insect-form parasites rely mainly on substrate level phosphorylation to produce ATP (Besteiro *et al.*, 2005)

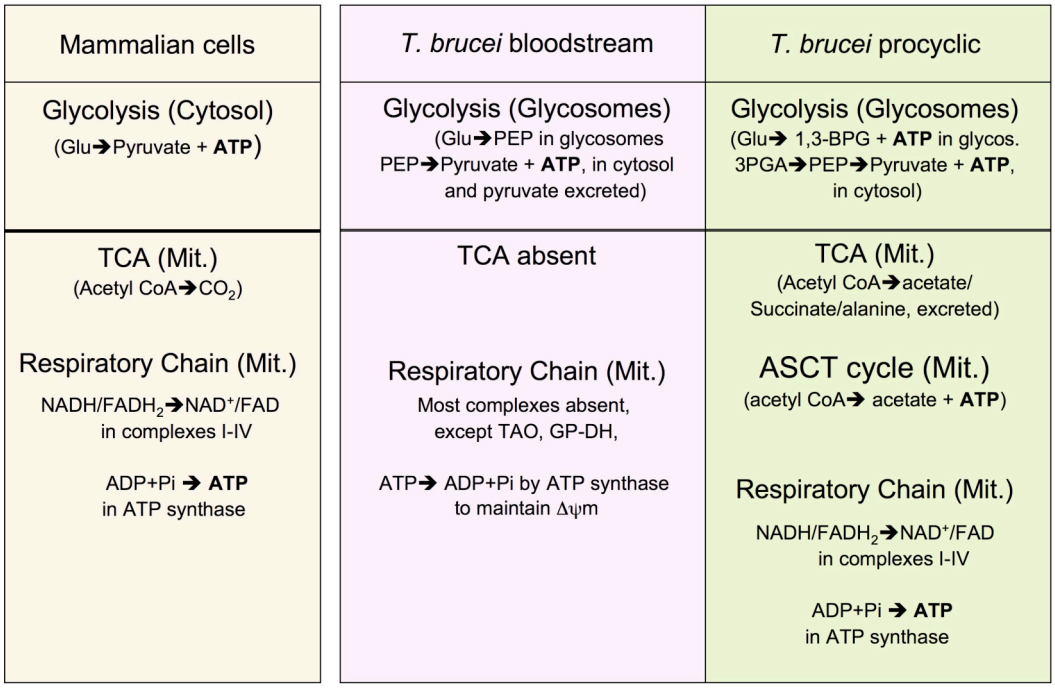

Figure 1.4 Schematic representation of *T. brucei* bloodstream and procyclic form metabolism. The main pathways and sites of cellular metabolism are shown in a schematic diagram to allow comparison between mammalian cells and *T. brucei* bloodstream and procyclic forms. In mammalian cells glycolysis is carried out in the cytosol, whereas it is compartimentalized in the glycosomes in trypanosomes; the Krebs Cycle (TCA) of higher eukaryotes is found in the mitochondrion (Mit.) of procyclic forms, although it does not convert acetyl CoA into CO_2 but only into acetate, succinate or alanine; procylic forms also metabolize acetyl CoA into acetate using the trypanosome-specific acetate: succinate CoA transferase and a succinyl-CoA synthetase (ASCT cycle). In bloodstream forms the TCA cycle is absent, and the mitochondrial respiratory chain lacks most of the components, with the exception of the glycerol-3-p dehydrogenase (GP-DH), the alternative oxidase (TAO) and the ATP synthase; however, the ATP synthase functions only to maintain the membrane potential ($\Delta\psi m$), whereas the main site of ATP production is the cytosol, from the degradation of the pyruvate.

1.6.4. The nucleus and gene regulation

The *Trypanosoma brucei* nucleus (**Figure 1.4** number **1**) is estimated to contain approximately 3.5 x 10^7 bp (35 Mb) per haploid genome (Borst *et al.*, 1982), harbouring about 9,000 protein coding genes (El-Sayed *et al.*, 2000; Berriman *et al.*, 2005). The chromosomes are divided into three classes according to their relative mobility on pulsed-field gel electrophoresis: mini-, intermediate- and megabase-chromosomes.
Mini chromosomes are 50-150 Kb, linear DNA sequences, which are about 100 per cell and consist mainly of 177-bp repeats (Van der Ploeg *et al.*, 1984). In addition, many minichromosomes contain a silent copy of the variable surface glycoprotein (VSG) genes and are thus highly susceptible to recombination events leading to translocation of the VSG gene to an expression site (Van der Ploeg *et al.*, 1984; Ersfeld *et al.*, 1999). Intermediate chromosomes range from 200 to 900 Kb, lack the repeats found in minichromosomes, they seem to serve mainly as a reservoir of VSG expression sites (Ersfeld *et al.*, 1999). The megabase chromosomes are diploid (Tait *et al.*, 1989) in the nucleus (whereas the mini- and intermediate chromosomes are of uncertain ploidy) and are 11 in number, ranging from 1 Mb to 6 Mb; they contain protein-coding genes with conserved synteny between different stocks but with DNA content varying up to 33% (Melville *et al.*, 1998).

Unlike in mammalian cells, in *Trypanosoma brucei* the majority of gene expression is not controlled by transcription initiation, but rather by RNA processing. Specifically genes that are next to each other and share a common orientation, are co-transcribed and subjected to a trans-splicing reaction, which adds a capped RNA of 40 ntd (called splice leader) to the 5'-end, and are then polyadenylated at the 3'-end (Johnson *et al.*, 1987; Ullu *et al.*, 1993). Moreover trypanosomes lack polymerase II promoters for protein coding genes, although most protein coding genes are transcribed by polymerase II (Clayton, 2002), with the exception of the major surface proteins of bloodstream and procyclic forms, VSGs and EPs, which are transcribed by polymerase I (Rudenko *et al.*, 1989). RNA polymerase III

transcribes most U RNAs (RNAs involved in splicing) and tRNAs (Nakaar *et al.*, 1997).

1.6.5. Surface glycoproteins

Bloodstream form *T. brucei* possess a thick surface coat made up of a variable surface glycoprotein (VSG), which are homodimers attached to the plasma membrane through C-terminal GPI (glycosylphosphatidylinositol) anchors (Cross, 1984). VSGs are synthesised in the ER and then sorted to the flagellar pocket by hydrodynamic forces on the swimming parasite (Engstler *et al.*, 2007). Once on the surface they are able to bind immunoglobulins of the host, which are then constantly internalised to the cell interior through the flagellar pocket (Webster *et al.*, 1990). By binding host immuneglobulins, VSGs prevent complement-mediated lysis of the parasite (Ferrante *et al.*, 1983). In addition, these surface coat proteins protect trypanosomes from antibody detection; indeed, the VSG coat allows penetration of small molecules but restricts the access of the antibodies to the buried VSG epitope, found at the C-terminal end of the protein (Cross, 1978; Overath *et al.*, 1994). During chronic infections trypanosomes keep changing their VSGs, in a process termed antigenic variation, whereby parasites expressing the dominant antigen type are killed by the immune response, but some trypanosomes survive and proliferate, having switched their VSG. The consequence of antigenic variation is the formation of repeated fluctuations of parasitaemia in the host (Vickerman, 1978).
Importantly, antigenic variation is responsible for trypanosome evasion of the mammalian immune response and for the inability to develop a vaccine against African trypanosomiasis (Vickerman, 1978). The stimulus inducing antigenic variation has not been identified, but it is known that the immune response plays only a selective and not an inductive role, since VSG switching can occur in the absence of an immune response (Myler *et al.*, 1985).

During parasite development from the bloodstream to the insect form stage, the VSG coat is shed and substituted by procyclin proteins, which are

detectable around 12-16 hr after differentiation (Roditi *et al.*, 1989). Procyclins, or PARPs (Procyclin Acidic Repetitive Proteins) are grouped into two classes, according to amino acid repeat motifs of their C-terminal domains (Roditi *et al.*, 1987).

EP-procyclin is characterized by the presence of a glutamic acid and proline dipeptide repeat (E-P), whereas GPEET-procyclin contains a pentapeptide repeat motif (gly-pro-glu-glu-thr) (Mowatt *et al.*, 1989). The function of these coat proteins was believed to be mainly protection from the proteases found in the tsetse fly midgut, conferred by their C-terminal domains containing the amino acid repeats (Ruepp *et al.*, 1997; Acosta-Serrano *et al.*, 2001). However, procyclin null mutant parasites were able to complete the life cycle in the tsetse fly and infect mice, thus proving that procyclins are not essential for cyclical transmission, although they do seem to provide a competitive advantage for the parasite (Vassella *et al.*, 2009).

1.7. The *Trypanosoma brucei* cell cycle

The events of the cell division cycle in trypanosomes are timely and orderly regulated in order to ensure proper duplication and segregation of the single copy organelles: the nucleus, the mitochondrion, the kinetoplast and the flagellum (Sherwin *et al.*, 1989). The trypanosome cell cycle can be divided in the typical four phases of the eukaryotic cell cycle: G1, S, G2 and M (**Figure 1.5 a**).

During G1 phase the parasite possesses a single nucleus, kinetoplast and flagellum (**Figure 1.5 b i**), and it is this latter one which is first duplicated when the cell progresses through S phase, resulting in a cell showing a single kinetoplast and nucleus but two flagella (1K1N2F) (**Figure 1.5 b ii**).

After the flagellum, the nucleus and kinetoplast are duplicated, and although their replication starts at approximately the same time, the kinetoplast DNA segregates before the nuclear DNA, thus giving rise to cells with two kinetoplasts, one nucleus and two flagella (2K1N2F) (**Figure 1.5 b iii**) (Woodward *et al.*, 1990; McKean, 2003).

In early G2 the basal bodies, the site where the flagellum originates, move apart causing the segregation of the two flagella and simultaneously of the kinetoplasts (Ogbadoyi *et al.*, 2003).
After G2, nuclear mitosis occurs, during which chromosomes are segregated in a microtubule-independent manner, unlike what is observed for higher eukaryotes, with maxichromosomes following a different pattern compared to minichromosomes (Ersfeld *et al.*, 1997). Nuclear mitosis results in the generation of cells possessing two kinetoplasts and two nuclei (2K2N2F) (**Figure 1.5 b v**). Finally, cytokinesis occurs through the formation of a cleavage furrow along the longitudinal axis, from the anterior to the posterior of the cell, passing between the two flagella, whose FAZs (flagellum attachment zones) provide the structural information required to position the cleavage furrow (Robinson *et al.*, 1995). At the end of cytokinesis the cells possess a single kinetoplast, nucleus and flagellum (1K1N1F) (**Figure 1.5 b i**). The completion of the cycle takes 6 hr in bloodstream forms (Vickerman, 1985) and 8.5 hr in procyclic forms (**Figure 1.5 a**).

Trypanosomes undergo proliferation in most of their life cycle stages (slender, procyclic and epimastigote forms) with the exception of transmissible stages (stumpy, mesocyclic and metacyclic forms), in which the parasites are cell-cycle arrested. Such observations suggested the presence of an interplay between the cell cycle progression and initiation of differentiation (Matthews *et al.*, 1994). This was supported by the fact that stumpy form cells were able to differentiate synchronously, whereas slender form cells were not (Ziegelbauer *et al.*, 1990; Matthews *et al.*, 1994). In addition, the first cell cycle event after differentiation was found to be S-phase, which suggested that only parasites in G0/G1 were competent to perceive the differentiation signal (Shapiro *et al.*, 1984; Matthews K R, 2004). However, once the parasites have initiated differentiation, their cell cycle position does not affect the completion of the developmental step, indeed inhibition of S-phase did not alter the stumpy transition to procyclic forms (Matthews K R, 2004).

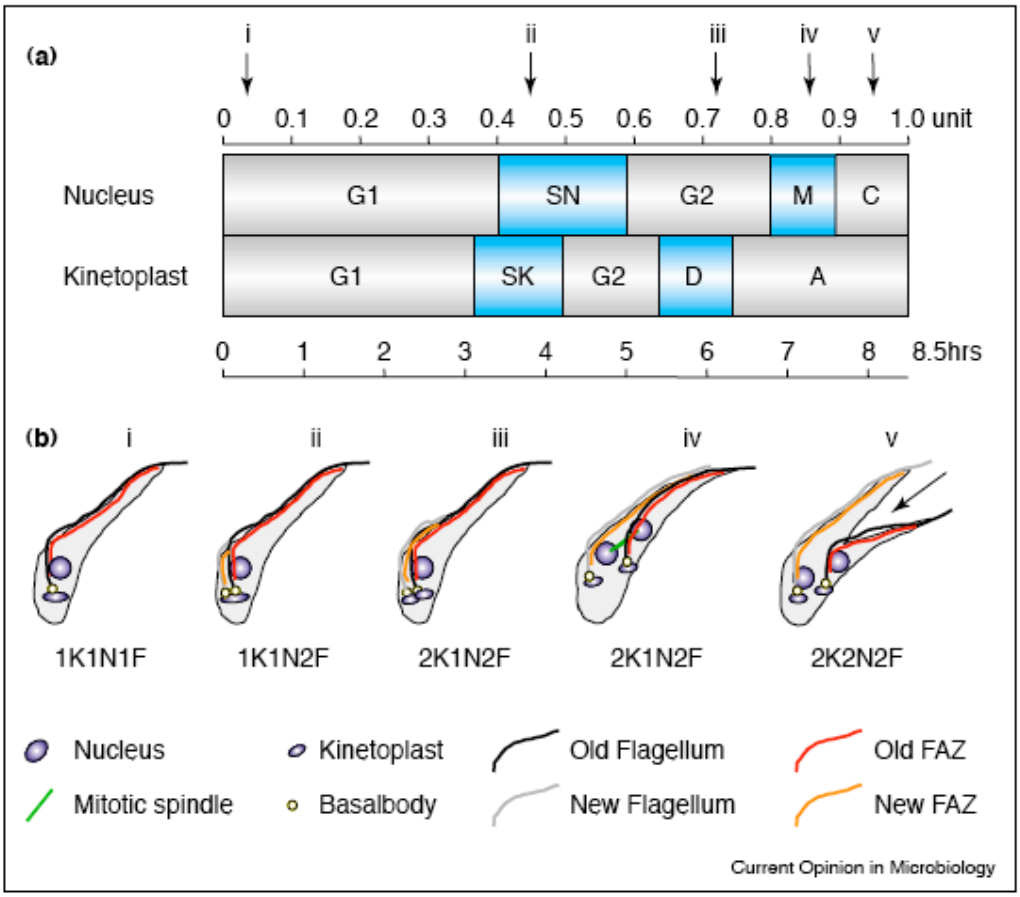

Figure 1.5 Diagram showing *Trypanosoma brucei* (procyclic form) cell cycle (from McKean, 2003). Schematic representation of the nuclear and kinetoplast cell cycle stages highlighting the timing of the different phases: gap phase 1 (G1), nuclear/kinetoplast synthetic phase (SN/SK), gap phase 2 (G2), kinetoplast segregation (D), nuclear mitosis (M), apportioning phase (A) –phase during which the basal bodies move apart-, and cytokinesis (C) (a). Diagram of the main morphological changes taking place during the cell cycle (b); the number of flagella (F), kinetoplasts (K) and nuclei (N) during the different stages (i-v) is shown graphically and with the common cell cycle nomenclature (1K1N1F, etc.).

1.8. The Life Cycle

In order to adapt to different environments, being transmitted between mammalian hosts by the tsetse fly, African trypanosomes undergo a series of programmed morphological and biochemical changes, referred to as the life cycle (Vickerman, 1965). The *Trypanosoma brucei* life cycle includes two bloodstream form stages (slender and stumpy forms) and four main insect form stages (procyclic, mesocyclic, epimastigote and metacyclic) (**Figure 1.6 and Table 1.2)**.

The need to adjust to different energy sources available in the bloodstream and fly environments, together with the necessity to evade the host's defence, are the main factors influencing the parasite metabolic and morphological changes (Vickerman, 1985). In addition, the transition to a different environment affects the cell cycle state, as cell proliferation is required to establish the parasite in a new environment, whereas cell cycle arrest enables a synchronous differentiation, which helps to protect the parasite when they are vulnerable, during transition between environments (**Table 1.2**).

1.8.1. Life in the bloodstream

When a tsetse fly bites the skin of a mammalian host, metacyclic form parasites are injected into the dermal connective tissue, pass to the lymphatic system and then enter the bloodstream.

In the bloodstream, long slender forms possess a post nuclear kinetoplast (trypomastigote arrangement) positioned towards the posterior of the cell, and a flagellum that extends to the anterior of the cell and then becomes free (Vickerman, 1985) (**Figure 1.6**). Slender forms proliferate causing an ascending parasiteamia, which peaks when the host develops an immune response against the dominant VSG type. After that, most of the slender form cells are killed, and are replaced by the non-dividing stumpy forms, thereby causing the parasitaemia to decline (Ferrante *et al.*, 1983).

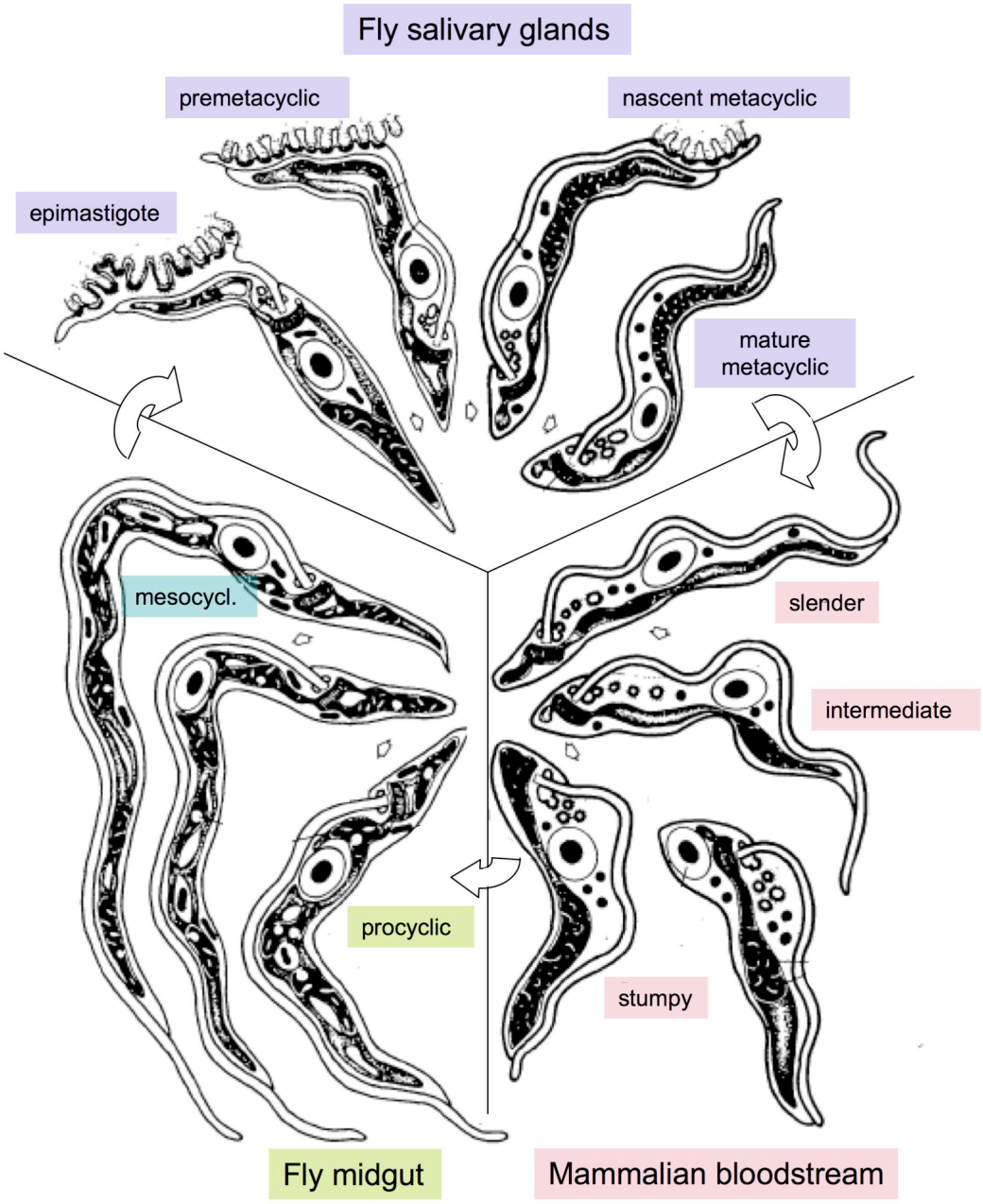

Figure 1.6 Schematic diagram showing the trypanosomes life cycle in the mammalian bloodstream and tsetse fly, modified from Vickerman, 1985. The main life cycle stages are highlighted: slender and stumpy forms in the bloodstream, procyclic and mesocyclic forms in the fly midgut, epimastigote, premetacyclic, nascent and mature metacyclic forms in the fly salivary glands. Changes in the mitochondrial morphology and in cell shape are also depicted.

	Location	Cell cycle profile	Kinetoplast Configuration	Surface coat	Peculiarity
Slender	Bloodstream	Proliferative	Trypomastigote	VSG	Glycolysis
Stumpy	Bloodstream + midgut lumen	Non-dividing	Trypomastigote	VSG	Fly transmissible
Procyclic	Midgut lumen	Proliferative	Trypomastigote	Procyclin	Branched mit. network
Mesocyclic	Proventriculus	Non-dividing	Trypomastigote	Procyclin	Asymmetric division
Epimastigote	Salivary gland epithelium	Proliferative	Epimastigote	BARP	Attachment to the villi and sexual exchange
Metacyclic	Salivary gland epithelium	Non-dividing	Trypomastigote	VSG	Mammalian host transmissible

Table 1.2 *Trypanosoma brucei* life cycle stages. The bloodstream form (slender and stumpy) and tsetse form stages are listed, together with their location, cell cycle profile, kinetoplast configuration, type of surface coat protein and peculiarity of that life cycle stage.

As previously mentioned, slender form cells obtain their energy from glycolysis (Vickerman *et al.*, 1988), utilizing the glucose present in the host's body fluids. However, when slender forms become stumpy forms, they start to switch to an amino acid-based energy metabolism through the elaboration of some mitochondrial activity, particularly $NADH_2$ oxidation (NAD diaphorase activity), with the first changes being detectable as soon as 12 hr post differentiation (Brown *et al.*, 1973). In addition, the mitochondrion acquires the ability to utilize Krebs cycle intermediates, thus metabolizing pyruvate. Overall, all these metabolic changes enable stumpy forms to pre-adapt to survive in the fly environment (Vickerman, 1965). Moreover, it has been shown that stumpy forms are more resistant than slender forms to acidic and proteolytic stress (Nolan *et al.*, 2000).

In parallel to the biochemical changes, the mitochondrion modifies its morphology by increasing its tube diameter and by developing well-defined cristae in its lumen (Vickerman, 1965) (**Figure 1.6**). At the same time, stumpy form cells become shorter, broader, they loose the free flagellum and increase the distance between their kinetoplast and the posterior end of the cell (Brown *et al.*, 1973).

Stumpy cells are important for the overall success of the parasite infection, as they limit the host parasitaemia by being non-proliferative (Shapiro *et al.*, 1984), and increase the chance of disease transmission by being capable to differentiate into insect form cells. Indeed, the expression of stumpy characteristics has proven to be a key event in regulating the ability of the parasite to differentiate (Tasker *et al.*, 2000).

The concomitant presence of stumpy and slender form cells in the mammalian bloodstream has lead to the use of the adjective "pleomorphic", when referring to these life cycle forms (Vickerman, 1965). However, pleomorphic lines can become "monomorphic" (i.e. showing only slender morphology) by long term passage in laboratory animals (Fairbairn *et al.*, 1947). These monomorphic lines, which are widely used in laboratories, have lost the capacity to become stumpy and thus are able to differentiate to procyclic forms only asynchronously (Overath *et al.*, 1986). The fact that pleomorphic and monomorphic lines are

able to differentiate to procyclic forms, although with different kinetics and efficiencies, suggests that both populations possess differentiation-competent cells (termed stumpy*), which are morphologically slender cells but are able to continue the life cycle (Tasker *et al.*, 2000) (**Figure 1.7**). The requirement for intermediate/stumpy* forms during the *in vitro* differentiation of a pleomorphic population has been contested by others, who reported as supportive evidence the fact that similar kinetics of VSG loss and procyclins expression exist, between monomorphic and pleomorphic cells (Bass *et al.*, 1991), although this argument was subsequently disputed (Matthews *et al.*, 1994). However, despite these controversial *in vitro* observations, the presence of intermediate/stumpy* and stumpy forms, in the course of a natural *in vivo* infection has been indisputable.

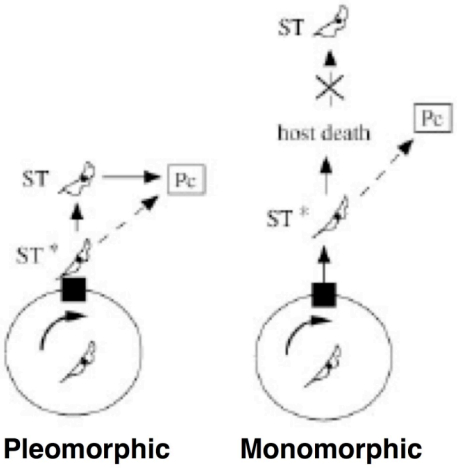

Figure 1.7 Model for the ability of pleomorphic and monomorphic trypanosomes to differentiate to procyclic forms (from Tasker, *et al.* 2000). In a pleomorphic population, slender form cells that are found in the G0/G1 window are able to progress to a transitional form, stumpy* (ST*), which possess some stumpy characteristics essential for differentiation, although are not morphologically stumpy; ST* can then differentiate to procyclic forms (Pc) either directly or through stumpy forms. In contrast, in a monomorphic population slender forms are able to achieve the differentiation competent state (ST*), but are less able to undergo morphological transformation to the stumpy form; consequently they cause very high parasitaemia that kills the host.

1.8.2. Life in the tsetse fly

In the tsetse fly, the bloodmeal enters the crop, and then the midgut, where further digestion is carried out (FAO, 1982). The trypanosomes ingested with the bloodmeal are transported into the lumen of the fly midgut, within the peritrophic matrix, a thick extracellular sheath that surrounds the bloodmeal **(Figure 1.8,** number **1)**.

In the anterior midgut, slender forms are killed, probably after glucose deprivation or of acidic/proteolytic stress, whereas stumpy forms continue swimming to the posterior midgut; here they start to lose the VSG coat and stop endocytosis from the flagellar pocket, thereby becoming procylic forms (Vickerman *et al.*, 1988).

The release of the VSG coat is partly achieved through the activation of the GPI-specific phospholipase C (GPI-PLC), (Bulow *et al.*, 1985) and in part through the action of a metalloprotease (Gruszynski *et al.*, 2003). In place of the VSG coat, EP protein is expressed at 4-6 hr after initiation of synchronous differentiation *in vitro* (Ziegelbauer *et al.*, 1990), and at 6-12 hr GPEET procyclin is also present (Vassella *et al.*, 2000). During this transition several metabolic and morphological changes also take place, some of which follow the differentiation events started in stumpy forms. Indeed the mitochondrial metabolism that was activated in stumpy forms, fully develops in procyclic forms, expanding into a branched network with discoid cristae.

In addition, glycosomes change from spherical to rod-shape (Vickerman *et al.*, 1988) and the posterior portion of the cell elongates, causing the kinetoplast to reposition further away from the posterior end of the cell and closer to the nucleus (Vickerman, 1985; Matthews *et al.*, 1995).

After four days from the infection, the proliferative procyclic form parasites invade the ectoperitrophic space, passing through the membrane over the anterior midgut (Ellis *et al.*, 1977). Inside the ectoperitrophic space, the trypanosomes migrate towards the proventriculus, a specialized muscular organ found in invertebrates, used to grind up food (FAO, 1982) (**Figure 1.8** number **2**).

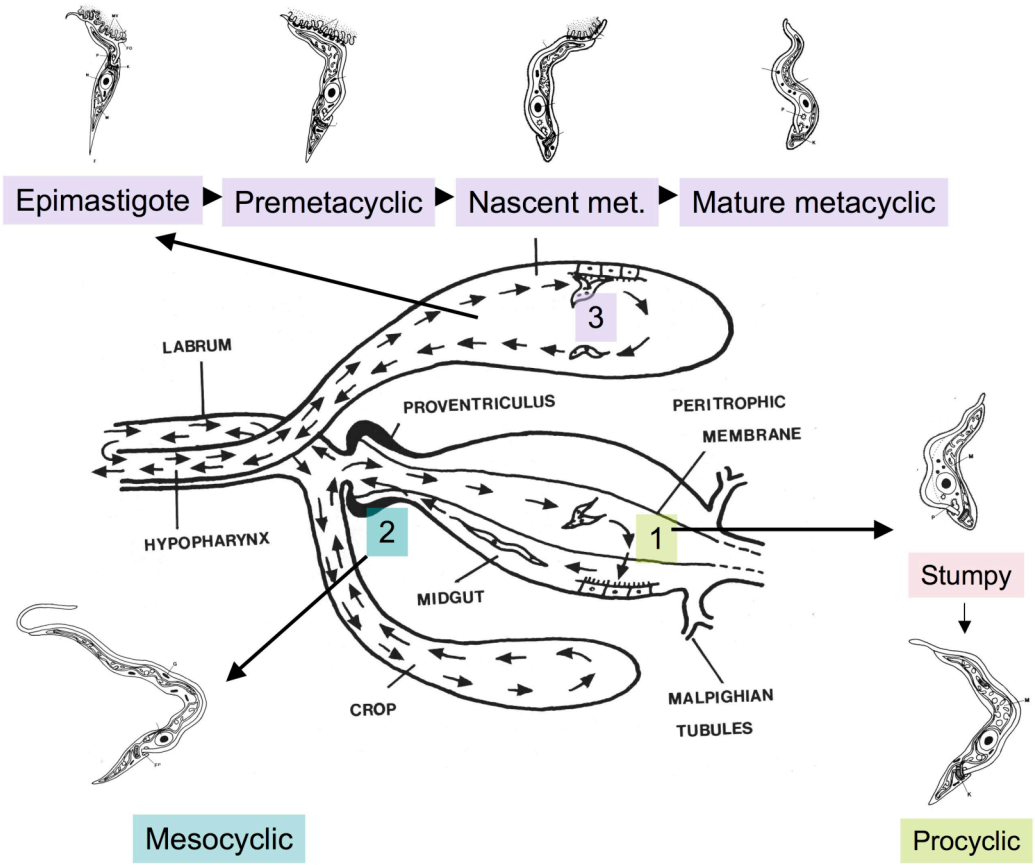

Figure 1.8 *Trypanosoma brucei* life cycle in the tsetse fly (modified from Vickerman, 1988). The location of the different life cycle stages within the tsetse fly is shown (1: posterior midgut, 2: proventriculus; 3: salivary gland; Nascent met.: nascent metacyclic).

On the way towards the proventriculus, procyclic forms become elongated mesocyclic (Sharma *et al.*, 2008b) and they arrest in G2 phase of the cell cycle. Once these mesocyclic parasites reach the proventriculus they further increase their length and retraverse the peritrophic membrane migrating towards the hypopharynx, reaching the salivary glands (Vickerman *et al.*, 1988) (**Figure 1.8** number **3**).

During this migration, mesocyclic trypomastigote trypanosomes become short epimastigotes (the kinetoplast is now prenuclear), which are created by an asymmetric cell division of the long trypomastigote (Sharma *et al.*, 2008b). This asymmetric division gives rise to one short and one long daughter epimatigote,

and the latter appears to die, whereas the short epimastigote colonizes the salivary glands.

In the salivary glands four different forms of the parasite exist: attached epimastigote, premetacyclics, nascent metacyclics and mature free metacyclics (Vickerman, 1985) (**Figure 1.8** number **3**).

The epimastigote forms are characterized by their attachment to the epithelium through a branched outgrowth of the flagellum ("flagellipodia"), which shows punctuate focal cup-like plaques at regular intervals. In addition, they possess a well developed mitochondrion and bacilliform glycosomes (Tetley *et al.*, 1985) and multiply still attached to the epithelium. Furthermore, epimastigote forms express a different surface protein, called BARP (brucei alanine rich protein), which is specific for this life cycle stage (Urwyler *et al.*, 2007).

Scattered among epimastigotes, premetacyclic forms are recognizable by their postnuclear kinetoplast and flagellar origin (trypomastigote configuration) and a reduced flagellar outgrowth, although they are still attached to the epithelium.

Premetacyclic forms then differentiate to nascent metacyclic forms, which further reduce their surface of attachment to the salivary gland, stop dividing and express VSG on their surface coat. In addition, nascent metacyclic forms already show a single stranded mitochondrion and spherical glycosomes, characteristic of mature metacyclic forms (Tetley *et al.*, 1985).

The complete coating of nascent metacyclic causes their release from the epithelium as free mature metacyclic forms. Metacyclic forms possess a blunt posterior end, in contrast to the pointed extremity of epimastigote and premetacyclic forms, and are heterogeneous with respect to the VSG expressed, which enables them to be infective to mammalian hosts (Tetley *et al.*, 1985). Metacyclic forms are produced after 3-5 weeks from the initial infection and in only 2-5 % of the flies (Vickerman *et al.*, 1988).

During *T. brucei* life cycle stages present in the fly salivary glands, before the development of metacyclic forms (Tait *et al.*, 2007), genetic exchange has been reported (Jenni *et al.*, 1986), with both cross- and self-fertilization taking place (Tait *et al.*, 1990). Observations have suggested that a meiotic division would be required, but a haploid stage has not been detected so far (Gibson, 2001).

However, sexual division is not an obligatory part of the life cycle, since it occurs only in a proportion of the parasites (Jenni *et al.*, 1986).

1.9. Molecular aspects of *T. brucei* differentiation

1.9.1. Slender to Stumpy transition

The first factor reported to induce differentiation of slender to stumpy forms was cell density (Black *et al.*, 1985); indeed it was noted that pleomorphic slender cells grown in culture became stumpy after reaching stationary phase, with no need of additional factors, and with the timing of differentiation dependent upon the initial cell density (Reuner *et al.*, 1997).

Further studies showed that density-dependent differentiation required a soluble factor released by the cell, which would cause cell cycle arrest and subsequent differentiation. Such a factor, termed "stumpy induction factor" (SIF), was found to be heat stable and with molecular weight lower than 500 Da, but has not been identified so far. Moreover SIF was suggested to act through the cAMP pathway, since a cell permeable analog of cAMP, successfully induced cellular differentiation. In addition, measurement of intracellular cAMP levels in differentiating cells detected a 2-fold increase 15 min after addition of conditioned media, reaching baseline levels after 30 min (Vassella *et al.*, 1997). Additional work identified the adenosine/5'-AMP product of cAMP hydrolysis as the triggering factor, thus suggesting that cAMP is not acting directly to induce differentiation but through its metabolic products (Laxman *et al.*, 2006). The mechanism of action of these products have not been identified, but potential molecular targets suggested are AMP kinases, cyclin-dependent kinases or mitogen-activated protein kinases (Laxman *et al.*, 2006).

Population density is a widespread parameter controlling initiation of differentiation or development in several prokaryotic and eukaryotic systems, however it is usually starvation that induces cell cycle arrest and the next developmental step is then triggered by a minimum number of cells (minimum density sensing)(Kaiser *et al.*, 1993). In contrast, *T. brucei* possesses a maximal

density sensing, thereby cell cycle arrest and transition to stumpy forms is induced when reaching high cell density. The choice of this mechanism is dictated by the environment, that once again plays a key role in the parasite development; indeed in the bloodstream, where glucose is abundant, the limiting factor is not energy source but host survival, and thus trypanosomes require to sense maximal rather than minimal cell density in order to survive (Vassella *et al.*, 1997), a phenomenon also observed in many bacterial populations.

1.9.2. Stimuli causing stumpy to procyclic form transition

1.9.2.1. Temperature shift and citrate/cis-aconitate

A temperature shift from 37° to 27°-25°C was the first stimulus identified to cause the transition from stumpy to procyclic forms *in vitro*, with the whole population showing procyclic morphology at 72 hr (Bienen *et al.*, 1980). Such a stimulus has been readily correlated to the natural tsetse feeding environment and habits, indeed they preferentially feed at dusk (Makumi *et al.*, 1998), when the temperature can drop significantly.

It was then found that the tricarboxylate Krebs cycle intermediates, citrate and cis-aconitate, also induced procyclic formation, in the presence of a temperature reduction to 27°C (Brun *et al.*, 1981). Specifically, cis-aconitate concentrations between 2 and 16 mM were found to be effective, resulting in 91 % of procyclic form cells after 48 hr of 3 mM cis-aconitate treatment; 3 mM citrate was found to be less effective than 3 mM cis-aconitate, resulting in a 1/5 and 1/3 lower absolute number of differentiated cells at 48 and 72 hr, respectively (Brun *et al.*, 1981).

It was postulated that incubation of cells with citrate/cis-aconitate (CCA) would cause an increased concentration of citrate, cis-aconitate and isocitrate inside the mitochondrion, through the action of the enzyme aconitase, which converts the first two compounds into isocitrate. Hence, a certain level of isocitrate would have then activated the Krebs cycle, triggering metabolic and morphological transformation (Brun *et al.*, 1981). The apparently contradictory observation that isocitrate alone did not induce differentiation was explained

by the fact that it did not cross the inner mitochondrial membrane (Brun *et al.*, 1981).

However, the millimolar concentrations of citrate/cis-aconitate required were considered unphysiological, since citrate levels in the mammalian bloodstream, where trypanosomes are bathed during transition to the fly midgut, reaches only 0.1 mM (Brun *et al.*, 1981) and in tsetse fly body fluids about 15 μM (Hunt *et al.*, 1994).

A major turning point in understanding the physiological role of CCA in trypanosome differentiation from stumpy to procyclic was the discovery by Engstler *et al.*, that a bigger temperature shift (cold shock) from 37° to 20°C, rather than 27°C, resulted in the acquisition of greater sensitivity to micromolar concentrations of CCA (Engstler *et al.*, 2004). This observation indicated that citrate/cis-aconitate is likely to play a key role in trypanosomes differentiation *in vivo*, as tsetse fly will experience cold temperatures after feeding (Rogers, 2000). Interestingly, it was also noticed that cold shock caused bloodstream form cells to express the insect-stage procyclin proteins, although not on the cell surface (Engstler *et al.*, 2004), suggesting that differential trafficking might be important during differentiation to procyclic forms.

More recently the genes encoding for CCA transporters have been identified as members of the transmembrane-spanning proteins of the major facilitator superfamily, called PAD ("proteins associated with differentiation") (Dean *et al.*, 2009). Specifically PAD1 and PAD2 were shown to be responsible for the sensitization of stumpy form cells to low physiological CCA concentrations, particularly under cold shock conditions (Dean *et al.*, 2009).

1.9.2.2. Mild acid and proteinase treatment

In addition to temperature reduction and CCA addition, treatment of bloodstream form cells with mild acid (Rolin *et al.*, 1998) or proteinases (Yabu *et al.*, 1988), in the presence of temperature reduction, have been reported to induce transformation to procyclic forms.

Mild acid was initially investigated because of its role in the development of *Leishmania* (Zilberstein *et al.*, 1991) and *Trypanosoma cruzi* (Tomlinson *et al.*,

1995), where a lower pH is characteristic of the extracellular environment encountered during the developmental steps. In *Trypanosoma brucei*, preincubation at pH 5.5, for 2 hr prior to incubation at 27°C, resulted in cellular differentiation in the absence of CCA. However, only 10% of the cells showed procyclic morphology, EP expression and mitochodrial activity after 72 hr, compared to 100% of transformation for CCA-treated cells (Rolin *et al.*, 1998). Mild acid treatment seemed to induce differentiation by causing death of slender forms but it was not clear whether that was the only mechanism responsible (Rolin *et al.*, 1998). Since the slower kinetics observed after mild acid treatment is probably unlikely to mirror the *in vivo* differentiation, and since the tsetse midgut pH has been shown to be alkaline (Van Den Abbeele *et al.*, 1999), the importance of this treatment during trypanosomes development is questionable. However, it cannot be excluded, that mild acid conditions are potentially encountered in the extracellular environment before reaching the midgut, acting together with other stimuli, such as CCA and cold shock to induce differentiation to procyclic forms *in vivo*.

Similarly to mild acid treatment, proteolytic stress has been shown to cause stumpy to procyclic form transition (Yabu *et al.*, 1988). Specifically trypsin treatment, coupled to temperature shift (37° to 27°C) of monomorphic *Trypanosoma brucei gambiense* induced the cells to become procyclics, with similar efficiency as CCA treatment (Yabu *et al.*, 1988) .

In contrast, other studies, performed on pleomorphic cells, reported different kinetics, with proteinase-treated cells differentiating faster than CCA-treated ones (Hunt *et al.*, 1994; Sbicego *et al.*, 1999). Furthermore, it was noticed that there was a high degree of slender cells death caused by trypsin or pronase (a mixture of bacterial proteases) treatment; however, it was demonstrated that trypsin did not cause differentiation solely by enriching for stumpy forms, but acted as a trigger itself (Sbicego *et al.*, 1999). The mechanism underlying proteolytic stress-induced differentiation is unknown, since it appears to include VSG release but also other morphological rearrangements, such as flagellar internalization and membrane fusion (Frevert *et al.*, 1986).

The physiological role of proteolytic stress is easy to envisage, as stumpy forms are found in the fly midgut, the site of bloodmeal digestion (FAO, 1982), where

trypsin-like enzymes have been implicated in the differentiation process (Imbuga *et al.*, 1992). Moreover, there has been a report showing that bloodstream form trypanosomes, from peak parasiteamia, release proteases into the external medium, perhaps in order to assis the penetration of the peritrophic membrane (Nwagwu *et al.*, 1988), but also potentially influencing cellular development.

1.9.3. Molecular events during transition to procyclic forms

The first detectable cytological event of pleomorphic lines of *Trypanosoma brucei* CCA-induced differentiation at 27°C to procyclic forms is expression of procyclin transcript, as early as 15 minutes after induction of differentiation, followed by gain of procyclin protein at 2 hr (Roditi *et al.*, 1989) (**Figure 1.9**). Between 4 and 6 hr the bloodstream form surface protein VSG is lost, which is partly achieved through the activation of the GPI-specific phospholipase C (GPI-PLC), (Bulow *et al.*, 1985) and in part through the action of a metalloprotease (Gruszynski *et al.*, 2003).

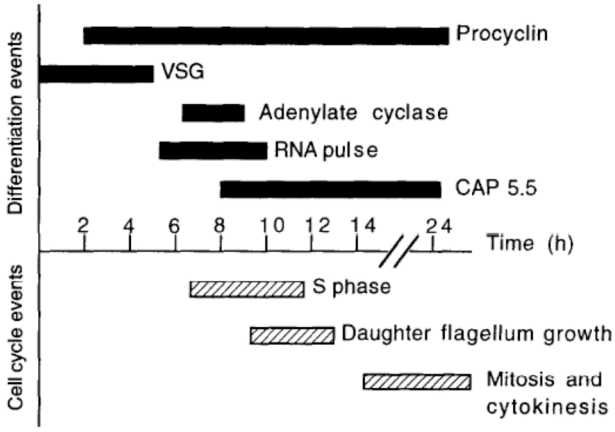

Figure 1.9. Summary the timing of the major event following induction of differentiation from stumpy to procyclic forms (from Matthews and Gull, 1994). The timing of the molecular events and cell cycle changes following initiation of differentiation (time zero) are highlighted as bars.

After VSG loss an increase in intracellular cAMP has been described at 6-10 hr and a second one after the first cell division (20-40 hr) (Rolin *et al.*, 1993). Together with the first cAMP increase, a pulse of RNA synthesis has been detected (Pays *et al.*, 1993), followed by expression of the cytoskeletal-associated protein CAP 5.5 (Matthews *et al.*, 1994). The cell-cycle arrested stumpy form cells start to differentiate between 6 and 12 hr after addition of citrate/cis-aconitate; entry into S-phase is then followed by daughter kinetoplast separation, mitosis and ultimately cytokinesis (Matthews *et al.*, 1994) (**Figure 1.9**).

Several factors controlling the events linked to differentiation have been identified, which include members of the phosphorylation signalling pathways, such as phosphatases and kinases.

1.9.1.1. Protein phosphatases involved in differentiation to procyclic forms

A protein tyrosine phosphatase, *Tb*PTP1, has been shown to negatively control transition to procyclic forms (Szoor *et al.*, 2006) by inactivating its tyrosine-phosphorylated substrate, *Tb*PIP39 (*Tb*PTP1 interacting protein of 39 kDa). Indeed, *Tb*PTP1 inhibition resulted in induction of differentiation through the increased level of phosphorylated and active *Tb*PIP39, which transduced the developmental signal to the glycosomes (Szoor *et al.*, 2010) (for a more detailed analysis of *Tb*PTP1 see paragraph 1.17).

1.9.1.2. Kinases involved in differentiation to procyclic form

In addition to protein phosphatases, a few protein kinases have been linked to the control of different aspects of differentiation to procyclic forms. Particularly, several homologues to the mammalian mitogen-activated protein kinases (MAPKs) have been shown to be involved in growth or differentiation processes. For example, *Tb*MAPK2 was found to control procyclic form proliferation, with null mutant stumpy form parasites

showing delayed differentiation kinetics, followed by cell-cycle arrest in insect form cells (Muller *et al.*, 2002).

In addition to MAPKs, a member of the AGC family of eukaryotic kinases (cAMP-dependent, cGMP-dependent and protein kinase C), PKC, has been shown to negatively regulate VSG shedding and cAMP production, this being observed soon after the initiation of differentiation. Indeed treatment of bloodstream forms with specific PKC inhibitors caused significant VSG release and stimulated adenylate cyclase activity (Rolin *et al.*, 1996) (For a more detailed analysis of *T. brucei* protein kinases see paragraph 1.13).

1.10. *Trypanosoma brucei* signalling

Trypanosoma brucei adaptation to changes in the extracellular environment is an essential requirement to ensure parasite survival. Since responses to environmental changes are mediated through signalling pathways, the factors involved in signal transduction are key components for understanding the cellular biology of these protozoan organisms, as well as for finding ways to compromise their ability to survive.

Homologues of mammalian receptors, protein kinases, protein phosphatases and second messengers have been found in *T. brucei*, although many of the components and connections have not yet been established (Parsons *et al.*, 2000). For example, the activating and deactivating phosphorylation sites of mammalian kinases, such as of ERK1, have been found to be conserved in *T. brucei*, but the canonical upstream receptors and downstream effectors are absent (Nett *et al.*, 2009b).

Interestingly, several differences between trypanosomes and higher eukaryotes can be ascribed to the peculiar biology of the parasite, as highlighted by the identification of signalling pathways involving RNA binding proteins (Chou *et al.*, 2010) and RNA processing (Nett *et al.*, 2009b) in trypanosomes, which were distinct to most mammalian pathways, that culminate in activation of transcription factors (**Table 1.3**).

1.10.1. Surface receptors

Mammalian cells possess mainly three classes of surface receptors: ion-channel linked receptors (such as neurotransmitter receptors), G-protein coupled receptors (or serpentine receptors, such as β2-adrenergic receptors) and enzyme-linked receptors (such as receptor kinases).
In trypanosomatids most of the genes encoding for serpentine and enzyme-linked receptors are missing or the extent of homology is not convincing (Parsons *et al.*, 2000) (**Table 1.3**).
An exception is represented by *T. brucei* adenylate cyclases (AC), which are membrane-bound enzymes that catalyze the formation of cAMP from ATP and, in mammalian cells, are regulated by G-protein coupled receptors. In *T. brucei* four AC genes have been found, ESAG4 and GRESAG 4.1, 4.2 and 4.3, which belong to the family of VSG expression site-associated genes and related genes (ESAGs and GRESAGs, respectively) (Paindavoine *et al.*, 1992).
Interestingly, *T. brucei* ACs possess a large extracellular N-terminal domain, in contrast to mammalian cells, whose adenylate cyclases do not have extracellular domains since they act as effectors of G-protein coupled receptors. Such differences indicate that the parasite enzymes probably serve as extracellular receptors, as also suggested by the variety of their N-terminal domains (Paindavoine *et al.*, 1992). In this regard, the structure of trypanosome adenylate cyclases is more reminiscent of mammalian guanylyl cyclases or of the receptor adenylate cyclase found in *Dictyostelium* (Pitt *et al.*, 1992), which possess both receptor and effector function. This one-step signal amplification, compared to the two-step system typical of mammalian cells, likely provides the advantage of eliciting and quenching the signal very rapidly, and it is coupled to a more limited magnification, which probably does not affect trypanosomes because of their smaller size (Seebeck T, 2001).
In bloodstream forms adenylate cyclase activity has been detected soon after VSG release, as previously mentioned, and is also found to occur in response to cellular stress. They are not to be obligatory coupled, however, as certain stimuli causing VSG shedding do not cause increased cAMP levels (Rolin *et al.*, 1996).

1.10.2. Second messengers

Second messengers are small molecules that are formed in or released into the cytosol in response to an extracellular signal and which transduce the signal to the interior of the cell, such as cAMP, IP_3 (inositol tri-phosphate), and Ca^{2+} (Berridge, 1993). *Trypanosoma brucei* possess all the main second messengers found in mammalian cells, but they sometimes show peculiar features and interactions, as seen in the case of surface receptors (**Table 1.3**).

1.10.2.1. The cAMP signalling

The second messenger cAMP is highly conserved among different organisms, while other upstream and downstream components are variable. In *T. brucei* cAMP is involved in the differentiation from slender to stumpy (Vassella *et al.*, 1997) and from stumpy to procyclic forms (Reed *et al.*, 1985), and involves the activity of four adenylate cyclases (Paindavoine *et al.*, 1992), as previously mentioned.
The levels of cAMP are controlled also by the action of phosphodiesterases (PDEs), of which two families are found in trypanosomes, compared to 11 groups in mammalian cells (Aravind *et al.*, 1997). Some members of class 2 PDEs were shown to be essential in bloodstream forms and thus are being pursued as drug targets (Oberholzer *et al.*, 2007).
In *T. brucei* the downstream signalling of cAMP is not known, since protein kinase A (PKA), which is the main cAMP effector in mammalian cells, has been shown to be activated by cGMP and not cAMP (Shalaby *et al.*, 2001).

1.10.2.2. Calcium signalling

Calcium is another highly conserved second messenger, which is found also in trypanosomes, although its role in the parasite biology and development has not been well characterized (Parsons *et al.*, 2000). However, some studies have highlighted its potential involvement in a variety of cellular processes, such as cell division (Dolan *et al.*, 1986), motility (Wu *et al.*, 1994), cell death

induced by reactive oxygen species (Ridgley *et al.*, 1999) and parasite differentiation (Ruben *et al.*, 1990).

Supporting the existence of Ca^{2+} signalling in trypanosomes is the presence of numerous downstream effectors, such as the calcium-binding protein calmodulin (CaM) (Ruben *et al.*, 1987). In addition to calmodulin, *T. brucei* possess several CaM-binding proteins, which include Ca^{2+}-ATPase in the plasma membrane (Benaim *et al.*, 1993) and the elongation factor 1α (Kaur *et al.*, 1994). Moreover, other EF-hand calcium binding proteins have been detected in the flagellum proteome, thus suggesting a possible role of Ca^{2+} in motility or environmental sensing (Wu *et al.*, 1994).

1.10.2.3. Phosphatidylinositol signalling

Phosphatidylinositol (PI) is a unique membrane lipid that can undergo reversible phosphorylation generating different inositol phospholipids, which represent important second messengers in mammalian cells. PI phosphorylation is regulated by PI3K (phosphatidylinositol 3-kinase), which generates PIP, PIP_2, PIP_3 (mono-, di- or tri-phosphorylated PI) and by PLC (phospholipase C), which gives rise to soluble IP_3 (inositoltriphosphate) and membrane bound DAG (diacylglycerol) (Berridge, 1993).

In *Trypanosoma brucei* GPI (glycophosphatidylinositol) is a glycolipid that anchors the VSG to the membrane of the parasite but the action of GPI-PLC (GPI phospholipase C) can release the GPI, which can be found free intracellualrly, as a mediator of signalling pathways (**Table 1.3**). For example, GPI-PLC has been found to increase endocytosis of transferrin, a mammalian plasma protein that transports iron, essential for parasite growth (Subramanya *et al.*, 2009). In addition to its intracellular effect, the GPI moiety has been shown to act extracellularly, causing host macrophages to release proinflammatory cytokines (Tachado *et al.*, 1994).

Nothing is known about GPI-PLC mediated IP_3 production in *T. brucei*, except the fact that IP_3 does not induce Ca^{2+} release from the ER (Nolan *et al.*, 1994), in contrast to what seen in mammalian cells.

One of the members of the PIK (phosphatidylinositol kinase) family has been identified in *T. brucei* which showed conserved functions with yeast and mammalian homologues, as a major regulator of vesicular trafficking endocytosis and Golgi complex segregation (Hall *et al.*, 2006). Other *T. brucei* PIK members, *Tb*TOR1 and *Tb*TOR2, are involved in cell growth control, cytokinesis and cytoskeletal remodeling (Barquilla *et al.*, 2008).

The PIK products PIP, PIP_2 and PIP_3 have not been characterized, however PH domains have been identified on several parasite protein kinases, such as in Nrk, a kinase potentially involved in differentiation to stumpy forms (Gale *et al.*, 1994), suggesting a possible role of PI signalling in the regulation of parasite development and other biological processes (**Table 1.3**).

	Conservation	Function	Peculiarity
Receptors			
Ion-channel linked	not conserved		
G-protein coupled	not conserved		
Enzyme-linked	substituted by AC	Development (Rolin *et al.*, 1996) Motility (?) (Paindavoine *et al.*, 1992)	AC with extrac. domain (Paindavoine *et al.*, 1992)
Second messengers			
cAMP	conserved	Development (Seebeck *et al.*, 2001)	No cAMP-activated PKA (Shalaby *et al.*, 2001)
Ca^{2+}	conserved	Cell division (Dolan *et al.*, 1986) Motility (Wu *et al.*, 1994) Cell death (Ridgley *et al.*, 1994) Development (?) (Ruben *et al.*, 1990)	
PI	conserved (GPI)	VSG release (Rolin *et al.*, 1996) Virulence (Webb *et al.*, 1997) Golgi segregation (Hall *et al.*, 2006) Endocytosis (Hall *et al.*, 2006) Vesicular trafficking (Hall *et al.*, 2006) Growth (Barquilla *et al.*, 2008) Development (Gale *et al.*, 1994)	No ER Ca^{2+} release (Nolan *et al.*, 1994)

Table 1.3 Summary of the main signalling pathway components of *T. brucei*. The cell surface receptors and second messengers found in *T. brucei* are listed and their conservation, function and main peculiarity are highlighted (AC: adenylate cyclase, extrac. domain: extracellular domain).

1.11. *T. brucei* protein phosphorylation

Protein phosphorylation is one of the main components of signalling pathways, controlling a variety of aspects of cellular physiology (Hunter, 1987). In *Trypanosoma brucei*, protein phosphorylation has been documented and showed to change during parasite development (Parsons *et al.*, 1990; Aboagye-Kwarteng T, 1991; Bakalara *et al.*, 1995). Particularly, two 30-45 kDa proteins were initially identified as showing increased tyrosine phosphorylation upon transition from slender to procyclic forms (Parsons M, 1991), and two proteins with similar size were also reported to increase serine and threonine phosphorylation levels during the same stages (Aboagye-Kwarteng T, 1991). Further studies have then revealed that the two phosphorylated proteins were nucleolar RNA binding proteins, Nopp44/46 (Das *et al.*, 1996; Das *et al.*, 1998), phosphorylated on serine by CK2 (Park *et al.*, 2002), tyrosine dephosphorylated by *Tb*PTP1 (Chou *et al.*, 2010) and important for ribosome biogenesis (Jensen *et al.*, 2005).

Moreover, analysis of protein phosphatase activity on cell extracts highlighted a different level of activity between bloodstream and procyclic form, with the former showing up to twice the activity of the latter (Bakalara *et al.*, 1995).

In addition to *T. brucei* development, protein phosphorylation has been found to play a role in the bloodstream parasite growth, as shown by the decrease in cell multiplication after treatment with the tyrosine kinase inhibitor genistein, which caused the alteration of tyrosine phosphorylation levels of a dozen proteins detectable by Western blot analysis (Wheeler-Alm *et al.*, 1992). Recently, more sensitive phosphoproteomic techniques have identified 491 cytosolic phosphoproteins in bloodstream form *T. brucei*, involved in several biological processes, such as DNA and RNA processing, protein synthesis and degradation, and metabolism (Nett *et al.*, 2009b) (**Figure 1.10**).

Moreover, some tyrosine phosphorylated proteins were found to localize in the flagellum basal body and axoneme in procyclic forms, thus suggesting

that tyrosine phosphorylation might be involved in flagellum formation and basal body segregation in this life cycle stage (Nett et al., 2009a).
Among the 491 phosphorylated proteins identified, 44 were kinases, the majority of which showed multiple phosphorylation sites on the MAP kinase activation loop, similarly to that observed for mammalian MAP kinases, thus suggesting some segments of higher eukaryotes signal transduction are conserved in *T. brucei*.

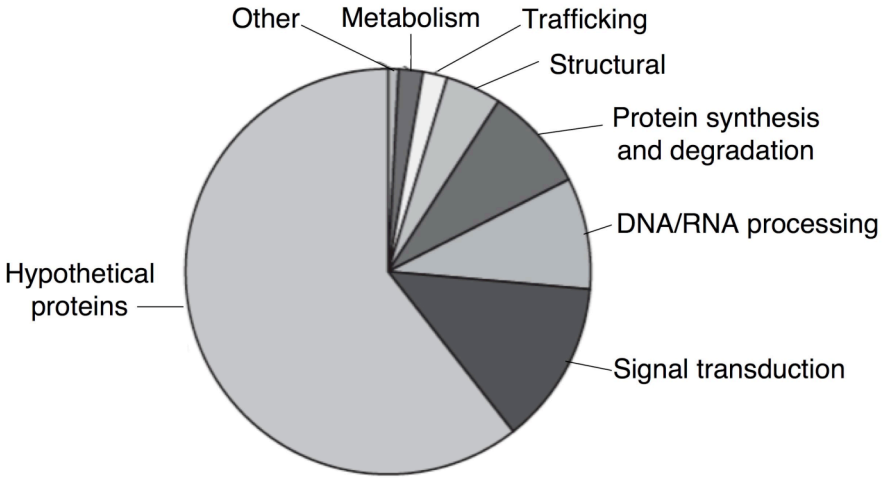

1.10 Role of phosphorylated proteins in bloodstream form *T. brucei*, as predicted by their genome annotation (modified from Nett *et al.*, 2009a). The biological processes potentially regulated by protein phosphorylation include signal transduction, DNA/RNA processing, protein synthesis and degradation, etc.; most of the phosphorylated proteins were found to be hypothetical proteins, with no homology to known proteins.

In contrast, trypanosomes are more similar to prokaryotes than to eukaryotes when analysing the ratio of phosphoserine/threonine/tyrosine present, being 75/21.5/3.5% in *T. brucei*, 70/20/10% in prokaryotes and 86/12/2% in eukaryotes (Nett et al., 2009b).
In addition to MAP kinases, the other phosphorylated kinases detected belong to different families, such as the cdc2-related protein kinases (CRK1, 2, and 3), which control the cell cycle (Mottram et al., 1995), the dual specificity kinases (DYRKs), which are involved in cell proliferation and development in *Drosophila* (Lochhead et al., 2003), GSK3β, which controls

glucose homeostasis in mammalian cells (Rayasam et al., 2009) and the STE family, which regulate MAP kinases.

Similarly, several tyrosine-phosphorylated proteins detected in procyclic form *T. brucei* were kinases, of which two were metabolic kinases (phospoenolpyruvate carboxykinase and 6-phospho-1-fructokinase) and 19 protein kinases belonging mainly to the MAP kinase and cdc-2 related protein kinase families (Nett et al., 2009a). Interestingly the tyrosine-phosphorylated proteins were found to be concentrated at the cytoskeleton, basal body, axoneme and nucleolar compartment in procyclic forms, in marked contrast with the localization of tyrosine-phosphorylated proteins in mammalian cells, which localize on the plasma membrane (Vuori, 1998).

1.12. *T. brucei* protein kinases

The analysis of the *T. brucei* genome reported the presence of 156 eukaryotic protein kinases (ePKs) and 20 atypical protein kinases (aPKs), which is approximately 30% of the number of kinases in humans (Parsons *et al.*, 2005), but twice the number of kinases found in other unicellular organism, such as *S. cerevisiae* or *P. falciparum*, thereby suggesting a more central role of protein phosphorylation in trypanosomes compared to other protozoa (Nett *et al.*, 2009b).

Moreover, the analysis of the different groups of ePKs, highlighted differences in the relative number of trypanosomatid kinases found in each group compared to the human counterpart (**Table 1.4**). One of the main differences in the kinome of *T. brucei*, and of other kinetoplastid parasite, was the complete absence of the PTK family (protein tyrosine kinases), which includes the enzyme-linked receptor family of receptor tyrosine kinases (Nett *et al.*, 2009b). The lack of tyrosine kinases indicates that tyrosine phosphorylation is probably performed by dual specificity kinases, which are able to phosphorylate serine/threonine and tyrosine residues (Dhanasekaran *et al.*, 1998), such as the MAP kinase kinases (STE7), and the CLK family, which are present in the *T. brucei* kinome (Parsons, 2005).

Furthermore, trypanosomes possess a smaller amount of kinases belonging to the AGC (cyclic nucleotide-regulated protein kinases) and CAMK (Ca^{2+}/Calmodulin-regulated protein kinases and AMP-activated protein kinases) groups, compared to the same groups in humans (**Table 1.5**). However, several important kinases that respond to second messengers are found in *T. brucei,* such as PKA, PKG and PKC. The CMGC kinase family (cyclin-dependent kinases) is better represented than other groups in mammalian cells, and includes 10 MAP kinases and 11 cyclin-dependent kinases. Similarly, the NEK family of "other" ePKs contains more kinases than the corresponding group in humans, and it also appears to possess a slightly bigger variety of accessory domains, which could indicate its involvement in parasite-specific signalling mechanisms (Parsons, 2005). Interestingly one member of this family has been characterized and shown to be upregulated during parasite differentiation from slender to stumpy forms (Gale *et al.*, 1994).

Among the 156 ePKs, 19 protein kinases were not found to be significantly similar to any enzyme of any other organisms, and were thus classified as "unique" PKs (Parsons, 2005).

The comparative analysis of the *T. bruc*ei kinome identified differences not only in the size of the different kinase families but also in the presence and combination of certain accessory domains, for example the lack of SH_2 (Src kinase homolgy domain) and SH_3 domains that bind phosphotyrosine and proline-rich sequences, respectively, thus suggesting, for the former, the evolution of different motifs interacting with parasite-specific tyrosine kinases (Parsons, 2005).

1.13. *T. brucei* Protein Phosphatases

Protein phosphatases are classified according to their substrate specificity into five main categories: serine/threonine phosphatases (STPs), protein tyrosine phosphatases (PTPs) and lipid phosphatases. The PTP family also includes the dual specificity phosphatases (DSPs), which dephosphorylate tyrosine and serine/threonine residues, and the family of smaller and simpler low molecular weight phosphatases (LMW-PTPs), which are specific for phosphorylated tyrosine (Fauman *et al.*, 1996).

An ontology based classification (Wolstencroft *et al.*, 2006) of *T. brucei* phosphatases highlighted the presence of the main classical families of phosphatases, but differences in their composition and in the type of accessory domains present, and the existence of parasite enzymes with no orthologues in other organisms, thus suggesting the evolution of parasite-specific signalling pathways (Brenchley *et al.*, 2007) (**Table 1.4**). The first difference observed was the small proportion of kinetoplastids PTPs, compared with humans, with 2.6% of *T. brucei* phosphatases being PTPs (2/78), and 30% in humans (43/140). The low proportion of PTPs seems to be compensated by the higher number of STPs detected, with 69% (54/78) present in *T. brucei* compared to 24% (33/140) in the human genome.

Moreover, a significant number of atypical phosphatases and kinetoplastid-specific enzymes were identified, belonging especially to the DSP family, whose members also were found to be significantly longer compared to their human counterparts (Brenchley *et al.*, 2007).

One subfamily of atypical DSP were shown to possess peculiar Leucine Rich Repeats (LRRs), found in some receptor-like kinases (RLKs) of *A. thaliana* (Shiu *et al.*, 2001), or in human phosphatase PHLPP. However, no enzyme has been identified which contains LRRs in a DSP domain, making this combination of domains kinetoplastid-specific. Interestingly, the LRRs sequences contained in kinetoplastid DSPs resulted to be similar to LRR proteins involved in Ras-mediated signalling, an important mammalian pathway that controls cell growth via the activation of the GTP-binding protein Ras and of the downstream Raf kinase (Alberts *et al.*, 2002), thus

suggesting a similar scaffolding role for this group of phosphatases (Brenchley *et al.*, 2007).

In addition to the LRRs, a second subfamily of atypical DSPs, were found to be composed of two pseudokinase domains, thus named "kinatases", from the union of kinase and phosphatase domains. Similar enzymes containing both kinase and phosphatase domains are present only in other protozoan organisms, indicating an evolutionarily conserved function of this group of DSPs (Brenchley *et al.*, 2007).

Another group of kinetoplastid DSPs that showed no orthologues with human enzymes, was the MAP kinase phosphatases (MKPs), which resemble MKPs of *Arabidopsis*, particularly AtMKP1, involved in the control of stress response (Ulm *et al.*, 2002), indicating, once again, the close evolutionary relationship of certain features of trypanosomes to plants. The same was also found to be true for some of the serine/threonine phosphatases, the kinetoplastid-specific phospho protein phosphatases (kPPP), whose sequences were mostly similar to plant and fungal phosphatases. However, not all the phosphatase families followed this trend, for example the PPM group (protein phosphatase, magnesium or manganese-dependent) of serine/threonine phosphatases showed closer homology to yeast and mammalian rather than plant enzymes (Brenchley *et al.*, 2007).

1.13.1 Characterized *T. brucei* Protein Phosphatases

The identification of the *T. brucei* phosphatome has given an insight into the composition and size of the different families of enzymes, as well as of their structural differences and similarities to other organisms. However, the function of most of these phosphatases is not known yet. Indeed only about 10 % (8/78) of *T. brucei* phosphatases have been characterized so far, five serine/threonine phosphatases and three tyrosine phosphatases (Szoor, 2010) (**Table 1.4**).

T. brucei PP1 and PP2A (*Tb*PP1 and *Tb*PP2A), belonging to the STP family, were found to be important for kinetoplast segregation and cellular cytokinesis (Das *et al.*, 1994), possibly regulating the kinetoplast cycle with

the cell cycle (Li *et al.*, 2006) and they were also shown to control the amount of β tubulin mRNA (Li *et al.*, 1995).

Another member of the serine/threonine phosphatases, *Tb*PP5, is involved in the regulation of Hsp90, an essential heat shock protein for parasite survival during stress, by promoting protein folding and maturation, particularly at 37°C (Jones *et al.*, 2008).

The fourth member of the STP family characterized in *T. brucei* is PP7 or PPEF (protein phosphatase with EF hands), whose gene does not possess the classical calmodulin binding and EF-hand motifs, and thus is likely not to be regulated by Ca^{2+} and which is involved in cell growth (Mills *et al.*, 2007).

The fifth STP characterized belongs to the subfamily of FCPs (TFIIF-stimulated CTD phosphatases), which in higher eukaryotic cells are responsible for the regulation of the carboxyl terminal domain of RNA polymerase II, thereby promoting enzyme recycling after transcription (Kobor *et al.*, 1999). In *T. brucei* one member of the FCPs has been identified, as *Tb*PIP39, a glycosomal phosphatase essential for parasite development (Szoor *et al.*, 2010).

One gene coding for a protein tyrosine phosphatase (PTP) has been identified in *T. brucei*: *Tb*10.70.0070 (*Tb*PTP1). *Tb*PTP1 has been shown to control parasite development (Szoor *et al.*, 2006) (see paragraph 1.17). Two dual specificity phosphatases (DSPs) were also identified, *Tb*PTP2 and *Tb*PTP3, which were found to be involved in cell cycle regulation (McElhinney, 2007; Szoor, 2010).

Kinome	Phosphatome
156 Total ePKs 20 atypical PKs 19 unique PKs absence of PTKs smaller AGC, CAMK bigger CMGC absence of SH2 and SH3 domains	78 Total 54 STPs (11 kinet-sp PPPs) 19 DSPs (6 atypical DSPs) 2 PTPs smaller PTPs bigger STPs presence of plant LRRs domains

Phosphatase	N°	Characterized	Function
PP1	8	*Tb*PP1	Kinet. segregation
PP2A	2	*Tb*PP2A	Kinet. segregation
PP2B	2	*Tb*PP2B	n.d
PP4	1	*Tb*PP4	n.d
PP5	1	*Tb*PP5	Heat shock response
PP6	0	*Tb*PP6	-
PP7	2	*Tb*PP7	Parasite growth
FCPs	14	*Tb*PIP39	Development St to Pcf
PTPs	1	*Tb*PTP1	Development St to Pcf
DSPs	19	*Tb*PTP2, *Tb*PTP3	Cell cycle regulation

Table 1.4 Summary of the main features of the *T. brucei* Kinome and Phosphatome and the list of Protein Phosphatases. The main differences of the *T. brucei* kinome (Parsons *et al.*, 2005) and the phosphatome (Brenchley *et al.,* 2007) compared to higher eukaryotes are highlighted in the table of the upper panel. In the table of the lower panel the classes of Ser/Thr Protein Phosphatases (PP1-PP7 and FCPs) and Protein Tyrosine Phosphatases (PTPs and DSPs) are listed, together with the number of genes identified in the *T. brucei* phosphatome, the names of the characterized enzymes and their function (Kinet. segregation: kinetoplast segregation; n.d: not determined; St: stumpy; Pcf: procyclic).

1.14. Mammalian Protein Tyrosine Phosphatases

In mammalian cells 81 active Protein Tyrosine Phosphatases (PTPs) have been identified, which are classified into four families according to their substrate specificity (Alonso *et al.*, 2004) (**Figure 1.11 A**).
Class I PTPs possess a cysteine-based catalytic mechanism and include classical PTPs, which are specific for phosphorylated tyrosine residues, and dual specific PTPs (DSPs), which can act on phosphorylated tyrosine as well as serine/threonine residues. Class II enzymes are low molecular weight phosphatases (LMPTP) that are characterized by a smaller and simpler structure and act on phosphorylated tyrosine residues. Class III PTPs are the cell cycle regulators CDC25s, which dephosphorylate cyclin-dependent kinases (CDKs) on tyrosine or threonine residues. The last family comprises PTPs possessing an aspartic acid as catalytic residue, instead of the cysteine found in the other three classes. Examples of enzymes belonging to this group are the transcription factors Eya, involved in *Drosophila* development (Jemc *et al.*, 2007).

Classical PTPs possess a catalytic site characterized by the active-site signature motif or "PTP loop" [I/V]HCX_5R[S/T], where X is any amino acid, and C is the cysteine residue essential for catalysis (Tonks, 2003). This family of enzymes is further divided into receptor-like (RPTPs) and non-transmembrane, cytoplasmic PTPs (NRPTPs) (Tonks, 2006).
Cytoplasmic classical PTPs comprise a large family of heterogeneous enzymes, particularly rich in protein-protein interaction domains that function in regulating the enzyme activity, substrate specificity and localization, for example, the SH_2, found in the phosphatase SHP1 (Pei *et al.*, 1996). In addition, some cytoplasmic PTPs possess targeting domains such as the PDZ binding motif, which binds to the PDZ motif, typically found on synapse and junction-associated molecules (Kim *et al.*, 1995) (**Figure 1.11 B**).

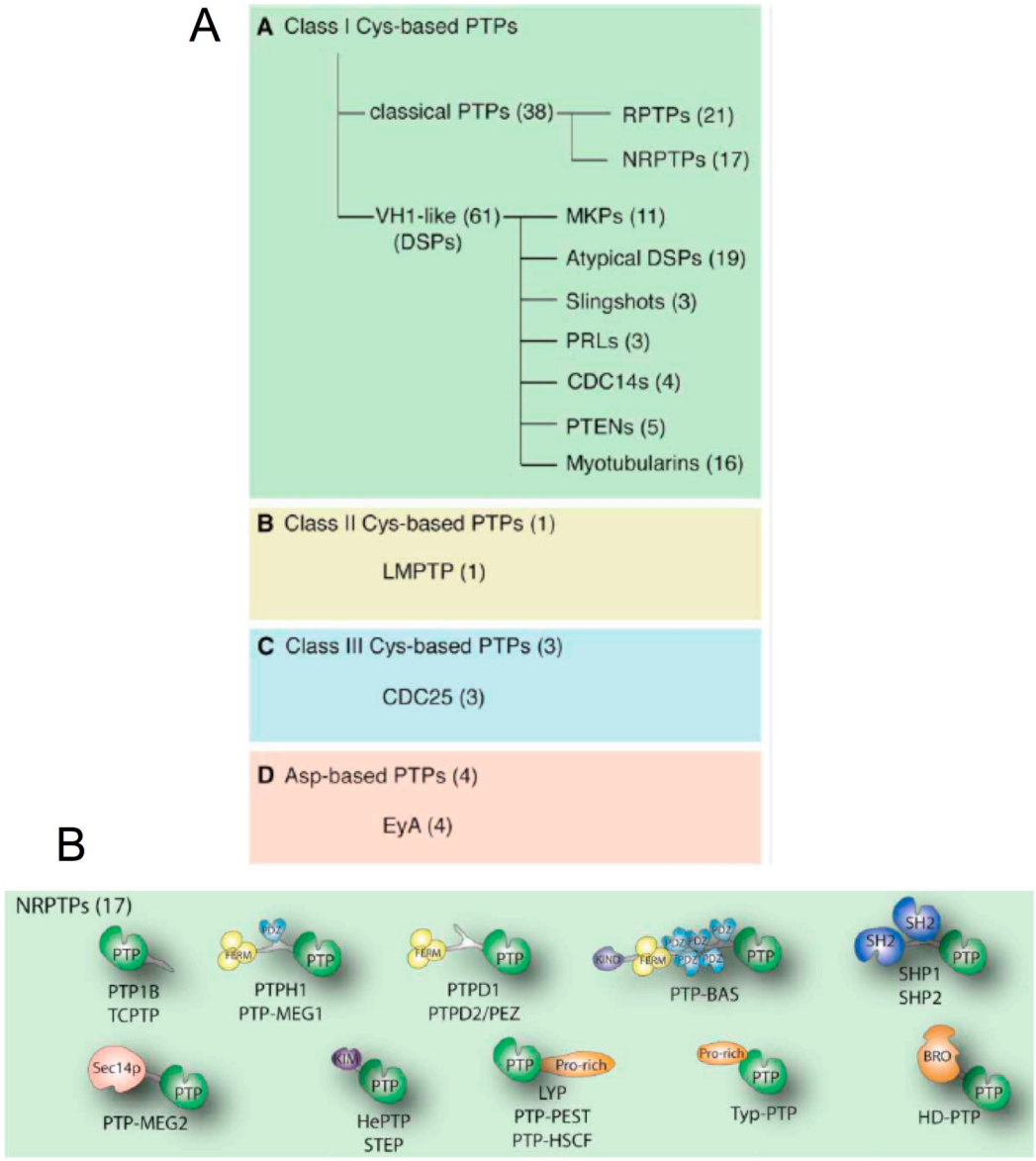

Figure 1.11. Classification of mammalian protein tyrosine phosphatases (PTPs) (from Alonso *et al.*, 2004). (A) The four classes of mammalian PTPs are shown (A to D: Class I to III of cysteine-based PTPs and the class of aspartic acid-based PTPs), together with their corresponding numbers (in parenthesis). (B) Schematic diagram of the domain structure of mammalian cytosolic PTPs. PTP: PTP catalytic domain; FERM: band 4.1/ezrin/radixin/moesin homology; PDZ: postsynaptic density-95/disc large/ZO1 homolgy; KIND: kinase N lobe-like domain; SH2: src homolgy 2; Sec 14 p: sec homolgy; KIM: kinase interaction motif; Pro-rich: proline rich; BRO: baculavirus BRO homolgy.

1.14.1 Structure and catalytic mechanism of mammalian protein tyrosine phosphatases

The characterization of the X-ray crystallographic structures of several classical PTPs has highlighted the presence of ten conserved motifs (M1 to M10) within the common PTP catalytic domain, which comprise approximately 280 aa (Andersen *et al.*, 2001).

Two of these domains (M4 and M9) are highly conserved among different classical PTPs: M9 is the PTP loop, which characterizes the PTP family, and M4 forms the core structure surrounding the catalytic site.

In addition to the PTP loop, the active site is structurally defined by three other motifs: the P loop, the WPD loop and the Q loop (M1, M8 and M10, respectively), which have been first characterized for the cytoplasmic PTP, PTP1B (Tonks, 2003) (**Figure 1.12**).

The phosphotyrosine recognition loop, or P loop (M1), defines the depth of the active site, thereby creating the selectivity for phosphotyrosine.

The WPD loop (M8) is critical for the dynamics of the catalytic site, since, by interacting with the PTP loop, it closes around the side chain of the phosphorylated tyrosine of the substrate thus positioning the aspartic acid residue (the D in the WPD loop) close to the tyrosyl group. This conformational change is essential to carry out the catalytic reaction initiated by the cysteine residue of the PTP loop. Indeed, the aspartic acid is responsible for the protonation of the substrate that follows the nucleophilic attack of the cysteine residue in the first step of catalysis (**Figure 1.13**, **step 1**). In addition, the aspartic acid of the WPD loop is important for the hydrolysis of the substrate in the second part of the reaction (Tonks, 2003) (**Figure 1.13, step 2**).

Finally the Q loop (M10) contains a glutamine residue (Q) that is responsible for the hydrolysis and release of the substrate, together with the aspartic acid of the WPD loop (**Figure 1.13, step 2**).

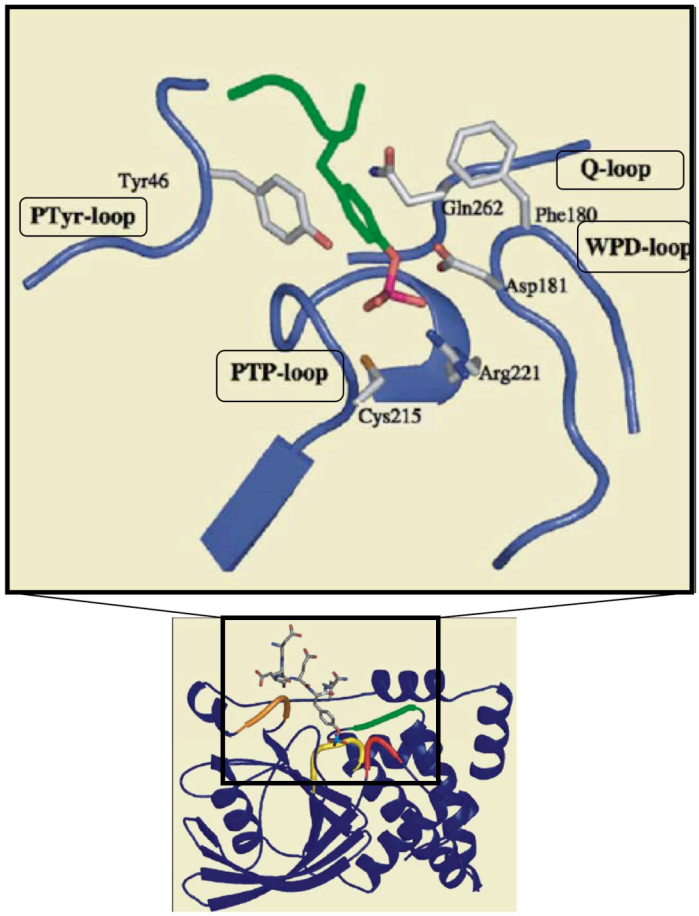

Figure 1.12 Structure of the PTP catalytic site (modified from Tonks, 2003). The structure and location of the active site of mammalian PTPs in the presence of a peptide substrate is shown in the upper and lower panel, respectively. The four motifs creating the structure of the catalytic cleft are highlighted: the phosphotyrosine-selectivity motif (PTyr-loop or P loop), the PTP signature motif containing the nucleophilic cysteine residue (PTP-loop), the motif containing the important aspartic acid (WPD-loop) and the glutamine residues (Q-loop) required for catalysis.

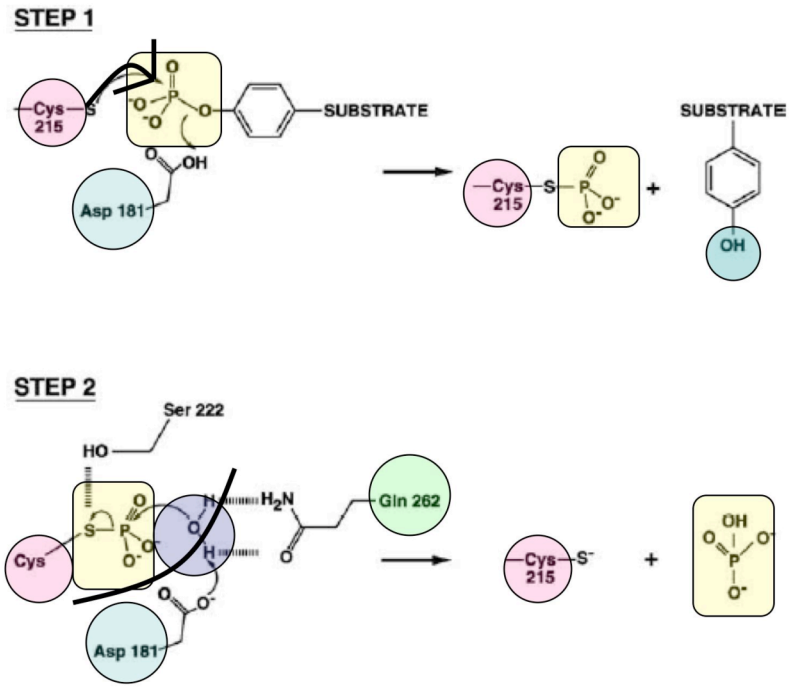

Figure 1.13. PTP catalytic mechanism (modified from Tonks, 2003). A schematic representation of the two-step catalytic mechanism of PTPs; in step 1 the sulphur atom of the catalytic cysteine attacks the phosphate of the substrate (arrow) and the side chain of the conserved aspartic acid of the WPD loop protonates the tyrosyl-leaving group of the substrate; in step 2 the same aspartic acid residue hydrolyses the catalytic intermediate (thick line), together with the glutamine residue of the Q loop. Residues of the enzyme are circled, whereas the phosphate of the substrate is highlighted by a yellow square. Residues are numbered according to the catalytic site of PTP1B.

1.15. The "substrate-trapping" mutant approach

The substitution of one of the amino acids required for catalysis has been used as a strategy to identify substrates of mammalian PTPs, and is known as the "substrate-trapping" approach (Garton *et al.*, 1996). Initially, two substrate-trapping mutant PTPs were created: one possessing a serine residue instead of the catalytic cysteine (Cys→Ser)(Guan *et al.*, 1991) and one possessing an alanine instead of the aspartic acid residue (Glu→Ala)(Flint *et al.*, 1997) required for catalysis. The Cys→Ser mutant enzyme was shown to retain some substrate binding ability, although it was not found to be an inactive enzyme. The Glu→Ala mutant phosphatase was also not completely inactive but was shown to interact more strongly with the substrates (Flint *et al.*, 1997). Indeed, mutation of the aspartic acid residue, found in the WPD loop, produces an enzyme that is not able to finish the first step of catalysis. Therefore the mutant enzyme maintains a high affinity for the substrate, provided by the catalytic cysteine, but it traps the substrate inside its catalytic cleft, without dephosphorylating it. This ability is clearly useful to facilitate the isolation and identification of substrates, which would otherwise be missed, due to the transient nature of the enzyme-substrate interaction.

1.16. *T. brucei* protein tyrosine phosphatases

Sequence analysis has classified kinetoplastid PTPs into three groups**,** based on the conservation of the ten hallmark PTP motifs (M1 to M10) (see paragraph 1.14.1) (Andersen *et al.*, 2001) **(Figure 1.14)**.

Group 1 contains parasite PTPs most similar to human enzymes and includes one *Leishmania major* enzyme (*Lm*PTP1) and one *Trypanosoma cruzi* enzyme (*Tc*PTP1)(Brenchley *et al.*, 2007). The only characterized PTP of this group is *Leishmania donovani* PTP1 (*Ld*PTP1), which has been implicated in the regulation of parasite virulence *in vivo* (Nascimento *et al.*, 2006; Brenchley *et al.*, 2007) (**Figure 1.14, Group 1**).

Group 2 PTPs lack motif 2 (M2) and possess up to six kinetoplastid-specific regions in both the pre-catalytic and catalytic domain of the proteins. This group contains three phosphatases: *Tb*PTP1 (which, despite its name, is not a homologue of *Lm*PTP1 or *Tc*PTP1), *Lm*PTP2 and *Tc*PTP2 (**Figure 1.14, Group 2**). The function of the kinetoplastid-specific regions is unknown but might be important in substrate recognition or regulation (Brenchley *et al.*, 2007). The only characterized enzyme of the second group is *Tb*PTP1(Szoor *et al.*, 2006), which will be talked about in detail in the next paragraph.

Group 3 PTPs show the most interesting variations from higher eukaryote enzymes, with substitutions and deletions in several motifs and includes two enzymes: *Lm*jF32.0640 and *Tb*11.01.5450 (*Tb*PTP2)(Brenchley *et al.*, 2007; Szoor, 2010) (**Figure 1.14, Group 3**).

Overall the main difference between mammalian protein tyrosine phosphatases and the homologues found in *T. brucei* and in other kinetoplastid parasites, lies in the lack of extracellular and trans-membrane regions or of any additional recognisable regulatory or targeting domains. This low homology suggests that kinetoplastid PTPs may be suitable targets for the design of specific and selective inhibitors against parasitic infection and transmission (Brenchley *et al.*, 2007).

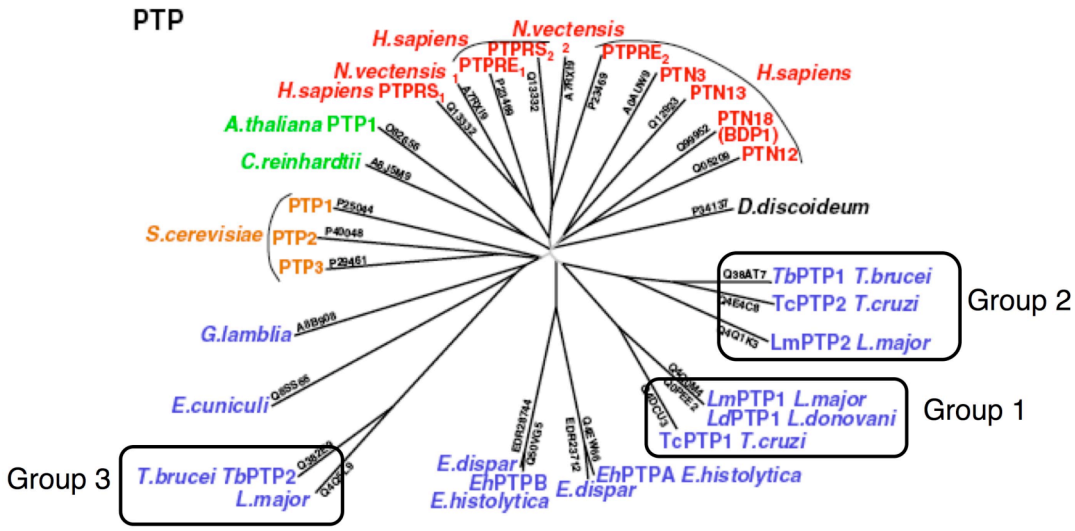

Figure 1.14. Phylogenetic tree of protozoan protein tyrosine phosphatases (PTPs) (modified from Andreeva *et al.*, 2008). The three groups of kinetoplastid PTPs are highlighted (Group 1, 2 and 3) and their relationship to mammalian PTPs are shown.

1.17. *T. brucei* protein tyrosine phosphatase 1

As previously mentioned, the only characterized kinetoplastid PTP belonging to group 2 is *T. brucei* protein tyrosine phosphatase (*Tb*PTP1) (Szoor *et al.*, 2006; Szoor *et al.*, 2010). *Tb*PTP1 is a 34 kD protein (306 aa) containing 9 of the 10 landmark motifs (M1-M10) present in classical tyrosine-specific phosphatases (see paragraph 1.14)(Andersen *et al.*, 2001) (**Figure 1.15**). The only motif missing is the less conserved motif 2 (M2), which is replaced by a trypanosome-specific motif (T1). In addition to T1, three other trypanosome-specific motifs are present in the enzyme sequence, two found in the catalytic region (aa 43-306) which were named T1 to T4, and two in the pre-catalytic region (aa 1-43), which were called PcT1 and PcT2 (Szoor *et al.*, 2006) (**Figure 1.15)**.

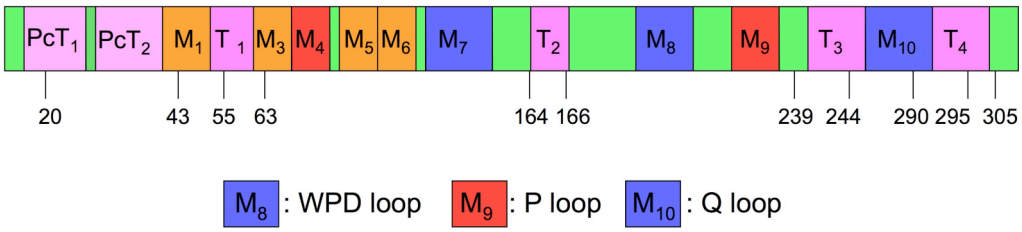

Figure 1.15. *Tb*PTP1 structure. Schematic diagram of *Tb*PTP1 highlighting the PTP motifs (M1-10) and the trypanosome-specific motifs (PcT1-2, T1-4). The ten conserved PTP motifs are shown (M1-M10) and coloured according to the degree of conservation among PTPs (red: high, orange: medium, blue: low); the trypanosome-specific motifs are coloured in pink (PcT1, PcT1, T1-T4). Numbers correspond to amino acid sequence of *Tb*PTP1 (Szoor *et al.*, 2006).

Beyond the pre-catalytic region, the *Tb*PTP1 catalytic domain is more homologous to the human protein tyrosine phosphatase 1B (PTP1B)(Tonks *et al.*, 1988) and to another human PTP upregulated in quiescent B cells (PTPROt) (Aguiar *et al.*, 1999), with 24% and 23% of identity, respectively (Szoor *et al.*, 2006).

Functionally, recombinant *Tb*PTP1 was shown to be active *in vitro*, with its activity being tyrosine-specific and sensitive to the general PTP inhibitor,

sodium vanadate, oxidation and pH changes (Szoor *et al.*, 2006). Importantly, *Tb*PTP1 inactivation by RNAi or by a PTP1B-specific pharmacological inhibitor resulted in the spontaneous transition from bloodstream to procyclic forms, showing the same kinetics as cis-aconitate treatment. Overall the data suggested that *Tb*PTP1 is kept active in bloodstream forms cells and upon induction of differentiation to procyclic forms the enzyme is inhibited thereby activating downstream signalling events (Szoor *et al.*, 2006).
More recently a *Tb*PTP1 target has been identified, as a glycosomal serine/threonine phosphatase (*Tb*PTP1-interacting protein, 39 kDa or *Tb*PIP39), which was shown to be dephosphorylated by *Tb*PTP1 (Szoor *et al.*, 2010). *Tb*PIP39 was also shown to be responsible for the downstream events leading to procyclic form transition, as demonstrated by the fact that its down-regulation by RNAi resulted in inhibition of differentiation. In addition, *Tb*PIP39 glycosomal localization was found to be essential for its role in the parasite life cycle, since the RNAi phenotype was not rescued by the ectopic expresssion of the protein lacking the C-terminal sequence responsible for its localization (Szoor *et al.*, 2010).
Very recently, a second *Tb*PTP1 substrate has been identified in procyclic form cells, as the RNA-binding protein Nopp44/46 (Chou *et al.*, 2010). Nopp44/46 is a nucleolar protein important for ribosome biogenesis (Jensen et al., 2005), whose tyrosine phosphorylation was shown to increase upon transition from slender to procyclic forms (Parsons M, 1991). However, the effect of the interaction between *Tb*PTP1 and Nopp44/46 is not clear, nor it is known whether this interaction is part of the events involved in differentiation to procyclic forms.

1.18. Human PTP1B

Human protein tyrosine phosphatase 1B (PTP1B), was one of the first tyrosine-specific phosphatases identified and named after its elution properties during purification from human placenta (Tonks *et al.*, 1988). PTP1B is a ubiquitously expressed protein, composed of 435 aa, which plays a role in several pathways: from cellular transformation, where it antagonizes the oncogenic kinases neu (Brown-Shimer *et al.*, 1992) and vSrc (Woodford-Thomas *et al.*, 1992), to cell adhesion (Liu *et al.*, 1998) and insulin signalling (Tonks *et al.*, 1990). Therefore, PTP1B is involved in a variety of pathologies, like leukemia or other cancers (LaMontagne *et al.*, 1998b; Lessard *et al.*, 2010), diabetes and obesity (Elchebly *et al.*, 1999). It was particularly this last observation that attracted the attention of pharmaceutical companies, as diabetes and obesity represent one of the main health challenges of the 21st century, with the WHO estimating that more than 700 million people will be obese by 2015 (WHO, 2006b). As a consequence, numerous PTP1B inhibitors have been developed, with the aim of finding a potent selective and highly specific compound (Zhang *et al.*, 2007).

1.18.1 The PTP1B inhibitor BZ3

Among the different PTP1B inhibitors developed, a group of benzbromarone derivatives (Wrobel *et al.*, 1999) were found to be particularly interesting, as they were bound to an allosteric site of the enzyme (Wiesmann *et al.*, 2004). A compound of this family, 3-(3,5-Di-bromo-4-hydroxy-benzoyl)-2-ethyl-benzofuran-6-sulfonicacid-(4-(thiazol-2-ylsulfamyl)-phenyl)-amide), was then successfully commercialized as PTP1B inhibitor (Calbiochem®), which will be referred to as BZ3, in the course of this work (Szoor *et al.*, 2006).
The crystallographic analysis of PTP1B bound to this compound showed that its binding to the allosteric site caused the phosphatase to adopt the "open" conformation. In the "open" conformation the catalytic site is accessible to the substrate, whereas in the "closed" conformation the catalytic WPD loop closes over the binding pocket to facilitate catalysis (Barford D *et al.*, 1994).

Importantly, BZ3 showed selectivity for PTP1B *in vivo*, as judged by the stimulation of insulin phosphorylation (Wiesmann *et al.*, 2004). In agreement with these data, BZ3 inhibited *Tb*PTP1 *in vitro* and *in vivo* (Szoor et al., 2006).

1.19. Aims

As evident from its complex life cycle, *Trypanosoma brucei* undergoes developmentally regulated morphological and biochemical changes in response to environmental cues, which are mediated through signalling pathways. However, our understanding of trypanosome signal transduction during differentiation is limited.

Protein Tyrosine Phosphatase 1 (*Tb*PTP1) is the one of the few factors identified to be responsible for differentiation from stumpy to procyclic form parasite (Szoor *et al.*, 2006), acting through the novel substrate *Tb*PIP39 (Szoor *et al.*, 2010). However the stimulus and the mechanism responsible for the physiological inhibition of *Tb*PTP1 upon initiation of differentiation is not known and only two *Tb*PTP1 substrates have been identified (Chou *et al.*, 2010; Szoor *et al.*, 2010).

The aims of this work were the validation of *Tb*PTP1-*Tb*PIP39 interaction, and the identification of novel substrates of *Tb*PTP1. In addition, it was interesting to characterize the stimulus and the mechanism responsible for *Tb*PTP1 inactivation upon differentiation to procyclic forms, in order to gain a deeper understanding of the role of the *Tb*PTP1-*Tb*PIP39 signalling pathway during this life cycle transition. Finally a part of this project investigated piggyback strategies targeting *Tb*PTP1, as a means to decrease the number of the fly-transmissible stumpy form cells in the bloodstream, thereby controlling parasite transmission.

Chapter 2

Materials and Methods

2.1. Trypanosomes cultures

2.1.1 Cell lines

Most of the cell lines used in this project were derived from *Trypanosoma brucei brucei* Lister 427 (427), which probably originated from the Shinyanga IIII strain, isolated in 1965 from cattle in Tanganiyka (http://tryps.rockefeller.edu).

For RNAi experiments "Single marker cells 16" or SMC 16 were used, which are cells originated from 427 cells and expressing the bacteriophage T7 RNA polymerase and tetracycline repressor protein (Wirtz *et al.*, 1999). These cells need to be grown in 2.5 μg/ml of G418 (Gentamicin) to retain the T7 RNA polymerase gene. The *Tb*10.389.0310 and *Tb*11.02.2090 SMC16 RNAi cell lines were grown in 2.5 μg/ml of G418 and 2.5 μg/ml phleomycin (to select for cells containing the p2T7 RNAi plasmid) and the induction of the RNAi was performed by addition of 1 μg/ml of tetracycline.

For stumpy form cells the pleomorphic *Trypanosoma brucei brucei* Antat 1.1, originally isolated in Uganda in 1966 (http://tryps.rockefeller.edu), were inoculated in mice, which were then sacrificed 5-6 days after infection.

The procyclic form cells, used mainly as positive control for EP protein expression, were the procyclic PTT, which express the T7 RNA polymerase and the tetracycline repressor protein.

2.1.2 Cell Media

For bloodstream form cells HMI-9 media (Sigma), supplemented with 20 % FCS and 1 mg/ml of penicillin/streptomycin (GIBCO), was used; cells were grown at 37°C with 5% CO_2 (Hirumi *et al.*, 1989) using vented flasks. Procylic form parasites were grown at 27° C in SDM-79 supplemented with 10 % FCS, 1 mg/ml penicillin/streptomycin and 7.5 mg/ml of sterile bovine haemin (Cross *et al.*, 1973).

Bloodstream or procyclic form cells were counted using a Z2™ Coulter Counter® Analyzer (Beckam Coulter) set to sample size range of 2.5-7 μm.

When needed, cells were frozen by centrifuging 10 ml of logarithmic-phase culture at 2,000 rpm for 10 min; then the pellet was resuspended in 0.5-1 ml

of media and an equal amount of freezing mix (HMI-9/14% glycerol for bloodstream form or SDM-79/14 % glycerol for procyclic forms) was added drop wise in order to slowly equilibrate the cells to the glycerol. Cryovials were then gently mixed and left standing for 2 minutes before being placed at -80° C, in a polystyrene box, to allow slow freezing; after about 2 days the vials were transferred to a normal freezing box or to liquid nitrogen (-196°C).

2.1.3 Purification of trypanosomes from blood

When stumpy form cells were needed, infected mice were sacrificed by heart puncture, (performed by Deborah Hall or Keith Matthews) and the blood was loaded on DEAE-cellulose (DE-52) pre-settled in a glass column, in order to absorb the particulate component of the blood (Lanham *et al.*, 1970); trypanosomes were eluted by addition of PSG buffer (3 mM NaH_2PO_4-$2H_2O$, 43.6 mM NaCl, 57 mM Na_2HPO_4 and 83 mM D-glucose, pH 7.8) on the top of the column. Cells were usually allow to recover a few hours in HMI-9 at 37°C, before starting any experiment.

2.1.4 Inducing differentiation of stumpy to procyclic forms

Stumpy form cells ($2x10^6$/ml) were induced to differentiate by addition of 6 mM cis-aconitate (Sigma 43412 , 0.6 M stock, in PBS, pH 7.6) to the HMI-9, then transferring the flasks into the 27° C incubator and substituting the vented lids with unvented ones. Similarly, 10 mM citrate was sometimes used to induce transformation to procyclic forms.

For BZ3-induced differentiation, the compound (PTP1B inhibitor, 3-(3,5-Dibromo-4-hydroxy-benzoyl)-2-ethyl-benzofuran-6-sulfonicacid-(4-(thiazol-2-ylsulfamyl)-phenyl)-amide) was purchased from Calbiochem (cat# 539741); a stock solution of 67 mM in DMSO was used and aliquoted at -80°C; freshly thawed aliquots were always used, to a final concentration of 150 μM in HMI-9.

When pronase was used to trigger differentiation (Hunt *et al.*, 1994), 4 units of pronase (from *Streptomyces griseus*, Biochemika 81748, 5 unit/mg) were

added to 1 ml of cells (approximately $2x10^7$) in PSG buffer; cells were left 10 minutes at 25°C then spun and washed twice with PSG before being resuspended in HMI-9.
Cold shock of stumpy form cells was also used to induce differentiation (Engstler *et al.*, 2004), by placing the un-vented flasks containing cells in an incubator set at 20° C overnight.

2.1.5 Transfection of bloodstream form cells

The Amaxa nucleofector® device (Lonza) was used for transfection of bloodstream forms *Trypanosoma b. b.* (Burkard *et al.*, 2007). Plasmid DNA for transfection was digested overnight and purified using a Nucleospin column (Macherey-Nagel); it was then precipitated by addition of 70% ethanol and resuspended in 5 μl of TE buffer (10 mM Tris-HCl, pH 8.0, 1 mM EDTA). Approximately $4x10^7$ cells were centrifuged at 2,000 rpm for 10 min and 100 μl of Amaxa T cell buffer or Ingenio™ electroporator solution (Mirus) was added to the pellet, which was resuspended and transferred into the provided cuvettes, together with the linearized DNA plasmid. The electroporation was perfomed placing the cuvette in the Amaxa nucleofector® device and selecting progamme X001. Immediately after that, the cells were transferred to a 10 ml flask containing HMI-9 and left to recover in the 37°C incubator overnight. The next day the cells were serially diluted 1:10 in a 24-well plate in HMI-9 supplemented with the antibiotic of choice, to select for cell containing the transfected plasmid. The selection was carried out over 10-12 days.

2.2. DNA manipulation

2.2.1 Polymerase chain reaction

For a standard polymerase chain reaction (PCR) a mixture was used containing the following: approximately 1 μg of template DNA, 0.1-1 μM of primers, 0.2 mM of deoxynucleotides, 1-4 mM of $MgCl_2$, 2 units of GoTaq®

DNA polymerase, autoclaved H_2O and 1X of the GoTaq® flexi buffer supplied (Promega M8305) to a final volume of 50 μl.
Reaction conditions were usually: 95°C for 4-6 min (initial denaturation step) for 1 cycle, then for 30 cycles at 94°C for 1 min (denaturation step) followed by the annealing step (1 min at 5°C lower than the T_m of the primers) and by 72°C for 2 min (elongation step, approximately 1 min per kb of DNA). At the end of the 30 cycles a final elongation step of 72°C for 2-3 min was added.
When primers containing restriction sites were designed, the chosen restriction site was added at the 5' end of the forward and reverse primer, usually including a 4 bp sequence at the 5' end to increase digestion efficiency. Primers were generally designed to be 18-30 bp long, with GC content between 40% and 60 %, containing G or C at the 3' end to allow stronger binding to the DNA template. The absence of self-complementarity and of palindromic sequences was checked by using the online server OligoCalc (http://www.basic.northwestern.edu/biotools/oligocalc.html).

2.2.2 Agarose gel electrophoresis

DNA was visualised in a 1% agarose gel in 1x TAE buffer (0.4 mM Tris-HCl, 0.1 mM EDTA, pH 7.7). Usually 100 ml of buffer was used for a small gel, with addition of 0.5 μg/ml of ethidium bromide or 5 μl of SafeView Nucleic Acid stain (NBS Biologicals). The gel was cast in a Fisher Brand DNA gel apparatus and run in TAE buffer at 120 Volts for approximately 20 min. DNA samples were added to a 1X DNA loading buffer (0.25% Bromophenol blue, 0.25 % Xylene cyanol FF and 15% Ficoll).

2.2.3 DNA purification

DNA purification from PCR reaction or from agarose gel was performed using a NucleoSpin Extract II kit (Machery-Nagel), according to manufacturer's instructions.

2.2.4 DNA digestion

DNA digestions were performed by incubating between 0.2 and 2 μg of DNA with 10 units of restriction enzyme, and 1X of the buffer required, in a final volume of 20 μl. The reactions were incubated at the suggested temperature for the enzyme of choice, for 2 hr. Restriction enzymes were purchased mainly from Promega, and New England Biolabs.

2.2.5 DNA ligation

Ligations were set up using a 5-10:1 insert:vector ratio with the corresponding quantities calculated using the formula ((ng vector x size insert in kb)/(size of vector in kb) x 5-10). Insert and vector, together with 10-20 units of T4 DNA ligase (Promega) were incubated overnight at 4°C in the buffer provided. Sometimes ligations were preceded by calf intestine alkaline phosphatase (CIAP, Sigma M182A) treatment of the linearized vector; CIAP causes the dephosphorylation of the 5' phosphate groups of the DNA, useful to prevent recircularization and religation of linerized DNA. For this purpose, the DNA was incubated with 0.05 units of CIAP in 1x CIAP buffer provided at 37°C for 30 minutes.

2.2.6 Bacteria transformation

Following ligation, the DNA was transformed by heat shock into competent *E. coli* XL-1 blue cells (Stratagene), for simple cloning; when transformation was needed for expression of recombinant protein the BL21-CodonPlus (DE3)-RIPL competent *E. coli* (Stratagene) were used, which are cells that contain extra copies of rare *E. coli argU, ileY, leuW, proL* tRNA genes to correct for codon bias and to improve expression.

For the transformation, 60 μl of bacteria per sample were gently thawed on ice and transferred to new 1.5 ml eppendorf tubes, where 10 μl of ligation were added. Bacteria containing the DNA to transform were kept on ice for 20 min and then heat shocked 90 seconds at 42°C. After that the tubes were left on ice for 2 min and 750 μl of LB broth (Luria Broth: 1% bactotryptone,

0.5% bacto-yeast extract, 1% NaCl, pH 7.0 (Gibco)) was added to allow the bacteria to recover. In addition, the tubes were placed in the 37°C shaking incubator for 1 hr. Finally, the bacteria were plated in plates containing LB agar (1.2% agar, 2.5 % LB) and ampicillin (100 μg/ml) or kanamycin (30 μg/ml), according to the resistance contained in the DNA plasmid used.

2.2.7 Mini-scale DNA preparation

For mini-scale DNA preparations one colony of bacteria was inoculated into 2 ml of LB broth containing the appropriate antibiotic (ampicillin (100 μg/ml) or kanamycin (30 μg/ml)), and left in the 37°C shaking incubator overnight. The next day, 1.5 ml of bacteria culture were harvested by centrifugation in an eppendorf tube. The pellet was resuspended in 100 μl of solution I (50 mM glucose, 25 mM Tris-HCl pH 8.0 and 10 mM EDTA pH 8.0); 200 μl of solution II (0.2 N NaOH and 1% SDS) were then added and the tube mixed by inversion several times. To allow separation of plasmid DNA from the rest, 150 μl of solution III (3 M KAc and 40% of Glacial Acetic acid) were added, the tube was kept on ice for 5 min and then centrifuged 10 min at 13,000 rpm. The resulting white precipitate consisted of chromosomal DNA, high-molecular-weight RNA and potassium/SDS/protein/cell wall complexes, whereas the supernatant contained the plasmid DNA. The supernatant was then transferred to a new tube and the DNA was precipitated by addition of 0.6 volume of 100% ethanol (900 μl for 450 μl of supernatant) and by incubation at -80°C for at least 20 minutes. The tube was centrifuged 15 min at 13,000 rpm, the resulting DNA pellet was washed once with 70% ethanol, centrifuged again for 5 min and allowed to dry on the bench. Finally the DNA pellet was resuspended into 40 μl of H_2O or of TE buffer (10 mM Tris-HCl pH 8.0, 1 mM EDTA).

2.2.8 Large-scale DNA preparation

Large-scale DNA preparations were performed using the QIAGEN Plasmid Purification Kit for Maxi, which requires the 1/100 dilution of a starter bacteria culture in 200 ml of LB supplemented with the appropriate

antibiotic. After an overnight growth in the 37°C shaking incubator, the bacteria were harvested by centrifugation 15 min at 6,000 g and the pellet was resuspended in 10 ml of ice-cold buffer P1 (50 mM Tris-HCl, pH 8.0, 10 mM EDTA and 100 μg/ml RNase A). Bacteria were then lysed by addition of buffer P2 (200 mM NaOH and 1% SDS) and cell debris, genomic DNA and proteins were precipitated by addition of 10 ml of buffer P3 (3 M KAc, pH 5.5). After 20 minutes on ice, the tube was centrifuged at 20,000 g for 30 minutes at 4°C and the resulting supernatant, containing plasmid DNA, was transferred in a new tube and centrifuged again at 20,000 g for 15 minutes, at 4°C. The plasmid DNA was then purified through the application of the supernatant to a QIAGEN column, which contains an anion-exchange resin. After three washes with buffer QC (1 M NaCl, 50 mM MOPS pH 7.0 and 15% isopropanol) the DNA was eluted by addition of 15 ml of elution buffer (1.25 M NaCl, 50 mM Tris-HCl pH 8.5 and 15% isopropanol). The DNA was then precipitated using 0.7 volumes of isopropanol, followed by a 30 minutes spin at 15,000 g at 4°C. The resulting pellet was washed with 70 % ethanol, centrifuged again 10 minutes at 15,000 g and air-dried on the bench. Finally the pellet was resuspended in 600 μl of TE buffer and the DNA concentration was quantitated using an Eppendorf Biophotometer and single use Eppendorf UVettes®.

2.3. Northern blot analysis

2.3.1 Probe preparation

The Northern blot probe was generated by PCR of the chosen sequence inserted in pGEM plasmid. The PCR was performed as previously described (see paragraph 2.2.1), using the M13 forward and reverse primers, and annealing temperature of 50°C. After visualization of the product on a DNA gel and its purification, the riboprobe reaction was carried out using the DIG RNA labeling kit (SP6/T7) (Roche). In the reaction 1 μg of DNA was incubated with 2 μl of 10 x NTP labeling mixture (10 mM ATP, 10 mM CTP, 10 mM GTP, 6.5 mM UTP, 3.5 mM DIG-11-UTP, pH 7.5), 5 mM DTT, 20 units of Protector RNase inhibitor to prevent RNA degradation during the

labeling reaction, 1x transcription buffer and 40 units of T7 RNA polymerase, which synthesizes RNA from a DNA template. The reaction was incubated at 37°C for 2 hr, after which the DNA template was degraded by addition of 20 units of DNase I, RNAase-free, for further 15 min at 37°C. In order to stop the reaction 2 μl of 200 mM EDTA (ethylene-diamino-tetraacetic acid, pH 8.0) were added. Finally, the probe was precipitated by incubation in 100 mM LiCl and 3 volumes of cold 100% ethanol at -70°C for 30 minutes. The tube was centrifuged 15 minutes at 12,000 g, the resulting pellet was washed once with 70% ethanol, air-dried and resuspended in 50 μl of water supplemented with 20 units of RNase inhibitor.

2.3.2 RNA sample and gel preparation

The RNA was extracted from 10-50 ml of bloodstream form cells using the RNeasy Mini kit (Qiagen), according to manifacturer's instructions. Cells were harvested by centrifugation and the resulting pellet was resuspended in 600 μl of lysis RLT buffer containing guanidine thiocyanate, which immediately inactivates RNases to ensure purification of intact RNA. One volume of 70% ethanol was then added to provide appropriate binding conditions of the RNA in the sample to the RNeasy spin column. The column is centrifuged for 15 seconds at 8,000 g to allow the binding, washed once with buffer containing ethanol and then eluted in 30-50 μl of RNase-free water.

The RNA agarose gel was prepared by heating 1.2 g of agarose in 80 ml of distilled water and by addition of 10 ml of 10 x MOPS (40 mM 4-morpholinepropanesulfonic acid, 10 mM sodium acetate, pH 7.0 and 1 mM EDTA). After allowing the solution to cool down, 3 ml of 37% formaldehyde were added, under the chemical hood, and the gel was poured into a Fisher brand DNA gel apparatus. The RNA samples were prepared firstly by the spectrophotometric (absorbance at 260 nm) quantification of the RNA using a NanoDrop device (Thermo Scientific). After that, 2 μg of RNA were transferred to a new 1.5 ml eppendorf tube, where 9 μl of 99.5% formamide, 3 μl of 37% formaldehyde, 2 μl of 10x MOPS and 2 μl of RNA loading buffer (6

% formaldehyde, 30 % formamide, 1x MOPS, 10% glycerol and 0.01% bromophenol blue) were added. The samples were heated at 60°C for 5 minutes and then loaded on the gel, which was run 90 minutes at 150 Volts. In order to visualize the RNA, the gel was stained by incubation in 1x MOPS with 1 μg/ml of ethidium bromide for 15 minutes, followed by three 40-minutes washes in distilled water. The visualization and quantification of the RNA loaded was performed using the Syngene G:Box apparatus and the GeneSnap (for pictures acquisition) and GeneTools (for picture analysis) softwares.

2.3.3 Blotting the RNA gel

A capillary blotting system was used to transfer the RNA from the gel to a positively charged nylon membrane (Roche). In order to do so, a plastic tray, properly cleaned with soap, 70 % ethanol and washed with water, was filled with 10 x SSC (1.5 M NaCl, 0.15 M Tri Na Citrate) up to 2 cm. After that, the nylon membrane of appropriate size to cover the gel was cut, and wetted in 10 X SSC, together with a long piece of filter paper (Fisher brand) covering the tray. Similarly, two pieces of filter paper of the same size of the gel were also cut and wetted in 2 X SSC. Inside the tray, one lunchbox was placed as to create a raised platform; on top of the box, the long piece of filter paper was positioned so that its extremities touch the solution in the tray. On top of the filter paper, a layer of parafilm was placed to cover the whole tray, in order to avoid evaporation of the SSC solution. The parafilm was cut in the area above the lunch box, where the gel was placed facing down, followed by the two pieces of pre-wetted nylon membrane and by two pieces of filter paper of the same size of the gel. A layer of paper towels covering the whole tray was then added to allow absorption of the SSC solution from the tray towards the gel. Finally, on top of the paper towels a weight was placed, as to create pressure evenly over the tray. The whole capillary blotting system was left at room temperature overnight. The next morning, the system was disassembled and the RNA was cross-linked to the nylon membrane by UV light, by placing the membrane in a Uvitec machine set at 0.125 Joules, for a couple of minutes.

2.3.4 Northern blot hybridization and detection

Initially the membrane was blocked in hybridisation buffer (5x SSC, 50% formamide, 0.02% SDS and 2% blocking solution) 1 hour at 68°C. After that, the membrane was incubated with 2 μl of boiled probe in 7 ml of prewarmed hybridisation solution, overnight at 68°C, in a rotating tube. The next day the blot was washed twice with 70 ml of 2x SSC/0.1% SDS at 68°C and once with 0.5 x SSC/0.1% SDS for further 40 minutes at 68°C. The membrane was then briefly washed with wash buffer (100 mM maleic acid, 150 mM NaCl, pH 7.4 and 0.3 % Tween 20) before blocking it with maleic acid buffer (100 mM maleic acid, 150 mM NaCl, pH 7.4) supplemented with 1% DIG (Blocking Reagent, Roche) block for 1 hr at room temperature. Detection of the DIG-labeled probe was performed using anti-Digoxigenin-Alkaline Phosphatase Fab fragment antibody (1:25,000 Roche) in maleic acid buffer/ 1% DIG block for 30 minutes at room temperature, followed by 3 washes for 5 minutes with wash buffer. The membrane was then soaked in detection buffer (100 mM Tris-HCl pH 9.5, 100 mM NaCl), before addition of the chemiluminescence substrate CDP-Star (1:100, Roche) for 2 minutes. The enzymatic reaction of CDP-Star reagent with alkaline phosphatase produces a light signal which can be detected by film or chemiluminescent-compatible instruments, specifically the quantification was performed using the Syngene G:Box apparatus and the GeneSnap and GeneTools softwares.

2.4. Western blot analysis

2.4.1 Protein extraction

Cells were harvested by centrifugation at 2,000 g for 10 min, washed once with PBS (137 mM NaCl, 3 mM KCl, 16 mM Na_2HPO_4, 3 mM KH_2PO_4, pH 7.6), centrifuged again and the resulting pellet was either frozen in liquid nitrogen or resuspended directly in Laemmli sample buffer (62.5 mM Tris-HCl, pH6.8, 2% SDS, 10% glycerol and traces of bromophenol blue). Alternatively, the cell pellet stored at -80°C was resuspended in cell lysis buffer (such as His-purification lysis buffer, see paragraph 2.7.2 or *Tb*PTP1

activity buffer, see paragraph 6.7.3) and subjected to 2 or 3 cycles of freezing-thawing to lyse the cells thoroughly.
Protein quantification was performed by the Bradford method, using the Bradford Reagent (Sigma), specifically 20 μl of sample was mixed with 600 μl of reagent in a disposable uvette (Eppendorf), for 10 minutes and absorption at 595 nm was measured using a spectrophotometer; the quantity corresponding to the absorbance measured was determined using a standard BSA (bovine serum albumin) curve.

2.4.2 SDS-PAGE

Proteins were resolved in 12%/13% or 15% polyacrylamide gels by mixing 1.86 ml of running buffer (1.5M Tris-HCl, pH8.8, 0.4% SDS) with 3 ml/3.25 ml or 3.75 ml of acrylamide solution (30% w/v acrylamide/bisacrylamide ratio 37.5:1), respectively, and adding water to a final volume of 7.49 ml; polymerisation was started by addition of 50 μl of 10% APS (ammonium persulphate, to a final concentration of 0.06%) and 7.5 μl of TEMED (N',N', N, N'-Tetramethylethylene-diamine, to a final concentration of 0.001%). After letting the running gel set, the stacking gel was cast by mixing 375 μl of stacking buffer (0.5 M Tris-HCl pH 6.8, 0.4% SDS) with 625 μl of acrylamide solution to a final volume of 2.5 ml. Polymerisation was started by addition of 0.05% APS and 0.001% TEMED. Gels were prepared and run in a Bio-Rad PROTEAN II apparatus at 150 Volts in running buffer (25 mM Tris-HCl, pH 8.3, 192 mM Glycine, 0.1% SDS). Between 5 and 50 $x10^6$ cells were loaded per lane, according to the type of experiment.
When needed gels were stained with SimplyBlue™ Safestain (Invitrogen) for 1 hr and destained in water for a further hour.

2.4.3 Proteins transfer

For Western blot analysis the gels were blotted onto nitrocellulose (Whatman Schleicher and Schuell, PROTRAN, 0.45 μm pore size) or PVDF membrane (Immobilon-P, Millipore) using either a semi-dry or a wet blot system, the

latter was always used for the detection of tyrosine phosphorylated proteins, whereas the former was used with the other antibodies, such as anti-*Tb*PIP39 or anti p-*Tb*PIP39.

Before blotting, the PVDF membrane was activated by a brief incubation in methanol, as suggested by the manufacturer's instructions.

For the wet blot, the gel, the membrane, two pieces of filter paper of the size of the gel and the two fiber pads provided were assembled in a Mini Trans Blot apparatus (Biorad). The gel sandwich was prepared by placing the provided cassette on a small tray containing blotting buffer (2.5 mM Tris, 192 mM Glycine and 20% methanol) with the black side facing down. On top of the black side of the cassette the other components were assembled in the following order: one of the fiber pads, one piece of filter paper, the gel, the membrane, the other piece of filter paper and the other fiber pad. The cassette was then closed and placed in the apparatus, with the black side facing the black side of the blotting device. Finally, a cooling unit containing ice was added and the apparatus was set running at 30 Volts overnight.

For the semi-dry transfer, the membranes and gels were soaked in transfer buffer (2.5 mM Tris, 15 mM Glycine, 0.02% SDS, 20% methanol), together with two sheets of extra thick filter paper; they were then assembled in the semidry blotter (Biorad, Trans-blot SD), placing one sheet of filter paper towards the bottom (towards the anode) then adding the membrane on top and the gel, followed by the second sheet of filter paper (towards the cathode). Air bubbles between each layer were then removed by gently rolling a pipette on the wet surface and the blotter was run at 15 Volts for 50 min.

To assess that the complete transfer had taken place, the membrane was stained with Ponceau Stain (0.4 % of Ponceau S and 3% tri-chloroacetic acid), for less than one minute, and destained with water.

2.4.4 Western blot detection and quantification

When analysing tyrosine phosphorylated proteins, the PVDF membrane was blocked by incubation for 1 hr at 37°C, according to the manufacturer's instructions. The p-Tyr antibody used was the 4G10 clone (Millipore) at

1:1,000 dilution in TBS-BSA (2%) for 1 hr, followed by 20 min wash in TBS-Tween (0.05%). The secondary antibody used was anti-mouse-HRP (Sigma) at 1:5,000 dilution, for 1 hr, followed by a 20 min wash with TBS-Tween (0.05%). Detection was carried out using the ECL Western blotting system (Amersham Biosciences) and by exposing the membrane on X-ray films (Kodak). Quantification was performed using the Syngene G:Box apparatus and the GeneSnap and GeneTools software.

For western blot against tubulin, the Odessey® infrared imaging system (LICOR Biosciences) was used, therefore all the incubation were performed in 50% Odyssey® block in PBS and the secondary antibody used was the anti-mouse green (LICOR Biosciences product n°: 926-32210, in 1:7,000 dilution).

For the analysis of tyrosine-phosphorylated proteins in stumpy cell extract, approximately 6 µg of proteins were loaded in the gel, corresponding to about 4 x 10^7 cells/100 µl. When phenyl phosphate (Sigma) was used, 200 mM of the compound were incubated 5-10 min with the primary antibody before proceeding with the Western blot.

When using the anti p-PIP39 antibody, the dry blot was used, and the blocking and the incubation steps were performed in 2% BSA. When using the anti-PIP39 or other antibodies, the dry blot was also used but 2% BSA was replaced by 5% milk, as blocking reagent, and TBS was replaced by PBS for incubations and washes.

The membrane was stripped by incubation in 0.2 N NaOH/ 1% SDS for 30-60 minutes followed by extensive washes in water. In order to check the complete disappearance of the signal, the membrane was treated with ECL reagents and exposed on the Syngene G:Box.

2.4.5 Primary antibody dilution

As mentioned in the previous paragraph, the anti phosphorylated tyrosine antibody (4G10, Upstate) was used at 1:1,000 dilution; similarly, the anti-*Tb*PIP39 and the anti His-tag antibody were used at 1:1,000 dilution, whereas

the anti p-PIP39 antibody (against Y278 of *Tb*PIP39) was used at 1:750 or 1:500 dilution; the anti BB2 antibody (anti TY tag: EVHTNQDPLD peptide) was used at 1:5 dilution.

2.5. Immunoprecipitation

Bloodstream form 427 overexpressing wild type *Tb*PTP1 were treated with tetracycline for 24 hr and then induced to differentiate with 6 mM cis-aconitate for 48 hr. After that, approximately $2x10^8$ cells were harvested by centrifugation and the resulting pellet was frozen in liquid nitrogen and stored at -80°C. The day of the immunoprecipitation the pellet was resuspended in 500 μl of IP lysis buffer (10 mM Tirs-HCl, pH 8.0, 0.05 mM EDTA and 150 mM NaCl) supplemented with one tablet of protease inhibitor cocktail (Roche). Cell lysis was completed by subjecting the sample to sonication, in a water bath for 5 minutes. After that, the cell extract was centrifuged at 13,000 rpm at 4°C for 10 minutes and the supernatant was transferred to a new 1.5 ml eppendorf tube containing 70 μl of Protein G agarose beads (Sigma). Following a 30-min incubation on ice, to allow the aspecific binding of proteins to the resin, the tube was centrifuged 3 min at 4°C to separate the agarose beads from the cell extract, which was transferred to two new tubes. The BB2 antibody, which recognizes the TY-tag (EVHTNQDPLD peptide) of *Tb*PTP1, was added to both tubes containing the cell extract using a 1:10 dilution. In one of the two tubes, the BB2 antibody was added together with the corresponding BB2 peptide, as negative control for the immune-precipitation (antibody and peptide were pre-incubated together for 30-40 min before addition of cell extract). The two tubes were left rotating at 4°C for 1 hr, and then 100 μl/100 μl of Protein G agarose beads (pre-washed in IP lysis buffer 2-3 times) were added to the cell extracts in order to precipitate the antibody. For this aim, the tubes were incubated for a further hour, rotating at 4°C. Finally, the agarose beads were washed 6 times with IP lysis buffer and the immunoprecipitated proteins were eluted from the agarose beads by addition of 30 μl SDS sample buffer.

2.6. Cell extract dephosphorylation

Stumpy cells from a mouse infection at 1 x 10^7/ml in HMI-9 were harvested and lysed in 100 µl of pNPP buffer plus protease inhibitor (Roche). Cell extracts were quantified using the Bradford method (see paragraph 2.4.1). A total of 32 µg of cell extract was used and incubated with 5 µg of recombinant *Tb*PTP1 for each reaction. The dephosphorylation reaction was allowed to proceed for 1 hour at 37°C.

2.7. Recombinant *Tb*PTP1

2.7.1 Creation of double mutants *Tb*PTP1 by site-directed mutagenesis

To produce the double mutants D199A/Q275A and D199A/C229S *Tb*PTP1, the single mutant D199A and C229S were used as template and the additional mutation was inserted using the following primers: FW 5′- GCG ATT CGG TAT GGT TGC ACG GTT AGA GCA GTA TG- 5′ and Rev 5′- CAT ACT GCT CTA ACC GTG CAA CCA TAC CGA ATC GC-3′for Q275A and FW 5′- C GTC GGT TGG CCC GCT CAC GGT GTT CCA G-3′ and Rev 5′- C TGG AAC ACC GTG AGC GGG CCA ACC GAC G-3′ for C229S (underlined bases indicate the inserted mutations). The in situ mutagenesis was performed following the manufacturer's instructions (QuikChange XL Site-Directed mutagenesis kit, Stratagene).

2.7.2 Expression and purification of the recombinant proteins

The *E. coli* XL1 strain transformed with the appropriate expression plasmid were grown in 50 ml of LB plus kanamycin 30 µg/ml at 37°C, shaking overnight. The bacteria were then diluted 1:20 in fresh LB plus antibiotic and grown 2 hr at 37°C. The O.D. of the bacteria at 600 nm was checked every hour and 0.4 mM IPTG (isopropyl-β-D-thio-galactose) was added when the O.D. was between 0.6-0.8. The cells were then grown at 30°C for further 4 hours. Cells were harvested by centrifugation, 20 min at 4,000 rpm and the

pellet resuspended in 5 ml of PBS plus 2-3 ml of His lysis buffer (20 mM Tris-HCl, pH 7.5-8.0, 250 mM NaCl, 1% Trition X-100, 1 mM β mercapthoethanol and 5 mM imidazole). Lysis was performed by sonicating the samples on ice 4 times for 30 seconds and debris were removed by centrifugation 20 min, 10,000 rpm at 4°C. The supernatant was incubated with 100-200 μl of NiNTA agarose beads (QIAGEN) 1 hr at 4°C, on a rotating wheel, and washed extensively with His lysis buffer. For protein elution, the beads were incubated 30 min with 1.5 ml of Wash 1 (20 mM Tris-HCl, pH 8.0, 250 mM NaCl and 5 mM imidazole), spun, the supernantant discarded and incubated further 30 min with 1.5 ml of Wash 2 (20 mM Tris-HCl, pH 8.0, 250 mM NaCl and 20 mM imidazole). Elution was performed in two steps: by addition of 200 μl of Elution 1 (20 mM Tris-HCl, pH 8.0, 250 mM NaCl and 250 mM imidazole) for 10 min at 4°C, and by addition of 200 μl of Elution 2 (20 mM Tris-HCl, pH 8.0, 250 mM NaCl, 500 mM imidazole and 1mM β mercapthoethanol) for 10 min at 4°C.

2.7.3 Tyrosine phosphatase activity assay

Phosphatase activity was assayed by measuring the ability of the phosphatase to catalyze the hydrolysis of *p*-nitrophenylphosphate (pNPP, Sigma N-2765), to p-nitrophenol, a chromogenic product with absorbance at 405 nm. Reaction mixtures (50 μl) contained 2–5 μg of purified *Tb*PTP1 with 20 mM final concentration of pNPP in 50 mM Tris, 50 mM Bis-Tris and 100 mM NaAc, pH 5.5. Reactions were incubated at 37°C for 15–30 min and quenched by addition of 100 μl of 0.2 M NaOH. The absorbance of the samples was measured at 405 nm in a microplate reader (ELx808 Absorbance Microplate Reader, BioTek).

2.7.4 Enzyme kinetics assay

*Tb*PTP1 maximal velocity (V_{max}) and K_M were determined by monitoring the hydrolysis of serial dilutions of the synthetic substrate p-nitrophenyl phosphate (pNPP) in presence of a constant quantity of enzyme (0.4 μg per

reaction); enzyme and pNPP were incubated in pNPP buffer (50 mM Tris, 50 mM Bis-Tris, 100 mM NaAc, pH 5.5) supplemented with 2 mM DTT in a final volume of 80 μl per reaction; the reactions were carried out in triplicate in 96-well plates and always included a blank control lacking the enzyme. After 15 min at 37°C, 0.1 ml of 2M NaOH was added, in order to detect the amount of hydrolysed substrate (pNP), which was then quantified by measuring the absorbance of the samples at 405 nm using a microplate reader (ELx808 Absorbance Microplate Reader, BioTek).

The velocity of pNPP hydrolysis was calculated dividing the average of O.D. measured minus the blank, by 18.8 x1x15, and multiplying the result by 1,000 to obtain millimoles released per minute (according to the Beer's law: $A=\varepsilon xcxI$, where A is the absorbance measured, ε is the extinction coefficient of p-nitrophenolate: 18.8 $mM^{-1}cm^{-1}$ (Montalibet *et al.*, 2005), c is the molar concentration of the substrate and I is the length through which the light passes (usually 1 cm) (Berg *et al.*, 2002) in order to convert experimental units (i.e. absorbance) into molecules of product formed (c) over 15 min, the above equation is used, thus $c= A/(18.8\ mM^{-1}cm^{-1} \text{ x1 cmx15 min})$. The velocity of hydrolysis obtained was plotted on the y-axis against the molar concentration of substrate on the x-axis and the graph was analysed with GraphPad Prism software using the Michaelis-Menten equation ($Y= (V_{max}xX)/(K_M+X)$, where Y is the enzyme velocity and X is the substrate concentration) in order to derive the V_{max} and K_M of the enzyme.

2.7.5 Enzyme inhibition assay

For the determination of the IC_{50} against *Tb*PTP1 (the amount of inhibitor required for 50% inhibition of enzyme activity) 0.3-0.4 μg of recombinant *Tb*PTP1 was incubated in the presence of 2 mM DTT in pNPP activity buffer (50 mM Tris, 50 mM Bis-Tris, 100 mM NaAc, pH 5.5) to a final volume of 80 μl per reaction, in a 96-well plate; the inhibitor to be tested was subsequently added to a final concentration of 200 μM, which was then serially diluted 1:2 to obtain ten different concentrations ranging from 200 μM to 0 μM. In order to start the reaction the synthetic substrate p-nitrophenyl phosphate (pNPP)

was added to a final concentration of 0.175 mM (importantly lower than the K_M determined for *Tb*PTP1 alone, see previous paragraph), the reactions were carried out in triplicate in a 96-well plate and always included a blank lacking the enzyme. Absorbance was measured after addition of 0.1 ml of 2M NaOH at 405 nm using a microplate reader (ELx808 Absorbance Microplate Reader, BioTek). The absorbance of the blank was subtracted from the average absorbance of the triplicate samples and the percentage of hydrolysis over the control was calculated dividing the obtained O.D. of the enzyme in presence of inhibitor by the O.D. of the enzyme without inhibitor, multiplied by 100; the percentage of hydrolysis over the control was then plotted on the y-axis vs. the logarithmic of the molar concentration of the inhibitor tested. The dose-response curve was drawn using GraphPad Prism software, which calculates the corresponding IC_{50} (using the sigmoidal dose-response equation: Y= Bottom+ (Top-Bottom)/(1+10 $^{LogIC50-X}$)), only data with R^2>0.9 was considered. When high 95% confidence intervals (95% CI) were obtained, the data were also fitted to a dose-response equation with fixed Top (=100) and Bottom (=0).

For inhibition assays against human PTP1B, 40 ng of recombinant protein (Sigma, P6244-50UG) was used per reaction and incubated with 10 μM of DiFMUP substrate (6,8-difluoro-4-methylumbelliferyl phosphate, Invitrogen D6567, ε= 17 mM^{-1}) in PTP1B buffer (25 mM Hepes pH 7.2, 50 mM NaCl, 2.5 mM EDTA and BSA 0.01 mg/ml). PTP1B was first incubated with the inhibitor tested for 30 min at 37°C, then the substrate DiFMUP was added for 10 min at 37°C. Changes in fluorescence were read at exc. 360 nm and em. 460 nm, using the Flx800 Plate Reader (BioTek). Data was graphed as for *Tb*PTP1.

2.7.6 Enzyme competition assay

For testing the nature of the inhibitor (competitive, non-competitive and mixed inhibitors) competition assays were carried out, in which a constant concentration of enzyme and inhibitor was tested in the presence of different concentrations of substrate (pNPP). *Tb*PTP1 was used, as previously done, at 0.3-0.4 μg per reaction, in the same buffer and 96-well plate format used for

enzyme kinetics and inhibition assays; the inhibitor to be tested was used at two or three different concentrations lower and higher than IC_{50} and added to the mix of enzyme and buffer. To start the reaction 40 µl of substrate was added to a final concentration of 33.3 mM for the first row of triplicate samples and then diluted 1:2 in the subsequent wells. The absorbance obtained was converted into velocity of hydrolysis, as done for the enzyme kinetics assay, and plotted against the linear molar concentration of substrate. The V_{max} and K_M were calculated by GraphPad Prism using the Michaelis-Menten equation ($Y= (V_{max}x\ X)/(K_M+X)$, where Y is the enzyme velocity and X is the substrate concentration); the V_{max} and K_M of the enzyme in presence of the inhibitor was compared with the ones obtained with enzyme and substrate alone.

2.7.7 Compounds preparation

All the DDP inhibitors tested were dissolved in DMSO (dimethyl sulfoxide) at 25 mM stock concentration of which aliquots were kept at -20°C in dark 0.2 ml eppendorf tubes. Similarly, Oleanolic acid (Sigma O5504) was dissolved to have a 20 mM stock solution, of which aliquots were kept at -20°C.

Sodium vanadate (Sigma) was activated by adjusting the pH of a 200 mM solution to pH 10 with 1 M NaOH or HCl (Gordon, 1991); the solution was then boiled until it turned colorless, cooled and adjusted to pH 10 again, followed by other cycles of boiling and setting the pH until the solution remained colorless with a stable pH of 10.

The PTP1B inhibitor 3-(3,5-Di-bromo-4-hydroxy-benzoyl)-2-ethyl-benzofuran-6-sulfonicacid-(4-(thiazol-2-ylsulfamyl)-phenyl)-amide), (Calbiochem®, product number 539741) was dissolved in DMSO to give a 67 mM stock solution.

2.8. Cell extract selection using recombinant *Tb*PTP1

Approximately $1.4x10^9$ stumpy form cells were treated with 150 µM BZ3 for 1.5 hr in HMI-9. They were then harvested by centrifugation, washed once in

PSG, and frozen in liquid nitrogen. Cells were then lysed by addition of 500 μl of His-purification lysis buffer (20 mM Tris, 250 mM NaCl, 1% Triton-X, 1 mM β mercaptoethanol, 5 mM Imidazole, pH 7.5-8) supplemented with complete, EDTA-free protease inhibitor cocktail (Roche). The extract was lysed by two cycles of freezing-thawing at -80°C, centrifugated for 20 min at 4°C 14,000 rpm and sonicated 3 min in a water bath. Quantification of cellular protein was performed by the Bradford method following the manufacturer's instructions.

A total of 15 mg of cell extract, in 800 μl of His-purification buffer, was first incubated with NiNTA agarose beads, 20 min at 4°C, in order to clear the cell extract from proteins that could aspecifically bind to the beads; then 3.8 mg and 11.6 mg of the cleared extract were incubated with 20 μl of beads alone or 40 μl of recombinant *Tb*PTP1, respectively. The reaction was allowed to proceed for 1.5 hr at 4°C on a slowly shaking platform. After 2-3 washes with PBS the proteins were eluted by addition of 40 μl of SDS sample buffer and boiled.

2.9. Mass spectrometry analysis

The Mass spectrometry analysis was performed by Richard Burchmore, at the Sir Henry Wellcome Proteomics Facility (University of Glasgow), using the electrospray ionization technique on a QSTAR Pulsar Hybrid LC/MS/MS System. The resulting spectra were then compared against the complete *T. brucei* proteome using the Matrix Science Mascot search engine. More details of the protocol used can be found in Szoor *et al.*, 2010.

2.10. Cellular ROS detection

For reactive oxygen species (ROS) detection using H_2DCF-DA (2', 7'-dichlorofluorescin diacetate, Sigma D6883) cells were stained with 50 μM H_2DCF-DA in HIM-9 for 20 min in the 37°C incubator then harvested by centrifugation 5-10 min at 2,000 rpm and washed once with PSG to remove excess dye. Cells were then resuspended in PSG and treated with cis-

aconitate/citrate/isocitrate or H_2O_2. Cells were then analysed by flow cytometry with the FITC channel using FACSCalibur (BD Biosciences) machine and the BD Cell Quest Pro software.
For quantification cells were analysed using a fluorimeter (Fluostar Galaxy, BMG Labtechnology and Fluostar Galaxy software) with excitation at 490 nm and emission at 520 nm and DCF (2', 7'-dichlorofluorescein, Sigma 410217) dilutions as standard. When the cell-permeable ROS-scavenger NAC (N-Acetyl-L-cysteine, Sigma A9165) was used, cells were grown in HMI-9 supplemented with NAC (250, 400 or 800 μM) for 1 hr prior the addition of the dye and treated again when the dye was added.

For ROS quantification using Ampliflu Red (Sigma 90101), cells were placed in HIM-9 containing 50 μM Ampliflu Red and 1unit/ml HRP before addition of cis-aconitate/citrate/isocitrate or H_2O_2. Fluorescence was measured in triplicate at excitation wavelength of 544 nm and emission at 590 nm in a black 96-well plate using Fluostar Galaxy, BMG Lab technology and Fluostar Galaxy software.

2.11. Cell proliferation assay using Alamar Blue®

Cells were grown in normal HMI-9, 20% FCS, in a 96-well plate with initial cell density of $1x10^5$/ml and were treated with serial dilution of the drug to be tested for 48 hr in the 37°C incubator; after that 10% v/v Alamar Blue® (Abd Serotec) was added (20 μl in 200 μl) for further 24 hr and absorbance of the samples was read at 540 and 595 nm, using ELx808 Absorbance Microplate Reader, BioTek and the Gen5 software. Cells were tested in triplicate and included a blank with the drug in HMI-9 without cells; the average absorbance of the triplicate samples minus the blank was calculated for both the wavelengths and the percentage difference in Alamar Blue® reduction of the cells treated with the drug versus untreated was calculated using the following formula, as suggested by the manufacturer: [A_{540}-(A_{595}xR_0) for test well)/(A_{540}-(A_{595}xR_0) for control well]x100 , where R_0 is the correction factor for different filters obtained from: [(A_{540}media+alamar)-

(A_{540}media)/(A_{595}media+alamar)-(A_{595}media)]. The percentage of Alamar Blue® reduction was then plotted on the y-axis against the logarithmic concentration of the drug tested using GraphPad Prism and the LD_{50} was calculated analyzing the data using the sigmoidal dose-response equation: Y= Bottom+ (Top-Bottom)/(1+10 $^{LogIC50-X}$)).

2.12. Flow cytometry for EP-procyclin surface expression

Approximately 2-4 x10^6 cells were centrifugated in FACS tube 5 min at 2,000 g , washed once with PBS and fixed in 200 µl PBS 2 % formaldehyde/ 0.05 % gluteraldehyde, overnight at 4°C. The next day the cells were first washed with PBS, then blocked in PBS 2% BSA for 30 min at 4°C; the primary antibody (anti EP-procyclin, 1:1,000) was then added in PBS 2% BSA for 30 min and secondary (anti mouse FITC, 1:1,000) was added for the same length of time after one wash with PBS. The samples were kept in PBS and analysed by flow cytometry using a FACSCalibur FACS machine (BD Biosciences). The percentage of EP-positive cells was counted by gating on the positive control (procyclic forms sample) and by excluding the negative control (undifferentiated cells).

2.13. Immunofluorescence

When needed the samples subjected to flow cytometry (see previous paragraph) were also used for immunofluorescence. After FACS analysis the same samples were briefly centrifuged, the pellet was resuspended in about 100 µl of PBS and spread over a glass slide (Menzel-Glaser slides 76 x 26 mm). After allowing the slides to air-dry, they were stained with 1 µg/ml of 4,6-diamidino-2-phenylindole (DAPI) for 2 minutes to highlight the nucleus and kinetoplast of the cells. Afterwards the slides were covered with a cover slip (Scientific Laboratories Supplies) mounted using 10% PDA (p-phenylenediamine) in MOWIOL (10% MOWIOL, 25% glycerol and 0.1 M Tri-HCl, pH 8.5). The slides were then analysed under a Zeiss Axioskop 2 plus Microscope.

2.14. Bioinformatics

*Tb*PTP1 3-D structure model was predicted using the online application Swiss-Pdb Viewer (Arnold *et al.*, 2006) (http://swissmodel.expasy.org/), selecting the "alignment mode" and as template PTP1B catalytic domain (PDB code: 1g7fA). The model (E value =$0.00e^{-1}$) was then visualized using Swiss-Pdb Viewer application.

2.15. Statistical analysis

Statistical analysis was performed using General Linear Model of the statistical software MINITAB (version 1.4). The cut off for significance used was $P<0.5$.

2.16. Plasmids used in this study

2.16.1 The pGEM®-T Easy plasmid

The pGEM®-T Easy plasmid (Promega) was used to clone PCR products. The vector is already linearized and contains 3′ thymidine overhangs that improve the efficiency of the ligation of PCR products by preventing recirculization of the plasmid.

2.16.2 The pET-28a and pET-30a plasmids

The pET-28a is a 5.3-kb plasmid (Novagen) containing an N-terminal His Tag® (a stretch of five His), a thrombin cleavage site and T7 Tag® coding sequence. It also contains the T7 promoter and terminator sequences and the kanamycin resistance gene. For the inducible expression of the tagged protein, the plasmid contains the *E. coli lac* operator and the *lacI* gene, coding for the *lac* repressor. The repressor is constitutively expressed and by binding to the *lac* operator, inhibits efficient transcription of the downstream sequence, containing the exogenous gene. However, when lactose or other analogues, like IPTG (isopropyl-β-D-thio-galactose), are present, the

repressor is inactivated and the exogenous gene is expressed. This plasmid was used for the expression of wild type *Tb*PTP1.

The pET-30a plasmid is identical to the pET-28a, except that it contains the S Tag® instead of the T7 Tag® and a C-terminal His Tag®, in addition to the N-terminal one. Consequently the pET-30a is slightly longer than the pET-28a (5422 bp compared to 5369 bp).
In both plasmids the *Tb*PTP1 gene was cloned using the XhoI and BamHI restriction sites. The pET-30a was used for the wild type and all the mutants *Tb*PTP1.

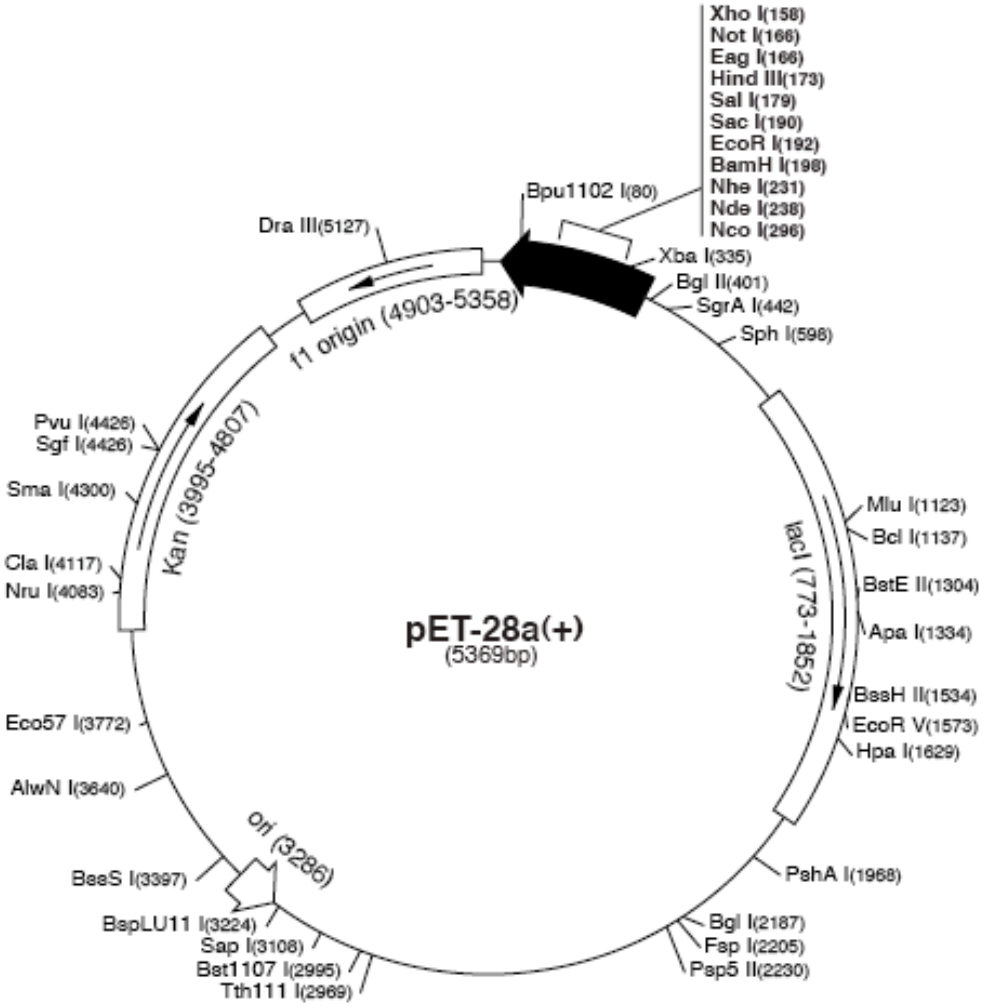

2.16.3 The p2T7 plasmid

The p2T7 is a plasmid developed from the p2rRNAprom for RNA interference in *T. brucei* (LaCount *et al.*, 2000), and it contains two bacteriophage T7 promoters on the opposite sides of the target gene. The primary advantage of this vector is that it allows the construct to be prepared in a single cloning step. In presence of G418 (1μg/ml), the sense and antisense RNAs, from the sequence located between the two promoters, are expressed and anneal to form dsRNA, which activate the RNAi pathways. The *Tb*10.389.0310 and *Tb*11.02.2090 gene fragments (688 bp and 525 bp, respectively) were both inserted in the p2T7 plasmid using the HindIII and BamHI restriction sites.

2.17. Primers used for RNAi

***Tb*10.389.0310**

*Tb*10.389.0310 FWD primer HindIII, BamHI: 5′-AAGCTT (Hind III) GGATCC (BamHI) TGT TGT GTC GCC GAT TAT GT; *Tb*10.389.0310 REV primer XhoI, NdeI: 5′-CAA CTG ACG CGA TAC CCG TAA AAG TG.

***Tb*11.02.2090**

*Tb*11.02.2090 FWD primer HindIII and BamHI: 5′-ATA AAGCTT (Hind III) GGATCC (BamH) ACC GGA TGT GACT TGC ACC A; *Tb*11.02.2090 REV primer XhoI/NdeI: 5′-TGCCATATGCTCGAGACCGCCATCGGTGTTGTTT.

Chapter 3

*Tb*PTP1 substrate identification

3.1. Introduction

Trypanosoma brucei Protein Tyrosine Phosphatase 1 (*Tb*PTP1) represents a major regulator of trypanosome differentiation from stumpy to procyclic forms (Szoor B *et al.*, 2006). In order to better characterize the *Tb*PTP1 signalling pathway responsible for this transition, the validation of the candidate interacting protein, *Tb*PIP39, and the identification of novel substrates was essential. For this purpose, two complementary approaches were investigated, which are the topic of this chapter.

The first approach involved the potential use of a *Tb*PTP1 substrate consensus sequence in order to identify novel substrates of the phosphatase *in silico*, similarly to what has been done with human PTP1B (Myers *et al.*, 2001). For this aim, the PTP1B substrate consensus literature was reviewed, and the 3-D structures of PTP1B and *Tb*PTP1 were compared.

The second approach consisted of the *in vitro* selection of candidate substrates from stumpy form cell extracts, using a recombinant substrate-trapping mutant *Tb*PTP1, which was employed to both validate the candidate protein and identify novel substrates.

3.2. Comparative analysis of PTP1B and *Tb*PTP1 structures

Published work on human PTP1B identified a specific motif in a group of substrates, required for their interaction with the phosphatase (Salmeen *et al.*, 2000); this motif was also successfully used to predict two novel physiological substrates for PTP1 (Myers *et al.*, 2001). Therefore, the possibility of using a similar approach for the identification of substrates of *Tb*PTP1 was examined.

Before investigating the presence of a potential *Tb*PTP1 substrate consensus sequence, it was essential to compare the primary sequence and 3-D conformation of *Tb*PTP1 and PTP1B, in order to assess whether the two enzymes share a conserved structure. Since the *Tb*PTP1 structure, which has been recently characterized (Chou *et al.*, 2010), was not known at the time in which the project was conducted, a model of its 3-D fold was predicted using the online workspace Swiss Model (Arnold *et al.*, 2006). It is worth noting

that the PTP1B C-terminal domain was missing in the 3D model as only the catalytic domain of the enzyme spanning aa 1-298 (Sun *et al.*, 2003) or 1-321 (Jia *et al.*, 1995) have been crystallized.

3.2.1 The ten landmark PTP motifs

As previously described, the alignment of the amino acid sequence of PTP1B and *Tb*PTP1 showed that all the ten landmark PTP motifs (M1 to M10) (Andersen *et al.*, 2001), except for motif 2 (M2), are present in the parasite enzyme (Szoor *et al.*, 2006).

A more detailed analysis of the alignments of these motifs revealed that all the invariant residues of the ten landmark PTP motifs (underscored bold letters in Table 2.1) are perfectly conserved in *Tb*PTP1 and that the overall identity of the motifs varies between 38 and 100%, with 7 out of 8 motifs scoring more than 50% (**Table 3.1**).

3.2.2 Conserved residues outside the landmark motifs

Outside the landmark motifs, seven residues have been reported to be conserved among PTPs (Andersen *et al.*, 2001), five of which are not identical in *Tb*PTP1, specifically Glu19, Arg156, Arg169, Leu192 and Arg254 of PTP1B are replaced by Phe25, Asp167, His188, Glu211 and Lys267 in the parasite enzyme (**Table 3.2**).

Of these five PTP residues, four are considered to be important for the definition of certain helices/sheets (Andersen *et al.*, 2001), all of which are predicted to fold into the same secondary structure in *Tb*PTP1. Specifically Phe25 defines the conserved α'2 helix, Asp167 and His188 the β10 and β11-sheet, and Glu211 the α3 helix.

The fifth substitution Arg254→Lys267 is potentially interesting, indeed Arg254 has been shown to form hydrogen bonds with the PTP loop of PTP1B, and has been hypothesized to function in enhancing the interaction with the phosphorylated tyrosine (pTyr) of the substrate and/or in stabilizing the thiolate form of the nucleophilic cysteine (Andersen *et al.*,

2001). Interestingly, mutations of Arg254 to Lys or Gln in PTP1B have been shown to have an inhibitory effect on the dephosphorylation of the artificial substrate pNPP (Salmeen *et al.*, 2000), thus the presence in *Tb*PTP1 of Lys267 could indicate a weaker nucleophilic activity of the catalytic Cys residue.

In addition, Arg254 has been shown to form the second phosphate-binding site, which has lower affinity for the substrate but that could be targeted, together with the main active site, to develop more specific inhibitors (Puius *et al.*, 1997). Indeed a peptide possessing two adjacent phosphorylated tyrosine residues (tandem pTyr), which targets both sites, has been shown to have a 70-fold higher binding affinity for PTP1B compared to the mono phosphorylated tyrosine peptide (Salmeen *et al.*, 2000).

Therefore, the observation that Arg254 is substituted by Lys267 in *Tb*PTP1 has two potentially important implications: the fact that the parasite enzyme might not prefer substrates containing tandem pTyr over mono pTyr, and the possibility of using this less conserved residue to design specific *Tb*PTP1 inhibitors.

A

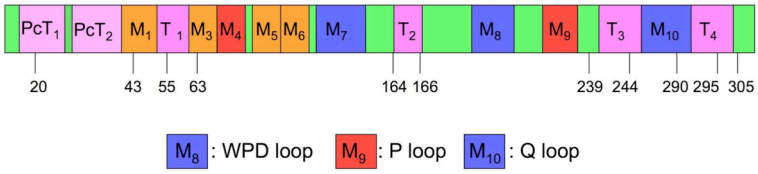

B

Motif	Consensus	*Tb*PTP1	Identity
PcT1		RMQREFVQLQR	
PcT2		ENPRNINFTTSK	
M1	NXX(**K/R**)N**R**Y	NRHKNRY	100
T1		LANEETIYP	
M2	DXX**R**(V/I)X**L**		
M3	D**Y**INA(N/S)	P**Y**INGN	67
M4	(F/Y)(I/V)AX**Q**GP	FVAC**Q**AP	85
M5	TXX**D**F**W**X(M/L/V)X(W)(E/Q)	GVLD**F**LETLSE	38
M6	(I/L/V)(V/I)**M**XT	VV**M**LT	100
M7	KCXX**Y**W**P**	KAER**Y**WP	57
T2		YEV	
M8	(Y/F)XX**W**P**D**XGX**P**	QYVG**WP**DHGV**P**	100
M9	PXX(**V/I**)**HCS**A**G**X**GR**(**T/S**)**G**	PILV**HCSAGIGRTG T**	100
T3		LIGAYA	
M10	(**V/I/L**)QTXXQ**Y**XF	**V**QRLEQYA V	67
T4		RLGVDI	

Table 3.1. Comparative analysis of the residues conserved between *Tb*PTP1 and mammalian PTPs. (A) *Tb*PTP1 structure highlighting the ten conserved landmark PTP motifs (Andersen *et al.*, 2001) and the trypanosome-specific ones. (B) The consensus sequences of the PTP motifs are compared to the residues found in *Tb*PTP1 (Szoor *et al.*, 2006). The percentage of amino acid identity is also shown (identity); invariant amino acids are underscored and bold, bold letters are conserved >90% and non bold >80% (from Andersen *at el.*, 2001).

PTP1B	*Tb*PTP1	Function
Glu19	Phe25	Definition of α'2 helix
Glu115	Glu126	H bond with Arg221
Arg156	Asp167	Definition of β10-sheet
Arg169	His188	Definition of β11-sheet
Leu192	Glu211	Definition of α3 helix
Arg254	Lys267	H bond with PTP loop
Arg257	Arg270	H bond with PTP loop

Table 3.2. Conservation of the important PTP residues outside the landmark motifs. The conserved residues in mammalian PTPs (Andersen *et al.*, 2001) (numbered for PTP1B) are compared with the corresponding amino acids of *Tb*PTP1; *Tb*PTP1 residues that are not conserved with PTP1B, and other mammalian PTPs, are highlighted. The proposed function of each residue, according to Andersen *et al.*, 2001 is also shown (H bond: hydrogen bond; α and β sheet are numbered according to Andersen *et al.*, 2001).

3.2.3 3-D structure prediction of the trypanosome-specific motifs

As previously illustrated (see paragraph 1.17), other interesting differences were highlighted from the comparative analysis of the primary sequence of *Tb*PTP1 and human PTP1B: the presence of six trypanosome-specific sequences, two pre-catalytic (PcT1 and PcT2) and four within the catalytic core (T1-T4) (Szoor *et al.*, 2006)(**Figure 3.1 A**).

Prediction of the secondary and 3-D structure for *Tb*PTP1, using the online available Swiss Model server (Arnold *et al.*, 2006; Bordoli *et al.*, 2009), and their superimposition with the PTP1B structure showed that most of the trypanosome-specific motifs align with the PTP1B backbone. However, these motifs are often arranged in random coils or U-turns, rather than α-helices or β-sheets, and are positioned on the surface of the enzyme (**Figure 3.1 B**).

The only exceptions are the motif T3, which is found within the core of the enzyme and motif T4, which is found outside in the 3-D structure prediction (aa 1-288).

According to the *Tb*PTP1 3-D model, the trypanosome-specific pre-catalytic motif PcT1 (aa 20-29) is found on the surface and folds into an α-helix, which aligns well with the corresponding PTP1B α2' helix, a motif that is conserved structurally but not at sequence level among PTPs (Andersen *et al.*, 2001).

In contrast, PcT2 (aa 32-43), which is predicted to form a coil, partly deviates (residue 33-35) from the backbone structure of PTP1B and protrudes towards the outside of the enzyme.

Similarly, the trypanosome-specific motif T1 (aa 55-63), which substitutes M2, is predicted to fold into a loop, in contrast to M2, which forms a β-sheet. Moreover Tyr62 of T1 is predicted to map on the edge of the loop, facing away from the central core of the enzyme. Similarly to T1, T2 (aa 164-166) also forms a U-turn on the surface of the enzyme (**Figure 3.1 B**).

The most interesting trypanosome-specific motif is probably T3 (aa 239-244), as it is found in the vicinity of the active site of the enzyme, although none of the corresponding residues in PTP1B have been shown to participate in catalysis. Motif T3 aligns well with the PTP1B backbone and, similarly to the human sequence, is predicted to fold into an α-helix. The only difference between T3 and the corresponding region of PTP1B are two *Tb*PTP1 residues,

Ala242 and Tyr243, which are not well conserved among PTPs, each of which is found only in one out of thirty-seven PTPs (Andersen *et al.*, 2001).

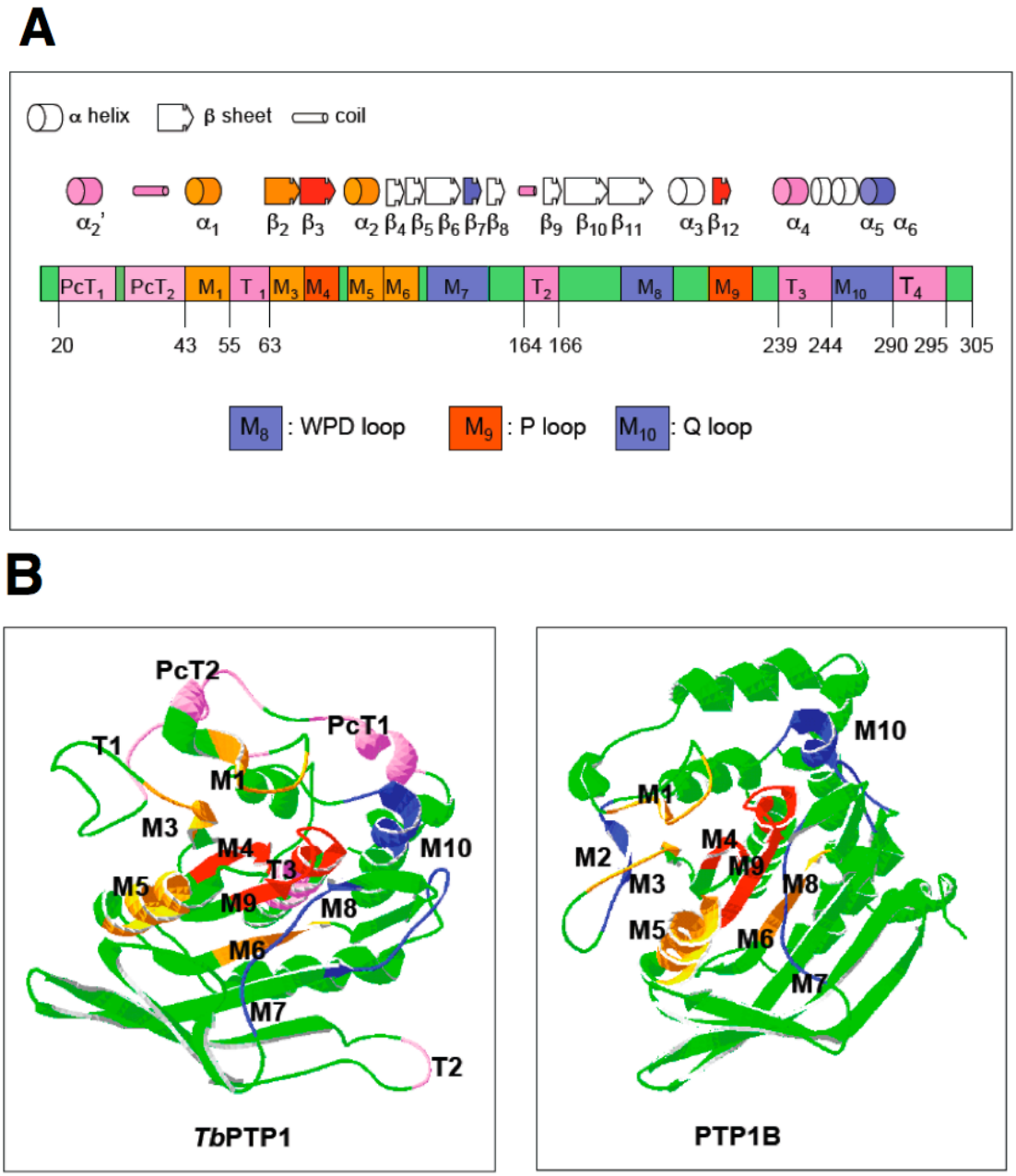

Figure 3.1. *Tb*PTP1 structure. (A) Schematic diagram of *Tb*PTP1 highlighting the PTP motifs (M1-10) and the trypanosomes-specific motifs (PcT1-2, T1-4). The ten conserved PTP motifs are shown (M1-M10) and coloured according to the degree of conservation among PTPs (red: high, orange: medium, blue: low); the trypanosome-specific motifs are coloured in pink (PcT1, PcT1, T1-T4). The secondary structure prediction for *Tb*PTP1 (α-helix, β-sheet and coil, predicted obtained using Swiss Model (Arnold *et al.*, 2006) is also shown and labeled according to Andersen *et al.,* 2001. (B) The 3-D structure of *Tb*PTP1 and PTP1B are shown, as predicted by the Swiss Model server and visualized using Swiss pdb-Viewer. The PTP motifs are labeled and coloured as for A.

3.3. *Tb*PTP1 substrate consensus analysis

The comparative analysis of the PTP1B and *Tb*PTP1 structure showed that the two proteins share most of the residues involved in substrate binding (**Table 3.1** and **Figure 3.1**). Consequently, it is possible that the two enzymes share the preference for certain types of amino acids surrounding the phosphorylated tyrosine.

A review of the literature published regarding the PTP1B substrate consensus sequence (i.e., the most commonly occurring amino acids, at each position of an aligned series of substrate proteins (Berg *et al.*, 2002)) revealed the existence of two groups of substrates. The first group includes the PTP1B targets that are phosphorylated in two adjacent tyrosine residues (tandem pTyr), such as the insulin receptor (Salmeen *et al.*, 2000). The second group comprises the substrates presenting only one phosphorylated tyrosine residues (pTyr), like the EGF receptor (Zhang *et al.*, 1993).

3.3.1 Tandem phosphorylated tyrosine consensus sequence

For the first group, a substrate consensus sequence was characterized (E/D-pY-pY-R/K), which was successfully used for the identification of two novel PTP1B targets (Myers *et al.*, 2001). The residue responsible for the binding to the second pTyr has been shown to be Arg254 (Puius *et al.*, 1997), which is not conserved in *Tb*PTP1 (see paragraph 3.2.2).

This observation, together with the fact that no tandem pTyr were detected in the list of *T. brucei* tyrosine phosphorylated proteins (Nett *et al.*, 2009b), suggested that the PTP1B substrate consensus E/D-pY-pY-R/K is probably not valid for *Tb*PTP1.

3.3.2 Mono phosphorylated tyrosine consensus sequence

In addition to the PTP1B substrate consensus sequence containing tandem pTyr, a lot of work has also been done to try and identify the consensus containing one pTyr residue (**Figure 3.2**).

Initial studies that used the substrate peptide DADEpYL, modeled on the auto-phosphorylation site of EGFR, highlighted the importance of the acidic residue N-terminal to the pTyr (Zhang *et al.*, 1993). Further crystallographic analysis of the PTP1B complex with the same peptide identified Arg47 as the major determinant of this preference (Sarmiento *et al.*, 1998), due to the guanidinium group of Arg forming salt bridges with the carboxylate group at the -1 position of the substrate peptide. However, other studies, which used random peptides, for example generated from phage display libraries, showed a wider preference at the -1 position (N-terminal) to the pTyr (Vetter *et al.*, 2000; Walchli *et al.*, 2004).

The observation that aromatic/aliphatic residues can also be accommodated at position -1 to the pTyr was then explained by the ability of the side chain of Arg47 to adopt two different conformations (Sarmiento *et al.*, 2000). Interestingly, *Tb*PTP1 possesses a Leu (Leu52) at the corresponding position of Arg47 of PTP1B, which suggests a possible preference for aliphatic or aromatic residues N-terminal to the pTyr (**Figure 3.2**).

In the list of tyrosine-phosphorylated proteins of bloodstream form *T. brucei*, hits containing non-charged residues at the -1 position represented 15/41 (36%), versus 6/41 (15%) proteins containing acidic residues in the same position. However, the confirmed *Tb*PTP1 substrate, *Tb*PIP39 possesses a glutamic acid (Glu278) N-terminal to the pTyr (DEpYTK) (Szoor *et al.*, 2010). These contrasting observations probably suggest that the *in silico* selection of *Tb*PTP1 substrates, based on the type of residue found in the vicinity of the phosphorylated tyrosine, is not feasible.

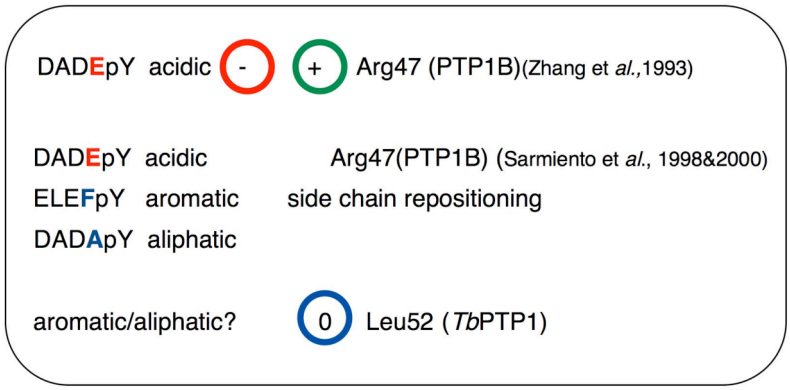

Figure 3.2 Substrate consensus sequence analysis. The schematic diagram summarizes the literature cited in the text concerning the PTP1B substrate consensus sequence for mono pTyr; the peptide used in the studies analysed is shown on the left (modifications of the EGFR peptide: DADEpY), and the residues N-terminal to the pTyr are highlighted in bold together with the corresponding aa type (acidic/aromatic/aliphatic). Acidic residues were initially identified as preferentially selected, due to their interaction with the basic side chain of Arg47 (Sarmiento *et al*., 1998); then a wider preference of aa N-terminal to the pTyr was recognized, explained by the repositioning of the Arg side chain (Sarmiento *et al*., 2000). *Tb*PTP1 possesses Leu52 in place of Arg47 of PTP1B, which might suggest a preference for aromatic or aliphatic aa N-terminal to the pTyr of its substrates. Red, green and blue colours indicate acidic, basic, aliphatic/aromatic residues, respectively.

3.4. The *Tb*PTP1 substrate-trapping mutant approach

In order to identify novel *Tb*PTP1 substrates, the method chosen was the use of a substrate-trapping mutant *Tb*PTP1, coupled to mass spectrometry analysis. Such a procedure, using the single mutant D→A, has been employed successfully in the case of PTP1B (Flint *et al.*, 1997; LaMontagne *et al.*, 1998a) and it is based on the fact that the substitution of the catalytic aspartic acid of the WPD loop causes the enzyme to retain the substrate, thus allowing its selection and identification (Flint *et al.*, 1997) (see paragraph 1.15).
The visualization of the trapped proteins is then possible by Western blot analysis against phosphorylated tyrosine residues. Therefore it was initially important to optimize the detection of tyrosine-phosphorylated proteins in *T. brucei* using Western blot.

3.4.1 Profile of tyrosine-phosphorylated proteins in stumpy cell extract

In order to optimize the detection of tyrosine-phosphorylated proteins several conditions of cell lysis and Western blot analysis were tested. Particularly important turned out to be the use of the more sensitive PVDF (polyvinylidene fluoride) membrane, compared to the normal nitrocellulose membrane, and the type of anti phosphorylated tyrosine antibody used (α-pTyr).
One example of a phosphorylated tyrosine profile, obtained from stumpy cell extracts is shown (**Figure 3.3**), together with a schematic comparison to the only published data available to date (Parsons *et al.*, 1990). As can be seen, the profile obtained is not identical to the analysis conducted by Parsons *et al.*, (compare **Figure 3.3 A** and **Figure 3.3 B**). In particular, proteins with a molecular weight of less than 30 kDa were not detected in the published profile. These discrepancies might be due to the different *T. brucei* strains, antibodies or blotting conditions used. Nevertheless it is possible to identify some proteins detected in both studies: two doublets at around 35 and 40 kDa and a strong band at around 55 kDa (**Figure 3.3 C**).
In order to test the specificity of the antibody for tyrosine-phosphorylated

proteins, the antibody itself was pre-incubated with phenyl phosphate, a phosphate analogue, which had been used for this purpose (Parsons *et al.*, 1990). In the presence of 200 mM phenyl phosphate (pp) most of the bands decreased in intensity, and the less abundant high molecular weight proteins nearly disappeared (**Figure 3.3 D**).

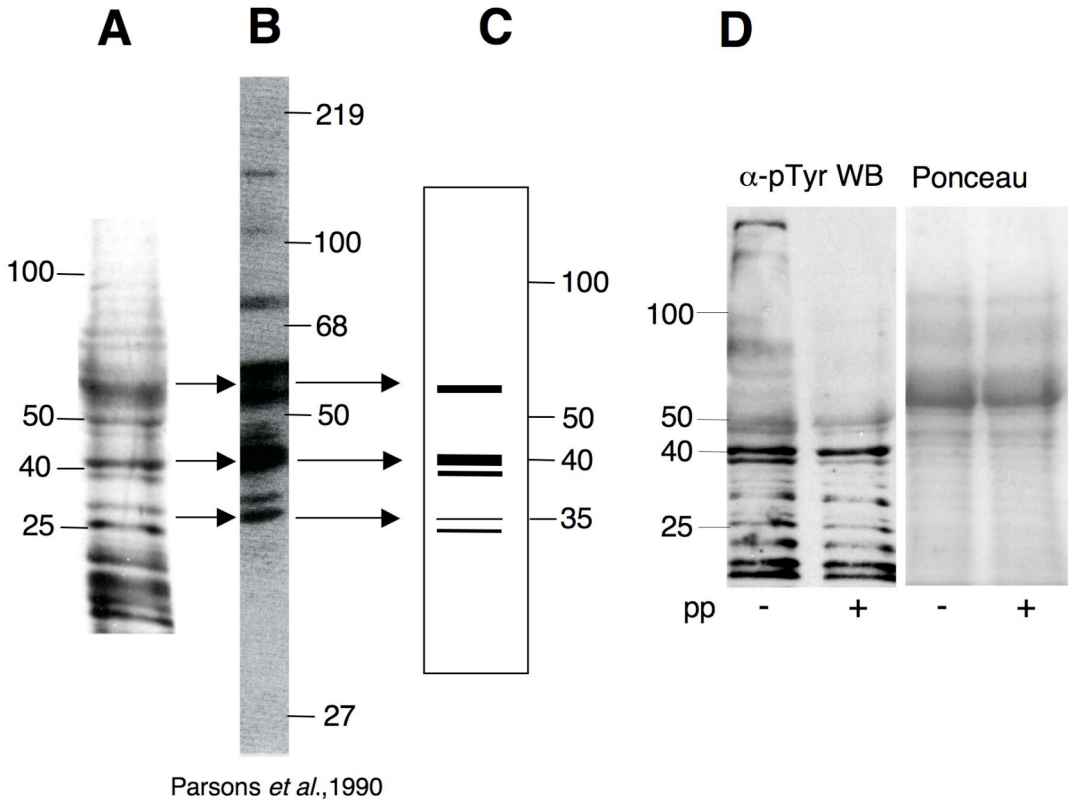

Figure 3.3 Profile of tyrosine-phosphorylated proteins in stumpy form cell extracts. Example of a Western blot performed on stumpy form cell extracts probed with anti phosphorylated tyrosine antibody (α-pTyr), 4G10 (Upstate) (panel A) and its comparison with the only published profile by Parsons *et al.*,1990 (panel B); the apparently common bands (arrows) are shown in the diagram of panel C. The same extract was probed with the same antibody in absence or presence of 200 mM phenyl phosphate (pp); the ponceau stain of the membrane is included to show equal loading (Ponceau of panel D). All the numbers indicate molecular weight markers in kDa.

3.5. Selection of stumpy form cell extract using substrate-trapping D199A/Q275A *Tb*PTP1

As previously mentioned, the substrate-trapping D181A mutant PTP1B has been extensively used for the identification of novel substrates of the phosphatase (Garton *et al.*, 1996; LaMontagne *et al.*, 1998a). However, more recent work has shown that the double mutant D181A/Q262A PTP1B displays a 6-fold greater substrate trapping ability compared to the D181A enzyme, as judged by *in vitro* binding assays to a substrate analogue and by *in vivo* immune-precipitations (Laiping *et al.*, 2001).

Therefore, in order to increase the substrate-trapping ability of the D199A *Tb*PTP1, the double mutant D199A/Q275A enzyme was created (**Figure 3.4**). The Q275A mutation was introduced in the pET30a plasmid containing the His-tagged D199A protein sequence. In parallel, an additional double mutant D199A/ C229S *Tb*PTP1 was also created (**Figure 3.4**), to be used as a negative control, since the corresponding PTP1B mutant has been shown to behave like the wild type protein (Laiping *et al.*, 2001).

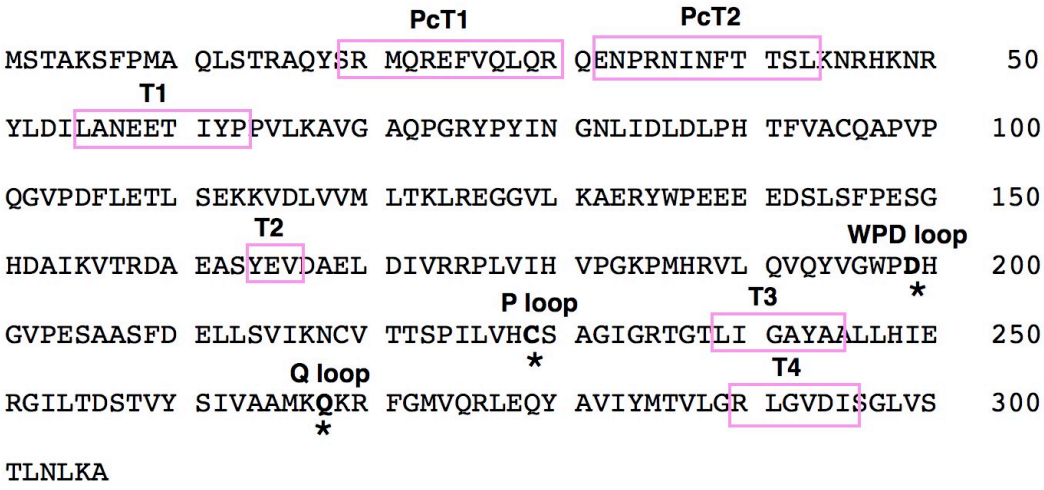

Figure 3.4. Double mutants D199A/Q275A and D199A/C229S *Tb*PTP1. The primary sequence of *Tb*PTP1 is depicted, with trypanosome-specific motifs highlighted (PcT1, PcT2, T1 to T4). The domains important in catalysis (see paragraph 1.15.3) are labeled (WPD loop; P loop; Q loop). The residues substituted in the different mutant forms (D199, C229 and Q275) are indicated by asterisks (*).

Both D199A/Q275A and C229S/D1994A *Tb*PTP1 mutants were expressed and purified in *E. coli* (**Figure 3.5**).

After successful expression and purification, the double mutants were used, together with the single mutant D199A, to select potential *Tb*PTP1 substrates from stumpy form cell extracts. Briefly, stumpy cells were harvested from a mouse infection and incubated with 150 μM BZ3, a commercially available PTP1B inhibitor (see paragraph 1.18.3), that is able to inhibit *Tb*PTP1 (Szoor *et al.*, 2006), for 1.5 hr at 37°C. Cells were then lysed and incubated for 1 hr at 4°C with the different His-tagged mutant versions of *Tb*PTP1. After 2-3 PBS washes, the bound proteins were eluted with the addition of SDS sample buffer, boiled and subjected to SDS-PAGE and Western blot.

Western blot was performed using the anti phosphorylated tyrosine antibody (α-pTyr), with the same conditions previously optimized (**Figure 2.3**), since the substrates trapped by the enzyme are still phosphorylated.

As expected the double mutant D199A/Q275A *Tb*PTP1 trapped several tyrosine-phosphorylated proteins, whereas the D199A/C229S and the WT enzyme did not (**Figure 3.5 B**).

In order to more specifically elute only the tyrosine phosphorylated proteins bound to the substrate-trapping enzyme, sodium vanadate was employed as a competitor. Indeed sodium vanadate is a powerful PTP inhibitor that binds the catalytic site of the enzyme and that has been used to elute proteins selected by substrate-trapping phosphatases (Blanchetot *et al.*, 2005; Chang *et al.*, 2008). However, vanadate did not elute tyrosine phosphorylated proteins bound to the D199A *Tb*PTP1 (data not shown), even at 120 mM, a concentration 8-fold higher than published. This was despite the use of a buffer lacking imidazole and β-mercaptoethanol, which have been reported to inhibit vanadate action (Huyer *et al.*, 1997). Since vanadate competition has been reported for only some PTPs, towards certain substrates and under specific conditions (Blanchetot *et al.*, 2005), it is likely that, in the experimental conditions used, the compound did not compete strongly enough with recombinant D199A *Tb*PTP1 to allow effective elution and visualization of the bound proteins.

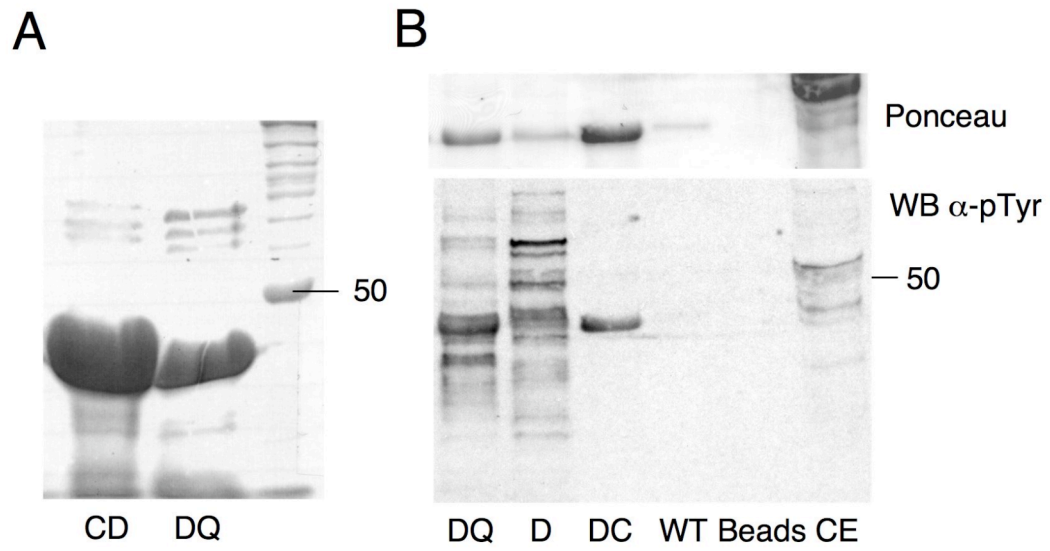

Figure 3.5. Purification of the recombinant mutant forms of *Tb*PTP1 and stumpy form cell extract selection. (A) Coomassie stain of purified His-tagged C229S/D199A mutant *Tb*PTP1 (CD) and D199A/Q275A mutant *Tb*PTP1 (DQ). (B) The same recombinant proteins of panel A were used to select potential *Tb*PTP1 substrates from stumpy form cell extract. In the upper panel the Ponceau staining of the membrane shows the loadings of the recombinant proteins (Ponceau). In the lower panel is shown the Western blot of the selection using the different recombinant forms of the enzyme probed with anti phosphorylated tyrosine antibody (WB α-pTyr). DQ: D199A/Q275A mutant *Tb*PTP1; D: D199A mutant *Tb*PTP1; DC: D199A/C229S mutant *Tb*PTP1, as negative control; WT: wild type *Tb*PTP1 as negative control; Beads: nickel agarose beads incubated with cell extract; CE: stumpy cell extract alone. Numbers indicate molecular weight markers, in kDa.

3.6. *Tb*PIP39 selection by *Tb*PTP1 in stumpy form cell extracts

*Tb*PIP39 was identified by mass spectrometry analysis of stumpy form cell extract selected by the D199A mutant *Tb*PTP1, before the start of this project. At that moment a specific antibody against *Tb*PIP39 was not available, and thus it was not possible to visualize the two proteins by Western blot analysis, thus validating their interaction.

Only during the course of this project, a specific antibody against *Tb*PIP39 was developed, which was then used to detect *Tb*PIP39 in the cell extract selections (**Figure 3.6**). As expected, *Tb*PIP39 was selected by the substrate-trapping mutants D199A ("D") and D199A/Q275A ("DQ") *Tb*PTP1 and not by wild type enzyme ("WT") or by the agarose beads alone ("Beads"). However, the C229S/D199A mutant *Tb*PTP1 ("DC"), which did not trap any tyrosine-phosphorylated proteins (**Figure 3.5 B**), did bind *Tb*PIP39 (**Figure 3.6 A**). This difference might be due to a lower sensitivity of the anti phosphorylated tyrosine antibody compared to the anti *Tb*PIP39 antibody.

The same selection was repeated using equal amounts of recombinant wild type ("WT") and D199A ("D") *Tb*PTP1 (**Figure 3.6 B**). The Western blot was probed with anti His tag antibody (α-His), to obtain a more accurate quantification of the His-tagged recombinant protein compared to Ponceau staining, and with anti *Tb*PIP39 antibody (α-PIP39). *Tb*PIP39 was found in the initial cell extract ("CE"), in the unbound cell extract (flow through, "FT") and, importantly, in the lane corresponding to the substrate-trapping D199A *Tb*PTP1 after incubation with the cell extract (arrowhead in "D + CE" lane of **Figure 3.6 B**). *Tb*PIP39 was also selected by the wild type *Tb*PTP1, after incubation with stumpy cell extract (arrowhead in "WT + CE" lane in **Figure 3.6 B**). This observation suggested that, under certain experimental conditions, the interaction between wild type *Tb*PTP1 and *Tb*PIP39 was stable enough to be detected, as seen when the two proteins were immune-precipitated (Szoor *et al.*, 2010).

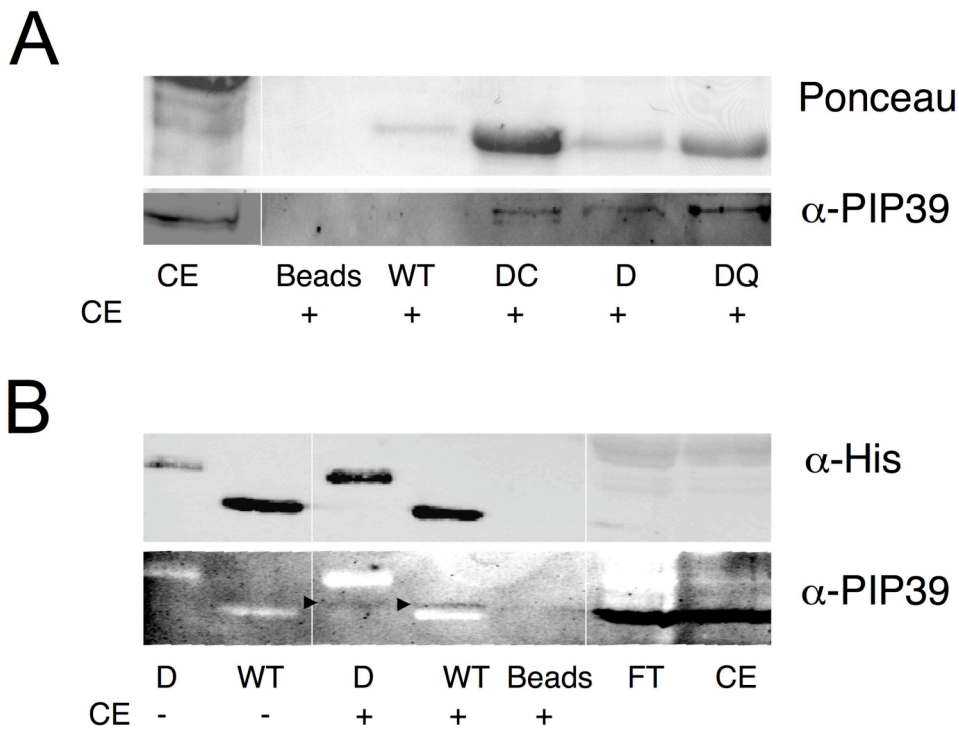

Figure 3.6 *Tb*PIP39 selection by *Tb*PTP1 in stumpy form cell extract. (A) The stumpy form cell extract selection of Figure 3.5 was probed with anti *Tb*PIP39 antibody (α-PIP39); the recombinant *Tb*PTP1 used are wild type (WT), C229S/D199A (DC), D199A (D), D199A/Q275A (DQ) and NiNTA agarose beads alone (Beads). All of them were incubated with stumpy form cell extract (+CE); cell extract prior incubation is also shown (lane CE). The Ponceau staining of the membrane is shown as loading control (Ponceau). (B) Western blot of another selection using wild type (WT), D199A (D) *Tb*PTP1 and NiNTA agarose beads alone (Beads), in absence or presence of stumpy cell extract (-/+ CE). The membrane was probed against *Tb*PIP39 (α-PIP39), and against His-tagged *Tb*PTP1 (α-His). FT: flow through (cell extract after incubation with the recombinant proteins). Note that the white bands in the lower panel of B, are the recombinant proteins visible on the membrane, but not detected by the anti phosphorylated *Tb*PIP39 antibody.

3.7. Selection of stumpy form cell extract using D199A *Tb*PTP1 and mass spectrometry analysis

The stumpy form cell extract selection was then used in larger scale cell extract selection experiments. The substrate-trapping mutant D199A *Tb*PTP1 was used, as it has been shown to trap more tyrosine phosphorylated proteins than the other mutants (**Figure 3.5 B**).

For the larger scale selections, approximately $1x10^9$ stumpy form cells were treated with BZ3 for 1.5 hr at 37°C. Subsequently the cells were lysed and the protein extract (11.6 mg) was incubated with the substrate-trapping D199A *Tb*PTP1. After 2-3 PBS washes, the bound protein were eluted by addition of SDS sample buffer and half the amount of each sample was visualized by Coomassie staining of the gel (**Figure 3.7**).

The substrate-trapping D199A *Tb*PTP1 selected several proteins from the cell extract, as judged by the darker appearance of the gel (lane "D199A + CE" in **Figure 3.7**); among them, one band, of approximately 120 kDa, appeared to be clearly visible (arrow in **Figure 3.7**). This band, cut from the gel, together with the remaining half of the other samples were subjected to mass spectrometry analysis.

The mass spectrometry (MS) analysis was carried out by Richard Burchmore (University of Glasgow), using the electrospray ionisation (ESI) technique on a QSTAR Pulsar Hybrid LC/MS/MS System. The resulting spectra were compared via Matrix Science Mascot search engine against the complete *T. brucei* proteome. The results of the mass spectrometry analysis are shown in **Table 3.3**, where the hits obtained from similar experiments to the one showed in **Figure 3.7** are also included. A total of four cell extract selections were performed, two before the start of this project (experiment 1 and 2 of **Table 3.3**), and two performed during the course of this project (experiment 3 and 4 of **Table 3.3**). The proteins listed have been selected by the D199A *Tb*PTP1 mutant and not by the agarose beads alone (negative control) in any of the experiments. In addition, proteins very similar to hits found in the negative control (such as tryparedoxin peroxidase 1 and tryparedoxin peroxidase 2), were not considered to be specifically selected by *Tb*PTP1.

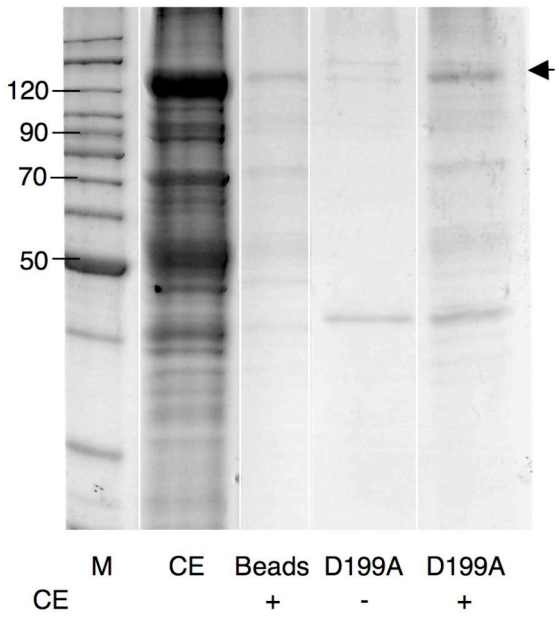

Figure 3.7 Selection of stumpy form cell extract using the D199A *Tb*PTP1. The Coomassie stained protein gel of stumpy cell extract selection showing the molecular weight marker (M, numbers are in kDa), approximately 5% of the extract used in the incubation with D199A *Tb*PTP1 (CE), NiNTA agarose beads incubated with the cell extract (Beads) and recombinant D199A *Tb*PTP1 in absence or presence of cell extract (D199A - and + CE). In addition the high molecular weight band visible in the D199A+ CE lane is highlighted (arrowhead).

Experiment number	GeneDB accession n°	Protein Function	Predicted MW
1 and 2	*Tb*09.160.4460	phosphatase (*Tb*PIP39)	39
1 and 2	*Tb*11.01.3010	dynein heavy chain	480
1 and 2	*Tb*927.7.920	dynein heavy chain	468
1 and 2	*Tb*11.02.2090	hyp. prot with HEAT repeat	197
3	*Tb*10.6k15.2800	hyp. prot.	25.7
3	*Tb*927.7.5700	hyp. prot.	45.5
3	*Tb*11.01.0400	Ser/Thr kinase	138
4	*Tb*10.389.0310	hyp. prot. with IQ CaM domain	96.3

Table 3.3. Summary of the proteins identified by MS analysis for the new and for the previous stumpy cell extract selection experiments. The experiments are numbered in chronological order: 1 and 2 (previously performed by B. Szoor on 27/10/06 and 16/05/07), 3 and 4 (performed during the course of this project). Proteins are identified by GeneDB database accession number (GeneDB accession n°), a description of the corresponding function is given (hyp. prot.= hypothetical protein; ser/thr= serine/threonine; IQ CaM= IQ–calmodulin binding domain), together with the predicted molecular weight in kDa (predicted MW).

The analysis of the MS hits identified four proteins common to more than one selection, corresponding to a putative CTD phosphatase (*Tb*09.160.4460), which was then characterized and named *Tb*PIP39,(Szoor *et al.*, 2010) (see paragraph 1.17), two dynein heavy chains (*Tb*11.01.3010 and *Tb*927.7.920), and one hypothetical protein (*Tb*11.02.2090) (**Table 3.3,** experiment 1 and 2). None of the proteins specifically selected by the D199A *Tb*PTP1 in the two selections performed in the course of this project (experiment 3 and 4) were found in the two previous selections (experiment 1 and 2), although the protocol followed was the same.

Four new hits were identified in the course of this project: two hypothetical proteins (*Tb*10.6K15.2800 and *Tb*927.7.5700) and one Ser/Thr kinase (*Tb*11.01.0400) (**Table 3.3**, experiment 3). In addition, another hypothetical protein (*Tb*10.389.0310), characterized by the presence of an IQ-calmodulin binding domain, was found when the band cut from the gel of selection number 4 (**Figure 3.6**, arrowhead) was analyzed (**Table 3.3**, experiment 4).

In order to assess the potential relevance of these hits to the *Tb*PTP1 pathway during differentiation to procyclic forms, the structural and functional role of the different candidate proteins was analyzed, with the exception of *Tb*09.160.4460 (*Tb*PIP39), which has already been validated as *Tb*PTP1 target (Szoor *et al.*, 2010).

*Tb*11.01.3010 and *Tb*927.7.920

Two of the hits identified, *Tb*11.01.3010 and *Tb*927.7.920 were large dynein heavy chains, of predicted molecular weight of 480 and 468 kDa, respectively (www.genedb.org).

Higher eukaryotes dyneins are multisubunit microtubule-dependent motor enzymes that act as the force-generating proteins of eukaryotic cilia and flagella. Specifically, dynein heavy chains exhibit ATPase activity and microtubule binding ability and are responsible for the movement of organelles and vesicles along the microtubules (Burgess *et al.*, 2003).

In *T. brucei* some dyneins are part of the intraflagellar transport apparatus, where they aid the transport of protein particles from the distal tip of the flagellum back to the basal body. RNAi of one such protein, *Tb*DHC1b (*Tb*11.02.0030), led to loss of the flagellum and to the disorganization of cell structure and polarity (Kohl *et al.*, 2003). This finding was particularly interesting in light of the observation that BZ3 treatment of slender cells caused a temporary loss of motility, apparent only within the first 5 min of drug treatment at 37°C (Szoor B., personal communication). Therefore dyneins might potentially play a role in the *Tb*PTP1 pathway in slender form cells.

*Tb*11.01.3010 expression, but not *Tb*927.7.920, appeared to increase in stumpy forms compared to slender forms, and then to be maintained constant throughout differentiation to procyclic forms (Kabani *et al.*, 2009).

However, no studies have been done on these two particular dyneins, and such big proteins, which carry numerous negative charges, may represent non-specific contaminants.

*Tb*11.02.2090

The fourth protein detected in both experiment 1 and 2 was a 197-kDa hypothetical protein (*Tb*11.02.2090), characterised by the presence of one HEAT repeat.

The HEAT repeat is a tandemly repeated, 37-47 amino acid long module, occurring in a number of cytoplasmic proteins, including the four name-giving proteins huntingtin, elongation factor 3 (EF3), the 65 kDa alpha regulatory subunit of protein phosphatase 2A (PP2A) and the yeast PI3-kinase TOR1 (Andrade *et al.*, 1995). Arrays of HEAT repeats consists of 3 to 36 units, which form a rod-like helical structure, made of antiparallel α-helices, and appear to function as protein-protein interaction surfaces, with each repeat corresponding to a structural unit of antiparallel helices (Kobe *et al.*, 1999).

It is difficult to predict whether the presence of a single HEAT repeat in *Tb*11.02.2090 (aa 765-801) is sufficient to form a protein-protein interaction domain, but the observation that 13/33 (39%) of *T. brucei* HEAT-containing

proteins possess a single repeat is intriguing. Twelve such proteins do not have a known function and do not possess any additional domain, whereas one is predicted to be a transportin-2 like protein (*Tb*10.6k15.3020); transportins mediate the nuclear transport of other proteins in higher eukaryotes (Harvey *et al.*, 2000). Other *T. brucei* HEAT-containing proteins are a PP2A regulatory subunit, a putative importin-β 1 subunit and the flagellar protein PF16, which contain 8, 5 and 3 repeats, respectively (www.genedb.org).

A Blast search for proteins similar to *Tb*11.02.2090 in other *Trypanosoma* species showed that the protein is conserved in *T. cruzi* and *L. major*, with a percentage of identity over *T. brucei* of 45 and 31, respectively; in addition, a particular tyrosine residue (Tyr409 of *Tb*11.02.2090) was shown to be conserved within these orthologues. No higher eukaryotic homologues could be found, only a human transcriptional regulator, homologous to the Drosophila Nipped-B (Krantz *et al.*, 2004), had a limited degree of identity (21%) with a small portion towards the C-terminal part of the protein (aa 1341-1581).

The *Tb*11.02.2090 mRNA expression profile showed a small level of down-regulation 18 hr after initiation of differentiation to procyclic forms, but no significant changes at earlier or later time points (Kabani *et al.*, 2009).

*Tb*10.6k15.2800, *Tb*927.7.5700 and *Tb*11.01.0400

In experiment number 3, three possible interacting proteins were identified, two of which were small hypothetical proteins (*Tb*10.6k15.2800 and *Tb*927.7.5700), with no particular structural domain (except the transmembrane helix of *Tb*927.7.5700), or any significant sequence similarity within the kinetoplastids or higher eukaryotes proteomes. They also did not show any change in mRNA levels during differentiation to procyclic forms (Kabani *et al.*, 2009).

The third protein (*Tb*11.01.0400) was a 138-kDa Ser/Thr kinase conserved among kinetoplastids and annotated as similar to the human Ser/Thr kinase 36 (STK36) (www.genedb.org). A Blast search revealed that the N-terminal 253 residues share 36 and 34 % of identity with mouse and human ULK4,

respectively, and 31% with human STK36, also known as "Fused homolog". ULK kinases have been involved in autophagy in yeast (Hosokawa *et al.*, 2009) and in cell-cell signalling in *Drosophila* development (Therond *et al.*, 1996). Similarly, STK36 has been shown to be important for postnatal development in mice (Murone *et al.*, 2000). *Tb*11.01.0400 has been identified in the kinome of *T. brucei* as a member of the ULK family, and reported to be catalytically inactive, due to mutations in essential residues, together with 12 other inactive protein kinases in *T. brucei*, which are supposed to play a regulatory role via protein-protein interactions (Parsons, 2005).
*Tb*11.01.0400 mRNA levels did not significantly change during differentiation to procyclic forms, except for a small decrease at 18 hr after cis-aconitate treatment (Kabani *et al.*, 2009).

***Tb*10.389.0310**

Experiment 4 identified more proteins than experiment 3 but only one (*Tb*10.389.0310) was specifically selected by *Tb*PTP1 and not found previously, corresponding to the 120 kDa band isolated from the gel of selection 4 (arrowhead of **Figure 3.7)**.
*Tb*10.389.0310 is a hypothetical protein with predicted molecular weight of 96.3 kDa; it is conserved within kinetoplastids, with 36% and 28% identity with *T. cruzi* and *L. major*, respectively, and showing a conserved tyrosine residue (Tyr104 of *Tb*10.389.0310). In addition, the protein contains an IQ-calmodulin binding domain (IQXXXRGXXXR at aa 115-140), which is found in proteins that bind calmodulin, such as myosins, and in many other proteins that have not been demonstrated to interact with calmodulin, such as PKC, connexin45 and sodium channel proteins (Rhoads *et al.*, 1997).
*Tb*10.389.0310 mRNA levels were found to be up-regulated in slender compared to stumpy forms, and to be maintained at constant levels during differentiation to procyclic forms (Kabani *et al.*, 2009).

Although it was difficult to estimate the importance of the identified hits as potential *Tb*PTP1 substrate, the most promising candidates appeared to be the 197-kDa hypothetical protein with the HEAT repeat (*Tb*11.02.2090) and

the 96.3-kDa hypothetical protein with an IQ-calmodulin binding domain (*Tb*10.389.0310).
The first one was chosen for further analysis because it was the only protein found in two different experiments, that seemed more specifically selected compared to the dynein heavy chains.
The second was selected for additional studies because it was identified from the mass spectrometry analysis of the high molecular weight band visible from the protein gel of experiment 4 (arrowhead of **Figure 3.6**). Therefore its identification was probably the most reliable. Moreover, since the sensitivity of protein detection from the analysis of a single band is higher compared to the analysis of the whole sample (R. Burchmore, personal communication), it is possible that this hit was missed in the previous selections.

3.8. *Tb*10.389.0310 and *Tb*11.02.2090 RNAi cell lines

*Tb*10.389.0310 and *Tb*11.02.2090 were considered the most interesting hits of the mass spectrometry analysis, and, in order to test whether the proteins were involved in *T. bru*cei differentiation, cell lines were created, which downregulated their expression.
In order to do so, both proteins were cloned into the p2T7 RNAi plasmid, which allows the tetracycline-inducible degradation of the targeted mRNA, and transfected into bloodstream form SMC 16 ("S16") cell lines. Transfectants selected with phleomycin were then tested for the down-regulation of the transcripts and for growth effects upon tetracycline treatment.

For *Tb*10.389.0310 the RNAi was not effective in downregulating the expression level of the gene, on the contrary induced cell possessed higher amounts of *Tb*10.389.0310 transcript, compared to uninduced (**Figure 3.8 A**). Growth capacity of induced *Tb*10.389.0310 RNAi cells was similar to the parental S16 cells (**Figure 3.8 B**). To avoid the possibility of a labeling mistake in the Northern blot, the analysis of the same samples was repeated twice. However, there could have been an error in the labeling of the

samples. Nonetheless, the lack of effect on cell growth (**Figure 3.8 B**) and differentiation (data not shown) ruled out the possibility for *Tb*10.389.0310 to play a role in parasite development to procyclic forms.

For *Tb*11.02.2090 RNAi cell lines, several clones were analysed, of which clone C gave the best knock down. Indeed, *Tb*10.389.0310 clone C RNAi resulted in a 47% downregulation of the transcript, compared to untreated cells, on the first day of induction, which then decreased to 9 % and 32% on the second and third day, respectively (**Figure 3.9**). However, induced *Tb*11.02.2090 RNAi cells showed a level of *Tb*11.02.2090 transcript equal to the parental S16 lines.

Next, the phenotype of induced *Tb*11.02.2090 RNAi cell lines was analysed, which resulted in a marked growth defect, visible from the first day of induction (black dashed line of **Figure 3.10 A**). The tetracycline-treated cells then slowly recovered until reaching untreated level of growth at day four.

Analysed under the microscope, *Tb*11.02.2090 RNAi cells, after 24 hr of tetracycline treatment, showed a small increase in 2K2N cells, from about 13% and 14% of uninduced and parental cells, respectively, to 22.7% of induced RNAi cells (**Figure 3.10 B**). In addition, the same cell line showed a small increase in aberrant cell types ("other" in **Figure 3.10 B**).

These data suggested that *Tb*11.02.2090 might be implicated in *T. brucei* cell cycle control, however more work will be needed to validate these preliminary observations.

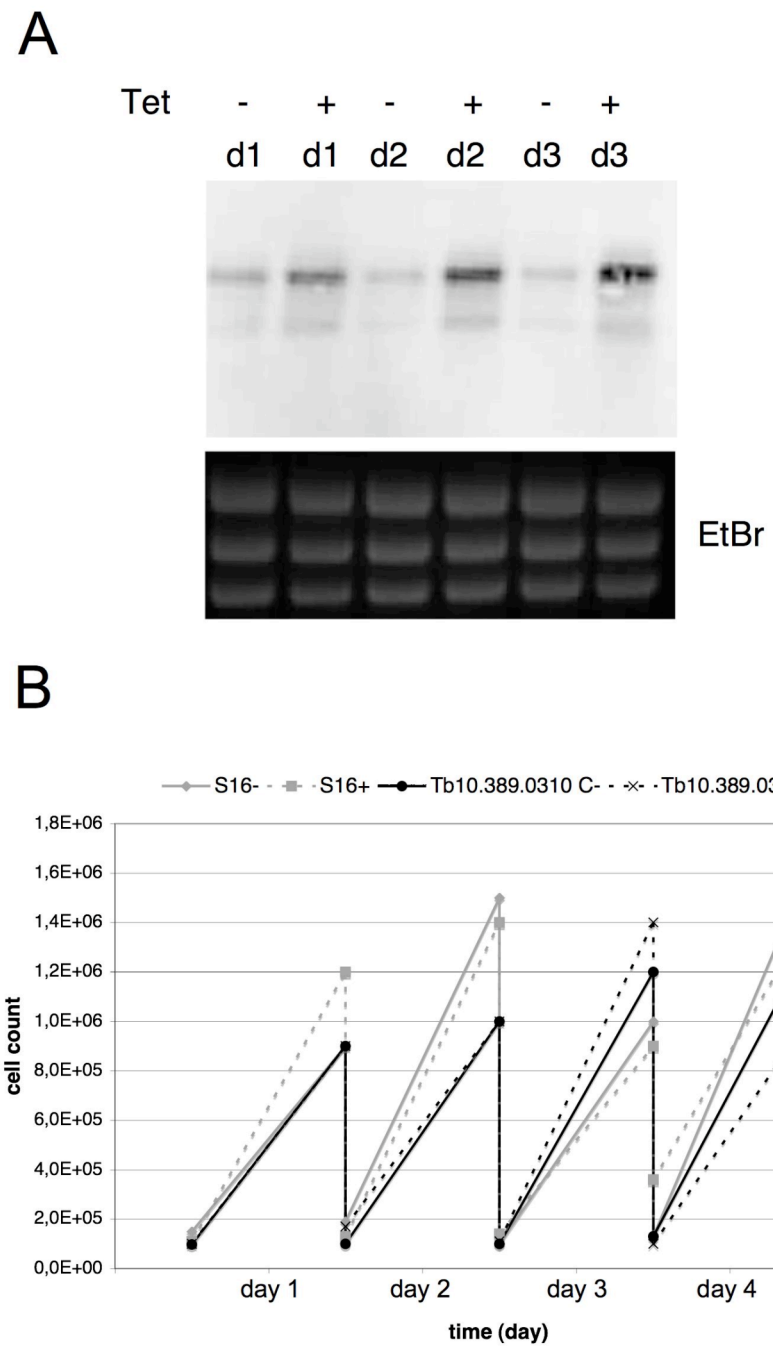

Figure 3.8 Analysis of *Tb*10.389.0310 RNAi cell line: expression and growth. (A) Northern blot analysis of the *Tb*10.389.0310 RNAi cell line C is shown, as one representative of three different cell lines. The levels of *Tb*10.389.0310 transcript, upon tetracycline addition (-/+ tet), to induce the RNAi, is shown for three consecutive days (d1-d3) (upper panel); the corresponding ethidium bromide stain (EtBr) is shown as loading control (lower panel). (B) The growth curves of parental S16 and *Tb*10.389.0310 RNAi lines in absence and presence of tetracycline (-/+ tet) are shown.

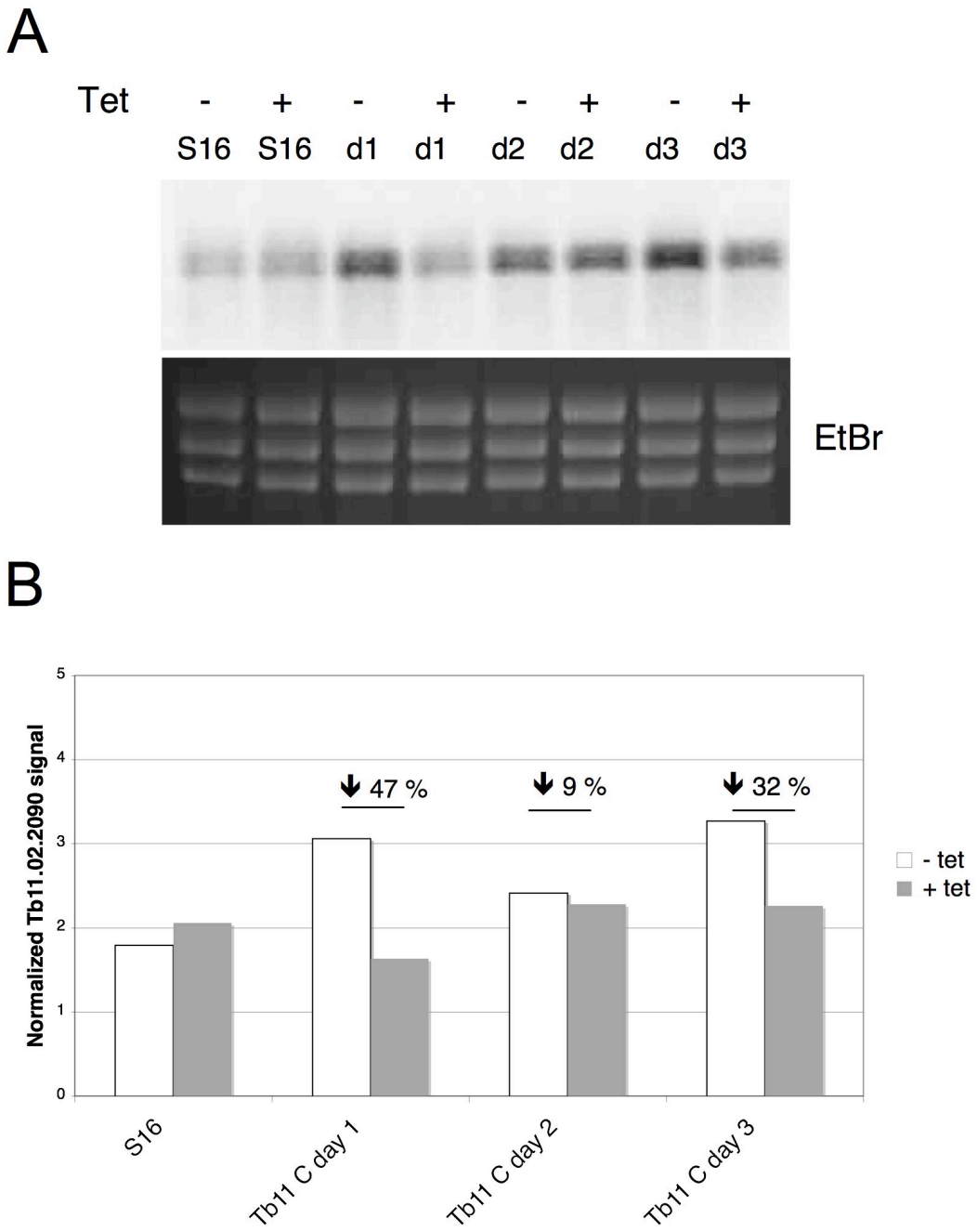

Figure 3.9 Expression of *Tb*11.02.2090 gene in the RNAi cell line C. (A) Northern blot analysis of the *Tb*11.02.1090 RNAi cell line C (Tb11 C) treated or not with tetracycline to induce the RNAi (-/+ tet) for three consecutive days (d1-d3) is shown (upper panel); the corresponding ethidium bromide stain (EtBr), as loading control, is also shown (lower panel). (B) The signal of the *Tb*11.02.2090 probe, normalized to the loading, has been quantified in order to calculate the percentage of *Tb*11.02.2090 transcript downregulation (number indicate percentage of downregulation of induced over uninduced *Tb*11.02.2090 RNAi).

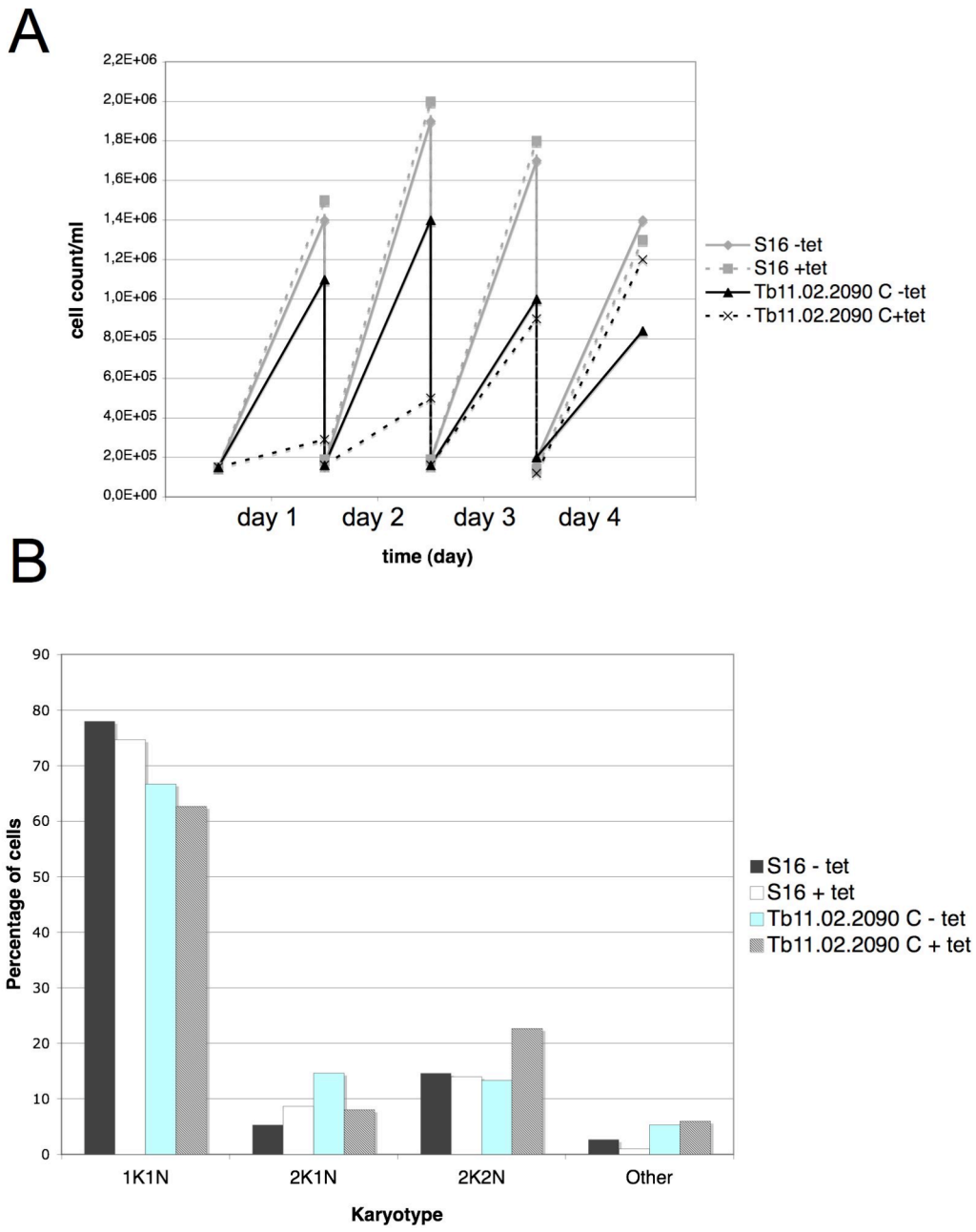

Figure 3.10 *Tb*11.02.2090 RNAi cell growth and cell cycle profile. (A) Growth of clone C of *Tb*11.02.2090 RNAi in absence or presence of tetracycline (-/+ tet) is shown (black lines), together with the parental lines (S16 -/+tet, grey lines). (B) The cell cycle profile (karyotype, determined by microscopy) of the *Tb*11.02.2090 RNAi cell line is shown, 24 hr after addition of tetracycline (Tb11.02.2090 C -/+ tet), and is compared to the karyotype of the parental line (S16 -/+ tet). The cell cycle stages are abbreviated as described in paragraph 1.7 (K: kinetoplast; N: nucleus). A total of 150 cells per cell line were counted.

3.9. Effect of *Tb*11.02.2090 RNAi on differentiation of bloodstream form to procyclic form cells

The role of *Tb*11.02.2090 on differentiation of bloodstream form to procyclic form *T. brucei* was investigated by inducing the RNAi in presence of the cis-aconitate. Specifically, cells were treated with tetracycline for 24 hr and then 6 mM cis-aconitate was added. After 72 hr the expression of the procyclic-specific surface protein EP was measured by flow cytometry to assess the degree of differentiation of the different cell lines (**Figure 3.11**).

Importantly, the cells were also analyzed by immunofluorescence in order to morphologically assess their degree of differentiation. This analysis revealed that 30% of the EP-positive *Tb*11.02.2090 RNAi lines treated with tetracycline and cis-aconitate did not possess procyclic form morphology, but were rounded. It is likely that the rounded cell phenotype was the consequence of the growth defect of the *Tb*11.02.2090 RNAi lines (**Figure 3.9**), exacerbated by the addition of cis-aconitate.

The flow cytometry data, which showed that 18% of the induced cells were EP-positive (versus 4.7% of uninduced cells), was then corrected for the false positives identified by immunofluorescence, thus resulting in 12.6 % of the induced cells showing real differentiation (**Figure 3.11**).

It is not known why the same cell line, in the absence of tetracycline, differentiated less well in response to cis-aconitate (Tb11C + CA, white rectangle of **Figure 3.11**). One possible reason could be the presence of a higher level of *Tb*11.02.20290 transcript in the uninduced RNAi cell lines versus the parental S16 line (**Figure 3.9**). This is more evident, if the change in EP and *Tb*11.02.2090 expression of the RNAi cell lines is compared to the parental lines (**Figure 3.12**). Indeed, the lower level of differentiation observed in the uninduced RNAi cell line could be explained by the higher level of *Tb*11.02.2090 mRNA (compared to parental line), if the protein was a negative regulator of differentiation.

Similarly, when the level of *Tb*11.02.2090 and EP expression is compared within the RNAi line, then *Tb*11.02.2090 also appeared to be a negative regulator of differentiation, as lower expression levels caused increase in EP expression (**Figure 3.12**).

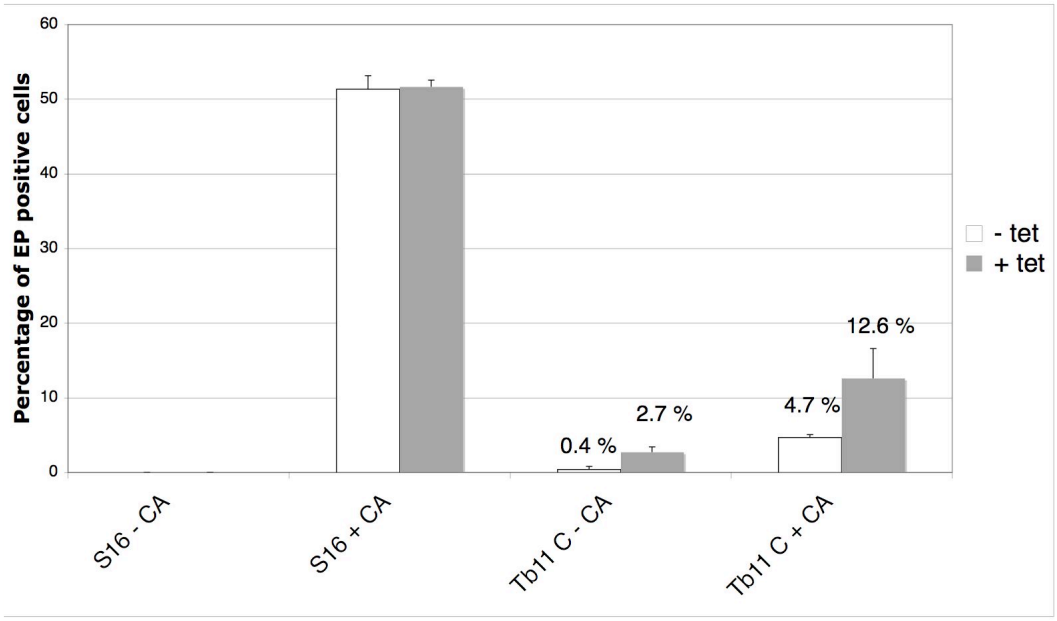

Figure 3.11. Effect of *Tb*11.02.2090 RNAi on differentiation to procyclic form cells. The degree of cellular differentiation to procyclic form in response to 6 mM cis-aconitate (CA) of clone C of *Tb*11.02.2090 RNAi (Tb11C) treated or not with tetracycline (white and grey rectangular), together with the parental cell line (S16) is shown. Differentiation is quantitated by EP protein expression after 72 hr of addition of cis-aconitate, and shown as percentage. Numbers above the histograms indicate the corresponding percentage of EP positive cells. Bars indicate standard deviation for three independent experiments.

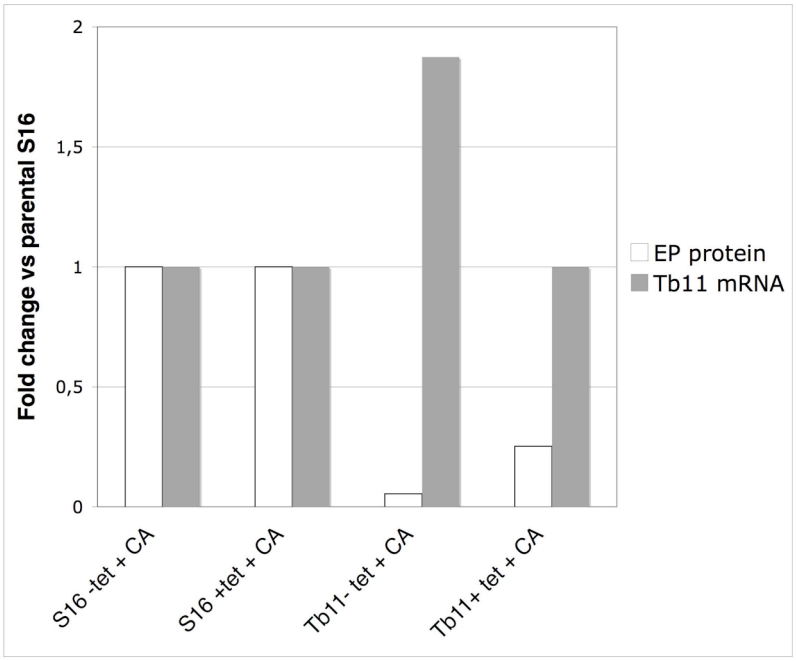

Figure 3.12 Expression of *Tb*11.02.2090 and EP protein in the parental S16 and in the *Tb*11.02.2090 RNAi cell line. The fold change in EP protein expression (EP protein) and *Tb*11.02.2090 mRNA expression (Tb11 mRNA) in the induced and uninduced (-/+ tet), parental (S16) and *Tb*11.02.2090 RNAi lines (Tb11), in presence of 6 mM cis-aconitate (+ CA) is shown.

3.10. Discussion

3.10.1 Comparative analysis of PTP1B and *Tb*PTP1 3-D structure

The analysis of the predicted *Tb*PTP1 3-D structure presented in the first part of this chapter was performed before the crystal structure of the phosphatase was published (Chou *et al.*, 2010). Interestingly, the preliminary observations derived from homology modeling (**Figure 3.1 B**) agree with the conclusions recently reported by Chou *et al*. This is likely due to the fact that the PTP1B template used in the *in silico* modeling is very similar to *Tb*PTP1. Indeed it has been shown that the more similar two sequences are, the closer the corresponding structures are expected and the more reliable the model is going to be (Chothia *et al.*, 1986). However, it has been reported that with a percentage of identity of less than 30%, model quality estimation becomes unreliable, particularly in the presence of large insertions (Bordoli *et al.*, 2009). *Tb*PTP1 shares 24% identity with PTP1B, but all the invariant residues of the PTP motifs (Andersen *et al.*, 2001) are perfectly conserved (**Table 3.1**), thus suggesting that the low degree of identity is mainly due to variations in the sequence connecting the domains. Consequently, the homology model obtained for *Tb*PTP1 is probably more reliable than expected for a 24% identity alignment and confirms the validity of such an *in silico* approach.

The analysis of *Tb*PTP1 3-D prediction showed that the backbone structure is very similar to the one of PTP1B and the trypanosome-specific sequences are found mainly on the surface of the enzyme (**Figure 3.1**). The crystallographic data of Chou *et al*., confirmed these observations by noting that the major differences of the superimposed structures of the parasite enzyme with human PTP1B or PTPRO were loops found on the surface of *Tb*PTP1. These parasite-specific regions were suggested to be involved in substrate recognition and regulation, being mapped at the periphery of the phosphatase, although not giving rise to new structural elements (Chou *et al.*, 2010).

The above observations indicate that a conserved PTP fold extends to distant eukaryotes such as *Trypanosoma brucei*, and that the specificity of function

possessed by these enzymes, in different organisms, is conveyed structurally in ways that do not affect the core conformation, for example by the use of parasite-specific motifs.

3.10.2 *Tb*PTP1 substrate consensus sequence

In addition to the 3-D structure of *Tb*PTP1, the crystallographic analysis highlighted the presence of a continuous electropositive region on the surface of the enzyme (Chou *et al.*, 2010). Since it has been reported that surface properties might account for PTPs substrate specificity (Barr *et al.*, 2009), such an electropositive region of *Tb*PTP1 has been suggested to indicate a preference for electronegative regions of its substrates. This hypothesis seemed to be validated by the fact that both its recently identified substrates, Nopp44/46 (Chou *et al.*, 2010) and *Tb*PIP39 (Szoor *et al.*, 2010), possess some negatively charged residues in the vicinity of the phosphorylated tyrosine (DDEApYDEDD and RTDEpYTKC). Chou *et al.*, supported this hypothesis by analogy with the negatively charged surface of PTP1B and the positively charged region of its substrate, the insulin receptor. However, the authors did not mention the fact that not all the PTP1B substrates possess acidic sequences around the pTyr, such as caveolin (Lee *et al.*, 2006), and the contradictory results reported by other studies were also not analysed (Sarmiento *et al.*, 2000; Vetter *et al.*, 2000; Walchli *et al.*, 2004).

In contrast to the hypothesis proposed by Chou *et al.*, the *Tb*PTP1 substrate consensus analysis reported in this chapter suggested a preference for aliphatic/aromatic residues. This hypothesis was based on the observation that *Tb*PTP1 possesses Leu52 in place of Arg47 of PTP1B (**Figure 3.2**). The presence of an aliphatic amino acid (Leu52) in the parasite phosphatase suggested a possible preference for less charged residues N-terminal to the pTyr, since Arg47 has been shown to represent the major determinant of PTP1B substrate selectivity (Sarmiento *et al.*, 1998).

Of course this second hypothesis is pure speculation, and it is likely that the overall surface charges of the enzyme will influence the interaction of the enzyme with its substrates, but conclusions need to be drawn with caution, as only two *Tb*PTP1 substrates have been identified so far.

The identification of additional substrates will probably reveal whether *Tb*PTP1 selectively targets certain types of residues in the vicinity of the pTyr and might lead to the delineation of a substrate consensus sequence. The data currently available for PTP1B and *Tb*PTP1 does not allow us to use any bioinformatics criteria to identify proteins that would more likely interact with the parasite enzyme.

3.10.3 *Tb*PTP1 substrate trapping mutants

The most widely used method for the characterization of physiological substrates of mammalian PTPs has been the use of substrate-trapping mutant forms of the enzymes (Garton *et al.*, 1996).

Several substrate-trapping mutants exist, which possess a very low enzymatic activity and bind efficiently to their substrates, thereby trapping them in their catalytic pocket (see paragraph 1.15). Among them, the most successful mutant PTP used has been the one possessing an alanine residue in place of the catalytic aspartic acid (D→A mutant) (Blanchetot *et al.*, 2005). However, the addition of a second mutation targeting the Q loop (Q→A), in the D→A mutant, has been shown to improve the substrate-binding capability of PTP1B (Laiping *et al.*, 2001) and SHP2 (Kontaridis *et al.*, 2004). Therefore the same approach was employed for *Tb*PTP1, and the Q→A mutation was introduced in the single D199A mutant, already in use in the lab (**Figure 3.4, A**). In parallel, the C229S/D275Q was also created, as negative control (**Figure 3.4**, **A**).

According to results published for PTP1B (Laiping *et al.*, 2001) the C→S/D→Q *Tb*PTP1 mutant was not a good substrate trapping enzyme (**Figure 3.4 B**). In contrast, the D199A/Q275A *Tb*PTP1 was found to trap several pTyr-containing proteins but not significantly better than the D199A enzyme (**Figure 3.4 B**), which was unexpected compared to what was reported for PTP1B (Laiping *et al.*, 2001). It is possible that other enzyme-specific factors contribute to such a difference, as it has been postulated for other PTPs. For example, the C→S mutant was shown to be a better substrate trapping mutant than the D→A for RPTPα (Blanchetot *et al.*, 2002) and SHP2

(Persson *et al.*, 2004), conversely to what was reported for most other enzymes. The exact reason for these differences is not known, but it has been suggested that the variable sensitivity to oxidation of the catalytic Cys, during the experimental procedure, might sometimes be the cause (Blanchetot *et al.*, 2005).

3.10.4 *Tb*PIP39 selection by the *Tb*PTP1 mutants

The different *Tb*PTP1 mutants were then used in a *in vitro* substrate trapping experiments, which possess the advantages of being easily up-scalable and usable in conjunction to mass spectrometry analysis. This approach was successfully used for the initial identification of *Tb*PIP39 (performed before the start of this project), which was then visualized by using the anti-*Tb*PIP39 antibody (**Figure 3.6**). Differences were noted in the substrate trapping abilities of the C229S/D199A *Tb*PTP1 between the amounts of tyrosine phosphorylated proteins detected (**Figure 3.5 B**) and the quantity of *Tb*PIP39 bound (**Figure 3.6 A**). This difference could be due to a more limited sensitivity of the anti phosphorylated tyrosine antibody compared to the anti *Tb*PIP39 antibody.

Another interesting observation was the fact that the *Tb*PTP1 wild type enzyme showed to bind *Tb*PIP39, under certain experimental conditions, such as in larger scale selections (**Figure 3.6 B**) and in immune-precipitations (Szoor *et al.*, 2010). The fact that the wild type *Tb*PTP1 interacts with *Tb*PIP39 in a manner stable enough for the substrate to be visualized *in vitro* or *in vivo*, has been noticed for other PTPs, suggesting that some phosphatases need to interact with the substrates through protein-protein domain prior to their dephosphorylation (Blanchetot *et al.*, 2005).

3.10.5 Mass spectrometry analysis

The mass spectrometry analysis carried out on the proteins selectively bound to the substrate trapping D199A *Tb*PTP1, identified a total of eight hits for

the four different large scale selections performed on stumpy cell extracts (**Table 3.3**).

In the first two selections (experiment 1 and 2 of **Table 3.3**) four hits were found in both experiments, which were carried out before the start of this project. Among these four hits, one was the already characterized CTD phosphatase (*Tb*PIP39) (Szoor *et al.*, 2010) and two were large dynein heavy chains, which were considered likely contaminants, although never detected in the negative controls (beads alone incubated with cell extract). The fourth hit, a hypothetical protein containing one HEAT repeat (*Tb*11.02.20290), was considered more interesting, as these repeats are involved in protein-protein interactions (Andrade *et al.*, 1995) .

In the other two selection experiments (experiments 3 and 4 of **Table 3.3**), four hits were identified, none of which were found in the previous selections. This variability was also detected in the negative controls, indeed no common hits among the four selections were found in the beads alone incubated with cell extract.

By comparing pairs of selections, the percentage of shared hits in the negative controls varied from 0 % (exp.4 and 1), to 10 % (exp. 1 and 2) and raised to a maximum of 55% (exp. 4 and 2). This variability could have been caused by the experimental set-up, although the same protocol for cell lysis and selection was used. In addition, the BZ3 treament of stumpy form cells that preceded protein extraction might also have been the cause of part of this variability. Similarly, the purity of the different batches of recombinant proteins employed was also likely to have played a role. Moreover, the biological variability always needs to be taken into account, for example the conditions of the cells might have differed between experiments. Consequently, it is maybe not surprising that no protein was found in all four or three of the selections.

In selection 3 and 4, the only hit that was considered of interest was a hypothetical protein (*Tb*10.389.0310) possessing an IQ-calmodulin binding domain and thus potentially involved in signalling.

3.10.6 *Tb*10.389.0310 and *Tb*11.02.2090

In order to characterize the potential roles played by *Tb*10.389.0310 and *Tb*11.02.2090 in the *Tb*PTP1 differentiation pathway, cell lines knocking down the two hits were created.

As quantified by Northern blot analysis, *Tb*10.389.0310 RNAi lines showed an increase in *Tb*10.389.0310 mRNA levels, which had no effect on their growth kinetics (**Figure 3.8)** or differentiation capability (data not shown). Therefore, a possible role for this protein and in *T. brucei* development can be excluded.

In contrast to this, *Tb*11.02.2090 expression was decreased of 47% upon induction of the RNAi for 24 hr in the cell line C (**Figure 3.8**). This level of downregulation was then lost on the second and third day of induction, likely due to a very high selection pressure on the treated cells. Indeed, a severe growth defect was observed in the same cell line as early as 24 hr of tetracycline treatment (**Figure 3.10 A**). These cells did not appear to present any other major morphological abnormality.

In addition, 24-hr induced *Tb*11.02.2090 RNAi cells showed a small increase in 2K2N (M phase cells) and aberrant cells (**Figure 3.10 B**), thus suggesting that *Tb*11.02.2090 might be involved in cell cycle control, directly or indirectly. Specifically *Tb*11.01.2090 could act by inhibiting S or G2 phase, which precede M phase, or by inducing cell division, that follows M phase.

Furthermore, cells expressing lower levels of *Tb*11.02.2090 transcript showed an increase in differentiation capacity (from 2.7% to 12.6 %), as judged by cell morphology and EP expression (**Figure 3.11**), thus suggesting that it might negatively regulate this life cycle transition.

From the above data, it could be hypothesized that *Tb*11.02.2090 might be important for cell division to occur, thus required for cell growth. Therefore, by inhibiting entry into G0/G1, *Tb*11.02.2090 could negatively regulate initiation of differentiation to procyclic forms. Consequently, the action of this hypothetical protein would need to be inhibited for differentiation to occur, potentially through its increased phosphorylation level caused by decreased *Tb*PTP1 activity (**Figure 3.13**).

In order to validate the potential role of *Tb*11.02.2090 during differentiation and as *Tb*PTP1 substrates, further work will be needed. First of all it would be important to confirm the reproducibility and to better characterize the cell cycle and differentiation phenotypes observed upon induction of *Tb*11.02.2090 RNAi. In addition, the interaction between *Tb*11.02.2090 and *Tb*PTP1 would need to be validated, similarly to what done for *Tb*PIP39, by generation of an antibody and by verification of its selection by *Tb*PTP1.

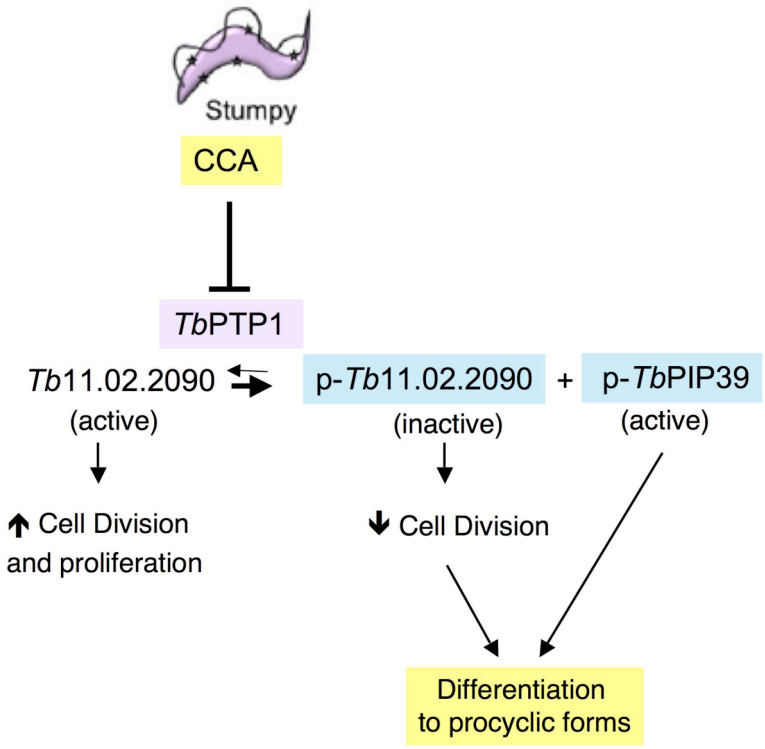

Figure 3.13. Model of the potential role of *Tb*11.02.2090 during differentiation from stumpy to procyclic form cells. Upon citrate/cis-aconitate (CCA) treatment of stumpy form cells, the inhibition of *Tb*PTP1 would cause the increased phosphorylation of the negative regulator of differentiation *Tb*11.02.2090. This would render *Tb*11.02.2090 inactive, thereby ceasing cell division and, together with the action of other downstream effectors (such as *Tb*PIP39), induce parasite differentiation to procyclic form cells.

Chapter 4

Dissection of *Tb*PTP1 signalling pathway during differentiation from stumpy to procyclic forms

4.1. Introduction

As mentioned in paragraph 1.17, the downstream effector and substrate of *Tb*PTP1 has recently been identified as a glycosomal phosphatase, *Tb*PIP39 (Szoor *et al.*, 2010), and a model has been proposed whereby citrate/cis-aconitate (CCA) would be transported into the cells via PAD expression (Dean *et al.*, 2009) causing *Tb*PTP1 inhibition and increasing the level of phosphorylated *Tb*PIP39, thus promoting the differentiation to procyclic forms (**Figure 4.1**). *Tb*PTP1 activity has been shown to significantly increase in the presence of *Tb*PIP39 and the addition of CCA have been shown to prevent such activation *in vitro*, potentially disrupting their interaction through the binding to the *Tb*PIP39 citrate-binding pocket (Szoor *et al.*, 2010). This part of the project aimed at investigating other potential mechanisms of *Tb*PTP1 regulation during parasite differentiation.

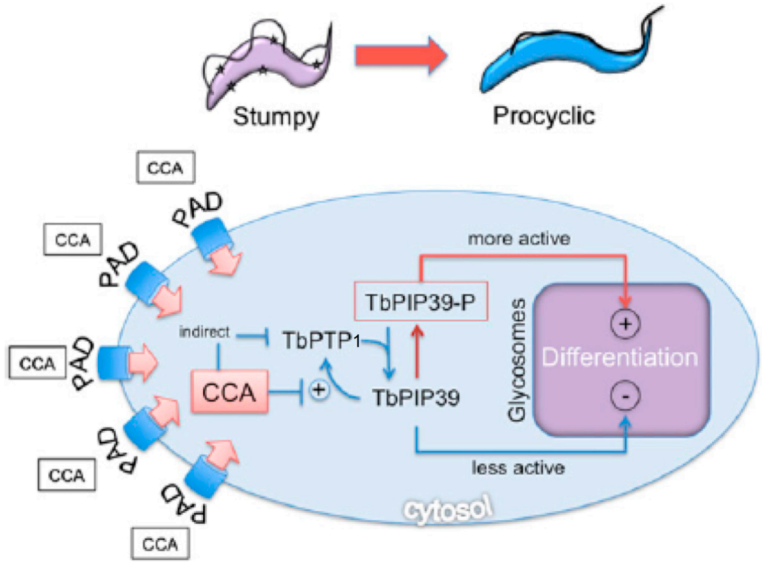

Figure 4. 1 Model of the *Tb*PTP1-*Tb*PIP39 pathway during differentiation from stumpy to procyclic forms (from Szoor *et al.*, 2010). Citrate/cis-aconitate (CCA) is imported into stumpy form cells via PAD proteins (PAD); intracellular CCA inhibits the activation of *Tb*PTP1 by *Tb*PIP39 directly, but other indirect ways of *Tb*PTP1 inactivation cannot be excluded. Upon *Tb*PTP1 inactivation, the level of phosphorylated *Tb*PIP39 would increase, which would promote differentiation to procyclic forms by acting on the glycosomes, through a yet uncharacterized mechanism.

4.2. Comparative analysis of *Tb*PTP1 mechanisms of regulation

4.2.1 Post-transcriptional regulation

In higher eukaryotes, the targeted and temporally modulated activity of PTPs is obtained through different levels of regulation, from post-transcriptional to post-translational (Bourdeau *et al.*, 2005).
In the case of PTP1B, one level of regulation is represented by alternative splicing, which produces two variants with slightly different C-terminal domains and whose quantities are controlled by growth factors and insulin (Shifrin *et al.*, 1993; Sell *et al.*, 1999). In *Trypanosoma brucei* only two genes have been shown to contain introns (Mair *et al.*, 2000; Berriman *et al.*, 2005), but there is growing evidence for the existence of differentially trans-spliced transcripts (Siegel *et al.*, 2010), therefore the potential regulation of *Tb*PTP1 by this mechanism cannot be excluded.

4.2.2 Post-translational regulation: proteolysis and differential targeting

In addition to post-transcriptional regulation, PTP1B is subjected to different post-translational modifications, such as proteolysis, phosphorylation, sumoylation and oxidation.
Proteolytic cleavage of PTP1B by calpains has been shown to generate a truncated form of the enzyme, lacking the 65-75 C-terminal residues, which is associated with enhanced enzyme activity, due to the loss of the C-terminal negative regulatory domain (Frangioni *et al.*, 1993).
The C-terminal domain of PTP1B is not present in *Tb*PTP1 and the final M10 domain is followed only by a short trypanosome-specific motif (T4) (see paragraph 1.17). The sequence of T4 is not predicted to be an Arg/Lys cleavage site, as assessed by using the ProP online programme (Duckert *et al.*, 2004), however aa 135-152 of *Tb*PTP1 have been identified as a PEST domain using the prediction programme Mobyle@Pasteur (http://mobyle.pasteur.fr) (Szoor *et al.*, 2006). The PEST motif is a region rich in Pro, Glu/Asp, Ser/Thr and flanked by Arg/Lys, which has been shown to be a high affinity substrate for calpains (Siman *et al.*, 1989). In addition, it is

interesting to note that some *Trypanosoma brucei* calpains are stage regulated during the parasite life cycle (Liu *et al.*, 2010).

The accessibility of PTP1B to its substrates is regulated in a spatial and temporal manner also by means of its 35 C-terminal residues, that are responsible for targeting the enzyme to the cytoplasmic face of the ER (Frangioni *et al.*, 1992). *Tb*PTP1 does not possess any recognizable targeting domain and cellular fractionation experiments have shown that the phosphatase is present mainly in the cytoskeletal fraction in slender, stumpy and procyclic form cells (Szoor *et al.*, 2006; McElhinney, 2007).

4.2.3 Post-translational regulation: phosphorylation

A more complex level of PTP1B regulation occurs via phosphorylation of five Ser and three Tyr residues, which have been shown to often affect enzyme activity in a cell and growth factor-specific manner. For example, Ser50 phosphorylation by AKT/PKB has been reported to decrease enzyme activity upon insulin stimulation (Ravichandran *et al.*, 2001); the same residue, together with Ser242 and 243, have been shown to be targeted by CLK1 and 2, with Ser50 being the main residue phosphorylated and causing a 2-fold increase in PTP1B activity (Moeslein *et al.*, 1999). In murine fat and skeletal muscle cells, insulin stimulation was also required for PTP1B Ser352 phosphorylation by PKA to occur, which resulted in an increased enzymatic activity (Ravichandran *et al.*, 2001; Tao *et al.*, 2001). In addition to insulin, the cell cycle position has been shown to affect PTP1B Ser phosphorylation, specifically transition from G2 to M phase has been linked to increased phosphorylation of Ser352 and Ser386 (Flint *et al.*, 1993).

Three Tyr residues have also been shown to be phosphorylated: Tyr66, Tyr152 and Tyr153 of PTP1B have been identified as *in vivo* substrates of the insulin receptor and shown to cause a 38-fold increase activity; moreover, these Tyr residues were dephosphorylated by PTP1B *in vitro*, and thus the possibility of the enzyme to auto-dephosphorylate itself has been suggested, as a way to modulate its activity upon insulin stimulation (Dadke *et al.*, 2001).

Among all the PTP1B phosphorylation sites mentioned above, *Tb*PTP1 shares only Tyr66 and Tyr152 (Tyr78 and Tyr164 of *Tb*PTP1) (**Figure 4.2**) and possesses Thr257 in place of Ser242 of the human phosphatase. Tyr78 and Tyr164 are conserved among trypanosomes (*T. congolense*, *T. vivax* and *T. cruzi*) but not in *Leishmania major*, whereas Thr257 is conserved only between *T. brucei* and *T. cruzi* (**Figure 4.2 A**). A bioinformatics analysis using three different prediction programmes (GPS (Xue *et al.*, 2005), NetPhos 2.0 (Blom *et al.*, 1999) and ScanSite (Obenauer *et al.*, 2003)) identified four potential phosphorylated residues of *Tb*PTP1 conserved among trypanosomes (Ser42, Thr238, Tyr280 and Tyr284) but it did not identify residues Tyr78, Tyr164 and Thr257 as possible phosphorylation sites. Of the four predicted *Tb*PTP1 phosphorylation sites two (Thr238 and Tyr284) are conserved in PTP1B, but there is no report of their phosphorylation in the literature; the other two predicted phosphorylation sites (Tyr280 and Ser42) are not conserved in the human homolog, and Ser42 is found in the trypanosome-specific motif PcT2. Since it is difficult to predict which sites of *Tb*PTP1 might be phosphorylated from the analysis of the primary sequence, the residues were also mapped on the 3-D model of the enzyme (**Figure 4.3**). Most of the phosphorylated PTP1B residues are found on the surface of the enzyme, with the exception of Ser242 and 243, which have been shown to be less preferred than Ser50 by CLK1 and 2 (Moeslein *et al.*, 1999); among the seven potential *Tb*PTP1 phosphorylation sites, three (Ser42, Tyr78 and Tyr164) are found on the surface of the enzyme, and thus might be more likely targets of kinases (**Figure 4.3**).

A

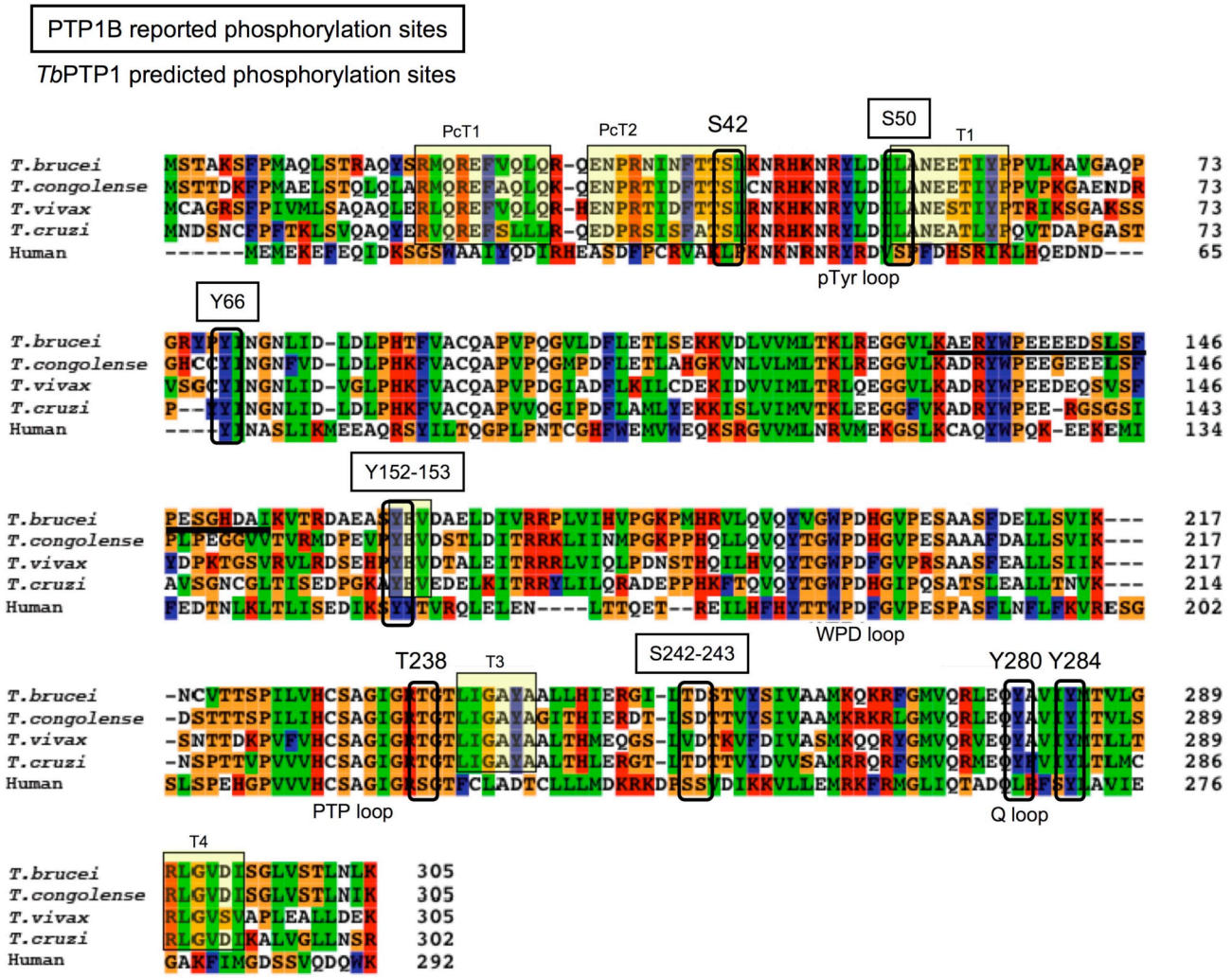
PTP1B reported phosphorylation sites
TbPTP1 predicted phosphorylation sites
PcT1
PcT2
S42
S50
T1
pTyr loop
Y66
Y152-153
WPD loop
T238
T3
S242-243
Y280 Y284
PTP loop
Q loop
T4
T.brucei
T.congolense
T.vivax
T.cruzi
Human

B

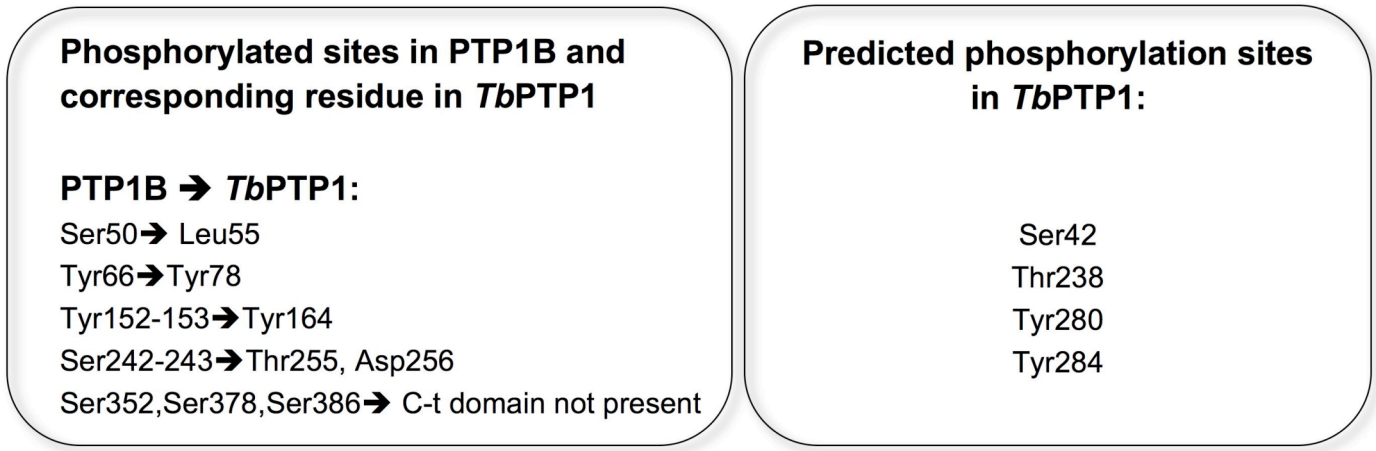

Figure 4.2. Comparative analysis of human PTP1B and *Tb*PTP1 phosphorylation sites. (A) Primary sequence alignment of *Tb*PTP1, *Tc*PTP1 and human PTP1B (modified from Szoor *et al*., 2006): residues experimentally shown to be phosphorylated in human PTP1B are highlighted above the alignment (rectangles) and residues predicted to be phosphorylated in *Tb*PTP1 are also indicated. In addition, the location the trypanosome-specific motifs (PcT1, PcT2, T1-T4) are underlined by yellow boxes, and the important catalytic motifs (pTyr, WPD, PTP and Q loops) are labeled below the alignment. (B) The list of the sites is shown in the diagram following the alignment. Accession numbers are Tb10.70.007 (*T. brucei Tb*PTP1), Tc00.1047053510187.234 (T. *congolense*), Tviv1180b04.p1k (T. *vivax*), Tc00.1047053508717 (*T. cruzi*), and NP_002818.1 (human PTP1B). The sequenced were aligned using ClustalW (Thompson *et al*., 1994) and visualized using BOXSHADE .

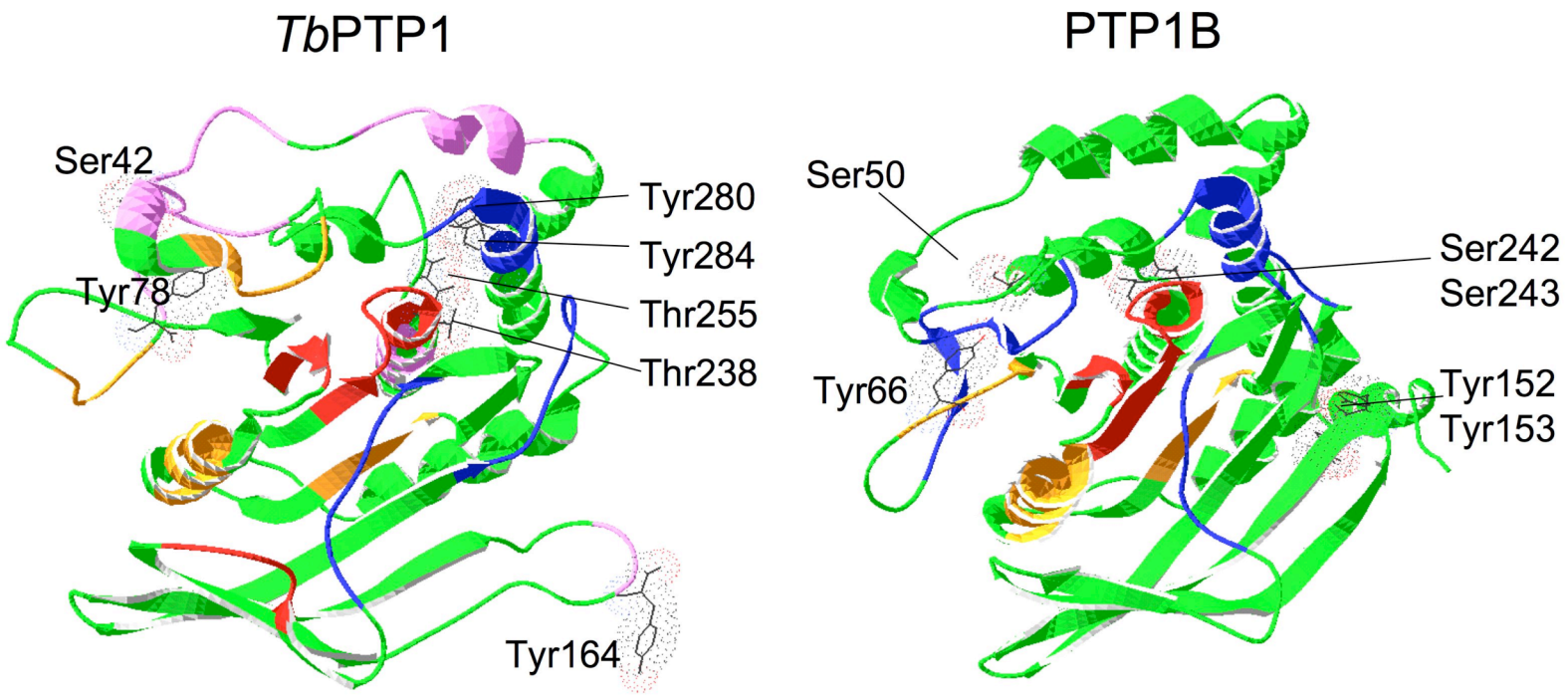

Figure 4.3. Comparative analysis of the locations of *Tb*PTP1 and PTP1B phosphorylation sites. The residues corresponding to PTP1B phosphorylated sites (Tyr78, Tyr164 and Thr255) are shown on the *Tb*PTP1 model, together with the four phosphorylation sites predicted using bioinformatics programmes (Ser42, Thr238, Tyr280 and Tyr284) listed in Figure 3.2 B, are mapped on the 3-D models of the two enzymes (predicted by Swiss Model server and visualized using Swiss pdb-Viewer (Arnold *et al.*, 2006)).

4.2.4 Experimental analysis of *Tb*PTP1 phosphorylation

Preliminary experiments in bloodstream form 427 cells over-expressing wild type *Tb*PTP1, suggested that the protein did not seem to be Tyr-phosphorylated after cis-aconitate treatment (**Figure 4.4**). Cells were induced to overexpress TY-tagged *Tb*PTP1 by addition of tetracycline for 24 hr, then they were treated with 6 mM cis-aconitate for a further 48 hr. Immunoprecipitated *Tb*PTP1 in presence or absence of cis-aconitate treatment was then subjected to Western blot analysis and the samples were probed with antibody anti TY-tag to determined the level of *Tb*PTP1 immune-precipitation and with antibody anti phosphorylated Tyr residues (pTyr) in order to detect potential enzyme phosphorylation (**Figure 4.4 A**).
Although the efficiency of the immune-precipitation was low, as only very faint bands were visible in the anti TY-tag Western blot (**Figure 4.4 A**, arrowheads at around 34 kDa), such bands were specifically blocked in presence of the TY peptide (**Figure 4.4 B**, arrowheads). The anti pTyr Western blot showed a weak band co-migrating with immune-precipitated *Tb*PTP1 (**Figure 4.4 A**, arrows) but this was not obviously blocked in the presence of the TY peptide (**Figure 4.4 B**, arrows), although the signal was somewhat obscured by the highly abundant 20-kDa protein G sepharose used to immunoprecipitate the antibody. Consequently, the pTyr positive band immunoprecipitated with *Tb*PTP1 must represent some other protein that non-specifically bound the beads and not *Tb*PTP1.

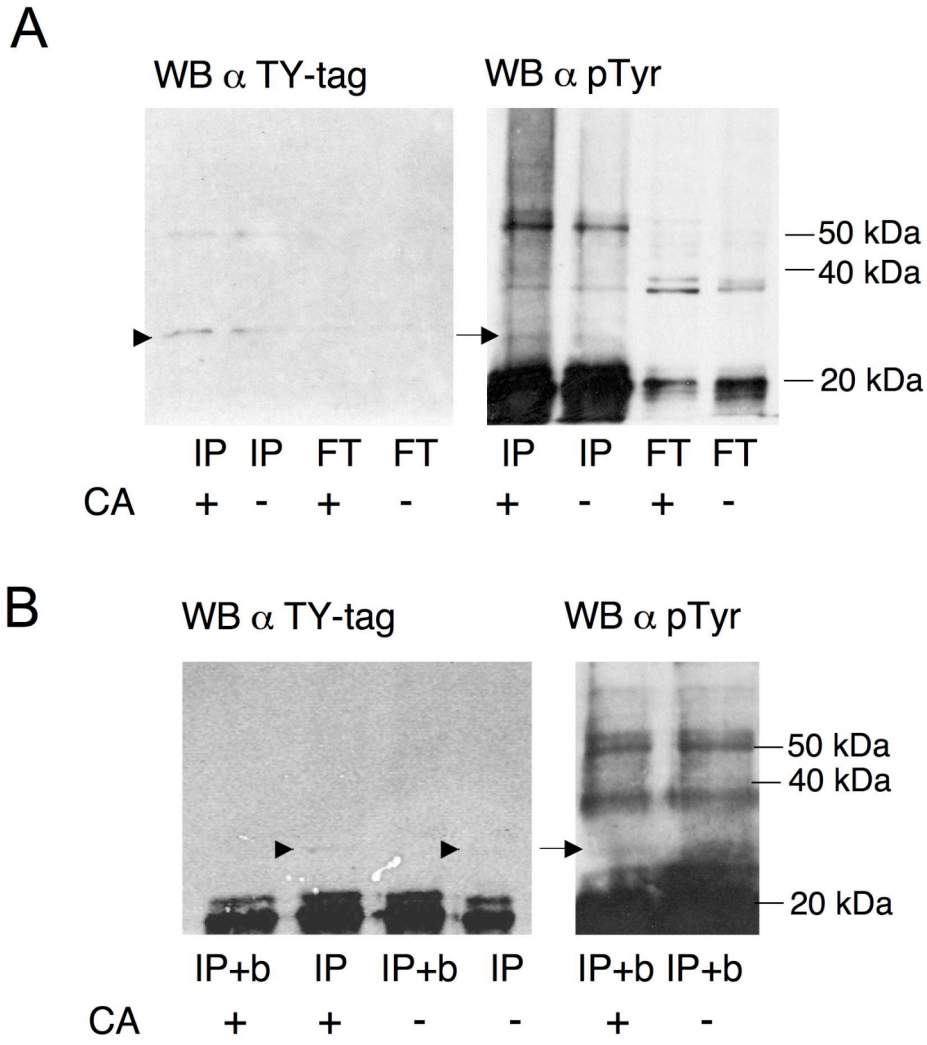

Figure 4.4 Detection of potential tyrosine-phosphorylated *Tb*PTP1 in presence or absence of cis-aconitate treatment (CA). (A) Western blot (WB) analysis of immunoprecipitated *Tb*PTP1 (IP) and flow-through after immuneorecipitation (FT) probed with anti TY-tag antibody (α TY-tag) and anti phosphorylated Tyr antibody (α pTyr). (B) Western blot analysis of the same experiment as in A, showing samples of the immunoprecipitation performed in presence of the blocking peptide (IP+b), specific for the TY-tag. Bands corresponding to immunoprecipitated TY-tagged *Tb*PTP1 are highlighted (arrowheads, about 34 kDa), together with a co-migrating pTyr-positive band (arrows). The molecular weight markers are shown on the right-hand side in kDa; eluted protein G is visible on the blot following immunoprecipitation (dark thick band at around 20 kDa), together with light and heavy Ig chains (about 20 and 55 kDa, respectively). Western blots were all exposed for 5-20 min, except the A left panel, which was exposed overnight.

4.2.5 Post-translational modification: sumoylation

In addition to protein phosphorylation, sumoylation has also been implicated in PTP1B regulation, specifically addition of small ubiquitin-like modifier (SUMO) on Lys335 and Lys347 has been shown to transiently inhibit the enzyme activity *in vivo* (Dadke *et al.*, 2007). The precise mechanism of PTP1B regulation by sumoylation has not been characterized, but it has been suggested that such modification might block or alter the catalytic domain of the enzyme (Dadke *et al.*, 2007).

In *T. brucei* only one recent study has been conducted to elucidate the role of sumoylation (Liao *et al.*, 2010), which revealed the existence of a SUMO homolog in *T. brucei* (*Tb*SUMO) and showed that *Tb*SUMO is essential for the completion of mitosis in procyclic forms. The observation that sumoylation is important in the cell cycle regulation is potentially interesting, as *T. brucei* cell cycle is intrinsically linked to its differentiation (see paragraph 1.7).

The comparative analysis of the residues sumoylated in PTP1B (Lys335 and Lys347) showed that none of them is conserved in *Tb*PTP1, indeed they are found in the C-terminal domain that is not present in *Tb*PTP1 (**Figure 4.5 A**). A bioinformatic prediction of sumoylation sites, using SUMOsp 2.0 (Ren *et al.*, 2009), identified Lys131 (L-K-A-E) of the parasite enzyme, as potentially sumoylated, according to the consensus sequence: Ψ-K-X-E (Ψ=A/I/L/M/P/F/V; X is any aa). Lys131 is conserved in PTP1B (Lys121) but is not found within a consensus sequence, as the Gln residue, at position +2 to the Lys residue, is substituted by Ala (L-K-C-A). Such observation could suggest that Lys131 might be sumoylated in *Tb*PTP1 and not in PTP1B. However, Lys 131 is located within the core of *Tb*PTP1 (K131 in **Figure 4.5 B**), in contrast, Lys335 and Lys347 of PTP1B are found in the C-terminal domain of the enzyme, and thus are probably more accessible to SUMO-conjugating enzymes.

A

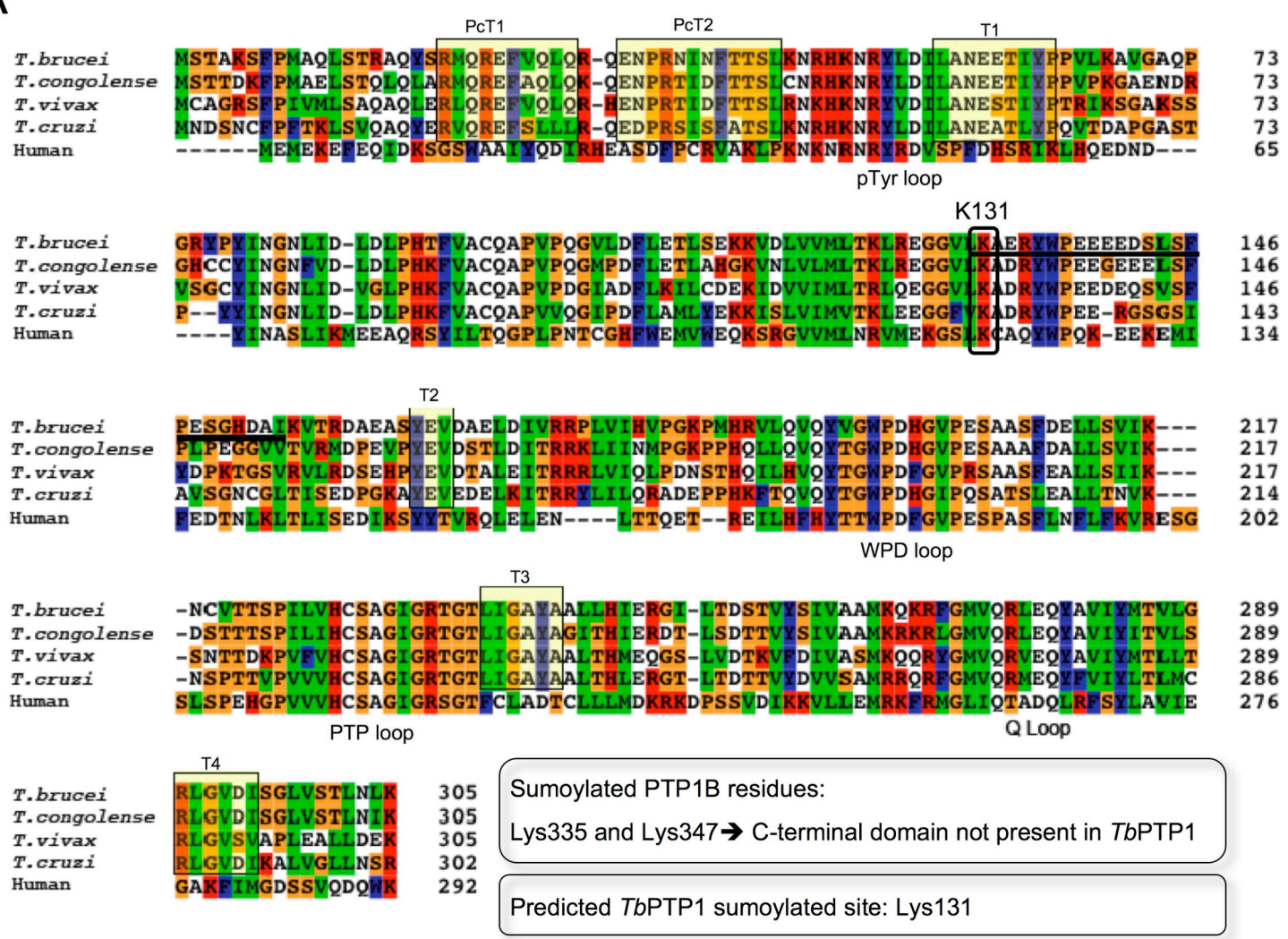
PcT1
PcT2
T1
T. brucei MSTAKSFPMAQLSTRAQYSRMQREFVQLQR-QENPRNINFTTSLKNRHKNRYLDILANEETIYPPVLKAVGAQP 73
T. congolense MSTTDKFPMAELSTQLQLARMQREFAQLQK-QENPRTIDFTTSLCNRHKNRYLDILANEETIYPPVPKGAENDR 73
T. vivax MCAGRSFPIVMLSAQAQLERLQREFVQLQR-HENPRTIDFTTSLRNKHKNRYVDILANESTIYPTRIKSGAKSS 73
T. cruzi MNDSNCFPFTKLSVQAQYERVQREFSLLLR-QEDPRSISFATSLKNRHKNRYLDILANEATLYPQVTDAPGAST 73
Human ------MEMEKEFEQIDKSGSWAAIYQDIRHEASDFPCRVAKLPKNKNRNRYRDVSPFDHSRIKLHQEDND--- 65
pTyr loop
K131
T. brucei GRYPYINGNLID-LDLPHTFVACQAPVPQGVLDFLETLSEKKVDLVVMLTKLREGGVLKAERYWPEEEEDSLSF 146
T. congolense GHCCYINGNFVD-LDLPHKFVACQAPVPQGMPDFLETLAHGKVNLVLMLTKLREGGVLKADRYWPEEGEEELSF 146
T. vivax VSGCYINGNLID-VGLPHKFVACQAPVPDGIADFLKILCDEKIDVVIMLTRLQEGGVLKADRYWPEEDEQSVSF 146
T. cruzi P--YYINGNLID-LDLPHKFVACQAPVVQGIPDFLAMLYEKKISLVIMVTKLEEGGFVKADRYWPEE-RGSGSI 143
Human ----YINASLIKMEEAQRSYILTQGPLPNTCGHFWEMVWEQKSRGVVMLNRVMEKGSLKCAQYWPQK-EEKEMI 134
T2
T. brucei PESGHDAIKVTRDAEASYEVDAELDIVRRPLVIHVPGKPMHRVLQVQYVGWPDHGVPESAASFDELLSVIK--- 217
T. congolense PLPEGGVVTVRMDPEVPYEVDSTLDITRRKLIINMPGKPPHQLLQVQYTGWPDHGVPESAAAFDALLSVIK--- 217
T. vivax YDPKTGSVRVLRDSEHPYEVDTALEITRRRLVIQLPDNSTHQILHVQYTGWPDFGVPRSAASFEALLSIIK--- 217
T. cruzi AVSGNCGLTISEDPGKAYEVEDELKITRRYLILQRADEPPHKFTQVQYTGWPDHGIPQSATSLEALLTNVK--- 214
Human FEDTNLKLTLISEDIKSYYTVRQLELEN----LTTQET--REILHFHYTTWPDFGVPESPASFLNFLFKVRESG 202
WPD loop
T3
T. brucei -NCVTTSPILVHCSAGIGRTGTLIGAYAALLHIERGI-LTDSTVYSIVAAMKQKRFGMVQRLEQYAVIYMTVLG 289
T. congolense -DSTTTSPILIHCSAGIGRTGTLIGAYAGITHIERDT-LSDTTVYSIVAAMKRKRLGMVQRLEQYAVIYITVLS 289
T. vivax -SNTTDKPVFVHCSAGIGRTGTLIGAYAALTHMEQGS-LVDTKVFDIVASMKQQRYGMVQRVEQYAVIYMTLLT 289
T. cruzi -NSPTTVPVVVHCSAGIGRTGTLIGAYAALTHLERGT-LTDTTVYDVVSAMRRQRFGMVQRMEQYFVIYLTLMC 286
Human SLSPEHGPVVVHCSAGIGRSGTFCLADTCLLLMDKRKDPSSVDIKKVLLEMRKFRMGLIQTADQLRFSYLAVIE 276
PTP loop
Q Loop
T4
T. brucei RLGVDISGLVSTLNLK 305
T. congolense RLGVDISGLVSTLNIK 305
T. vivax RLGVSVAPLEALLDEK 305
T. cruzi RLGVDIKALVGLLNSR 302
Human GAKFIMGDSSVQDQWK 292
Sumoylated PTP1B residues:
Lys335 and Lys347➔ C-terminal domain not present in TbPTP1
Predicted TbPTP1 sumoylated site: Lys131

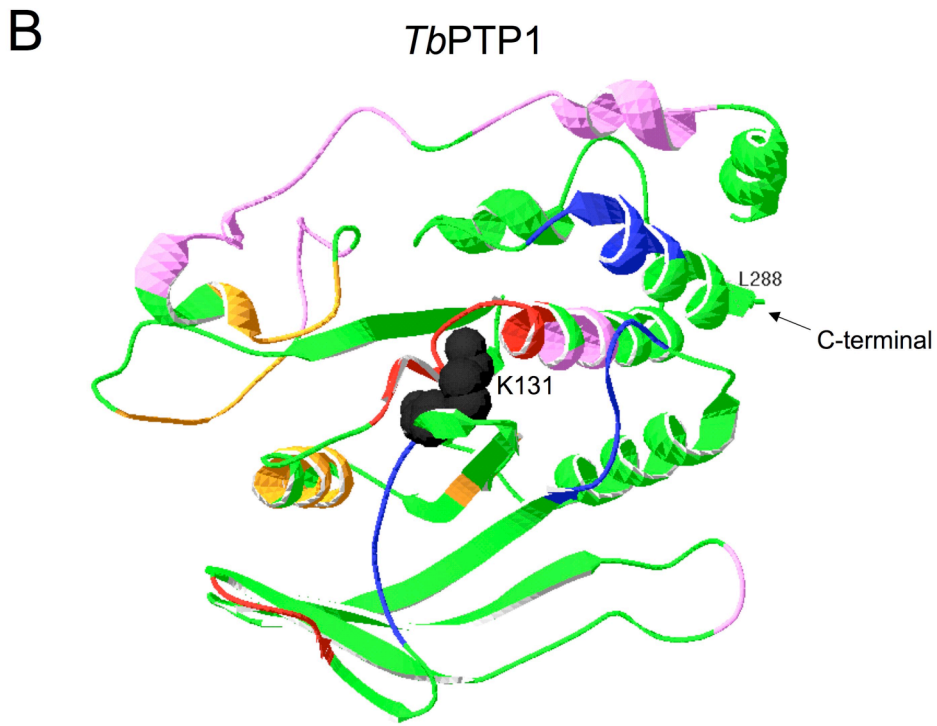

Figure 4.5 Comparative analysis of PTP1B and *Tb*PTP1 sumoylation. (A) The alignment of *T. brucei Tb*PTP1, *T. congolense*, *T. vivax*, *T. cruzi* and human PTP1B (Human) homologues is shown, with the residue predicted in to be sumoylated in *Tb*PTP1 (K131) highlighted. A summary diagram is shown underneath the alignment. Protein accession numbers and the alignment software used are the same as in Figure 3.2. (B) The location of the potentially sumoylated K131 is shown in the 3D model of *Tb*PTP1 (B); the C-terminal *Tb*PTP1 residue included in the model is highlighted (L288) to show the approximate location of the PTP1B sumoylation sites.

4.3. The role of reactive oxygen species (ROS) during differentiation to procyclic form

In addition to proteolysis, phosphorylation and sumoylation, oxidation has been characterized as a physiological mechanism to regulate the activity of several mammalian PTPs *in vivo* (Monteiro *et al.*, 1996; Denu *et al.*, 1998). According to the work carried out for PTP1B, an intracellular oxidase would be activated in a ligand-dependent manner, causing a localized increase in intracellular reactive oxygen species (ROS), which would oxidize the catalytic Cys of the phosphatase, thus resulting in its reversible inactivation (Tonks, 2003).

The possibility of *Tb*PTP1 to be regulated via oxidation was particularly interesting since the enzyme had already shown to be sensitive to oxidation *in vitro* (Szoor *et al.*, 2006). Moreover tyrosine phosphorylation has been shown to be, at least in part, hydrogen peroxide-sensitive in procyclic form cells (Nett *et al.*, 2009a). In addition, differentiation of stumpy form cells to procyclic forms can be triggered by extracellular stress conditions, and it is generally known that aerobic organisms respond to environmental stress and to some physiological stimuli through production of ROS (Fedoroff, 2006).

In *Trypanosoma brucei* the real role of environmental stress on differentiation to procyclic forms is not known, but it has been noticed that several stress conditions induce such transformation, although with different kinetics and thus likely through several mechanisms (Rolin *et al.*, 1998). For example, citrate, one of the differentiation triggers, was found to be associated with high rates of cell death in monomorphic lines, at concentration between 0.1 and 3 mM (Hunt *et al.*, 1994). Similarly, mild acid treatment of pleomorphic cells has been shown to cause death of slender form cells with concomitant transformation of stumpy form into procyclic form cells (Rolin *et al.*, 1998). Moreover, treatment of bloodstream form with trypsin (Yabu *et al.*, 1988) or pronase, a mixture of proteinases, have also been identified as inducers of trypanosome differentiation (Hunt *et al.*, 1994; Sbicego *et al.*, 1999) and the same compounds have been linked to increased oxidative stress in other cell types (Aoshiba *et al.*, 2001).

In addition, in the tsetse fly midgut, the site where trypanosome differentiation to procyclic form takes place, the pro-oxidant action of large amounts of heme generated during hydrolysis of hemoglobin produces a pro-oxidant environment which is counteracted by production of antioxidants by the fly (Souza *et al.*, 1997). In such an environment, trypanosomes have been shown to be sensitive to oxidant-induced stress, which affected parasite survival and life cycle progression (MacLeod *et al.*, 2007).

The work carried out for PTP1B has shown that a ligand-dependent localized increase in ROS, can reversibly inactivate the PTP found in its vicinity, thus promoting downstream tyrosine phosphorylation-dependent signalling (Tonks, 2003). According to this model, physiological differentiation of stumpy form cells to procyclic forms would require the production of intracellular ROS, which would cause oxidation of *Tb*PTP1 and induce cellular transformation.

To test this hypothesis, bloodstream form cells were treated with different concentrations of cis-aconitate or citrate (0.1, 4, 6 and 18 mM cis-aconitate and 10 or 18 mM citrate) and the formation of intracellular ROS was monitored using H_2-DCFDA, a cell permeable indicator of ROS (Myhre *et al.*, 2003). Specifically *Trypanosoma brucei* bloodstream S16 cells or stumpy forms from an infected mouse, were incubated with 50 μM H_2-DCFDA in PSG buffer at 37°C for 20 min, washed once, in order to remove the extracellular dye, transferred in HMI-9 and treated with different concentrations of cis-aconitate or citrate and then monitored by FACS to detect ROS production (**Figure 4.6 A**). As visible in Figure 4.6 A, initial experiments showed a small but significant ($P<0.01$) increase in H_2-DCFDA fluorescence after 40-50 minutes, upon all treatments. However, further experiments indicated that cis-aconitate, citrate and isocitrate (another tricarboxylic acid, which does not trigger differentiation (Hunt *et al.*, 1994)) reacted with the ROS indicator in a cell-free environment (**Figure 4.6 B**). This observation was surprising since H_2-DCFDA is supposed to be sensitive to oxidation only intracellularly, as it first needs to be acetylated by cellular esterases; therefore the detection of fluorescence in the cells must have been caused by the de-esterification and oxidation of the ROS indicator by cis-aconitate/citrate outside the cell,

followed by its intracellular diffusion. In order to eliminate the artifact potentially caused by overloading, a lower concentration of H_2-DCFDA was also tried; as visible in Figure 4.6 C, cis-aconitate and isocitrate reacted with the dye, in the absence of cells, even at 5 μM H_2-DCFDA.

To overcome the incompatibility of H_2-DCFDA, another ROS indicator, Ampliflu™ red, was employed, which detects ROS expelled from the cell, and which has also been used as indicator of PTPs oxidation (Lou *et al.*, 2008). Ampliflu™ red did not react with cis-aconitate, citrate or isocitrate in the absence of cells and did not show increased fluorescence upon induction of cellular differentiation (**Figure 4.7**). This suggested that oxidation is probably not involved in *Tb*PTP1 inactivation during transition to procyclic form cells.

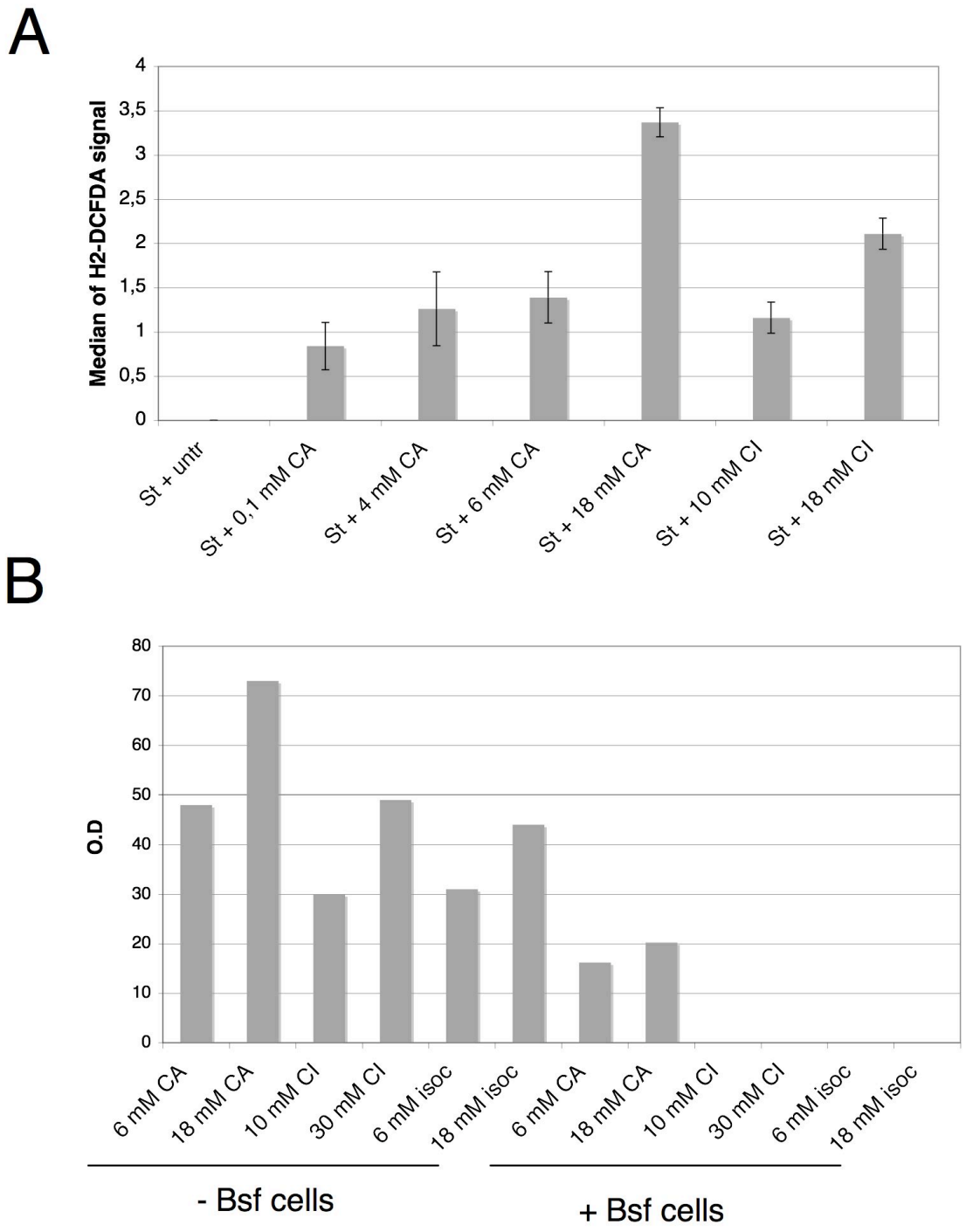
A
Median of H2-DCFDA signal
4
3,5
3
2,5
2
1,5
1
0,5
0
St + untr
St + 0,1 mM CA
St + 4 mM CA
St + 6 mM CA
St + 18 mM CA
St + 10 mM CI
St + 18 mM CI
B
O.D
80
70
60
50
40
30
20
10
0
6 mM CA
18 mM CA
10 mM CI
30 mM CI
6 mM isoc
18 mM isoc
6 mM CA
18 mM CA
10 mM CI
30 mM CI
6 mM isoc
18 mM isoc
- Bsf cells
+ Bsf cells

C

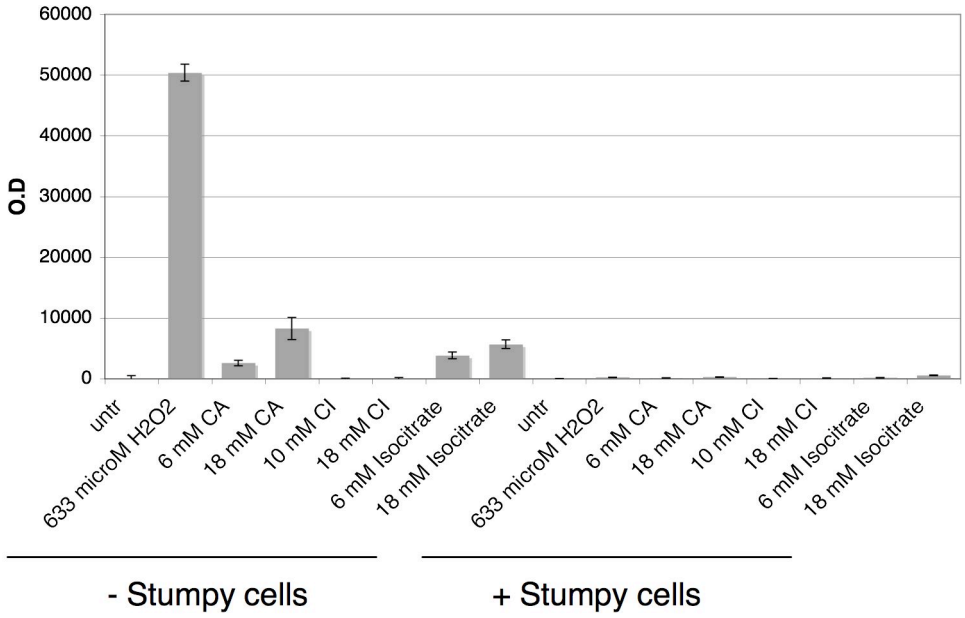

Figure 4.6 Detection of intracellular ROS upon induction of differentiation with cis-aconitate or citrate using H_2-DCFDA. (A) Stumpy form cells (+ St) were treated with 0.1, 4, 6 and 18 mM cis-aconitate (CA), 10 and 18 mM citrate (CI), or 6 and 18 mM isocitrate (as negative control) and ROS production was monitored using 50 μM H_2-DCFDA by FACS for 60 min and FITC channel geometric mean intensity at 50 min is shown (B). Monomorphic bloodstream form cells (+ Bsf cells) were treated with 6 or 18 mM cis-aconitate (CA), 10 or 30 mM citrate (CI), 6 or 18 mM isocitrate (isoc) in PSG buffer supplemented with 50 μM H_2-DCFDA, and ROS production was measured using a fluorimeter (exc. 490 nm, em. 520 nm); the same compounds in the absence of cells were also included, as negative control (-Bsf cells). (C) Stumpy form cells (+ Stumpy cells) and controls (- Stumpy cells) were treated as in B but using 5 μM H_2-DCFDA. Bars in A and C represent S.E.M. at 50 min.

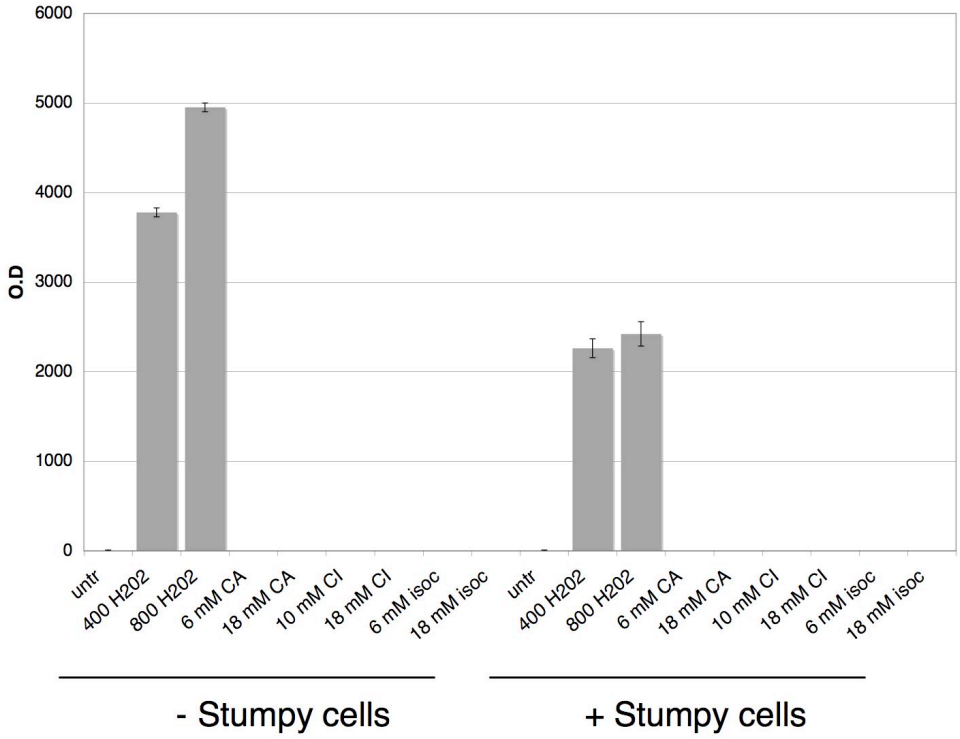

Figure 4.7 Detection of intracellular ROS upon induction of differentiation with cis-aconitate/citrate using Ampliflu™ red. Stumpy form cells (+ Stumpy cells) were treated with 0.1, 4, 6 and 18 mM cis-aconitate (CA), 10 and 18 mM citrate (CI) or 6 and 18 mM isocitrate (isoc., as negative control) and ROS production was monitored using Ampliflu™ red and quantified using a fluorimeter (ex. 544 nm, em. 590 nm). PSG buffer with cis-aconitate, citrate or isocitrate and no cells was included (- Stumpy cells) and H_2O_2 treatment was used as positive control.

4.4. Effects of H_2O_2 and N-acetyl cysteine (NAC) on differentiation

Exogenously supplied H_2O_2 has been shown to mimic the effect of insulin in mammalian cells through the inhibition of PTPs and activation of protein tyrosine kinases (Heffetz *et al.*, 1992). Therefore it was interesting to investigate the effect of exogenous ROS on the differentiation of stumpy forms to procyclic forms. For this purpose, cells were treated with different concentrations of H_2O_2 and monitored for EP protein expression using FACS analysis. Stumpy form cells treated with 5 μM H_2O_2 for up to 48 hr did not show any sign of transformation (**Figure 4.8 A**) and concentrations of 50 and 100 μM H_2O_2 on monomorphic bloodstream form were also ineffective (data not shown).

Since, in this context, exogenous ROS might not possess the selectivity shown by stimuli-induced ROS, the effect on differentiation of endogenous ROS neutralization was also tested. For this purpose, the cell permeable anti-oxidant N-acetyl cysteine (NAC) was employed, which has been used in trypanosomes to attenuate the effect of intracellular ROS (Figarella *et al.*, 2006). Initially the anti-oxidant properties of NAC against H_2O_2 were assessed (**Figure 4.8 B**). As visible in Figure 4.8 B, cells treated with increasing concentrations of NAC showed decreased H_2-DCFDA fluorescence over time upon H_2O_2 treatment, compared to untreated cells. The observed decrease in fluorescence indicated that 1-hr treatment with NAC concentrations between 0.25 and 2 mM neutralized most of the exogenous H_2O_2 supplied within 80 min of H_2O_2 addition; as expected, the level of NAC neutralization was directly proportional to its concentrations, with 0.25 and 0.4 mM NAC effectively neutralizing all of the exogenus H_2O_2 supplied up to 40 min after H_2O_2 addition, and 0.8 and 2 mM NAC lasting twice as long.

The same pre-treatment on stumpy cells subsequently induced to differentiate with 6 mM cis-aconitate did not result in a significant alteration of the number of EP positive cells (**Figure 4.8 C**). High concentrations of NAC, however, were found to be cytotoxic, as suggested by a marked

decrease in cell growth upon treatment with 0.8 and 2 mM NAC (**Figure 4.8 D**).

Nonetheless it was clear that ROS generation by H_2O_2, or its inhibition by NAC, did not affect the differentiation efficiencies of the cells. Apparently, therefore, ROS generation does not represent a major regulatory component of the differentiation signal, despite the effects of ROS on *Tb*PTP1 activity observed *in vitro*.

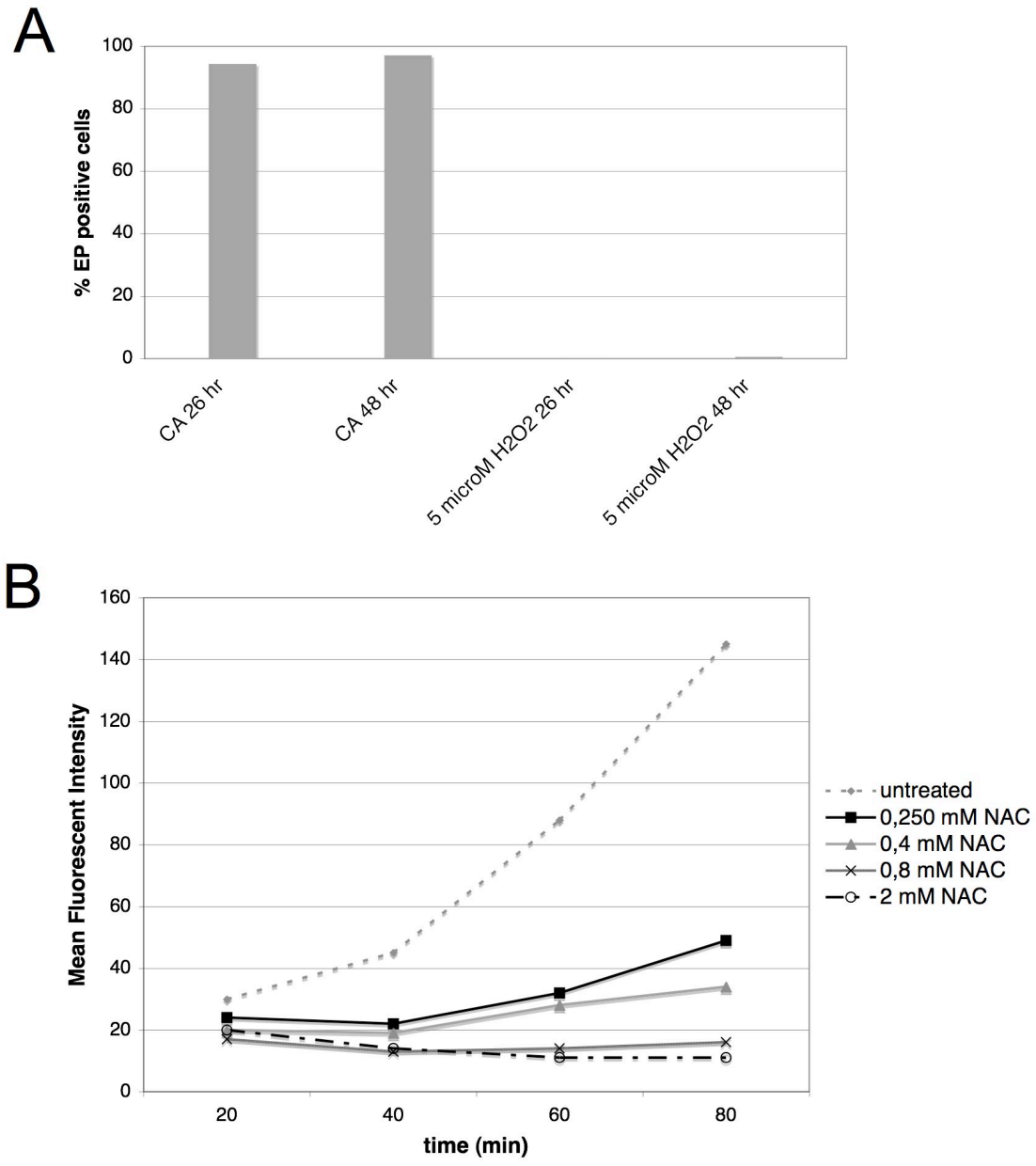

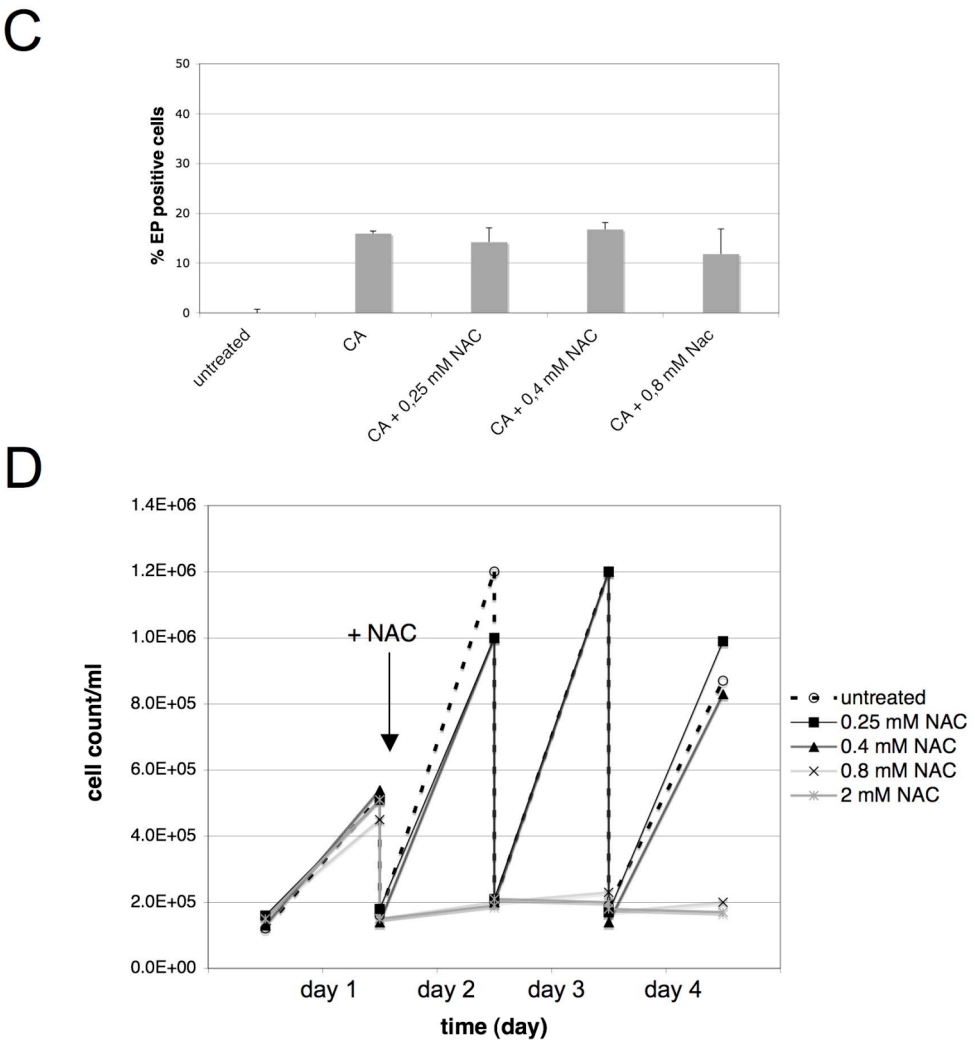

Figure 4.8. Effect of H_2O_2 and N-acetyl Cysteine (NAC) on differentiation. (A) Stumpy form cells were treated with 5 mM H_2O_2 and stained for EP expression after 26 and 48 hr. (B) Bloodstream form S16 cells were treated 1 hr with 0.25, 0.40, 0.80 and 2 mM NAC prior stimulation with 0.2 mM H_2O_2 and the intracellular ROS level was quantified by monitoring the increase in H_2-DCFDA fluorescence over time; (C) S16 cells were treated 1 hr with 0.25, 0.40, 0.80 and 2 mM NAC and then induced to differentiate with 6 mM cis-aconitate. (D) Effect of NAC on cell growth. Growth of bloodstream form S16 cells in presence of 0.25, 0.4, 0.8 and 2 mM NAC was monitored up to 48 hr after treatment; NAC was added after 24 hr (arrow).

4.5. Monitoring *Tb*PIP39 phosphorylation

In parallel to investigating the possible physiological mechanisms of *Tb*PTP1 regulation during differentiation, it was also interesting to test whether different compounds reported to induce stumpy to procyclic form transition acted through the same *Tb*PTP1-*Tb*PIP39 pathway as CCA signalling.

In order to do so, changes in *Tb*PIP39 phosphorylation were monitored under different conditions, using an antibody developed specifically to detect the phosphorylated tyrosine 278 (p-PIP39) of *Tb*PIP39 (Szoor *et al.*, 2010). Initially, validation of the anti p-PIP39 antibody was carried out, as Figure 4.9 shows, the signal of the antibody completely disappeared when procyclic form cell extract, which contains phosphorylated *Tb*PIP39, was incubated with recombinant *Tb*PTP1.

Interestingly, the anti p-PIP39 antibody reacted with two proteins of approximately 40 and 50 kDa, but only the lower band (arrow in **Figure 4.9**) reacted also with the anti-PIP39 antibody; therefore the 50-kDa band is not *Tb*PIP39 but another protein, potentially possessing a phosphorylated tyrosine residue, which is also substrate of *Tb*PTP1 *in vitro*. A Blast search against the *T. brucei* genome database, using the peptide sequence against which the p-PIP39 antibody was raised (ELDHWRTDEpYTKC) (Szoor *et al.*, 2010), found only *Tb*PIP39 (*Tb*09.160.4450) and the almost identical protein (*Tb*09.160.4480); the same analysis carried out using a shorter sequence (DEYT), identified two other hits with similar molecular weight to *Tb*PIP39 (*Tb*10.70.1520: 41.2 kDa and *Tb*09.211.0590: 49.2 kDa). However, none of these two proteins were present in the list of proteins selected by the WT or D199A mutant *Tb*PTP1 (see Chapter 3), or in the published *T. brucei* phosphoproteome (Nett *et al.*, 2009b), hence the identity of the cross reacting band migrating at approximately 50 kDa remains uncertain.

The tyrosine-phosphorylation status of *Tb*PIP39 in the different life cycle forms was then assessed using the p-PIP39 antibody and the ratio of phosphorylated *Tb*PIP39 over a loading control, such as tubulin, was quantified (**Figure 4.10 A**). As expected the ratio was greater in procyclic forms compared to stumpy and bloodstream forms, specifically showing a 2.6 fold increase from stumpy to established procyclics. Similarly, the ratio of

phosphorylated *Tb*PIP39 was quantified 1.5 hr after induction of differentiation with cis-aconitate or with the *Tb*PTP1 inhibitor, BZ3 (**Figure 4.10 B**). Also in this case a significant increase in the p-PIP39 signal was detected upon both treatments, this being 3-4 times the untreated level. Interestingly such increase was slightly greater than the 2.6 fold increase seen comparing stumpy and established procyclic cell extracts (**Figure 4.10 A**).

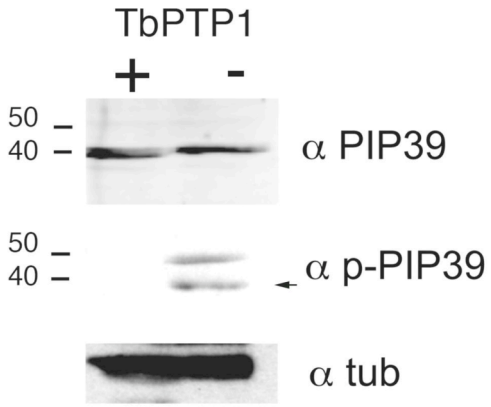

Figure 4.9 *Tb*PTP1 dephosphorylation of *Tb*PIP39 in procyclic forms cell extracts. Western blot of procyclic forms cell extracts incubated in presence or absence (+/-) of recombinant active *Tb*PTP1 for 1 hr, at 37°C. The membrane was then probed with anti-*Tb*PIP39 antibody (α PIP39), anti- phosphorylated Y278 antibody (α p-PIP39) and anti-tubulin antibody, as loading control (α tub). The molecular weight marker is shown on the left-hand side, numbers indicate kDa. The *Tb*PIP39 signal (arrow) disappears upon *Tb*PTP1 treatment, as does the reactivity with a cross-reacting protein migrating at about 50 kDa.

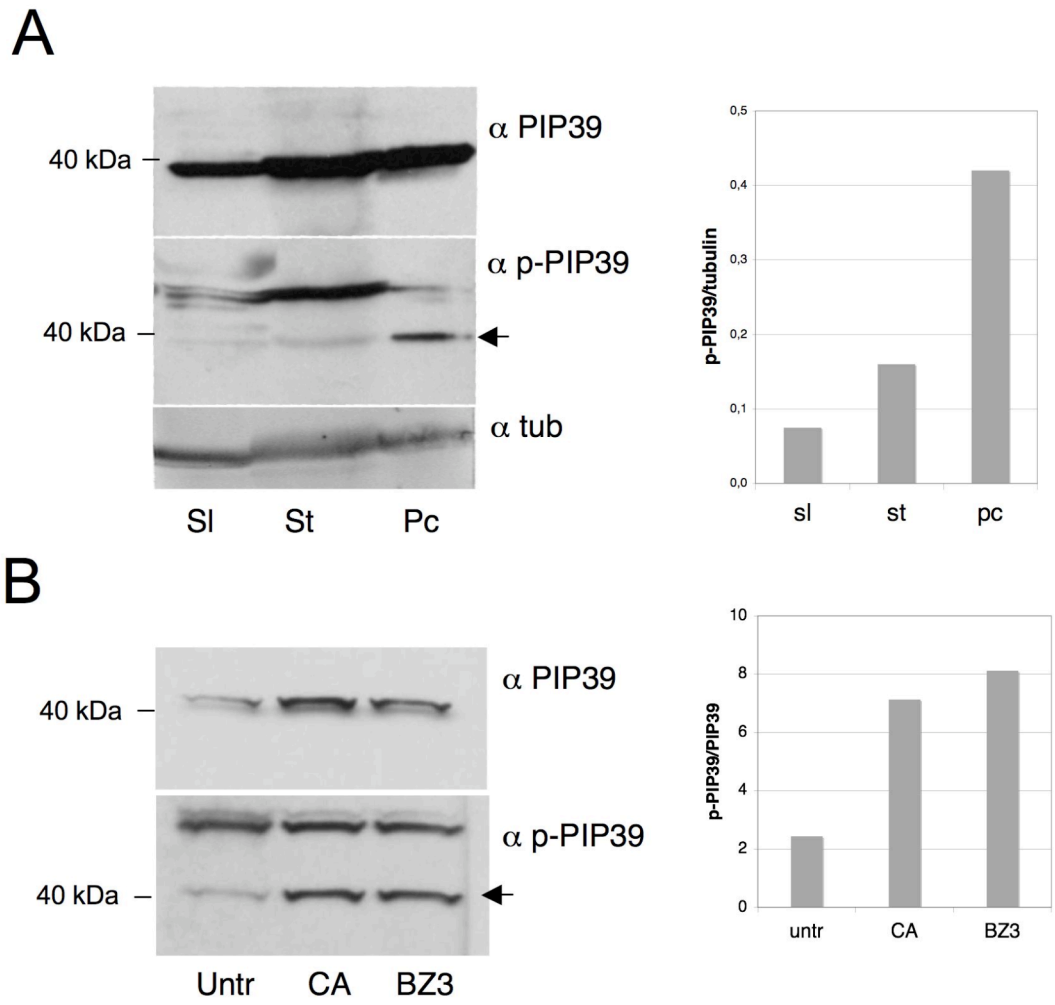

Figure 4.10 *Tb*PIP39 phosphorylation analysis in the different life cycle forms and soon after induction of differentiation. (A) Western blot of slender (Sl), stumpy (St) and procyclic (Pc) form cell extracts probed for total *Tb*PIP39, p-*Tb*PIP39 and tubulin (α PIP39, α p-PIP39 and α tub) (left panel); the corresponding quantification of p-PIP39/tub signal is shown in A, right panel. (B) Western blot of untreated stumpy form cell extract (untr), cells treated for 1.5 hr with 6 mM cis-aconitate (CA) or with 150 μM BZ3 (BZ3), probed for total *Tb*PIP39 and p-*Tb*PIP39 (α PIP39 and α p-PIP39) (left panel); the corresponding quantification of p-PIP39/PIP39 signal is shown in the right panel. Quantifications are performed using Syngene G:Box for p-PIP39 and PIP39, and LICOR Odissey® imager system for tubulin (note that the p-PIP39/PIP39>1 is likely due to the processing of the Western blot, as the same membrane was first probed with α p-PIP39, stripped and reprobed with α PIP39, see Materials and Methods) .

4.6. Monitoring *Tb*PIP39 phosphorylation upon treatment with citrate/cis-aconitate (CCA) and with other differentiation triggers

In order to compare the effect of different triggers of differentiation on the *Tb*PTP1-*Tb*PIP39 signalling cascade, it was first important to characterize in more detail the size and timing of the increase in *Tb*PIP39 phosphorylation upon citrate/cis-aconitate (CCA) treatment. Therefore the p-PIP39 signal normalized to tubulin, was compared at different time points after addition of 6 mM cis-aconitate (**Figure 4.11**). One representative Western blot is shown in Figure 4.11 A and the mean of the p-PIP39/tubulin signals of several experiments is shown in Figure 4.11 B; as evident from the Western blot and corresponding quantification, increasing p-PIP39 levels were detectable from 2 hr after addition of 6 mM cis-aconitate (CA) and appeared to peak at 6 hr (**Figure 4.11 A and B)**. However, the level and timing of p-PIP39 increase among experiments was variable, such that the changes in level of p-PIP39/tubulin signal over time did not result to be statistically significant (General linear model, P= 0.42). In parallel, cellular differentiation was analysed, by FACS analysis of EP protein expression, which did not show the same variability seen with the levels of p-PIP39 (**Figure 4.11 C**).

In addition to cis-aconitate, the effect of citrate, the other citric acid cycle intermediate known to induce differentiation (Czichos *et al.*, 1986), on *Tb*PIP39 phosphorylation was assessed in the same way. As expected, 10 mM citrate induced a similar p-PIP39 increase in parallel to cellular transformation (**Figure 4.12 A and B**).

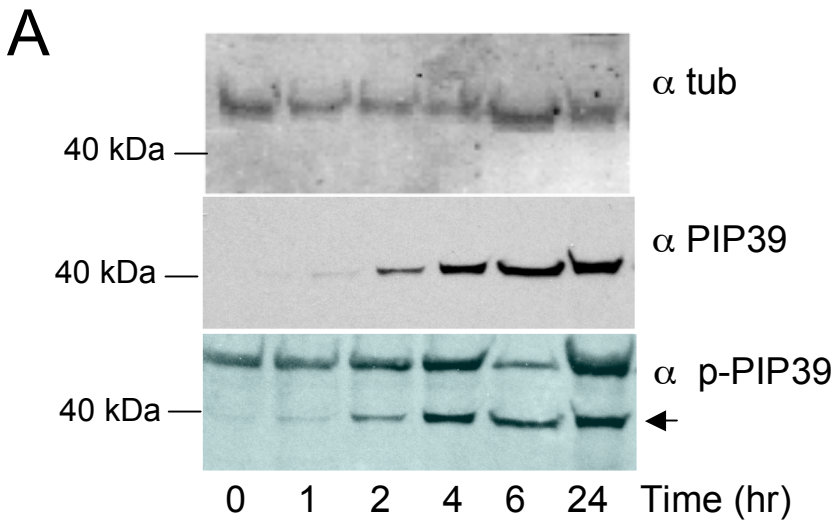
A
α tub
40 kDa
α PIP39
40 kDa
α p-PIP39
40 kDa
0 1 2 4 6 24 Time (hr)

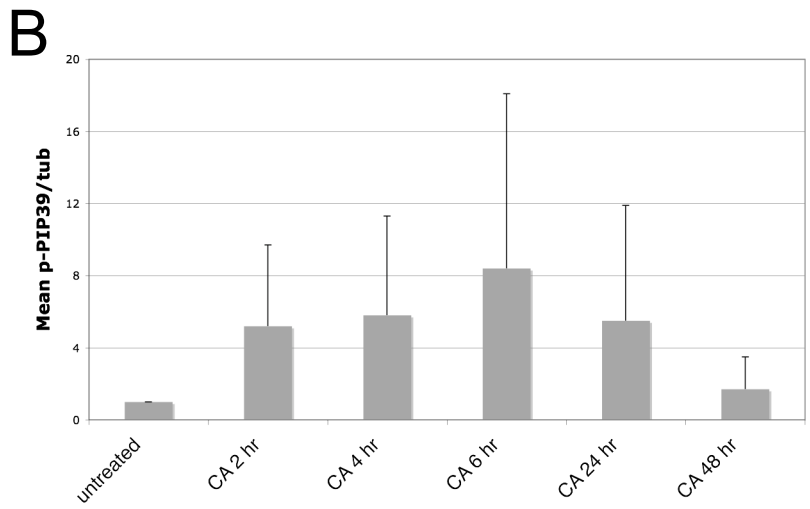
B
Mean p-PIP39/tub
20
16
12
8
4
0
untreated
CA 2 hr
CA 4 hr
CA 6 hr
CA 24 hr
CA 48 hr

C

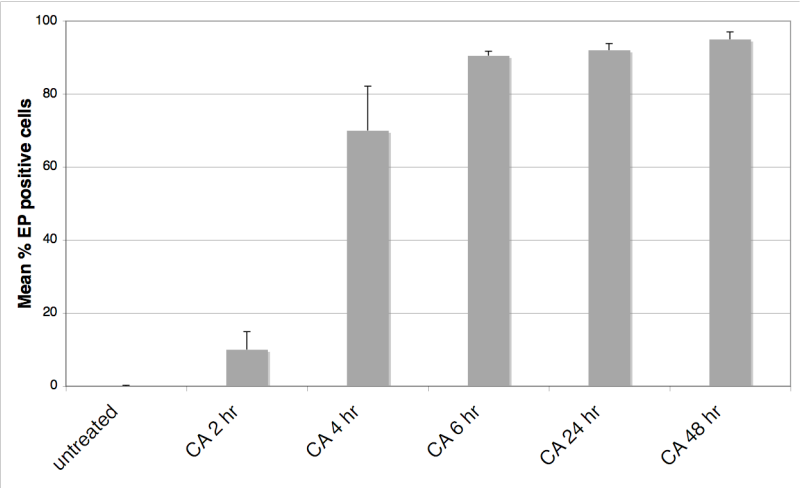

Figure 4.11 Monitoring the phosphorylation levels of *Tb*PIP39 upon cis-aconitate (CA) treatment of stumpy form cells. (A) An example of Western blot analysis of stumpy form cells induced to differentiate by addition of 6 mM cis-aconitate (CA). Samples were probed with anti-PIP39, anti p-PIP39 or tubulin antibodies (α PIP39, α p-PIP39 and α tub, respectively). (B) The mean quantification of the p-PIP39/tubulin signal of different experiments (n=6 for untreated, 2 hr and 4 hr; n=4 for 6 hr; n=5 for 24 hr and n=2 for 48 hr) is shown, together with the corresponding percentage of cellular differentiation to procyclic forms, as judged by EP protein expression analysed by FACS (C). Error bars are S.E.M.

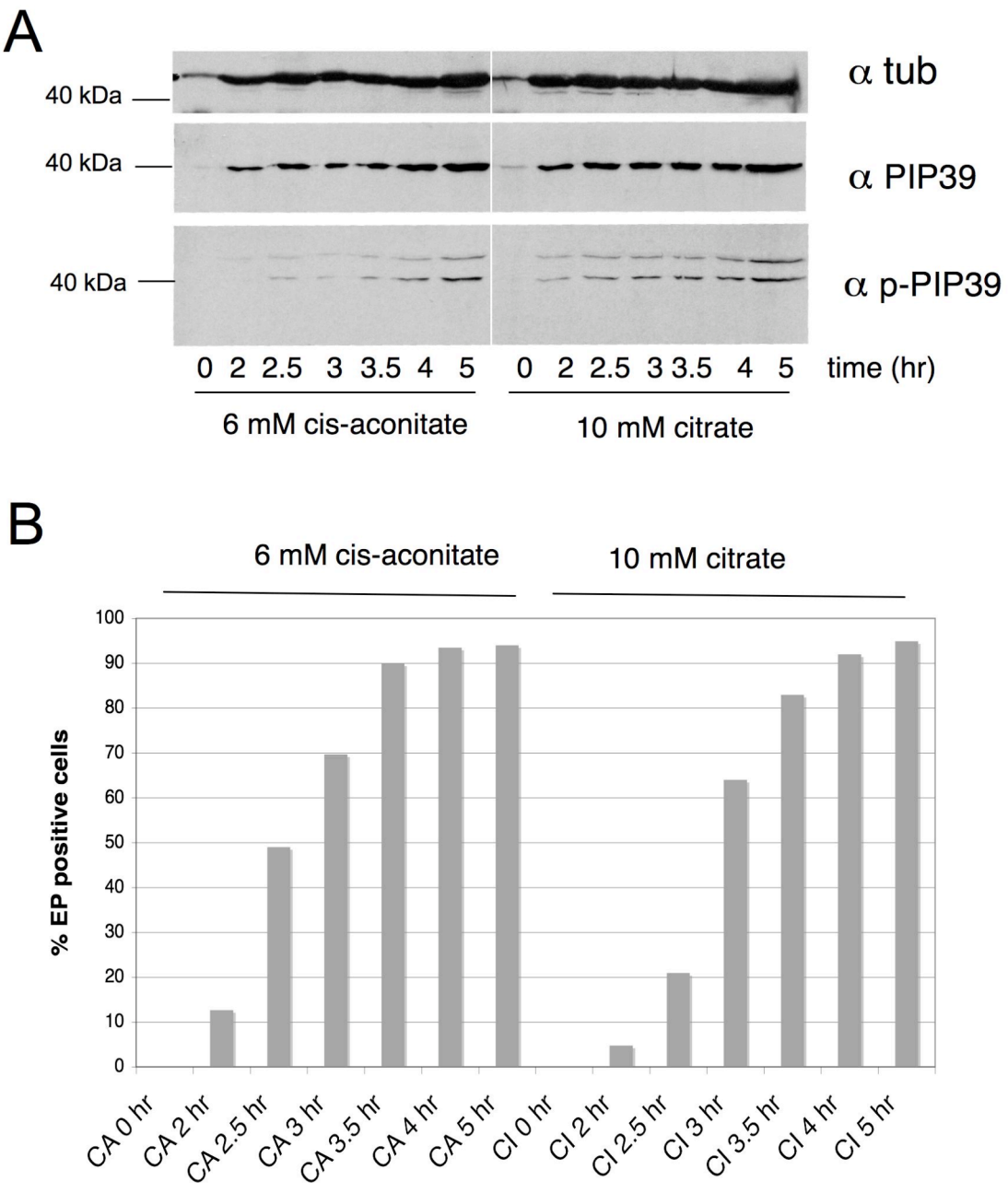

Figure 4.12 Analysis of the phosphorylation levels of *Tb*PIP39 upon cis-aconitate (CA) and citrate (Ci) treatment of stumpy form cells. (A) Western blot analysis of stumpy form cells induced to differentiate by addition of 6 mM cis-aconitate (CA) or 10 mM citrate (CI). Samples were probed with anti-PIP39, anti p-PIP39 or tubulin antibodies (α PIP39, α p-PIP39 and α tub, respectively). (B) Corresponding percentage of cellular differentiation to procyclic forms, as judged by EP protein expression quantified by FACS.

Since the physiological differentiation of stumpy form to procyclic form cells is believed to be mediated through the cooperative effect of cis-aconitate and temperature reduction (Engstler *et al.*, 2004), the consequences of cold shock on the PIP39 phosphorylation were investigated. Initially it was interesting to test the effect of cold shock alone, which has been reported to cause EP protein expression on the stumpy cell surface, but not to induce cell proliferation and differentiation to procyclic forms (Engstler *et al.*, 2004). Accordingly, Figure 4.13 shows that cold shock treatment did not induce an increase in the p-PIP39 signal (**Figure 4.13 A**) but it did cause EP protein expression in 15-20 % of the cell population at 2-4 hr (**Figure 4.13 B**).

Next, the effect of cis-aconitate in the absence or presence of cold shock on the levels of phosphorylated PIP39 was tested. The shift from the bloodstream temperature of 37°C to 20°C, likely corresponding to the vector feeding environment, renders trypanosomes more sensitive to cis-aconitate. Therefore cis-aconitate concentrations such as 1 mM or lower, which at 27°C do not induce differentiation, are as effective as 6 mM, in presence of cold shock (Engstler *et al.*, 2004). Hence, stumpy form cells were treated with 6 mM or 1 mM cis-aconitate in presence or absence of an overnight incubation at 20°C (cold shock). Under these conditions, however, similar levels of p-PIP39 were detected and no significant difference was visible between cells exposed to 1 mM cis-aconitate without or with cold shock (1 mM CA -/+ CS) (**Figure 4.14**).

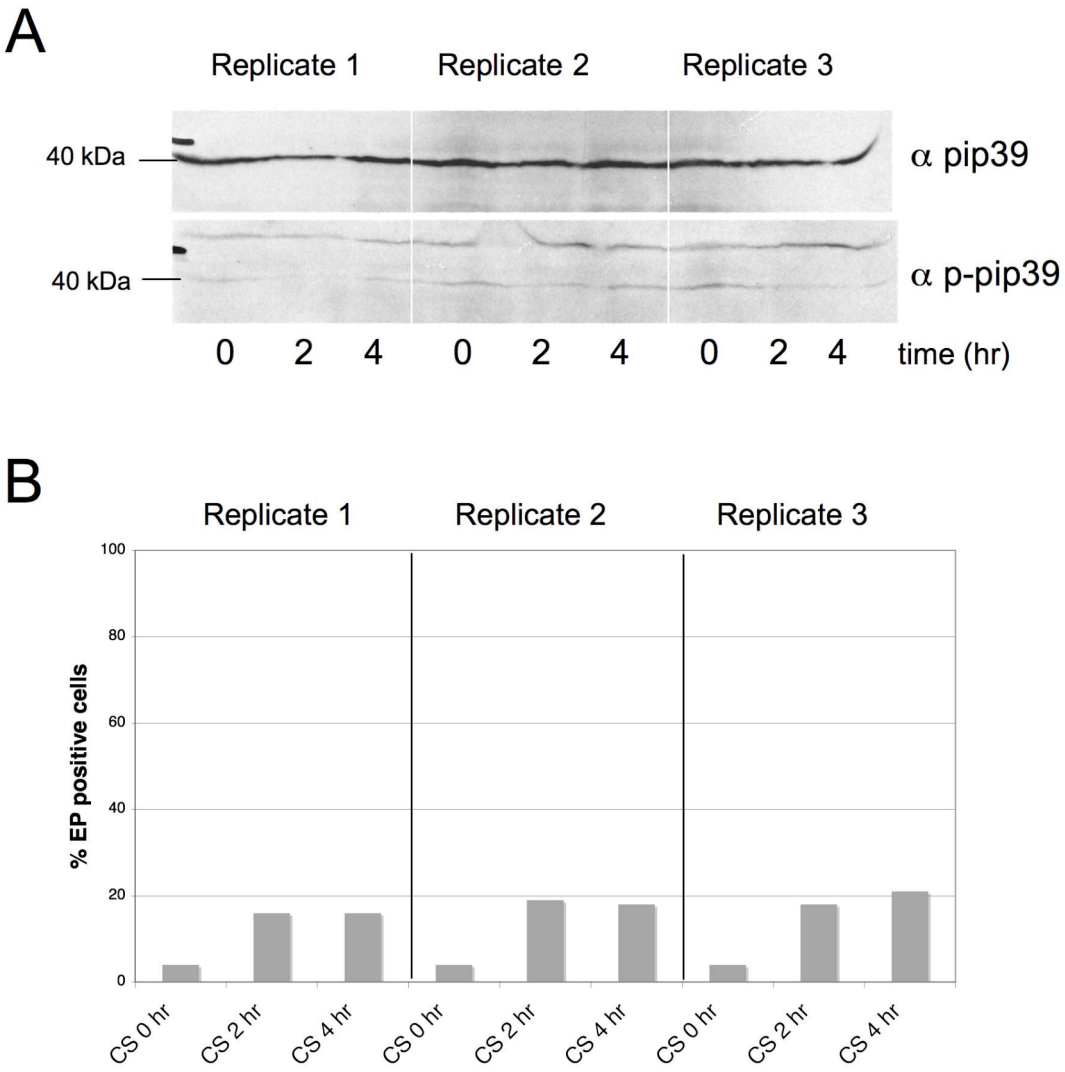

Figure 4.13 Effect of cold shock on the phosphorylation levels of *Tb*PIP39. Three independent Western blots of stumpy form cells cold shocked overnight at 20°C are shown in A; the 0 hr time point represents samples taken after an overnight incubation at 20°C. The experiment was conducted in triplicate, with cells from the same mouse kept at 20°C in three different flasks. As for the previous figures, samples were probed with anti-PIP39, anti p-PIP39 or tubulin antibodies (α PIP39, α p-PIP39 and α tub, respectively). (B) Corresponding percentage of cellular differentiation to procyclic forms, as judged by EP protein expression.

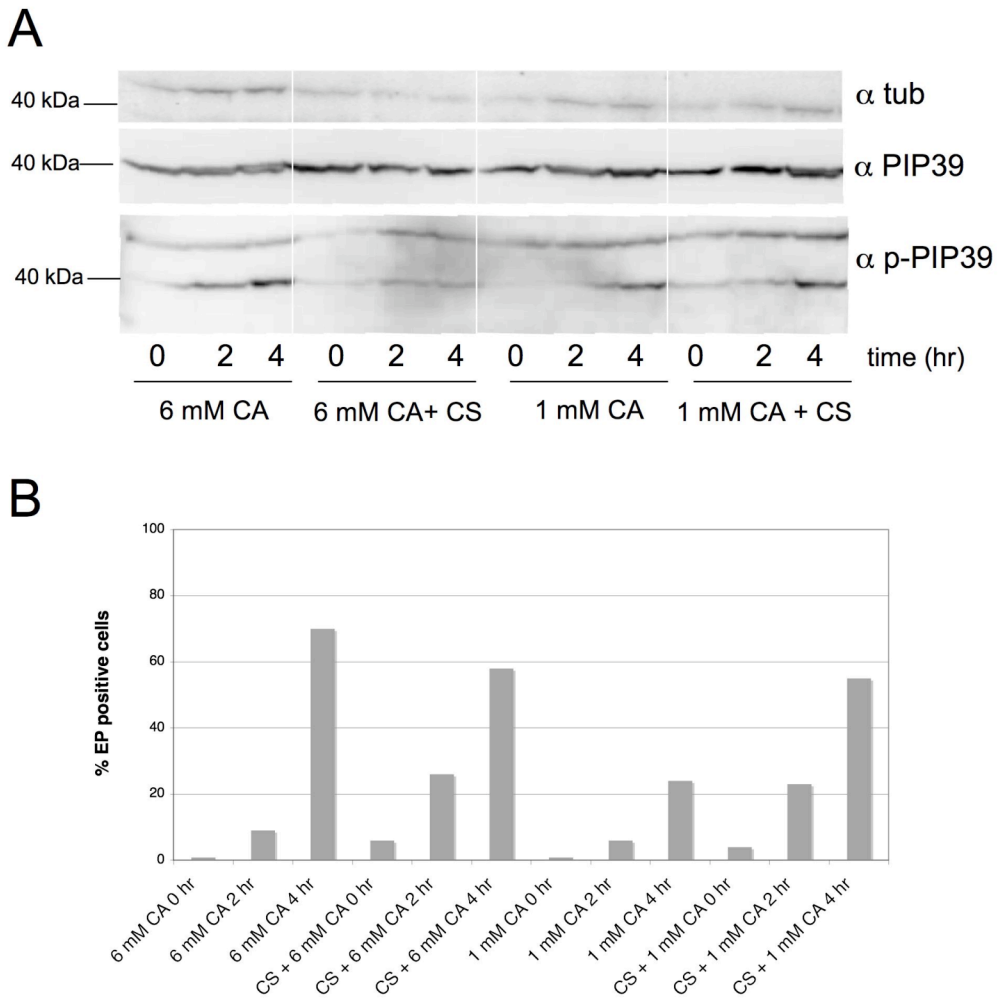

Figure 4.14 Effect of cis-aconitate (CA) without or with cold shock (CS) on the phosphorylation levels of *Tb*PIP39. (A) Western blot analysis of stumpy form cells induced to differentiate by addition of 6 mM or 1 mM cis-aconitate (CA) in presence of absence of cold shock (CS) (the 0 hr time point represents samples taken after an overnight incubation at 20°C). Samples were probed with anti-PIP39, anti p-PIP39 or tubulin antibodies (α PIP39, α p-PIP39 and α tub, respectively). (B) Corresponding percentage of cellular differentiation to procyclic forms, as judged by EP protein expression is also shown.

In addition to citrate/cis-aconitate, another trigger of differentiation to procyclic forms is mild acid treatment, which has been shown to induce transition to procyclic forms in absence of CCA, albeit with different kinetics (Rolin *et al.*, 1998) (see paragraph 1.9.2.2). Indeed, a pre-incubation in HMI-9 media at pH 5.5 for 2-hr before transferring the cells in HMI-9 at normal pH (pH 7.8) at 27°C, resulted in limited differentiation, reaching less than 50 % after 48 hr (**Figure 4.15 B**). Moreover, the level of *Tb*PIP39 phosphorylation during this time did not seem to visibly increase compared to CCA-treatment (**Figure 4.15 A**, compare with Figure 4.11 A).

In addition to mild acid, proteolytic stress, such as trypsin or pronase treatments, have been shown to induce transformation of stumpy form cells into procyclics through an unknown mechanism (Hunt *et al.*, 1994; Sbicego *et al.*, 1999). In order to test whether the *Tb*PTP1-*Tb*PIP39 pathway is involved in proteolytic stress-induced differentiation, the level of *Tb*PIP39 phosphorylation was assessed under pronase treatment. Such treatment resulted in a much weaker p-PIP39 signal compared to that seen for CCA-treated cells (**Figure 4.16 A** and **B**), despite a similar degree of EP expression (**Figure 4.16 C**). The difference was particularly striking at 2 and 4 hr, as no increase in p-PIP39 levels was detected for pronase-treated cells compared to a 1 and 1.5 fold increase for cis-aconitate treated cells, although the degree of cellular differentiation was higher for the first treatment.

In conclusion, both cis-aconitate and citrate-induced differentiation stimulated *Tb*PIP39 phosphorylation, whereas cold shock, mild acid and, particularly, pronase did not. This indicates the presence of alternative signalling pathways operating with these differentiation triggers.

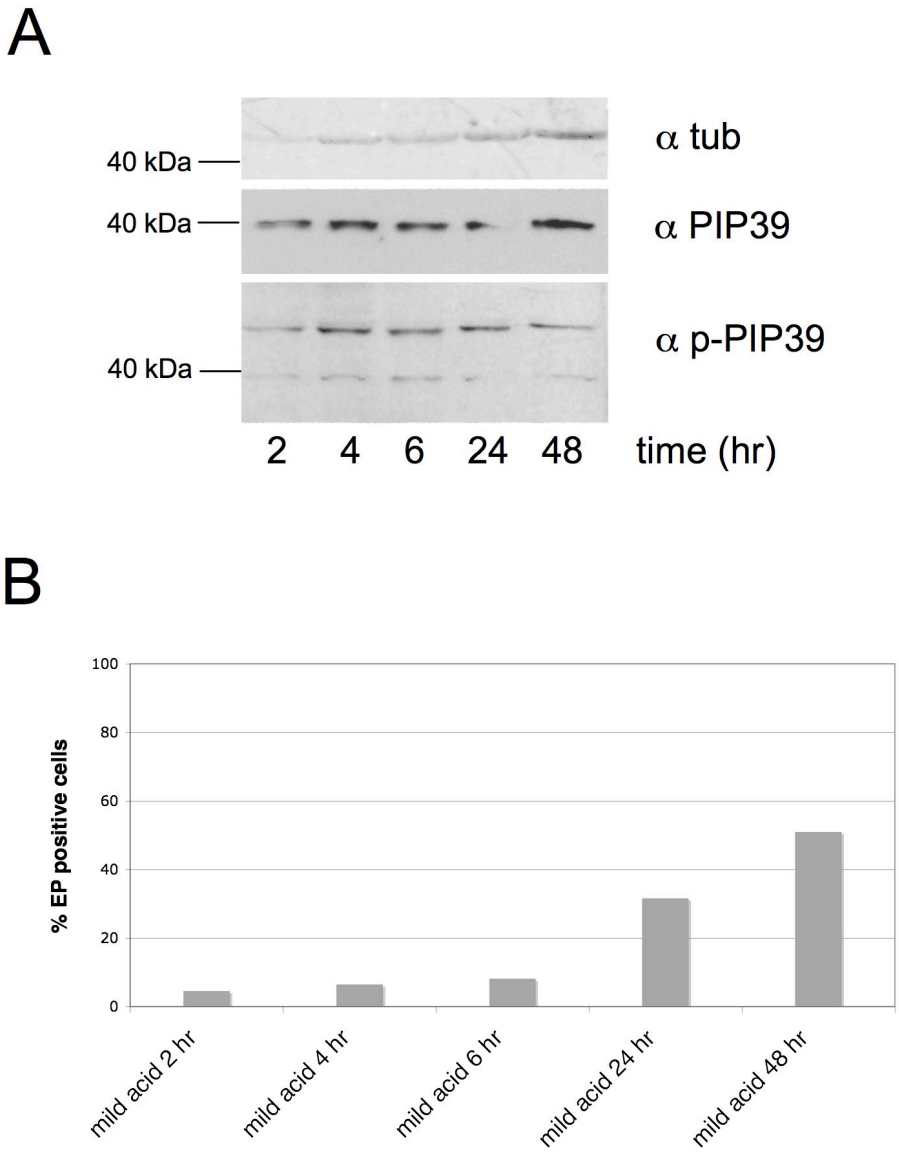

Figure 4.15 Effect of mild acid treatment on the phosphorylation levels of *Tb*PIP39. (A) Western blot analysis of stumpy form cells placed in HMI-9 media at pH 5.5 for 2 hr and then in normal HIM-9 at 27°C, according to Rolin *et al.*, 1998; as for the previous figures, samples were probed with anti-PIP39, anti p-PIP39 or anti tubulin antibodies (α PIP39, α p-PIP39 and α tub, respectively). (B) Corresponding percentage of cellular differentiation to procyclic forms, as judged by EP protein expression. The 0 hr time point corresponds to the end of the mild acid treatment.

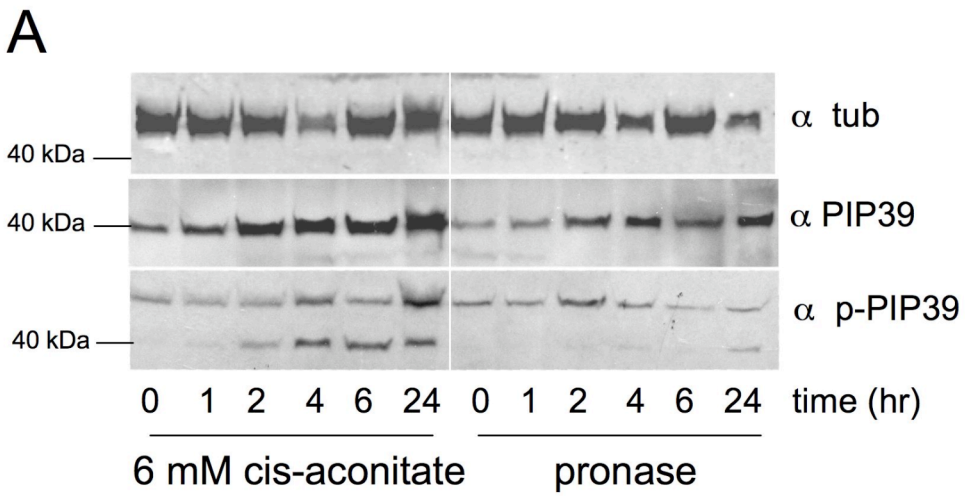
A
40 kDa
40 kDa
40 kDa
α tub
α PIP39
α p-PIP39
0 1 2 4 6 24 0 1 2 4 6 24 time (hr)
6 mM cis-aconitate
pronase

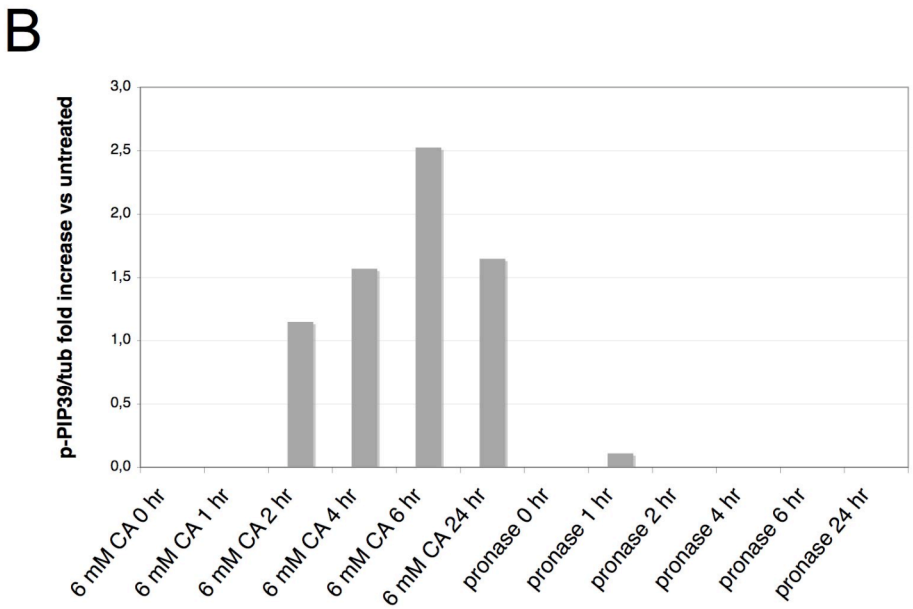
B
p-PIP39/tub fold increase vs untreated
3,0
2,5
2,0
1,5
1,0
0,5
0,0
6 mM CA 0 hr
6 mM CA 1 hr
6 mM CA 2 hr
6 mM CA 4 hr
6 mM CA 6 hr
6 mM CA 24 hr
pronase 0 hr
pronase 1 hr
pronase 2 hr
pronase 4 hr
pronase 6 hr
pronase 24 hr

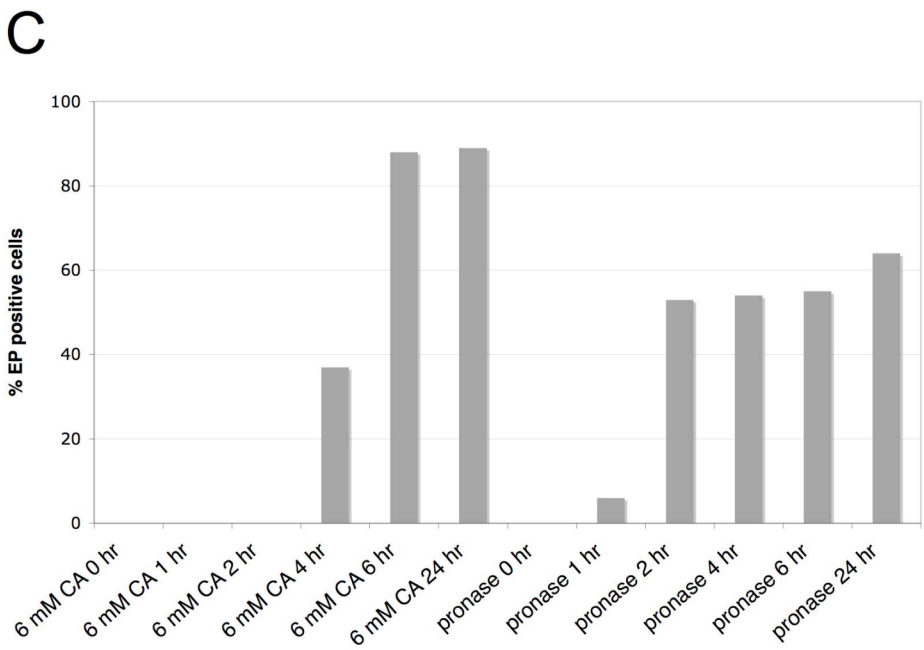

Figure 4.16 Effect of pronase treatment on the phosphorylation levels of *Tb*PIP39. (A) Western blot analysis of stumpy form cells treated with pronase according to Sbicego *et al*., 1999; as for the previous figures, samples were probed with anti-PIP39, anti p-PIP39 or anti tubulin antibodies (α PIP39, α p-PIP39 and α tub, respectively). (B) Quantification of the fold increase compared to untreated cells of the p-PIP39 signal normalized to tubulin. (C) Corresponding percentage of cellular differentiation to procyclic forms, as judged by EP protein expression.

4.7. Discussion

4.7.1 Comparative analysis of *Tb*PTP1 mechanism of regulation during differentiation to procyclic forms

The spatial and temporal regulation of Protein Tyrosine Phosphatases (PTPs) is essential to ensure the proper propagation of cellular signalling in response to different stimuli (den Hertog *et al.*, 2008). In mammalian cells, 81 active PTPs are present (Alonso *et al.*, 2004) that are involved in a plethora of cellular functions, from cell cycle, shape and motility, to gene transcription and mRNA processing, and which display a variety of regulatory mechanisms.

In the trypanosomatid genomes, the large number of protein kinases clearly indicates that protein phosphorylation is an important mechanism of signal transduction. However, the lack of recognizable tyrosine kinases (Parsons, 2005), together with a very limited number of classical tyrosine phosphatases (Brenchley *et al.*, 2007) could suggest the presence of a more discrete repertoire of proteins regulated by tyrosine phosphorylation compared to serine/threonine phosphorylation. If this is the case, it is then possible that a less tight PTP regulation may be needed in these protozoan organisms. However, experimental evidence has also shown that a certain degree of tyrosine phosphorylation is present in *Trypanosoma brucei*, with two developmentally regulated phosphotyrosine-containing proteins being characterized (Parsons *et al.*, 1994; Chou *et al.*, 2010; Szoor *et al.*, 2010) and 13 phosphorylated tyrosine sites being identified on protein kinases (Nett *et al.*, 2009b). Moreover, the lack in kinetoplastid PTPs of additional structural domains, such as targeting motifs or protein-protein interaction domains, (Brenchley *et al.*, 2007) might indicate a greater requirement for regulatory mechanisms.

In the context of *Tb*PTP1, the inhibition of phosphatase activity responsible for the transition from stumpy to procyclic forms, suggests the need for an enzymatic regulation sensitive to the environmental changes that the parasite encounters (Szoor *et al.*, 2006).

Higher eukaryote PTPs, particularly PTP1B, have been shown to be regulated at different levels: transcriptionally, post-transcriptionally, translationally and post-translationally (Bourdeau *et al.*, 2005).
Within the transcriptional regulation level several mechanisms are present in mammalian cells to obtain tissue or stimuli-dependent control of PTPs, for example downregulation through promoter methylation, upregulation via enhancer elements or differential expression by the alternate use of promoters (den Hertog *et al.*, 2008). In *Trypanosoma brucei*, gene regulation is mainly post-transcriptional due to lack of recognizable promoters in the protein-coding genes (Clayton, 2002), therefore *Tb*PTP1 transcriptional regulation can probably be excluded.

4.7.1.1. Post-transcriptional regulation of *Tb*PTP1

Only a few studies have addressed the issue of post-transcriptional, translational or protein stability control of mammalian PTPs, showing that increase in mRNA stability (Rajendrakumar *et al.*, 1993) or reduced rate of protein degradation (Gebbink *et al.*, 1995) can be responsible for changes in PTPs quantity, although the extent of this level of regulation compared to others is not clear. In *Trypanosoma brucei,* altered mRNA processing, mRNA degradation or stabilization and translational control, are all mechanisms that account for the developmental regulation of more than 30 transcripts (Clayton, 2002), and thus could potentially play an important role in *Tb*PTP1 regulation. However, whilst *Tb*PTP1 gene expression through the different life cycle stages has been reported to increase 1.5-3 fold in stumpy form compared to slender and procyclic forms (Szoor *et al.*, 2006), this change is not reflected by increased protein levels, which are maintained equal throughout differentiation. Likewise, since the size of the *Tb*PTP1 transcript was found to be the same in the different *T. brucei* life cycle stages (Szoor *et al.*, 2006), it is unlikely that trans-splicing plays a role in the phosphatase regulation. Hence, post-transcriptional mechanism cannot account for *Tb*PTP1 inactivation upon differentiation to procyclic forms.
A constant *Tb*PTP1 level could still result in differential enzyme activity if coupled to changes in protein subcellular localization, as it is achieved

through the presence of protein-protein interaction or targeting domains in various mammalian PTPs (den Hertog *et al.*, 2008). For example, cytoplasmic PTPs can be recruited to sites of cell-cell adhesion or cell-surface tyrosine phosphorylation through FERM, PDZ or SH2 motifs (Alonso *et al.*, 2004); similarly, some PTPs, such as PTP1B, possess ER-anchoring sequences that target them to the ER, where they are able to interact with ER-transported proteins, such as EGFR and PGFR (Haj *et al.*, 2002). However *Tb*PTP1, together with the other kinetoplastids PTPs, lack any additional recognizable regulatory or targeting domains (Brenchley *et al.*, 2007); in addition, *Tb*PTP1 cytoskeletal localization has not been shown to change during the parasite life cycle (Szoor *et al.*, 2006; McElhinney, 2007), likely excluding differential targeting as a regulatory mechanism.

In addition to protein localization, another mechanism identified for PTP1B recruitment to specific cellular targets has been through adaptor molecules, for example it has been shown that phospholipase Cγ1 mediates the interaction between PTP1B and its target Jak2 by directly binding to both proteins (Choi *et al.*, 2006). *Tb*PTP1 possesses several trypanosome-specific motifs located on the surface of the protein, which have been proposed to play a role in protein-protein interaction (Chou *et al.*, 2010), and thus could potentially mediate the phosphatase recruitment to a target protein through adaptor molecules. Experimental evidence would be needed to validate this hypothesis, however.

Another example of PTP regulation at the protein level is represented by limited proteolysis. Several mammalian PTPs, including PTP1B, have been shown to undergo limited cleavage by calpain upon platelet activation, resulting in increased activity due to the removal of a negative regulatory domain (Frangioni *et al.*, 1993; Falet *et al.*, 1998). It is not known whether *Tb*PTP1 possesses negative regulatory motifs or if it can be proteolytically cleaved under certain stimuli, but residues 135-152 have been identified as predicted PEST motif (Szoor *et al.*, 2006), a region rich in Pro, Glu/Asp, Ser/Thr and flanked by Arg/Lys, a high affinity substrate for calpains (Siman *et al.*, 1989). Moreover, some *T. brucei* calpain-like proteins, have been shown to be developmentally regulated, although their catalytic domain is not

perfectly conserved and their proteolytic activity has not been demonstrated (Hertz-Fowler *et al.*, 2001; Liu *et al.*, 2010). Due to the limited characterization of *T. brucei* proteases, there is a lack of tools, such as calpain inhibitors or stimulators, with which to assess the potential involvement of these molecules in *Tb*PTP1 regulation. Indeed proteolytic cleavage of PTP1B was only visualized by the change in electrophoretic motility of the phosphatase, after treatment with calcium ionophores, which activate calpains by raising intracellular calcium concentration, or with calpain inhibitors (Frangioni *et al.*, 1993).

4.7.1.2. *Tb*PTP1 phosphorylation

Probably the best characterized mechanism of PTP regulation, particularly for PTP1B, is phosphorylation. As previously mentioned, PTP1B activity has been shown to be modulated in a growth factor-dependent manner through phosphorylation of three serine and three tyrosine residues (Bourdeau *et al.*, 2005) and in a cell cycle-specific manner via phosphorylation of Ser352 and Ser386 (Flint *et al.*, 1993). Although these phosphorylation events have been shown to affect enzyme activity, little is known about their mechanism of action. Generally it is believed that this post-translational modification either directly interferes with catalysis or indirectly recruits phosphate-binding proteins, which are responsible for the change in enzymatic activity (den Hertog *et al.*, 2008). For example, PTP1B phospho-Tyr66 was found to be located within the consensus sequence for the SH2 domain of Grb2, an adaptor protein which binds to the EGFR, and thus it has been suggested to mediate PTP1B inhibition by competing with other substrates (Bandyopadhyay *et al.*, 1997).

A comparative analysis of PTP1B and *Tb*PTP1 phosphorylation sites showed that, among the eight phosphorylated residues of the human phosphatases, only two (PTP1B Tyr66 and Tyr152) are conserved in the parasite enzyme (*Tb*PTP1 Tyr78 and Tyr164), and also in the *T. congolense*, *T. vivax* and *T. cruzi* but not in *Leishmania major* homologues (**Figure 4.2**). Both these sites are predicted to map onto the surface of *Tb*PTP1 (**Figure 4.3**) and thus could possibly be phosphorylated. PTP1B Ser242 is substituted by Thr255 in

*Tb*PTP1, but is found within a sequence showing very low similarity to the human counterpart, and not found on the surface of the phosphatase (**Figure 4.3**), and thus may be less likely to be phosphorylated. Among the four *Tb*PTP1 residues predicted to be phosphorylated by bioinformatics analysis (Ser42, Thr238, Tyr280 and Tyr284) (**Figure 4.2**), only Ser42 is found in a more accessible position on the enzyme, compared to the others (**Figure 4.3**); in addition, Ser42 is conserved among trypanosomes and is found in the trypanosome-specific motif PcT2, and thus might represent a different phosphorylation site acquired by this family of kinetoplastid protozoa.

Although the presence and position of the conserved Tyr66 and Tyr152 could support the hypothesis of *Tb*PTP1 being tyrosine-phosphorylated, preliminary experimental evidence does not show any presence of pTyr residues in the enzyme, either before or after induction of differentiation to procyclic form (**Figure 4.4**). One reason for the lack of detectable pTyr residues in *Tb*PTP1 enzyme might be the limited amount of immuno-precipitated enzyme; moreover the phosphorylation could be transient and thus not visible after 48 hr of cis-aconitate treatment. Similarly, it could be argued that monomorphic cell lines, like the ones used for the immuno-precipitation, do not mimic physiological differentiation, as they do not pass through stumpy form stage. Consequently monomorphic lines might display a different mechanism of *Tb*PTP1 regulation, or the potential level of enzyme phosphorylation might be too low to be detectable, given the limited amount of cellular differentiation.

In order to address this issue, the creation of a pleomorphic cell line overexpressing *Tb*PTP1 would be needed, or alternatively, the endogenous phosphatase could be immunoprecipitated from wild type stumpy form cells. This however, would require a better *Tb*PTP1-specific antibody than the one available. In addition, the potential phosphorylation of the enzyme should be monitored from minutes to a few hours after induction of differentiation, in order to detect the transient or very early phosphorylation in the developmental pathway. Indeed, in the case of PTP1B, the phosphorylation of Tyr66 has been detected 5 minutes after insulin stimulation (Bandyopadhyay *et al.*, 1997). The stumpy-specific and likely transient nature of the potential *Tb*PTP1 phosphorylation, could also account

for the absence of the phosphatase in the list of *T. brucei* phosphorylated protein (Nett *et al.*, 2009b).

Taken together, the above observations indicate that more experiments will be needed to definitely rule out the possibility of *Tb*PTP1 being regulated by Tyr or Thr/Ser phosphorylation.

4.7.1.3. *Tb*PTP1 sumoylation

A relatively recently described post-translational modification regulating PTPs activity is sumoylation. Generally, sumoylation can affect protein function by masking or creating binding sites on the sumoylated molecule, or by changing its conformation (Wilkinson *et al.*, 2010). In the case of PTP1B, the only PTP identified to date as being regulated by this modification (Dadke *et al.*, 2007), sumoylation of Lys335 and Lys347 has been suggested to block the catalytic domain of the phosphatase thus inhibiting its activity upon insulin stimulation.

Interestingly, *Tb*PTP1 also possesses the sumoylation consensus motif on Lys131 (ΨKxD/E, where Ψ is A/I/L/M/P/F/V and X is any aa), which is conserved among *T. congolense*, *T. vivax*, *T. cruzi* and *L. major* but not with human PTP1B (which lacks the D/E residue) (**Figure 4.5 A**). However, *Tb*PTP1 Lys131 is not found on the surface on the enzyme, whereas the residues shown to be sumoylated in PTP1B are found in the C-terminal domain of the protein, which is probably much more accessible to SUMO-conjugating enzymes (Dadke *et al.*, 2007). Moreover, although about 75% of sumoylation occurs within the consensus motif, it can also occur at lysine residues outside the motif and not all ΨKxD/E sequences are sumoylated (Wilkinson *et al.*, 2010).

The role of protein sumoylation in *T. brucei* is not known, but one SUMO homologue has been recently characterized and showed to be essential for the cell-cycle regulation of procyclic forms (Liao *et al.*, 2010). As visualization of protein sumoylation is often missed in absence of strong SUMO isopeptidase inhibitors (Dadke *et al.*, 2007), the conserved functionality of such inhibitors in *T. brucei* would have to be tested before being used to experimentally validate the presence of sumoylated *Tb*PTP1. Consequently,

conclusions on the potential role of this modification on *Tb*PTP1 regulation can not be drawn at this time.

4.7.1.4. *Tb*PTP1 oxidation

A well-established post-translational mechanism of PTPs regulation is oxidation (Monteiro *et al.*, 1996; Denu *et al.*, 1998). Most PTPs are sensitive to oxidation due to the unique environment of the active site, which renders the catalytic cysteine particularly vulnerable to oxidative agents (Meng *et al.*, 2002). Crystallographic studies performed on PTP1B have characterized the mechanism in detail, whereby the oxidation of the cysteine to sulphenic acid (S-OH) causes the formation of a covalent bond between the cysteine sulphur atom and the main chain nitrogen of the adjacent serine residue (Salmeen *et al.*, 2003). Such modifications result in changes in the architecture of the active site, which have been suggested to protect the enzyme from further irreversible oxidation and to facilitate reduction back to the active form of the phosphatase (Tonks, 2005). PTP inactivation through reversible oxidation has been shown to happen in response to several physiological stimuli, such as insulin (Mahadev *et al.*, 2001) and growth factors (Chen *et al.*, 2006), and is often mediated by the action of ligand-activated NADPH oxidases (Chen *et al.*, 2008). The interaction between ROS-generating enzymes and PTPs is believed to convey signal specificity, since phosphatases are not the only ROS target present in the cell. For example, PTP1B has been shown to be inhibited by oxidation upon interleukin-4 stimulation in T cells, through the activation of the NADPH oxidase NOX1 (Sharma *et al.*, 2008a). However, exogenous H_2O_2 has also been shown to mimic insulin activity on PTPs (Heffetz *et al.*, 1992).

Trypanosoma brucei possesses a peculiar redox metabolism compared to higher eukaryotes. Indeed trypanosomes lack the proteins responsible for mammalian detoxification from ROS, such as glutathione reductase, thioredoxin reductase, and catalase. Neutralization of hydrogen peroxide is obtained through the action of Prx (2-Cys-peroxiredoxin) and Px (glutathione-peroxidase-type enzymes), which derive their reducing

equivalents from the cascade composed of T(SH)2 (trypanothione) and TXN (tryparedoxin) (Krauth-Siegel *et al.*, 2008).

ROS have been shown to play a role in *T. brucei* programmed cell death (Figarella *et al.*, 2006), drug resistance (Tsuda *et al.*, 2006) and parasite clearance in the tseste fly (Hao *et al.*, 2003), but their potential involvement in parasite differentiation has not been studied. However, some stress conditions, which are generally known to produce increase in intracellular ROS in higher eukaryotes (Fedoroff, 2006), have been linked to parasite differentiation from stumpy to procyclic forms. Notably treatment of bloodstream form cells with trypsin (Yabu *et al.*, 1988) or pronase, a mixture of proteinases, have been shown to induce expression of the procyclic form-specific EP protein (Hunt *et al.*, 1994; Sbicego *et al.*, 1999). Moreover, mild acid treatment of pleomorphic cells has been shown to cause transformation of stumpy form into procyclic form cells (Rolin *et al.*, 1998). However, it is also worth noting that it is not known whether these triggers possess a real physiological role in trypanosome differentiation or if they act in a similar way. Interestingly, trypsin and pronase have also been involved in the induction of intracellular ROS in lung fibroblasts, and although their mechanism of action have not been characterized, potential ways in which these compounds could act have been suggested, such as through proteinase-activated receptors or ion channels, or via increase membrane permeability and loss of intracellular antioxidants (Aoshiba *et al.*, 2001).

Although the links between ROS and mammalian PTPs inactivation and ROS and cellular stress are well established, there is no example in the literature showing phosphatase oxidation under stress conditions, as the only stimuli identified so far to produce ROS-mediated enzyme inhibition have been insulin (Mahadev *et al.*, 2001) and growth factors (Chen *et al.*, 2006; Sharma *et al.*, 2008a). It is possible that PTP regulation via oxidation requires a more localized increase in ROS, achievable through activation of cellular oxidases in a ligand-dependent manner, as reported for PTP1B under certain stimuli (Tonks, 2003; Sharma *et al.*, 2008a), rather than a generalized ROS production usually originated from the mitochondria (Aoshiba *et al.*, 2001). However, as mentioned earlier, exogenous H_2O_2 has been shown to mimic the insulin effect on protein phosphorylation in intact cells (Heffetz *et al.*, 1992). For

these reasons the potential role of both stimulus-dependent and exogenous H_2O_2-induced increase in intracellular ROS during trypanosome differentiation were investigated.

Since the physiological trigger of parasite differentiation to procyclic forms is considered to be citrate/cis-aconitate (CCA) (Overath *et al.*, 1986; Engstler *et al.*, 2004) it was particularly interesting to test whether CCA could cause *Tb*PTP1 inhibition through production of intracellular ROS, similarly to what is observed for insulin and PTP1B (Mahadev *et al.*, 2001). In order to do so, it was first necessary to monitor intracellular ROS upon CCA treatment of bloodstream form cells. Unexpectedly, the most widely used redox-sensitive probe H_2-DCFDA, reacted with CCA in a cell-free environment (**Figure 4.6**), thus excluding this dye as a useful tool to assess ROS formation. To overcome this problem a different compound (Ampliflu™ red) had to be used, as most of the redox-sensitive compounds share the fluorescein moiety found in H_2-DCFDA. Cells were monitored continuously from 5 minutes after CCA addition, since ROS signalling events have been shown to start as early as 5 minutes after EGF stimulation (Bae *et al.*, 1997) or peak at 45 minutes after integrin-mediated cell adhesion (Chiarugi *et al.*, 2003). In fact, 3 hr was chosen as upper limit for detection of potential signalling events leading to differentiation, since the first detectable cytological event is the appearance of EP protein at 2-4 hr after CCA addition (Ziegelbauer *et al.*, 1990). During this time, Ampliflu™ red did not show increased fluorescence upon CCA treatment of bloodstream or stumpy form cells (**Figure 4.7**).

These results suggest that CCA do not induce formation of intracellular ROS under these conditions, however it is also possible that Ampliflu™ red might not be sensitive enough to detect potentially small ROS increase, since it reacts with H_2O_2 outside the cell and thus might require a greater ROS gradient. Indeed Ampliflu™ red has been used mainly to compare baseline levels of ROS among different cell types, rather than to detect transient increase of ROS upon stimulation (Lou *et al.*, 2008). It is also possible that a different stimulus or stimuli might be needed, as PTP inactivation by oxidation has been shown to be growth factor-specific (Meng *et al.*, 2002).

Since CCA-induced differentiation did not result in increased intracellular ROS, the possibility of exogenous H_2O_2 regulating *Tb*PTP1 activity was then

investigated. To test this hypothesis, bloodstream or stumpy form cells were treated with different concentrations of H_2O_2 ranging between 5 and 100 μM. The lack of EP protein expression, even after 48 hr of treatment, indicated that exogenous H_2O_2 was not able to induce trypanosome differentiation to procyclic forms (**Figure 4.8 A**), unlike what seen in mammalian cells (Heffetz *et al.*, 1992).

Having shown that CCA and exogenous H_2O_2 are unlikely to be responsible for *Tb*PTP1 oxidation, it was then interesting to test the role of endogenous ROS, potentially produced by stimuli other than CCA, in cellular differentiation. For this purpose, cells were treated with the ROS scavenger N-acetyl cysteine (NAC), at 0.25 and 0.4 mM, concentrations found to be effective in preventing intracellular ROS increase upon H_2O_2-exposure but not to be cytotoxic (**Figure 4.8 B** and **D**, respectively). The results showed that NAC treatment did not affect the number of EP positive cells (**Figure 4.8 C**), thus suggesting that H_2O_2 is unlikely to play a role in the parasite differentiation pathway.

The above observations indicate that *Tb*PTP1 might not be regulated through oxidation *in vivo*. Indeed, although *Tb*PTP1 has been shown to be sensitive to this modification *in vitro*, reaching 0% of activity after 15 min of 0.25 mM H_2O_2 treatment (Szoor *et al.*, 2006), another PTP, PTEN, has shown similar inhibition after only 5 min of 0.1 mM H_2O_2 (Ross *et al.*, 2007). Therefore it is possible that *Tb*PTP1 might be relatively resistant to oxidation, as reported for other PTPs (Ross *et al.*, 2007), but to validate this hypothesis a more uniform and detailed comparative analysis would be needed.

Differences in PTPs oxidation levels have also been noted to be cell type-specific, probably due to the different oxidative environment of the cell lines (Weibrecht *et al.*, 2007). This phenomenon, although not directly relevant to the signalling events leading to differentiation, could maybe account for the maintenance of *Tb*PTP1 inactivation in procyclic forms, since insect-stage cells display higher mitochondrial activity than bloodstream forms and thus have potentially higher ROS production (Vickerman *et al.*, 1988).

In addition, recent experimental evidence has shown that *Tb*PTP1 is regulated by its own substrate, *Tb*PIP39, in a CCA-dependent manner, with CCA inhibiting the increase in activity seen when *Tb*PTP1 is incubated with

*Tb*PIP39 *in vitro* (Szoor *et al.*, 2010). If this observation reflects the *in vivo* situation, then *Tb*PTP1 would be positively regulated by its own substrate in stumpy form cells and addition of CCA would neutralize such regulation. It is not known how *Tb*PIP39 affects *Tb*PTP1 activity, but one possibility might be through enzyme-substrate interaction leading to conformational changes in the enzyme and resulting in its increased activity. In this case, CCA would interfere with this interaction by binding to the *Tb*PIP39 citrate binding pocket, thus loosening the enzyme-substrate cooperative interaction and decreasing its activity. Such a mechanism might not require additional levels of *Tb*PTP1 control and would represent a novel way of PTP regulation, different from the ones described in literature to date (den Hertog *et al.*, 2008).

In order to dissect the physiological importance of the possible different *Tb*PTP1 regulatory mechanisms it would be necessary to assess the *in vivo* activity of this phosphatase during differentiation. Monitoring enzyme oxidation through techniques such as the in-cell oxidation assay (Ross *et al.*, 2007), in-gel phosphatase assay (Meng *et al.*, 2004) and through the use of oxidation-specific antibodies (Persson *et al.*, 2004) or by mass spectrometry (Caselli *et al.*, 1998) would be an obvious choice to address this question. In addition, it would be important to test phosphatase activity under a certain stimulus by performing activity assays "ex-vivo" on the immuno-precipitated enzyme (Chiarugi *et al.*, 2003). All these techniques require very specific conditions of cell lysis and protein manipulation to avoid spontaneous enzyme oxidation, for example lysing cells under anearobic conditions, and thus are relatively laborious. In addition, they require the phosphatase to be immunoprecipitated, which is technically difficult in the absence of a good antibody against endogenous *Tb*PTP1 or of a pleomorphic line expressing the tagged enzyme, as already mentioned. In the future, it would also be useful to express mutant versions of *Tb*PTP1, lacking the potential phosphorylation/sumoylation sites or PEST sequence, to dissect the role of these different modifications on the phosphatase activity. Similarly, monitoring *Tb*PTP1 activity *in vivo*, in cells expressing different versions of *Tb*PIP39, for example possessing a mutated citrate-binding site,

would be needed to address the importance of *Tb*PIP39 and the CCA-mediated regulation of *Tb*PTP1.

4.7.2 Monitoring *Tb*PIP39 phosphorylation upon treatment of stumpy form cells with different differentiation triggers

Parallel to the dissection of *Tb*PTP1 regulation during differentiation, it was interesting to investigate whether other triggers of the transition to procyclic forms also act through the *Tb*PTP1-*Tb*PIP39 signalling cascade, as seen for CCA (Szoor *et al.*, 2010).

The antibody developed for the phosphorylated Y278 residue of *Tb*PIP39 (p-PIP39) was a useful tool for this purpose. As expected, the signal of the anti p-PIP39 antibody disappeared in the presence of recombinant active *Tb*PTP1 (**Figure 4.9** middle panel, arrow) and detected the same 40-kDa band recognized by the anti-PIP39 antibody (**Figure 4.9** upper panel), thus demonstrating its specificity. Moreover, analysis of cell extracts from different life cycle stages showed an increasing level of phosphorylated *Tb*PIP39 progressing from slender, to stumpy and procyclic form (**Figure 4.10 A**), with established procyclics showing approximately a 2.6 fold increase compared to stumpy forms. Similarly greater levels of phosphorylated *Tb*PIP39 were detected after 1.5 hr treatment with cis-aconitate or with the *Tb*PTP1 inhibitor BZ3 (**Figure 4.10 B**). Interestingly, a slightly greater increase in p-PIP39 signal was obtained at 1.5 hr after induction of differentiation compared to established procyclics (3-4 fold versus 2.6 fold, compared p-PIP39 quantification in Figure **4.10 B** and **A**). This observation suggests that *Tb*PIP39 phosphorylation might peak soon after induction of differentiation after which it is maintained at somewhat lower levels in established procyclic forms. However, because of the small difference in p-PIP39 signal, repeats of this analysis will be needed to statistically validate these preliminary results.

In order to better characterize the degree and timing of p-PIP39 increase during CCA-induced differentiation, the p-PIP39 signal, normalized to tubulin, was compared at different time points and among several experiments; the level of p-PIP39 showed a reproducible increase from 2 to 24 hr of treatment (**Figure 4.11 B**). However, because of the variability

between different blots of the same experiment and among different experiments, this increase was not statistically validated. Variations in p-PIP39 quantification were not matched by variations in cellular differentiation, as most experiments showed very similar levels of EP protein expression at the different time points (**Figure 4.11 C**). Therefore, it is likely that Western blot processing and quantitation account for most of the variability observed and consequently, it was not possible to identify the time point after cis-aconitate treatment at which the p-PIP39 level peaked. As expected, citrate, the other citric acid cycle intermediate known inducer of differentiation (Czichos *et al.*, 1986), also generated an increase in *Tb*PIP39 phosphorylation levels similar to those obtained with cis-aconitate (**Figure 4.12 A**).

4.7.2.1. Effects of cold shock on the phosphorylation levels of *Tb*PIP39

Since the physiological differentiation of stumpy form to procyclic form cells, is believed to be achieved through the cooperative effect of cis-aconitate and temperature reduction (Engstler *et al.*, 2004), the consequences of cold shock on p-PIP39 were investigated. It was first interesting to test the effect of cold shock alone, which has been shown to cause EP protein expression but not cell proliferation and differentiation (Engstler *et al.*, 2004). Upon overnight incubation at 20°C (cold shock), no increase in p-PIP39 level was detected (**Figure 4.13 A**), in accordance with the lack of differentiation previously reported. In contrast, increased p-PIP39 levels were observed when cells were cold shocked in presence of 1 mM cis-aconitate (**Figure 4.14 A**), which was able to induce differentiation, as the temperature shift renders the cells sensitive to concentrations of cis-aconitate lower than 6 mM (Engstler *et al.*, 2004). However, the increase in p-PIP39 detected under these conditions was comparable to what seen if cells were treated with 6 mM cis-aconitate with or without cold shock (**Figure 4.14 A**).

Taken together, the above results suggest that cold shock does not directly affect the levels of *Tb*PIP39 phosphorylation, and that cold shock-induced sensitization of stumpy form cells to cis-aconitate does not seem to be achieved through increased p-PIP39 levels. The latter observation, which

apparently contradicts the hypothesis that cold shock-induced expression of *Tb*PIP39 would increase the level of phosphorylated *Tb*PIP39 promoting differentiation (Szoor *et al.*, 2010), in reality indicates that *Tb*PIP39 upregulation might not always be required to induce transition to procyclic forms, as long as increased levels of p-PIP39 are present. Therefore cold shock would sensitize trypanosomes to cis-aconitate by promoting its transport into the cell, through expression of the PAD transporter (Dean *et al.*, 2009). Thereafter, the presence of higher intracellular CCA would inhibit the feedback activation of *Tb*PTP1 by *Tb*PIP39, thus increasing the levels of phosphorylated *Tb*PIP39, responsible for transmitting the differentiation signal to the glycosomes (Szoor *et al.*, 2010).

4.7.2.2. Effects of mild acid treatment on the phosphorylation levels of *Tb*PIP39

In addition to CCA and cold shock, mild acid treatment has been reported to induce differentiation to procyclic form cells, although with different kinetics (Rolin *et al.*, 1998). A 2-hr incubation of pleomorphic cells in media at pH 5.5 resulted in loss of slender forms and a concomitant increase in stumpy forms, probably due to the death of the less resistant slender forms to acidic stress and likely mediated by the glycophosphatidilinositol-specific phospholipase C (GPI-PLC) (Rolin *et al.*, 1998; Nolan *et al.*, 2000). According to the published data, mild acid treatment induced a more limited degree of cellular differentiation compared to CCA, with less than 50 % of the cells showing EP positivity after 48 hr (**Figure 4.15 B**). No visible change in the level of phosphorylated *Tb*PIP39 was detected during the treatment (**Figure 4.15 A**) suggesting that acid stress might not act through the *Tb*PTP1-*Tb*PIP39 pathway. However, due to the more limited degree of differentiation after mild acid treatment and to the potentially transient nature of *Tb*PIP39 phosphorylation, comparison with CCA-induced differentiation is difficult and thus more experiments would be needed to draw convincing conclusions.

4.7.2.3. Effects of pronase treatment on the phosphorylation levels of *Tb*PIP39

Proteolytic stress has also been shown to induce trypanosome differentiation to procyclic forms (Hunt *et al.*, 1994; Sbicego *et al.*, 1999). The importance of the potential role of proteolytic stress in the physiological transition from bloodstream to the vector stage parasite has been supported by the observations that bloodstream form cells have been shown to release proteinases (Nwagwu *et al.*, 1988) and that trypsin-like enzymes have been found in the tsetse fly midguts (Imbuga *et al.*, 1992).

Studies looking at the effect of pronase or trypsin treatment on pleomorphic bloodstream form trypanosomes have reported a different kinetic of EP protein expression and timing of morphological changes compared to CCA-treatment; specifically a faster EP protein expression has been shown, with 100% of positive cells at 6 hr after pronase treatment compared to 90% after CCA-induced differentiation (Sbicego *et al.*, 1999). Similarly, a faster acquisition of the typical procyclic-form morphology has been reported, with 95% of procyclic-like cells visible at 72 hr after pronase treatment, compared to 55% of CCA-treated cells at the same time point (Hunt *et al.*, 1994). Moreover both studies have highlighted the fact that the protease-treated cells showed some degree of cell death, reaching 5-6 times lower cell density than for CCA treated (Sbicego *et al.*, 1999), with slender form cells being more sensitive than stumpy forms (Hunt *et al.*, 1994). The latter observation prompted the investigators to test whether the effect of pronase treatment on pleomorphic cells differentiation was merely due to selection of stumpy forms. For this reason they subjected to pronase treatment a population of pure stumpy cells, which resulted in transition to procyclic form cells, thus demonstrating that proteinase treatment acted directly, triggering differentiation (Sbicego *et al.*, 1999).

Interestingly, both papers made two other potentially important observations. Firstly that proteinase and CCA seemed to act through a different mechanism, as judged by different kinetics of differentiation (Hunt *et al.*, 1994) and demonstrated by the fact that addition of the soybean trypsin inhibitor did not inhibit CCA-induced differentiation (Sbicego *et al.*, 1999).

Secondly, they both observed an additive effect of pronase/tryspin and CCA treatment compared to CCA treatment alone.

According to the published results, treatment of stumpy form cells with 4 U/ml of pronase, for 10 min at 25°C, resulted in higher EP protein expression than what is usually seen with 6 mM cis-aconitate, with almost 50% of EP-positive cells detected at 2 hr compared to 0% of CCA-treated (**Figure 4.16 C**). However, the pronase-treated cells never reached 90-100% of EP positivity, probably caused by the high rate of cell death, possibly due to the use of a stronger proteinase treatment than published (Hunt *et al.*, 1994).

In addition, the procyclic morphology that was seen at 72 hr of pronase treatment by Hunt *et al.*, and Sbicego *et al.*, was not present after 24 hr of treatment in the experiments presented here. The only report monitoring in detail the morphological changes during pronase treatment (Frevert *et al.*, 1986) highlighted the presence of major structural changes, such as removal of the surface coat, flagellar internalization and dissolvement of the flagellar pocket, between 10 seconds and 20 minutes of treatment. However, these morphological changes do not mirror the ones induced by cellular differentiation, with the exception of surface coat removal. Furthermore, the concentration of pronase used by Frevert *et al.*, is difficult to compare with other studies, due to the different origin of the enzymes, and thus the massive morphological changes reported could be explained by a higher and unphysiological pronase concentration. Interestingly, pronase treatment had a much weaker effect on the phosphorylation levels of *Tb*PIP39 compared to cis-aconitate, with only faint bands visible at most of the timepoints (**Figure 4.16 A** α p-PIP39) and in at least three different experiments. This observation supports the hypothesis suggested by both Hunt *et al.*, and Sbicego *et al.*, regarding a potential different mechanism of pronase and CCA-induced differentiation. For example, it is possible that proteinase treatment induces a fast EP expression by bypassing the initial signalling events required for CCA-induced differentiation (**Figure 4.17**).

In order to draw conclusions about these two potentially different pathways, I believe, that it would first be necessary to monitor the effect of pronase treatment on EP expression and the morphology of stumpy cells in more

detail. In parallel, it would also be useful to investigate the kinetics of the events *in vivo*, as differences have been observed between the timing of transformation in culture and in the fly (Turner *et al.*, 1988). If the physiological roles and the different kinetics of the two triggers are confirmed, then the hypothesis of the existence of two pathways should seriously be considered. Although the presence of more than one mechanism of trypanosome differentiation may be unexpected, pronase and CCA might actually act complementarily and might both be required for differentiation in the vector. Indeed, the cooperative action of pronase and CCA has been suggested from the observation that the simultaneous treatment of cells with both triggers resulted in a twice as fast kinetics of EP expression (Sbicego *et al.*, 1999).

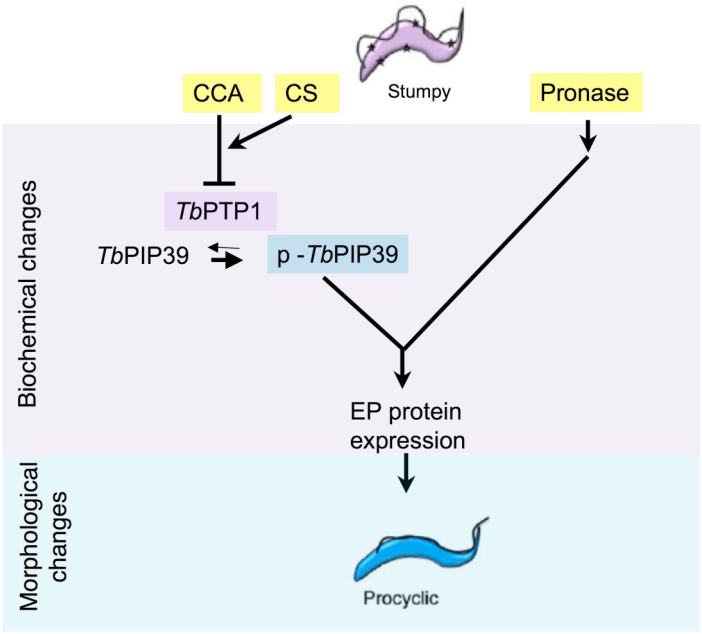

Figure 4.17 Signalling pathways involved in *T. brucei* differentiation from stumpy to procyclic forms. Diagram depicting the potentially different pathways involved in parasite differentiation triggered by citrate/cis-aconitate (CCA), cold shock (CS) (which acts together with CCA, although here is represented as different for clarity), and pronase. CCA acts by inhibiting *Tb*PTP1, thereby promoting *Tb*PIP39 phosphorylation, which leads to EP protein expression and the subsequent functional and morphological changes. Pronase treatment of stumpy forms does not seem to act through *Tb*PIP39, but via another pathway resulting in a faster EP protein expression and probably in morphological changes characteristic of differentiation, although some differences were noted in this study.

Chapter 5

Investigation of *Tb*PTP1 as a therapeutic target for the control of disease transmission

5.1. Background

The rationale behind targeting *Tb*PTP1 as a means to control sleeping sickness transmission lies in the fact that inhibition of the phosphatase causes bloodstream stumpy form parasites to differentiate into procyclic form cells (Szoor *et al.*, 2006). Stumpy forms are the only bloodstream form cells that are pre-adapted to survive in the vector (Vickerman *et al.*, 1988), therefore treating an infected individual or animal with a drug inhibiting *Tb*PTP1 would decrease the chance of disease transmission.

*Tb*PTP1 is 24% identical at protein level with the human protein tyrosine phosphatase 1B (PTP1B) (see paragraph 1.17), which is one of the most attractive PTPs in the field of drug discovery; indeed PTP1B is a negative regulator of the insulin and leptin pathways, and mice deficient for such protein have shown increased sensitivity to insulin and resistance to obesity, thus establishing PTP1B as a therapeutic target for the treatment of type 2 diabetes and obesity (Elchebly *et al.*, 1999). Several pharmaceutical companies have been working to develop potent and selective PTP1B inhibitors (Zasloff *et al.*, 2001; van Montfort *et al.*, 2003), as obesity represents a hugely lucrative market: according to the WHO projections, approximately 2.3 billion adults will be overweight and more than 700 million will be obese by 2015.

The possibility of using a PTP1B inhibitor to target the parasite enzyme would provide a "piggy-back" strategy to control sleeping sickness transmission. "Piggy-back" denotes a drug discovery approach for neglected tropical diseases, which relies on the existence of a molecular target in the parasite, that has been pursued for other commercial indications (Nwaka *et al.*, 2006). This strategy facilitates the identification of chemical entities active towards the parasite target, and has been used for the screening of antimalarial drugs from mammalian inhibitors of histone deacetylase (Andrews *et al.*, 2000) and of cysteine proteases (Semenov *et al.*, 1998), originally developed for treatment of cancer and osteoporosis, respectively. The additional advantage of the "piggy-back" approach is the potential use of existing drugs to target the parasite protein ("label extension" or drug

repositoning) (Nwaka *et al.*, 2006). The use of an existing drug for the treatment of a disease, different to the one the drug was originally developed for, has the advantage that the candidate has known safety and pharmacokinetics properties, since it has been through some clinical development, and thus represents a less risky, cheaper and faster pathway to the market (Ashburn *et al.*, 2004). The possibility of delivering a drug more quickly and at lower costs is particularly attractive for sleeping sickness and for other neglected tropical diseases, because they affect mainly poor people, and therefore do not represent lucrative markets for pharmaceutical companies (Trouiller *et al.*, 2001). For this reason, label extension is considered the most successful drug discovery strategy for the treatment of neglected tropical diseases, and it has resulted in the identification of several anti-parasitic drugs in use today, such as eflornithine for sleeping sickness (see paragraph 1.5.5), ivermectin for filariasis and praziquantel for schistosomiasis (Nwaka *et al.*, 2006).

For the above reasons, seventeen PTP1B inhibitors, derived from the Drug Discovery Portal (DDP) at the University of Strathclyde in Glasgow, were tested against *Tb*PTP1 *in vitro* and their IC_{50} and K_i values were calculated in order to identify the most potent compounds. In addition, *in vitro* competition assays were performed to find out whether the compounds bind the catalytic site of the enzyme, thus further characterizing their mechanism of action. The inhibitors with lower IC_{50} were also tested on stumpy form *T. brucei* to evaluate their specificity against *Tb*PTP1 *in vivo*.

In addition to the seventeen compounds received from the Drug Discovery Portal, two other known PTP1B inhibitors were tested: oleanolic acid (Zhang *et al.*, 2008) and suramin (McCain *et al.*, 2004). Oleanolic acid was chosen because it is a natural compound discovered from traditional Chinese medicinal herbs, like several well-established anti-protozoal drugs, such as quinine and artemisinin (Klayman, 1985); moreover its cheapness, commercial availability and safety (Zhang *et al.*, 2008) represented valuable properties for a potential drug, particularly for the control of a neglected tropical disease. Oleanolic acid is a triterpenoid compound present in a wide variety of foods, and in more than 120 plant species and demonstrating a

plethora of effects, including anti-inflammatory, antimicrobial, hepatoprotective and antitumoral activity (Liu, 1995). In addition, oleanolic acid has been found to have antimalarial properties (Steele *et al.*, 1999) and to be trypanocidal for bloodstream form *T. b. brucei* (Salem *et al.*, 2006).

Suramin is a drug already in use for the treatment of early stage HAT, whose mode of trypanocidal action has not been definitely proven. Although it has been shown to inhibit glycerolphosphate oxidase and other glycolytic enzymes (Fairlamb *et al.*, 1977), it is believed to have additional targets due to its six negative charges, which can easily form strong electrostatic interactions with a variety of enzymes (Fairlamb *et al.*, 1977; Wierenga *et al.*, 1987; Barrett *et al.*, 2007). Moreover it has been found to be an effective inhibitor of human PTP1B (McCain *et al.*, 2004). In order to elucidate suramin activity and to potentially further characterize its mode of action, it was interesting to test the drug against *Tb*PTP1 *in vitro* and *in vivo*.

5.2. *In vitro* Screening of PTP1B inhibitors against *Tb*PTP1

Among the variety of assays available to monitor protein tyrosine phosphatase activity (Montalibet *et al.*, 2005) the method chosen was the use of p-nitrophenyl phosphate (pNPP), a colorless substrate that upon hydrolysis to p-nitrophenol (pNP) becomes yellow, and the formation of which can be monitored by absorbance at 405 nm. Since the phenolate ion has a pKa of 7.2, the pNP absorbs mostly at alkaline pH, which is not the ideal pH of many tyrosine phosphatases (including *Tb*PTP1 (Szoor *et al.*, 2006)). Hence the reaction needs to be stopped and the pH raised in order to detect the product formed (Montalibet *et al.*, 2005).

In order to determine the optimal reaction rate before performing enzymatic assays, it was important to perform a rate assay: an assay with serial dilutions of enzyme and at saturating concentrations of substrate (pNPP). Enzyme concentration was then plotted against the initial rate of the reaction, which was calculated by dividing the absorbance measured by the

reaction time (**Figure 5.1 A**). From the rate assay graph it could be determined the minimum enzyme concentration found within the linear range of the reaction (between approximately 100 and 300 nM, since higher concentrations gave a O.D measure that was outside the software test range of 0-2.5). Converting moles into grams (for a 34-kDa protein 100 pmoles= 3 μg), the concentration range, in order to have detectable level of product within the linearity of the reaction, was between approximately 0.24 and 0.8 μg per reaction.

The next step important for enzyme characterization and necessary for further assays was the determination of the Michaelis and Menten kinetics. The Michaelis and Menten model describes the rate of catalysis of most enzymes, which rises with increasing concentration of substrate, until it reaches a maximum and begins to level off (hyperbolic plot) and is formalized in the following equation: $Y= (V_{max}x\ X)/(K_M+X)$, where Y is the enzyme velocity, X is the substrate concentration, K_M is the Michaelis and Menten constant and V_{max} the maximal rate or enzyme turnover. Both K_M and V_{max} depend on the substrate and on the environment of the enzyme (buffer pH and composition); the K_M is equal to the substrate concentration when V is equal to $(½)V_{max}$ and thus provides a measure of the substrate concentration required for significant catalysis to occur. In addition, the K_M is a measure of the strength of the enzyme-substrate complex: low K_M values indicate strong binding, high K_M values indicate weak binding. The maximal rate of enzyme reaction (V_{max}) is defined as the number of substrate molecules that are converted into product in a unit time when the enzyme is fully saturated with substrate (Berg *et al.*, 2002). In order to obtain K_M and V_{max}, a constant concentration of enzyme was assayed against increasing concentrations of substrate (pNPP) and the velocity (V_0) of pNPP hydrolysis was plotted against the pNPP concentration (**Figure 5.1 B**). The velocity of pNPP hydrolysis was calculated using the following formula: $V=A/(\varepsilon \times 1\ cm \times 15\ min)$, where A is the absorbance measured and ε is the pNPP extinction coefficient (see Materials and Methods). The data were then analysed with GraphPad Prism software, which calculated a V_{max} of 3.03 mmol/min and K_M

of 2.72 mM, when the quantity of enzyme used was 0.4 μg/reaction (**Figure 5.1 B**).

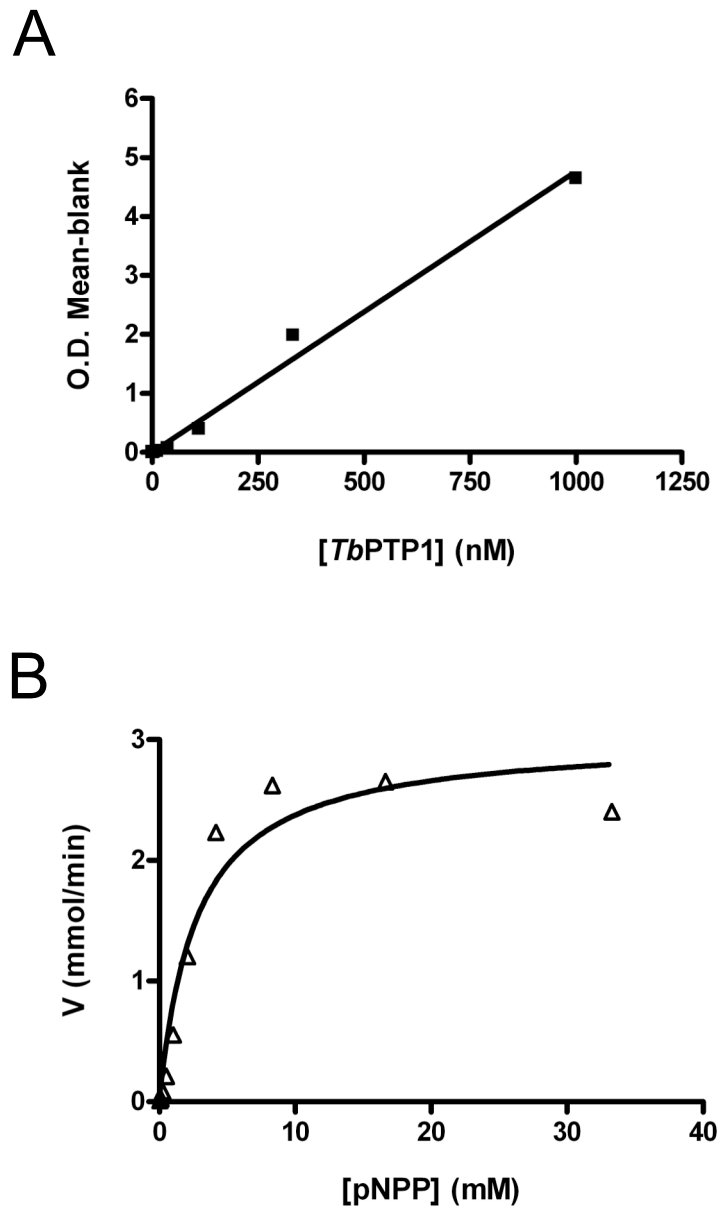

Figure 5.1.*Tb*PTP1 rate assay and Michaelis and Menten kinetics. A shows the plot of the initial rate of reaction; on the y-axis is plotted the absorbance at 405 nm of the enzyme and substrate minus the absorbance of buffer and substrate alone (blank), and on the x-axis is plotted the concentration of enzyme ([*Tb*PTP1]). B shows the Michaelis and Menten plot of enzyme velocity, measured in millimoles per minute (mmol/min), versus substrate concentration ([pNPP]); the calculated V_{max} and K_M were 3.03 mmol/min and 2.72 mM, respectively.

In order to compare the activity of different inhibitors for a certain enzyme it was important to determine the concentration of the inhibitor that reduced the maximum enzyme velocity by half (IC_{50}). The IC_{50} value can be calculated from the sigmoidal dose-response curve, formalized in the following equation: $Y= Bottom+ (Top-Bottom)/(1+10^{LogIC50-X})$, where Y is the enzyme velocity, X is the logarithmic concentration of the inhibitor, the variable Bottom is the Y value at the bottom of the plateau, the Top is the Y value at the top of the plateau and $LogIC_{50}$ is the X value when the response is halfway between Bottom and Top (Motlusky *et al.*, 2003). In order to calculate the IC_{50} a series of reactions were carried out, each containing a different concentration of inhibitor; the enzyme and substrate concentrations were maintained constant and the latter was kept lower than the saturating concentration (usually at K_M) in order to allow the competition of the inhibitor for the enzyme.

Since the IC_{50} value depends on the reaction conditions, it cannot be used to compare the affinity of a certain inhibitor under different experimental conditions, for this purpose the dissociation constant (K_i) can be used. K_i is the concentration of inhibitor that will bind to half the enzyme sites in the absence of substrate. The dissociation constant is inversely proportional to the binding affinity of the inhibitor: if K_i is low, the affinity is high (Motlusky *et al.*, 2003). In order to compare the activity of the inhibitors for PTP1B and for *Tb*PTP1, K_i values were calculated using GraphPad Prism software, by choosing the one-site binding equation: $Y=(V_{max}x\ X)/(K_M+X)$, where X= log[In] and Y= V, then selecting the option of calculating K_i from IC_{50} using the K_M value of the enzyme in absence of inhibitor, and the concentration of substrate used for the competition assays (0.175 mM).

Seventeen DDP PTP1B inhibitors were tested against *Tb*PTP1 and the relative IC_{50} were calculated (**Table 5.1 and** see **Appendix A** for their dose-response curves). Among them four (DDP inhibitor 2, 5, 7 and 12) possessed IC_{50} between 50 and 100 μM, with 95% confidence interval between 10 and 300 μM) (**Figure 5.2** and highlighted in blue in **Table 5.1**); three compounds (DDP inhibitor 11, 15 and 17) showed an IC_{50} between 100 and 200 μM (highlighted in pink in **Table 5.1**), and three (DDP inhibitor 1, 12 and 13)

showed IC_{50} between 200 and 350 μM (**Table 5.1**). For the remaining seven DDP inhibitors it was not possible to calculate accurate values, probably due to very low inhibitory activities or sometimes to precipitation of the compounds.

In addition to the DDP inhibitor 2, 5 and 7, BZ3, suramin and vanadate showed K_i and IC_{50} values of less than 100 μM, whereas oleanolic acid was found to have a K_i and IC_{50} between 100 and 200 μM. BZ3 and vanadate represented positive controls, as their inhibitory activity on *Tb*PTP1 had already been tested (Szoor *et al.*, 2006).

The comparative analysis of the inhibitory activities of the same compounds against *Tb*PTP1 and PTP1B (**Appendix A** and **B** and **Table 5.1**), revealed no significant differences in K_i and IC_{50} values for most of them; only DDP inhibitor 6 showed a significantly greater inhibition of the human enzyme compared to the parasite homolog.

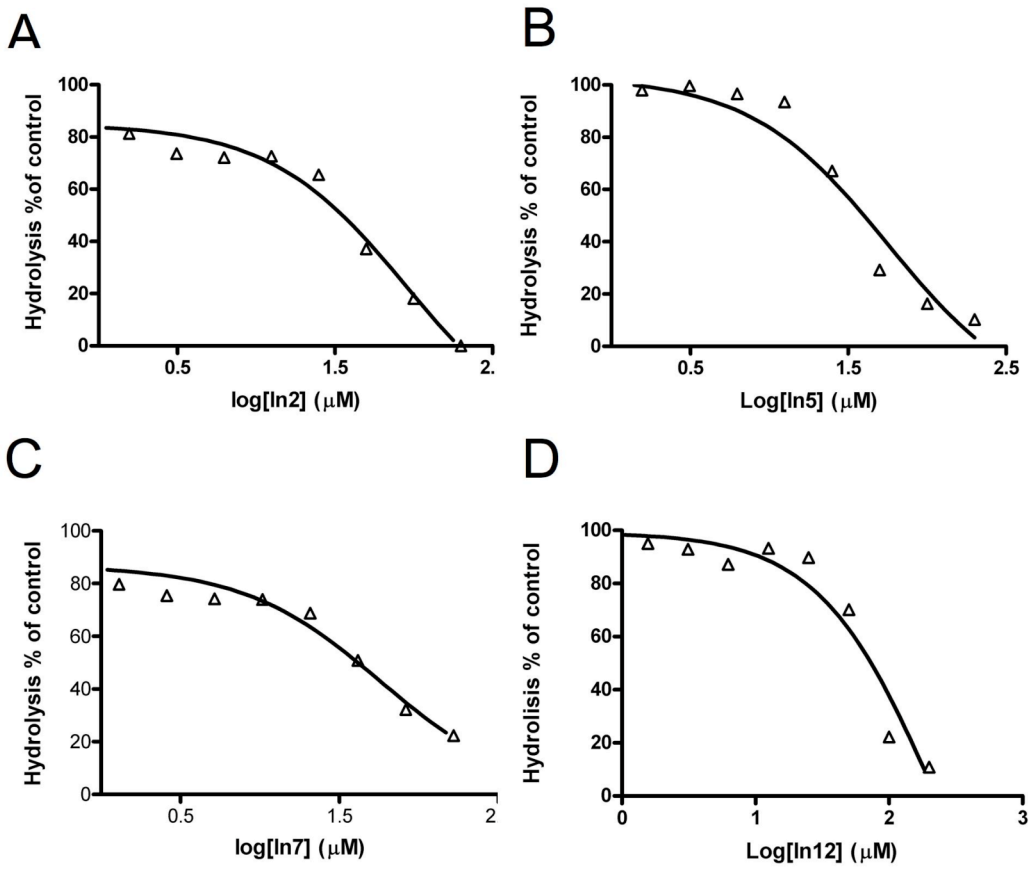

Figure 5.2 Dose-response curves for DDP inhibitors 2, 5, 7 and 12 against *Tb*PTP1. A constant concentration of enzyme (0.3-0.4 μg/reaction) and substrate (0.175 mM) was incubated with serial dilutions of inhibitors (from 200 to 0 μM). The percentage of substrate hydrolysis in presence of inhibitor compared to control without inhibitor (Hydrolysis % of control) is plotted against the logarithmic concentration of inhibitor (Log[In]); The calculated IC_{50} values for inhibitor 2, 5, 7 and 12 were 90, 56, 57 and 66 μM, respectively (A, B, C and D).

Inhibitor	K_i *Tb*PTP1	K_i PTP1B	IC_{50} *Tb*PTP1	IC_{50} PTP1B
In. 1	294 (32-2688)	51 (13-205)	319 (34-2922)	36 (0.3-3549)
In. 2	83 (26-269)	61 (37-103)	90 (28-292)	53 (41-67)
In. 5	51 (21-127)	30 (11-137)	56 (22-138)	32 (28-38)
In. 6	n.d	39 (12-131)	1786 (246-12963)	33 (28-38)
In. 7	53 (13-126)	16 (7-39)	57 (14-234)	16 (14-19)
In. 11	116 (49-294)	n.d	126 (49-319)	n.d
In. 12	62 (36-106)	196 (22-1755)	66 (54-80)	113 (7-1734)
In. 13	306 (12-7495)	55 (34-89)	330 (13-8151)	70 (40-124)
In. 15	118 (49-284)	204 (140-299)	128 (53-308)	199 (168-236)
In. 17	102 (31-331)	42 (13-138)	111 (34-360)	35 (29-42)
BZ3	40 (7-234)	n.d	43 (7-254)	8
Oleanolic ac.	120 (54-266)	n.d	111 (60-206)	24
Suramin	6 (3-14)	n.d	7 (3-15)	12
Vanadate	54 (14-200)	0.4	58 (15-217)	n.d

Table 5.1 Summary of the IC_{50} and K_i calculated for the different inhibitors against *Tb*PTP1 and PTP1B. The number of the DDP inhibitors tested (In. 1-17), together with the other four PTP1B inhibitors are listed with the corresponding K_i and IC_{50} values for *Tb*PTP1 and PTP1B. Values are expressed in μM and the 95% confidence interval are shown in parethesis. The DDP inhibitors that showed calculated IC_{50} or K_i between 50 and 100 μM (within a 95% CI between 100 and 200 μM) are highlighted in blue, whereas compounds showing calculated IC_{50} or K_i values between 100 and 200 μM are highlighed in pink. The values listed for BZ3, oleanolic acid (Oleanolic ac.), suramin and vanadate against PTP1B are the published ones (Huyer *et al.*, 1997; McCain *et al.*, 2004; Wiesmann *et al.*, 2004; Zhang *et al.*, 2008); n.d is not determined. See **Appendix A** and **B** for *Tb*PTP1 and PTP1B dose-response curves.

5.3. *Tb*PTP1 competition assays

In order to further characterize the mechanism of action of the inhibitors tested, competition assays were performed between the compounds and the synthetic substrate pNPP. A constant enzyme and inhibitor concentration was tested against increasing concentrations of substrate and the Michaelis and Menten equation was used to calculate V_{max} and K_M. The comparison of the Michaelis and Menten constants, between enzyme alone and enzyme in presence of inhibitor, defines the type of inhibition; if an inhibitor binds to the same site as the substrate (competitive inhibitor) (**Figure 5.3**), it reduces enzyme velocity at low concentrations of substrate, thus increasing K_M, but it does not alter the maximum velocity (V_{max}) at saturating concentrations of substrate. An example of a competitive PTP inhibitor is vanadate, which has been shown to inhibit PTPs (Swarup *et al.*, 1982) by binding to the active-site cysteine (Denu *et al.*, 1996), with a calculated K_i for PTP1B of 0.38 μM (Huyer *et al.*, 1997).

Contrasting with this, if the inhibitor does not bind to the same substrate-binding site (non-competitive inhibitor), the reaction will be partly inhibited, even at saturating concentrations of substrate, thus resulting in a decreased V_{max} and constant K_M. Non-competitive inhibitors bind with equal affinities to both the enzyme alone and to the enzyme-substrate complex, whereas competitive inhibitors, by targeting only to the active site, are unable to bind to the enzyme-substrate complex (**Figure 5.3**).

In addition it is possible that a certain inhibitor can both hinder the binding of the substrate and decrease the turnover number of the enzyme (mixed inhibitor), thus lowering V_{max} and increasing K_M (Berg *et al.*, 2002). From the molecular point of view, mixed type inhibitors bind with different affinities to both the enzyme and the enzyme-substrate complex and therefore interfere with enzyme-substrate binding as well as with the activity of the enzyme-substrate complex formed (**Figure 5.3**).

Non-competitive and mixed-type inhibitors are allosteric inhibitors, which bind to a different site on the enzyme (Berg *et al.*, 2002). An example of a non-

competitive allosteric inhibitor of PTP1B is a derivative of benzbromarone (BZ3), which was shown to bind a novel site of the enzyme and to trap the phosphatase into the inactive conformation by preventing the closure of the WPD loop (Wiesmann *et al.*, 2004) (see paragraph 1.18.1).

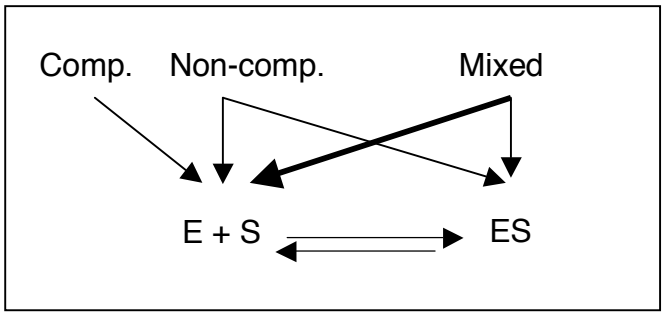

Figure 5.3 Diagram showing the mode of action of competitive, non-competitive and mixed type inhibitors. Schematic representation of the mode of action of competitive (Comp.), non-competitive (Non-comp.) and mixed type inhibitors (Mixed); competitive inhibitors can bind only the enzyme alone (E), whereas non-competitive and mixed inhibitors bind to both the enzyme and the enzyme-substrate complex (ES); non-competitive inhibitors bind with equal affinities to E and ES, whereas mixed type bind preferentially to E (thick arrow).

As shown in Table 5.2 A and in the Michaelis and Menten plots of Appendix C, the two positive controls included for competitive and mixed type inhibition, vanadate and BZ3, respectively, showed the expected changes in V_{max} and K_M. Of the nine DDP inhibitors tested six (In.5, 11, 12, 13, 15 and 17) showed a non-competitive type of inhibition, indicated by a decreased V_{max} but constant K_M, compared to control assays without inhibitors (highlighted in blue in **Table 5.2 A**). Only DDP inhibitor 7 was found to be competitive, causing a 4-fold increase in K_M (highlighted in green in **Table 5.2 A**). The K_M and V_{max} values for DDP inhibitor 2 were not confidently determined due to poor fitting of the data to the Michealis and Menten equation for unknown reasons. DDP inhibitor 1 did not significantly affect V_{max} and K_M at half IC_{50} concentration and inhibitor 6 was excluded from the competition assays, being a very weak *Tb*PTP1 inhibitor (IC_{50} >1 mM). Among the other PTP1B inhibitors, oleanolic acid was found to be a non-competitive inhibitor,

similarly to most of the DDP inhibitors, whereas suramin showed to be a competitive inhibitor of *Tb*PTP1 (**Table 5.2 A**).

The comparative analysis between the data obtained with *Tb*PTP1 and with the human PTP1B (Rachel Clark, personal communication) is shown in Table 5.2 B. Most of the DDP inhibitors showed the same type of behavior for the two enzymes, with the exception of inhibitor 7, which was found to be competitive for *Tb*PTP1. Oleanolic acid, which has been shown to be a competitive PTP1B inhibitor (Zhang *et al.*, 2008), resulted instead not to bind the *Tb*PTP1 catalytic site. Contrasting with this, suramin was found to be a competitive inhibitor for both enzymes (McCain *et al.*, 2004) (**Table 5.2 B**).

A

	[In.]	V_{max}	K_M	Inhibition
***Tb*PTP1** (batch 1)		2.0-4.0	0.1-5.0	
In. 5	11	1.78 (1.3-2.1)	3.3 (0.9-5.6)	non-comp
	56	0.35 (0.3-0.6)	2.5 (0.6-8.3)	non-comp
	111	0.25 (0.02-0.3)	2.23 (0.6-3.8)	non-comp
In. 7	28	1.56 (1.2-1.8)	6.0 (2.9-9.2)	non-comp
	57	2.9 (2.3-3.5)	21.0 (12.5-29.4)	competitive
In. 11	11	0.68 (0.4-0.8)	3.71 (0.2-7.2)	non-comp
In. 12	43	0.19 (0.05-0.33)	1.3 (-2-4.9)	non-comp
	217	0.34 (0.19-0.48)	2.40 (-1-5.9)	non-comp
In. 13	35	1.70 (1.3-1.8)	3.60 (1.5-4.5)	non-comp
	17.7	1.57 (1.4-1.9)	3.0 (1.9-5.4)	non-comp
In. 15	11	1.86 (1.4-2.2)	2.15 (0.4-3.8)	non-comp.
In. 17	27	0.48 (0.3-0.56)	7.42 (3.0-11.4)	non-comp
BZ3	43	0.27 (0.0-0.65)	80 (0.0-238)	mixed
Oleanolic ac.	3	0.41 (0.2-0.5)	3.28 (0.2-6.3)	non-comp.
	18	0.40 (0.3-0.5)	1.92 (0.2-3.6)	non-comp.
***Tb*PTP1** (batch 2)		1.8-3.1	0.2-4.4	
Suramin	3	1.7 (0.7-2.6)	12.6 (0.0-28.2)	competitive
***Tb*PTP1** (batch 3)		1.1-1.7	0.7-4.0	
Vanadate	25	1.43 (1.2-1.6)	7.7 (4.3-11.0)	competitive

Vmax =	K_M ↑	competitive
Vmax ↓	K_M =	non-comp
Vmax ↓	K_M ↑	mixed type

B

Inhibitor	*Tb*PTP1	PTP1B
In. 5	non comp.	non comp.
In.7	competitive	non comp.
In. 11	non comp.	non comp.
In. 12	non comp.	non comp.
In. 13	non comp.	non comp.
In. 15	non comp.	non comp.
In. 17	non comp.	non comp.
BZ3	mixed	mixed
Oleanolic acid	non comp.	competitive
Suramin	competitive	competitive
Vanadate	competitive	competitive

Table 5.2. Competition experiments performed with *Tb*PTP1. (A) In Table A the name of the inhibitor tested is listed in the first column from the left-hand side, together with the concentration of the inhibitor used in the assay in the second column ([In.] in μM); the third and fourth columns show the calculated V_{max} and K_M for the compounds (including the corresponding 95% confidence interval) and the last column summarizes the type of inhibition, according to the changed in V_{max} and K_M (as shown by the legend in the lower right-hand side panel); all the concentrations are in μM units. Note that BZ3 has been classified as "mixed" because of its clear increase in K_M, despite the wide 95% confidence interval. (B) In Table B the comparative summary of the type of inhibitors tested for *Tb*PTP1 and human PTP1B is shown. The type of inhibition (competitive in pink, non competitive in blue and mixed in purple) is shown for the DDP inhibitors tested (In.5-17), oleanolic acid, suramin and the controls used for mixed type and competitive inhibitor (BZ3 and vanadate, respectively). Data for *Tb*PTP1 was obtained from competition assays performed during the course of this project, whereas PTP1B data is reported from personal communication with Rachel Clark (DDP inhibitors) or from published work for oleanolic acid (Zhang *et al.*, 2008), suramin (McCain *et al.*, 2004), and vanadate (Huyer *et al.*, 1997). See **Appendix C** for the corresponding *Tb*PTP1 graphs.

5.4. Activity on stumpy form cells of the PTP1B inhibitors

After the *in vitro* characterisation of the different PTP1B inhibitors, it was important to test the compounds *in vivo*, on stumpy form cells. The specificity of the compounds for *Tb*PTP1 was assessed by determining whether they induced differentiation of stumpy to procyclic forms, the phenotype that has been observed in *Tb*PTP1 RNAi lines and in cells treated with BZ3 (Szoor *et al.*, 2006). The eight most potent DDP inhibitors, together with inhibitor 4 as negative control, were tested at 150 μM and 300 μM, concentrations that have been shown to be effective for BZ3 (Szoor *et al.*, 2006). Stumpy form cells were treated with the various inhibitors or with DMSO alone, in HMI-9 at 27° C for 4 hr; this time point was chosen because it had been reported to be the earliest time point at which EP protein expression, a marker of procyclic form cells, is detectable in about 90% of the cells after cis-aconitate or BZ3 treatment (Szoor *et al.*, 2006). It was important to minimize the incubation length, since some of the inhibitors altered the pH of the media, which could have affected their overall viability. Together with the DDP inhibitors, oleanolic acid and suramin were also tested, but at lower concentrations, as they had shown to be trypanocidal (Fairlamb *et al.*, 1977; Salem *et al.*, 2006).

The results are shown in Figure 5.4, where it is visible that none of the compounds caused EP protein expression, as detected by FACS stain of the cells. Inhibitor 2 showed some positivity to EP staining, but that was only an artifact probably due the intrinsic fluorescence of the compound, as judged by immune-fluorescence analysis of the same samples. The positive control, cis-aconitate and the inhibitor BZ3, did however, induce efficient procyclin expression (**Figure 5.4**).

Unexpectedly, the DDP inhibitor 12 was found to have trypanocidal activity when tested on stumpy form cells at 150 μM and 300 μM, and thus its LD_{50}, the dose resulting to be lethal for 50% of the population (Albrecht *et al.*, 1996), was calculated in order to quantify its potency. For this aim, the Alamar Blue® assay was employed, which is based on the reduction of the

redox indicator in the media upon cell growth. Due to its simplicity and reproducibility, this method has been extensively used for anti-protozoan drug discovery (Raz *et al.*, 1997; de Oliveira-Silva *et al.*, 2008). As shown in Figure 5.5 A, DDP inhibitor 12 generated a LD_{50} of approximately 40 μM (with 95% CI between 11 and 74 μM) or 9.4 $x10^6$ ng/ml; this value was determined on bloodstream S16 *T. brucei brucei*, by plotting the decrease in the reduction of Alamar Blue®, due to inhibition of cell growth, over different concentrations of inhibitor (**Figure 5.5 A**). Suramin was also included, as positive control, which showed a LD_{50} of 20 nM (3380 ng/ml) (Figure 5.5 B), in agreement with data obtained using the same cell type and assay (Ishiyama *et al.*, 2008).

Unlike to DDP inhibitor 12, the other DDP inhibitors did not cause cell death when tested for differentiation at 150 and 300 μM on stumpy forms and thus were not subjected to cell viability assays. Indeed it was considered unlikely that compounds ineffective against stumpy forms at milimolar concentrations would display significant trypanocidal activity on slender form cells.

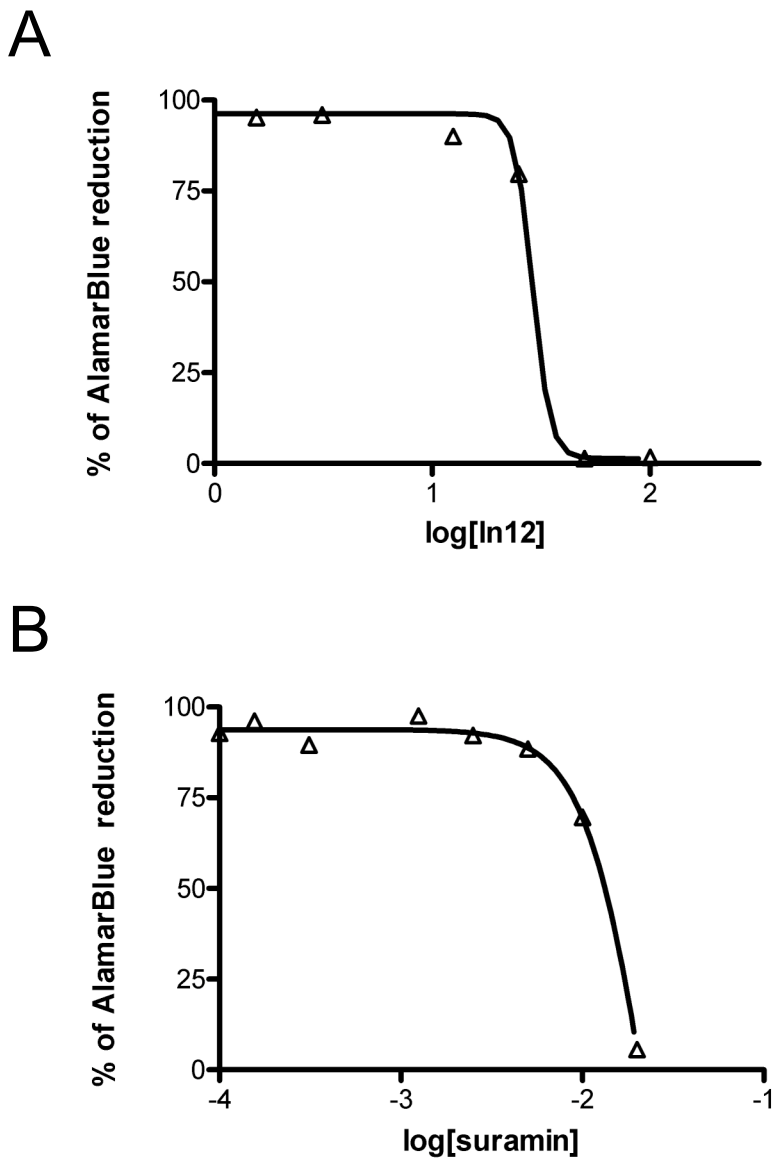

Figure 5.5 Trypanocidal activity of DDP inhibitor 12 and suramin. DDP inhibitor 12 and suramin were tested on bloodstream form S16 cells and their effect on cell viability was quantified as LD_{50} using the Alamar Blue® assay and found to be 40 and 0.02 μM, respectively (A and B); the percentage of Alamar Blue® reduction of treated versus untreated cells is shown on the y-axis and the logarithmic of concentration in μM is shown on the x-axis.

5.5. Discussion

*Tb*PTP1 is an unusual drug target candidate, since it does not meet the classical requirements of being essential for parasite survival and of lacking closely related mammalian homologues (Aguero *et al.*, 2008). Nevertheless, the peculiar and unique function of *Tb*PTP1 in regulating the transition from bloodstream form to insect form parasite represents an opportunity to control African trypanosomiasis transmission. So far, research targeting sleeping sickness transmission has not been considered a priority, since other strategies, such as vector control or animal reservoir treatment, are already in use (Welburn *et al.*, 2001), and safer drugs to cure the disease are still under-developed (Barrett *et al.*, 2007). Nevertheless, in a scenario where African trypanosomiasis incidence has been reduced and the focus is on its elimination, the use of a drug targeting disease transmission would be beneficial. HAT elimination has already been considered a reasonable aim in countries reporting less than 100 cases per year (Welburn *et al.*, 2009); in these countries, the removal of the vector altogether has been chosen as the main solution for disease elimination. However, tsetse re-invasion remains possible making this strategy questionable (Hargrove, 2003). In addition, tsetse control has been successful only where transmission sites are localized, such as in the savanna and along forest galleries, whereas vector control has proven to be more difficult in forest habitats where *Glossina spp*. are more dispersed (Fevre *et al.*, 2006b).

For the above reasons it is clear that, in order to avoid African trypanosomiasis re-occurence, additional strategies to vector controls are going to be needed. Treatment of the animal reservoir is a possible strategy, but useful only for Rhodesian sleeping sickness and not for the Gambiense form (Welburn *et al.*, 2001), which represents the majority of the cases (WHO, 2006a). For this form of the disease, active case finding and treatment is nowadays the only control measure, but the remoteness of the rural areas and the weakness of the local health system make this approach unsustainable. Moreover, Gambiense HAT is characterized by a chronic infection, often with the first signs and symptoms appearing after years (WHO, 1998), thus rendering its control even more challenging. Therefore,

in areas with low sleeping sickness incidence, the possibility of treating the human host with a safe oral drug reducing the number of transmissible forms of the parasite would provide a novel and valuable approach to minimize the risk of diseases re-occurence, particularly for the Gambiense form. In the context of Rhodesian HAT, such a drug could also be employed for the treatment of the animal reservoir, in combination with curative trypanocides.

The apparently undesired similarity of *Tb*PTP1 with the human PTP1B could, on the other hand, be exploited to use inhibitors developed for the human enzyme. The interest of pharmaceutical companies for PTP1B and the possible future release to the market of an oral drug treating diabetes and obesity, could provide a way to overcome the financial limitations of drug discovery for sleeping sickness. HAT has already witnessed a similar situation with eflornithine, a drug initially developed as an anti-cancer agent, then commercialized mainly as a hair growth inhibitor cream and discovered to be effective against trypanosomes (TDRnews, 2001). Currently eflornithine is in use, in combination with Nifurtimox, for the treatment of phase II Gambiense HAT (Priotto *et al.*, 2006; Priotto *et al.*, 2009) and represents the only new drug registered in the last 50 years. The potential impact of a drug controlling African trypanosomiasis transmission, together with the possibility of exploiting pharmaceutical pre-clinical and clinical studies carried out for PTP1B inhibitors, prompted us to test some of such inhibitors against *Tb*PTP1.

5.5.1. Inhibitory activities of the compounds on *Tb*PTP1 and PTP1B

The PTP1B inhibitors were obtained from the Drug Discovery Portal (DDP) of the University of Strathclyde in Glasgow, and were identified as inhibitors of human PTP1B. In addition to these seventeen compounds, two published PTP1B inhibitors were also included: oleanolic acid (Zhang *et al.*, 2008) and suramin (McCain *et al.*, 2004). As mentioned at the beginning of this chapter, it was interesting to test oleanolic acid because it is a natural compound,

commercially available and safe; similarly suramin represented an attractive candidate, being a drug used for treatment of first stage HAT. The initial screening was conducted *in vitro*, on recombinant *Tb*PTP1, in order to assess the degree of activity of the compounds. For ten out of the seventeen DDP inhibitors an accurate IC_{50} value was calculated (**Table 5.1** and **Appendix A**), whereas for the remaining seven a dose-response curve was not confidently extrapolated from the data, likely due to low inhibitory activity and sometimes precipitation of the compound in the buffer used. Four of the DDP inhibitors (inhibitors 2, 5, 7 and 12) were found to have a calculated IC_{50} or K_i between 50 and 100 μM (or between approximately 20 and 300 μM, if the 95% confidence intervals are considered) (**Figure 5.2**); three DDP inhibitors (inhibitors 11, 15 and 17) showed IC_{50} values between 100 and 200 μM and three (inhibitors 1, 6 and 13) between 200 and 350 μM. Oleanolic acid displayed a moderate inhibitory activity (IC_{50} of 111 μM) and suramin was found to be the most powerful of the compounds screened (IC_{50} of 7 μM) (**Table 5.1** and **Appendix A**).

A comparative analysis of the same inhibitors tested against *Tb*PTP1 and PTP1B showed that most of them had a similar activity towards the two enzymes (**Table 5.1** and **Appendix B**). Indeed, despite the fact that calculated IC_{50} and K_i values seemed to indicate differences in inhibitory activities, the confidence intervals of the constants need to be taken into account, which vary from compound to compound. Therefore, even if a cut-off of 0.9 was used for the coefficient of determination (R^2), which quantifies the goodness of fit of the data, in order to confidently extrapolate the IC_{50} and K_i values, these values need to be compared with caution. Larger confidence intervals were usually found for the assays performed against *Tb*PTP1 compared to assays against PTP1B, maybe indicating a less ideal combination of buffer/substrate/enzyme.

Among the compounds tested, the DDP inhibitor 6 was the only one to show a significantly different IC_{50}, being more powerful against PTP1B than against the parasite phosphatase, with calculated IC_{50} values of 39 μM and 1786 μM, respectively (**Table 5.1**). However, the wide 95% confidence interval of the IC_{50} value for *Tb*PTP1 and the fact that its corresponding K_i

value was not confidently extrapolated from the data, suggested that the fit of DDP inhibitor 6 was probably not very sensible, although the reason for this was not clear.

5.5.2. Type of inhibition of the compounds against *Tb*PTP1 and PTP1B

A large variety of compounds have been identified as PTP inhibitors, most of which are nonhydrolyzable phospho-tyrosine mimics. By targeting the PTP active site, this type of compounds are usually potent inhibitors but often show limited selectivity and poor cell permeability (Vintonyak *et al.*, 2009). Examples of competitive PTP1B compounds are oleanolic acid (Zhang *et al.*, 2008), suramin (McCain *et al.*, 2004) and vanadate (Huyer *et al.*, 1997). Suramin and vanadate were found to retain the same type of inhibition for *Tb*PTP1, whereas oleanolic acid showed to bind the catalytic site of the human enzyme, but not of the parasite one (**Table 5.2**). Moreover, one of the DDP inhibitors tested, inhibitor 7, showed to be competitive for *Tb*PTP1 but not for PTP1B. These observations suggest the presence of potential structural differences between the two proteins. This difference must be found in the regions located in the vicinity of the catalytic site, since the catalytic residues are perfectly conserved (see paragraph 1.17).

In addition to phospho-tyrosine mimics, allosteric PTP1B inhibitors have also been developed. The best characterised example of this type of PTP1B inhibitors is BZ3, which was shown to bind to a second site on the enzyme, far from the catalytic pocket (Wiesmann *et al.*, 2004). Since this second site is much less conserved than the catalytic one, compounds targeting this region are likely to show increased selectivity for PTP1B over other PTPs. Therefore the development of allosteric PTP1B inhibitors has been considered one of the most promising strategies for the identification of lead compounds (Vintonyak *et al.*, 2009). In agreement with the published data, BZ3 was found to be an allosteric ("mixed type" of inhibition) inhibitor of *Tb*PTP1. Similarly all the DDP inhibitors tested, except inhibitor 7, (inhibitor 5, 11, 12, 13, 15 and 17) were found to be non-competitive, i.e. to bind to a site different

from the catalytic site of the enzyme, which was true also for PTP1B (Rachel Clark, personal communication) (**Figure 5.2** and **Appendix C**).

5.5.3. *In vivo* activity of the compounds

The eight most potent *Tb*PTP1 DDP inhibitors were then tested *in vivo* on stumpy form cells but did not specifically inhibit the phosphatase, as judged by lack of expression of the procyclic surface protein EP (**Figure 5.4**). The possibility that the compounds did not permeate the trypanosome's membrane is unlikely, since DDP inhibitor 12, which belongs to a similar chemical family (**Figure 5.6**), was found to have a lethal effect on the cell (**Figure 5.5 A**). In addition, it is improbable that the concentrations used (150 and 300 μM) were insufficient to inhibit *Tb*PTP1 *in vivo*, as BZ3, which displayed an *in vitro* inhibitory activity comparable to DDP inhibitors 2, 5 and 7, showed a specific effect at concentrations between 50 and 150 μM (Szoor *et al.*, 2006). Similarly, oleanolic acid and suramin did not induce stumpy to procyclic form transition (**Figure 5.4**).
The most likely explanation for the lack of activity of the inhibitors tested is a limited *in vivo* specificity for *Tb*PTP1, which was less surprising for oleanolic acid and suramin. Indeed, oleanolic acid has been reported to affect a wide variety of physiological functions (Liu, 1995), and suramin has shown to bind different enzymes probably because of its six negative charges (Fairlamb *et al.*, 1977; Wierenga *et al.*, 1987; Barrett *et al.*, 2007).

During the course of the screening for *Tb*PTP1 inhibitors, one of the DDP compounds tested showed an unexpected lethal activity against S16 bloodstream form *Trypanosoma brucei brucei*. The calculated LD_{50} for DDP inhibitor 12 was found to be 9.4 ng/ml or 40 μM (11-74 μM, 95% confidence interval) (**Figure 5.5 A**), which is higher than the 0.2 μg/ml or 10 μM threshold set by the current drug discovery programme for HAT (www.dndi.org; Nwaka *et al.*, 2006). However, the activity of the compound should also be tested on *T. brucei rhodesiense* and *gambiense*, as some drugs

can show a certain degree of species-specific variability (Raz *et al.*, 1997). In addition, its cytotoxicity on mammalian cells has should also be assessed.

5.5.4. Analysis of the structure/activity relationship of the compounds

The screening of compounds for drug discovery is a complex process that includes several phases. Initially, a hit or a set of hits, which are molecules with adequate activity towards the chosen target, need to be identified and then refined, in order to find a smaller subset of compounds with improved activity and selectivity. This phase involves the analysis of structure/activity relationship, which is the correlation of structural features or groups with the biological activity of the compounds. These lead compounds will then be subjected to further optimization, aiming at the generation of a clinical candidate, possessing the required pharmacological properties (Bleicher *et al.*, 2003).

The screening of the PTP1B inhibitors reported here represents only the very initial phase of drug discovery, which would aim at the identification of a set of hits acting against *Tb*PTP1. However, the generation and refinement of the hits usually requires the screening of thousands of compounds, whereas a much more limited number of molecules were tested during the course of this study. Consequently, the analysis of structure/activity relationship of these inhibitors is very difficult with the current set of data. In addition, a better understanding of the chemical structures and their reactivity would be required to properly interpret the results. Furthermore, the wide 95% confidence intervals obtained for the IC_{50} and K_i values of some of the compounds renders their comparison not particularly useful.

At the moment, only a few general observations on the data can be made. For example, it is interesting to note that DDP inhibitors with similar structure (as indicated by their DDP identification number), such as inhibitor 12 and 13 (DDP_1113_03578 and DDP_1113_04818) (**Figure 5.6 A** and **C**) were found to display different inhibitory activities (IC_{50} of 66 μM and 330 μM, respectively). In addition, compounds showing IC_{50} or K_i values between 50 and 100 μM seemed to have a more "compact" structure, possessing two

aromatic rings, compared to three in the second group of inhibitors (with IC_{50} or K_i values between 100 and 200 μM) (**Figure 5.6 A** and **B**). However, some compounds of the third group (IC_{50} or K_i values between 200 and 300 μM) also showed two aromatic rings (**Figure 5.6 C**). Moreover, it is interesting the fact that the three DDP inhibitors (DDP inhibitor 8, 9 and 10) that lacked activity against *Tb*PTP1, possessed a similar formula, thus suggesting that their structure might not be particularly active against *Tb*PTP1, and that similar compounds could be excluded from future drug screenings (**Figure 5.6 D**).

A Inhibitors showing IC_{50} or K_i 50-100 μM against *Tb*PTP1

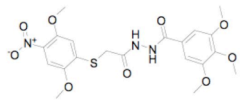

DDP in. 2
DDP_022002_02361
(IC_{50}: 90 μM)

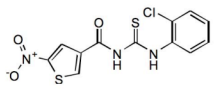

DDP in. 5
DDP_040616_00129
(IC_{50}: 56 μM)

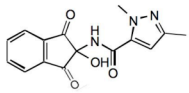

DDP in. 7
DDP_082019_01976
(IC_{50}: 57 μM)

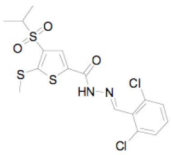

DDP in. 12
DDP_1113_03578
(IC_{50}: 66 μM)

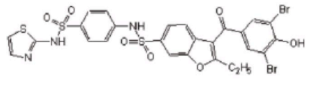

BZ3
(IC_{50}: 43 μM)

Competitive inhibitors

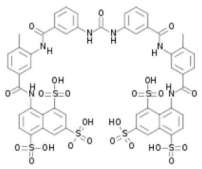

Suramin
(IC_{50}: 7 μM)

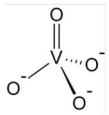

Vanadate
(IC_{50}: 58 μM)

B Inhibitors showing IC_{50} or K_i 100-200 μM against *Tb*PTP1

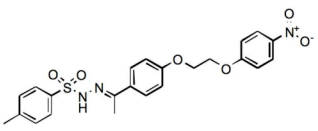

DDP in. 11
DDP_100604_03984
(IC_{50}: 126 μM)

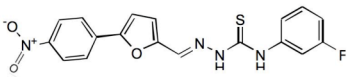

DDP in. 15
DDP_180418_01375
(IC_{50}: 128 μM)

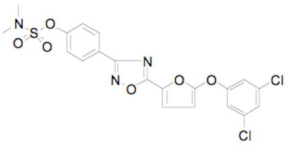

DDP in. 17
DDP_1916_00892
(IC_{50}: 111 μM)

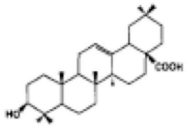

Oleanolic acid
(IC_{50}: 111 μM)

C Inhibitors showing IC_{50} or K_i 200-350 μM against *Tb*PTP1

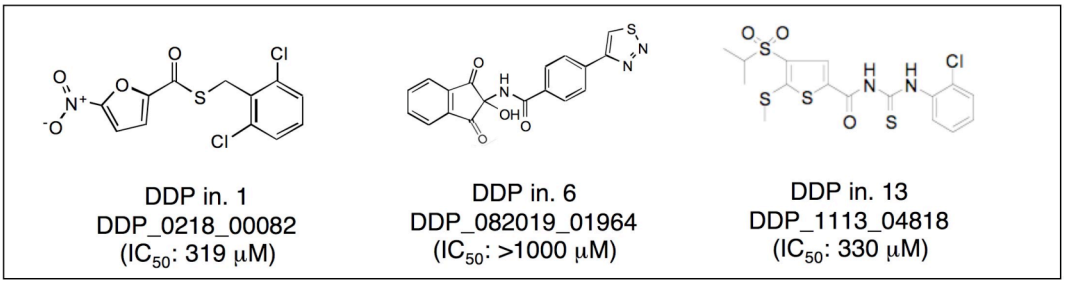

DDP in. 1
DDP_0218_00082
(IC_{50}: 319 μM)

DDP in. 6
DDP_082019_01964
(IC_{50}: >1000 μM)

DDP in. 13
DDP_1113_04818
(IC_{50}: 330 μM)

D Inhibitors lacking inhibitory activity against *Tb*PTP1

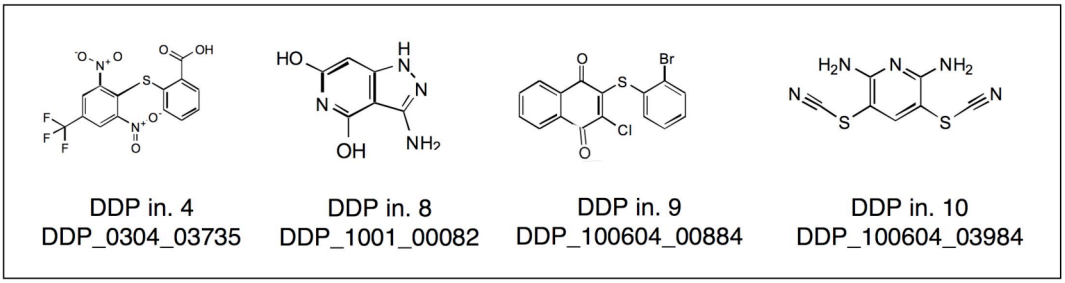

DDP in. 4
DDP_0304_03735

DDP in. 8
DDP_1001_00082

DDP in. 9
DDP_100604_00884

DDP in. 10
DDP_100604_03984

Figure 5.6 Chemical formulae of the different inhibitors tested on *Tb*PTP1. (A) Chemical formulae of the inhibitors that showed an IC_{50} or K_i values between 50 and 100 μM, together with the corresponding DDP ID and calculated IC_{50}; suramin and vanadate are grouped together since they are both competitive inhibitors, whereas all the other compounds were non-competitive inhibitors, with the exception of DDP inhibitor 7, which was found to be competitive as well. (B) Chemical formulae of the inhibitors that showed an IC_{50} or K_i values between 100 and 200 μM. (C) Chemical formulae of the inhibitors that showed an IC_{50} or K_i values between 200 and 350 μM. (D) Chemical formulae of the inhibitors that lacked activity against *Tb*PTP

5.5.5. Future directions

In future drug screenings, more compounds will need to be tested in order to better analyze their structure/activity relationship. In addition, future studies should focus more on the identification of candidates with *in vivo* specificity, for example through larger scale analysis that could provide an insight into the chemical requirements for achieving such specificity. The comparison of the structure of BZ3 with the ones of the DDP inhibitors would be the first step to understand their different activity and to select new compounds with potentially better specificity. For example, it would be interesting to "virtually" screen compound libraries using the ligand-based design (Jacob *et al.*, 2008), which would exploit the knowledge available from the numerous studies done on PTP1B inhibitors (Zhang *et al.*, 2007). Moreover, since the *Tb*PTP1 structure has been recently characterized (Chou *et al.*, 2010), it is now possible to find more specific inhibitors *in silico*, through the method of Structure Based Design (Cavalli *et al.*, 2009).
It would also be important to test PTP1B inhibitors further down the drug development line, in order to maximize the benefits of the "piggy-back" approach. Unfortunately pharmaceutical companies are often unwilling to share their lead compounds for financial reasons or, when they are, bureaucratic procedure can be long and exhaustive. Indeed during this project a small American pharmaceutical company was contacted, which possessed the PTP1B inhibitor trodusquemine (MSI-1436) (Takahashi *et al.*, 2004) in phase I clinical trial, and a material transfer agreement was initiated but with no outcome for almost two years. The compound in question was particularly attractive as it was found to be effective *in vitro* against PTP1B and in an *in vivo* animal model of obesity (Zasloff *et al.*, 2001; Ahima *et al.*, 2002).

The identification of a hit or set of hits with a good inhibitory activity is not the only requirement to further develop the compounds. Indeed successful inhibitors require the detailed characterization of their mode of action, particularly the identification of their binding site on the enzyme. Competitive inhibitors target the active site of the enzyme, but allosteric

inhibitors (non-competitive or mixed inhibitors), like most of the DDP compounds tested, can bind anywhere on the protein. Therefore, it would be essential to find out where the best DDP inhibitors, or other good inhibitors that will potentially be identified, bind on *Tb*PTP1. In order to do so, one possible approach would consist in the use of competition assays with other inhibitors, for which the binding site is known. For example the compound OBA5, whose interaction with PTP1B is stabilized by the closure of the WPD loop, only has been used to identify whether a certain PTP1B inhibitor prevents the closure of this loop (Wiesmann *et al.*, 2004). A complementary approach has been the use of mass spectrometry to monitor the dephosphorylation reaction, so that the stage at which the inhibitor binds to the enzyme can be identified (Wiesmann *et al.*, 2004). Probably the most accurate method to determine the binding site of a non-competitive compound would be the resolution of the crystallographic structure of the compound bound to the enzyme.

Drug discovery is a notoriously difficult process that requires long-term commitment and huge resources, and thus, is mainly carried out by big pharmaceutical companies. Nonetheless, the initial proof-of-principle often comes from research carried out in Universities. Consequently small projects investigating new therapeutic or preventive strategies, such as the one described in this chapter, represent essential first steps and important contributions of research to the improvement of global health.

Chapter 6

General Overview

6.1. General overview

Protein Tyrosine Phosphatase 1 (*Tb*PTP1) is the one of the few factors identified to be responsible for differentiation from stumpy to procyclic form parasite (Szoor *et al.*, 2006), acting through the novel substrate *Tb*PIP39 (Szoor *et al.*, 2010). However, the stimulus and the mechanism responsible for the physiological inhibition of *Tb*PTP1 upon initiation of differentiation are not known and only two *Tb*PTP1 substrates have been identified (Chou *et al.*, 2010; Szoor *et al.*, 2010). Moreover, the unique function of *Tb*PTP1 in regulating transition from the stumpy form to the insect form parasite, could be targeted as a means to decrease disease transmission.

6.2. *Tb*PTP1 substrate identification

In order to identify novel *Tb*PTP1 substrates, the potential use of a substrate consensus sequence was investigated, as this approach has been successfully used for human PTP1B (Myers *et al.*, 2001). For this aim, it was first important to compare the 3-D structure of the two phosphatases. Since the *Tb*PTP1 crystal structure was not known during the course of this project, the phosphatase 3-D structure had to be predicted *in silico*. The homology modeling of the 3-D structure of *Tb*PTP1 revealed the presence of a conserved catalytic structure with human PTP1B, in agreement with its published crystallographic structure (Chou *et al.*, 2010). In addition, the bioinformatics model correctly predicted the position of the four trypanosome-specific motifs, which are mainly found on the surface of the enzyme and thus might be involved in substrate recognition and regulation.

A review of the literature analysing the potential presence of a substrate consensus sequence for PTP1B highlighted the existence of a clear consensus mainly for the tandem phosphorylated substrates, which have not been detected in *T. brucei* (Nett *et al.*, 2009b). Moreover the residue responsible for

the formation of the second phosphate binding site in PTP1B (Arg254) (Puius YA *et al.*, 1997) is not conserved in *Tb*PTP1 (Lys267), suggesting that the parasite phosphatase might not prefer substrates containing tandem pTyr over mono pTyr. The data currently available for the mono pTyr consensus sequence of PTP1B does not allow the use any bioinformatics criteria to identify proteins that would be more likely substrates of *Tb*PTP1. However, the presence of a leucine residue in *Tb*PTP1 (Leu52) instead of an arginine residue in the corresponding position of PTP1B (Arg47), might suggest a possible preference for aliphatic/aromatic residues N-terminal to the phosphorylated tyrosine of the substrates of the parasite enzyme. This hypothesis is in contrast with the one supported by Chou *et al.*, which proposed the preference for negatively charged residues in the vicinity of the phosphorylated tyrosine, as suggested by the presence of a nearly uninterrupted acidic sequence in the *Tb*PTP1 procyclic stage substrate Nopp44-46. Similarly, acidic residues are also found in the stumpy stage *Tb*PTP1 substrate *Tb*PIP39. Nonetheless, only the identification of additional substrates will reveal which hypothesis was right and might lead to the delineation of a substrate consensus sequence for *Tb*PTP1.

In order to identify novel *Tb*PTP1 substrates the substrate trapping approach was used in selections of stumpy form cell extracts. In agreement with the data for human PTP1B, the D→A mutant was a better substrate trapping enzyme than the wild type *Tb*PTP1. Similarly, the D→A/Q→A double mutant was also able to bind to more substrates then wild type enzyme, although less than the D→A mutant. Moreover the C→S/D→A mutant *Tb*PTP1 was shown not to trap tyrosine phosphorylated proteins, as seen for PTP1B. However, this double mutant enzyme did bind to *Tb*PIP39, with similar efficiency as the D→A and D→A/Q→A mutants *Tb*PTP1. Overall the mutants *Tb*PTP1 showed similar substrate trapping ability as the PTP1B mutants, particularly when tyrosine phosphorylated proteins were visualized by Western blot. The main exception was the D→A/Q→A mutant *Tb*PTP1 that did not seem to display the 6-fold increase binding efficiency reported for the human enzyme (Laiping X *et al.*, 2001).

Consequently, the D→A *Tb*PTP1 mutant (D199A) was used in larger scale stumpy cell extract selections, both to validate the phosphatase interaction with its first identified substrate, *Tb*PIP39, and to identify novel substrates. Confirming the mass spectrometry analysis performed before the start of this project, *Tb*PIP39 was found to bind the substrate trapping mutants *Tb*PTP1, as well as to the wild type protein, under certain experimental conditions.
Two new mass spectrometry analyses of stumpy cell extract selections were performed, and the data obtained was examined, together with the results of previous experiments. Two hits were considered the most interesting, *Tb*10.389.0310 and *Tb*11.02.2090, and thus were chosen for further studies. Although *Tb*10.389.0310 downregulation by RNAi did not succeed, changes in its transcript level did not affect cell growth or differentiation capacity, thus excluding the protein from playing a role in parasite differentiation.
On the contrary *Tb*11.02.2090 mRNA downregulation, to almost half the wild type level, caused a marked growth defect in bloodstream form cells, and the accumulation of cells in the 2K2N cell cycle stage. Moreover, the same cells treated with cis-aconitate showed increased differentiation levels compared to uninduced cells (from 4.7 % to 12.6 %). These preliminary results suggested that *Tb*11.02.2090 might act as a negative regulator of differentiation, likely by affecting the parasite cell cycle. Further experiments will be needed to validate *Tb*11.02.2090 RNAi phenotype and its interaction of with *Tb*PTP1.

6.3. Dissection of *Tb*PTP1 signalling pathway during differentiation from stumpy to procyclic forms

Higher eukaryotic PTPs, particularly human PTP1B, have been shown to be regulated in a variety of ways, from post-transcriptionally to post-translationally (den Hertog *et al.*, 2008). In contrast, it is not known how the activity *T. brucei* PTPs, and particularly *Tb*PTP1, is controlled.
In order to understand the mechanism by which *Tb*PTP1 is physiologically inactivated during differentiation from stumpy to procyclic forms, the mechanisms of regulation of the human homolog, PTP1B, were examined. This comparative analysis highlighted a few potential interesting differences,

as the parasite enzyme appeared to lack several levels of regulation reported for human PTP1B. Indeed, in contrast to PTP1B, *Tb*PTP1 activity during differentiation is unlikely to be controlled post-transcriptionally, since no changes in the size of the transcript and in the protein quantity have been detected in the different life cycle stages (Szoor *et al.*, 2006). Similarly, differential targeting has also been excluded, as the phosphatase showed the same cellular fractionation profiles in stumpy and procyclic forms (McElhinney, 2007).

In addition, *Tb*PTP1 regulation through oxidation could be excluded, as no increase in intracellular ROS was detected upon treatment of stumpy form cells with the differentiation triggers citrate or cis-aconitate, as shown by the experiments included in chapter 3. Moreover, the differentiation capacity of the parasites did not appear to be influenced by addition of exogenous H_2O_2 or by neutralization of endogenous H_2O_2.

Likewise, no evidence for *Tb*PTP1 tyrosine phosphorylation during differentiation was found, despite the presence of two conserved tyrosine residues (Tyr78 and Tyr164 of *Tb*PTP1). However, the existence of a potentially transient tyrosine phosphorylation could still be a possibility. Furthermore, Ser/Thr phosphorylation of the *in silico* predicted phosphorylation sites of *Tb*PTP1 (Ser42 and Thr238) has not been tested, although none of them is conserved in PTP1B, and Thr238 is substituted by a serine residue that was not shown to be phosphorylated in the human phosphatase.

Other potential mechanisms of *Tb*PTP1 regulation, like proteolysis and sumoylation, have not been tested, since the tools required for these analyses, such as protease and SUMO inhibitors, have not been fully characterized in *T. brucei*.

*Tb*PTP1 regulation might also, and maybe solely, be achieved via its interaction with substrates, adaptor proteins, or other molecules, like the changes in the *in vitro* activity of the *Tb*PTP1-*Tb*PIP39 complex in the presence of CCA have suggested (Szoor *et al.*, 2010).

Overall *Tb*PTP1 was shown to lack most of the regulatory mechanisms found in higher eukaryotic PTPs, suggesting that, despite a conserved catalytic

structure, the parasite enzyme possesses different ways to control its activity compared to its human homolog.

In order to characterize the stimuli responsible for *Tb*PTP1 inhibition during differentiation, *Tb*PIP39 phosphorylation was monitored in stumpy form cells treated with different differentiation triggers. Citrate and cis-aconitate resulted in an increase in *Tb*PIP39 phosphorylation, whereas mild acid treatment and, particularly, pronase did not. This difference suggested the presence of two separate, but potentially complementary, pathways responsible for *T. brucei* differentiation to procyclic forms, in agreement with other published data (Hunt *et al.*, 1994; Sbicego *et al.*, 1999).
Therefore, despite the presence of a small repertoire of structurally simple protein tyrosine phosphatases, *T. brucei* appears to possess different signalling pathways involved in the parasite development from stumpy to procyclic forms.
Future studies will need to confirm these observations, for example by monitoring *Tb*PIP39 activity or function, once they have been characterized, rather than merely its phosphorylation. In addition, it would be important to analyse in more detail the role of CCA, pronase and the other differentiation triggers *in vivo*, in order to better understand the physiological relevance of the *Tb*PTP1 signalling.

6.4. Investigation of *Tb*PTP1 as therapeutic target for the control of disease transmission

The peculiar and unique function of *Tb*PTP1 in regulating the transition from bloodstream to insect form parasites, represents an opportunity to limit disease transmission, as an alternative to vector control. Moreover, the interest that pharmaceutical companies are showing in developing human PTP1B inhibitors could be used to identify compounds active against *Tb*PTP1. This strategy could result in a less risky, cheaper and faster development of a drug, which is particularly valuable for the control of a neglected tropical disease, like sleeping sickness, since these diseases do not

represent a lucrative market for pharmaceutical companies (Trouiller *et al.*, 2001).

The preliminary screening of nineteen PTP1B inhibitors showed that most of them retained their inhibitory activity and type of inhibition for *Tb*PTP1. However, none of the compounds tested displayed *in vivo* specificity for the phosphatase, when tested on stumpy form cells. Supporting the hypothesis of the lack of *in vivo* specificity towards *Tb*PTP1, was also the observation that one of these compounds caused death of bloodstream form parasites, which is not the phenotype expected from *Tb*PTP1 inhibition. Therefore, future studies will need to focus more on the identification of the chemical requirements to achieve this specificity. Moreover, larger scale screenings will be needed in order to better analyse the structure/activity relationships of different classes of compounds. Nonetheless, the results reported in chapter 4 validated the use of a "piggy back" strategy targeting *Tb*PTP1, as most PTP1B inhibitors showed the same inhibitory activity and mode of action for both human and parasite enzymes.

Appendix A

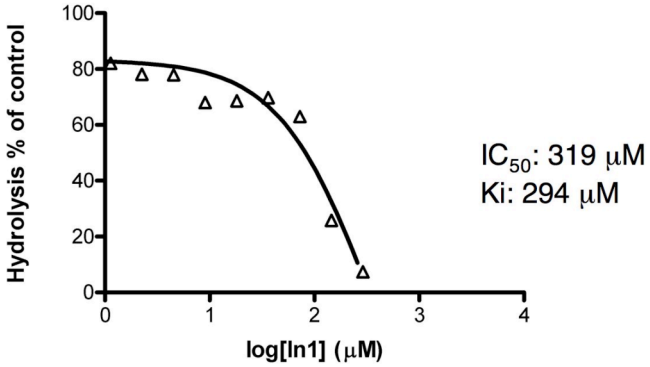
Hydrolysis % of control
100
80
60
40
20
0
0
1
2
3
4
log[In1] (μM)
IC50: 319 μM
Ki: 294 μM

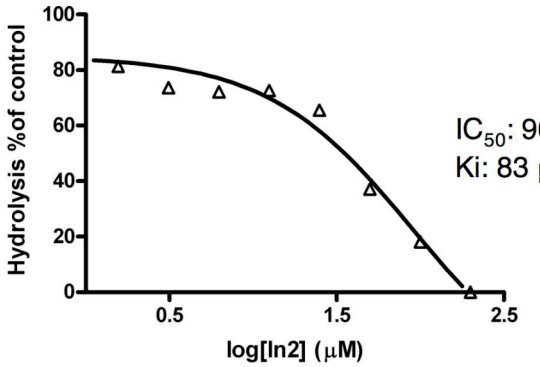
Hydrolysis %of control
100
80
60
40
20
0
0.5
1.5
2.5
log[In2] (μM)
IC50: 90 μM
Ki: 83 μM

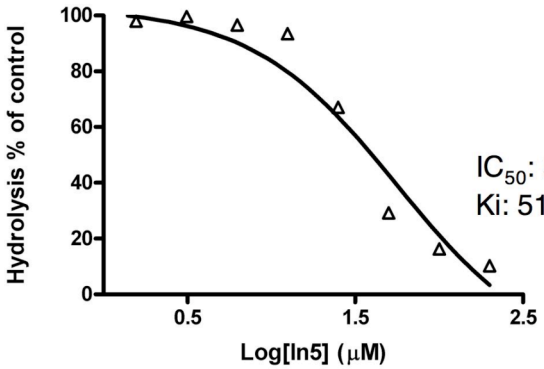
Hydrolysis % of control
100
80
60
40
20
0
0.5
1.5
2.5
Log[In5] (μM)
IC50: 56 μM
Ki: 51 μM

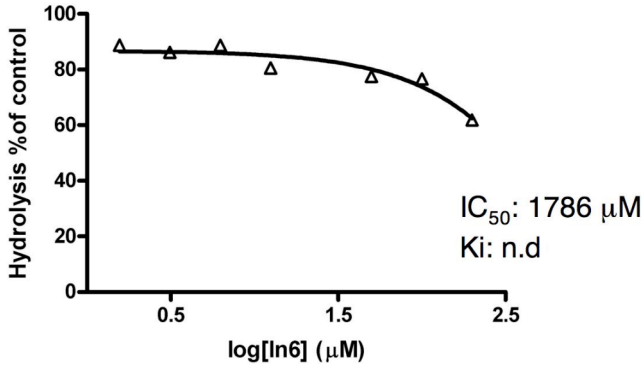
Hydrolysis %of control
100
80
60
40
20
0
0.5
1.5
2.5
log[In6] (μM)
IC50: 1786 μM
Ki: n.d

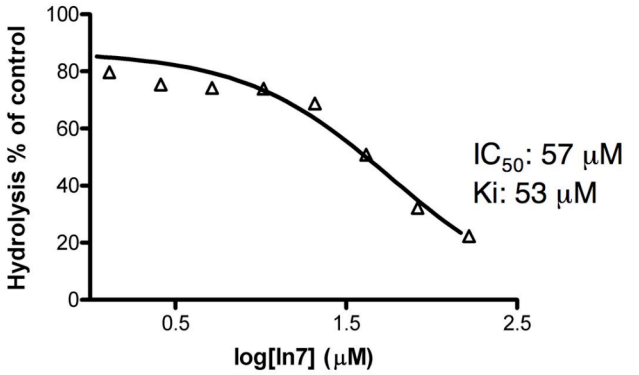
Hydrolysis % of control
100
80
60
40
20
0
0.5
1.5
2.5
log[In7] (μM)
IC50: 57 μM
Ki: 53 μM

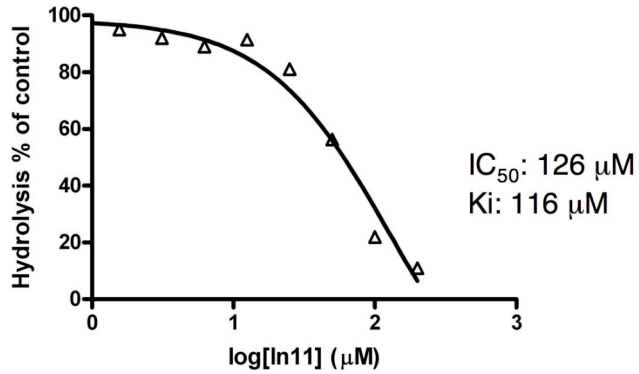
Hydrolysis % of control
100
80
60
40
20
0
0
1
2
3
log[In11] (μM)
IC50: 126 μM
Ki: 116 μM

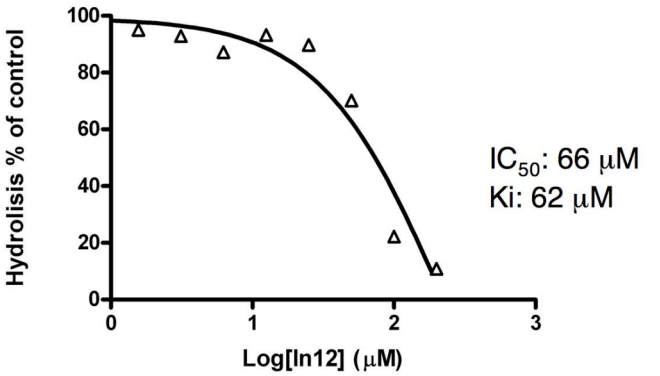
Hydrolisis % of control
100
80
60
40
20
0
0
1
2
3
Log[In12] (μM)
IC50: 66 μM
Ki: 62 μM

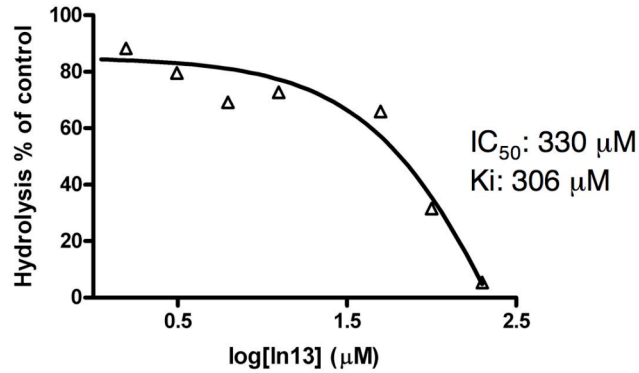
Hydrolysis % of control
100
80
60
40
20
0
0.5
1.5
2.5
log[In13] (μM)
IC50: 330 μM
Ki: 306 μM

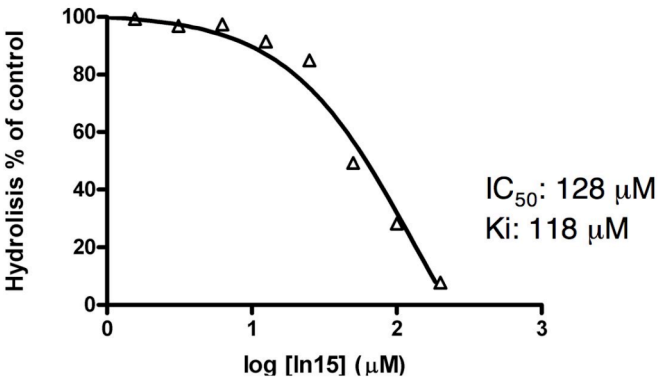
Hydrolisis % of control
100
80
60
40
20
0
0
1
2
3
log [In15] (μM)
IC50: 128 μM
Ki: 118 μM

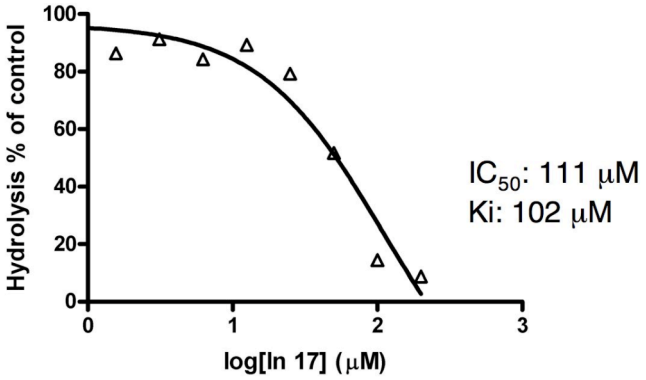
Hydrolysis % of control
100
80
60
40
20
0
0
1
2
3
log[In 17] (μM)
IC50: 111 μM
Ki: 102 μM

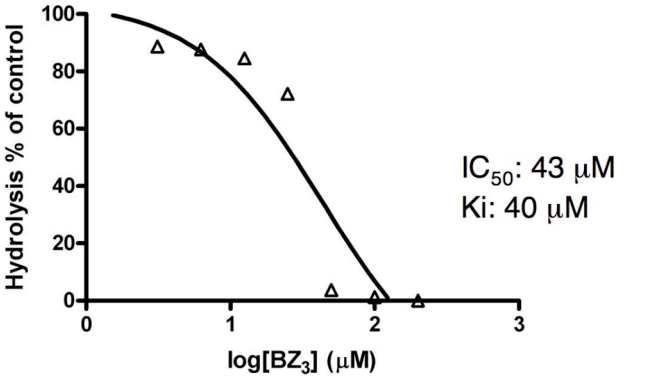
Hydrolysis % of control
100
80
60
40
20
0
0
1
2
3
log[BZ3] (μM)
IC50: 43 μM
Ki: 40 μM

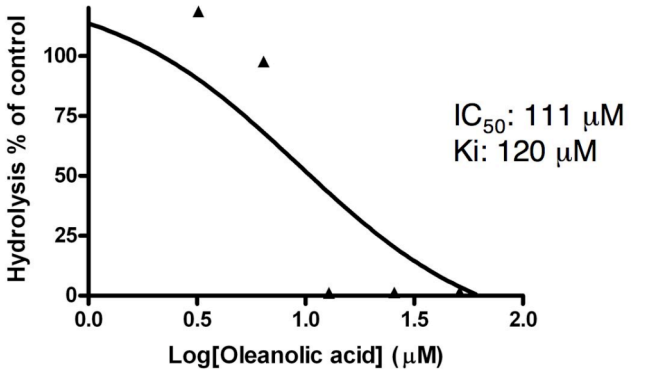
Hydrolysis % of control
100
75
50
25
0
0.0
0.5
1.0
1.5
2.0
Log[Oleanolic acid] (μM)
IC50: 111 μM
Ki: 120 μM

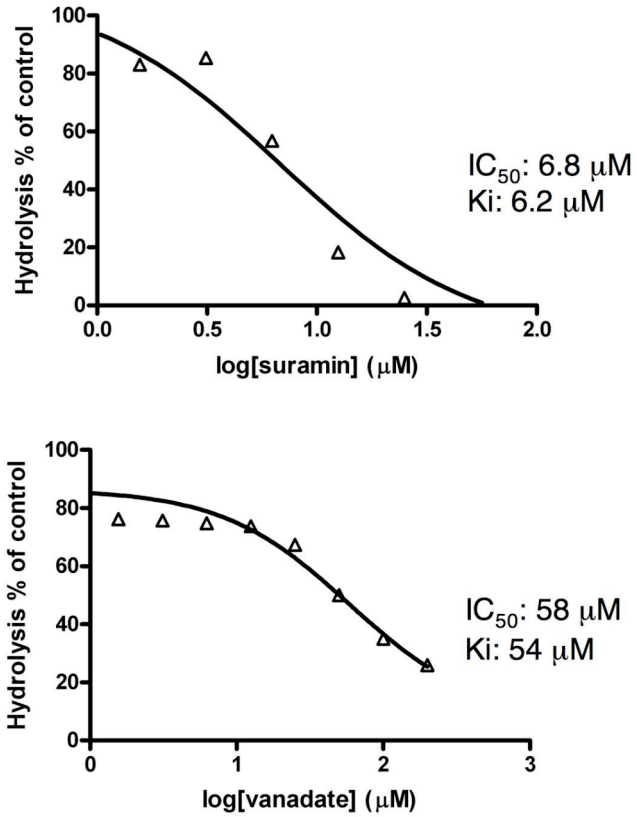

***Tb*PTP1 dose-response curves for the different PTP1B inhibitors.** The dose-response curve of ten DDP inhibitors (In. 1, 2, 5, 6, 7, 11, 12, 13, 15 and 17), together with BZ3, oleanolic acid, suramin and vanadate are shown; the relative IC_{50} and Ki are shown next to each graph. The graphs and IC_{50}/K_i calculations were performed using GraphPad Prism® Version 4.

Appendix B

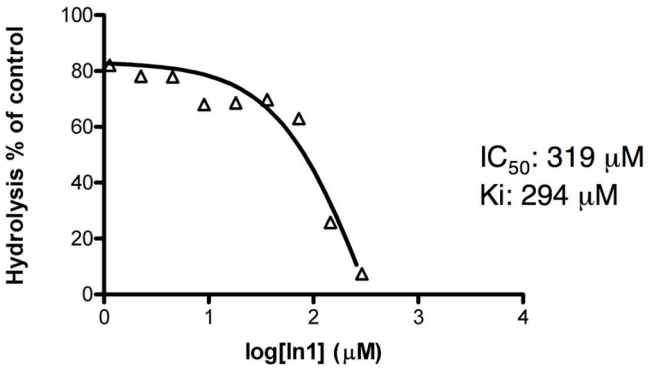
Hydrolysis % of control
100
80
60
40
20
0
0
1
2
3
4
log[In1] (μM)
IC50: 319 μM
Ki: 294 μM

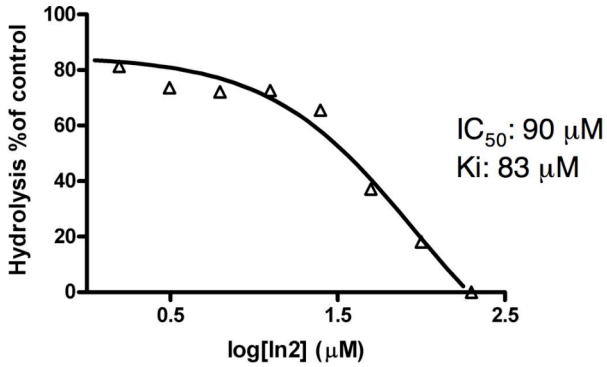
Hydrolysis %of control
100
80
60
40
20
0
0.5
1.5
2.5
log[In2] (μM)
IC50: 90 μM
Ki: 83 μM

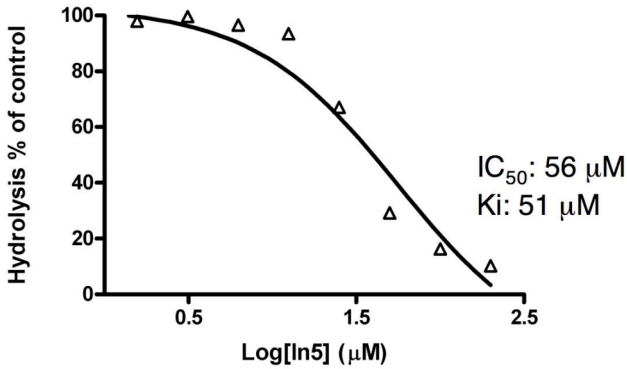
Hydrolysis % of control
100
80
60
40
20
0
0.5
1.5
2.5
Log[In5] (μM)
IC50: 56 μM
Ki: 51 μM

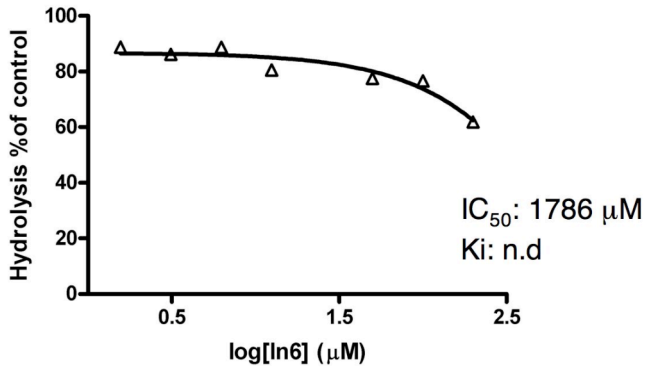
Hydrolysis %of control
100
80
60
40
20
0
0.5
1.5
2.5
log[In6] (μM)
IC50: 1786 μM
Ki: n.d

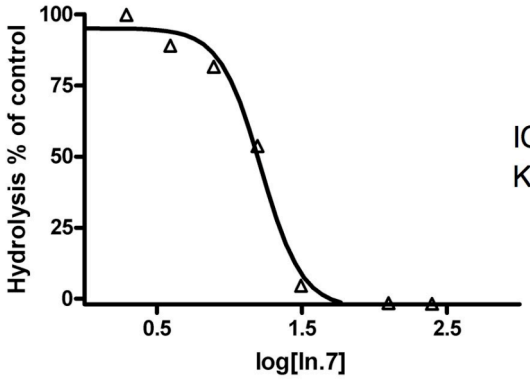

IC_{50}: 16 μM
Ki: 16 μM

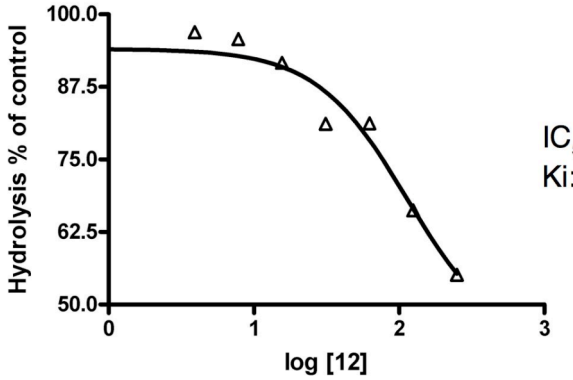

IC_{50}: 113 μM
Ki: 196 μM

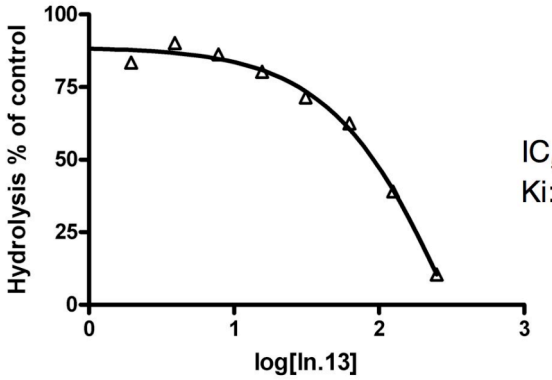

IC_{50}: 70 μM
Ki: 55 μM

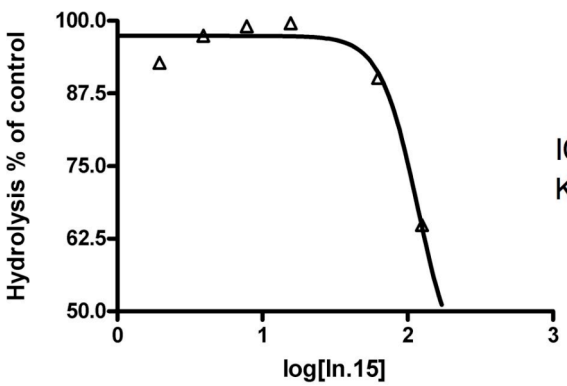

IC_{50}: 199 μM
Ki : 204 μM

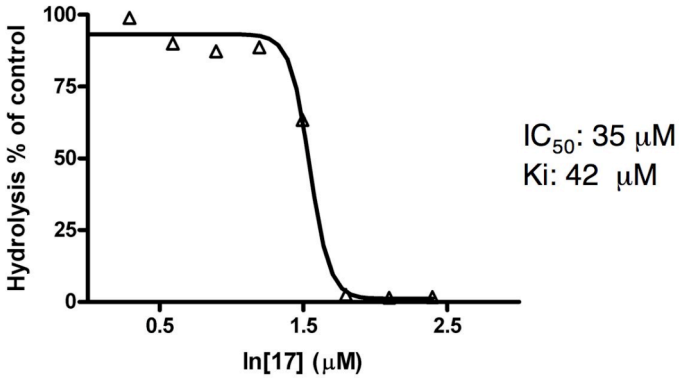

PTP1B dose-response curves for the different DDP inhibitors. The dose-response curves of nine DDP inhibitors (In.1, 2, 5, 6, 7, 12, 13, 15 and 17) are shown, with the relative IC_{50} and K_i values listed next to each graph. Graphs and calculations were performed using GraphPad Prism® Version 4.

Appendix C

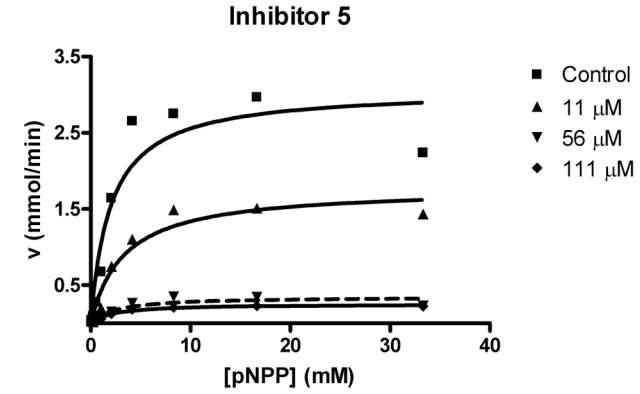
Inhibitor 5
v (mmol/min)
[pNPP] (mM)
Control
11 μM
56 μM
111 μM

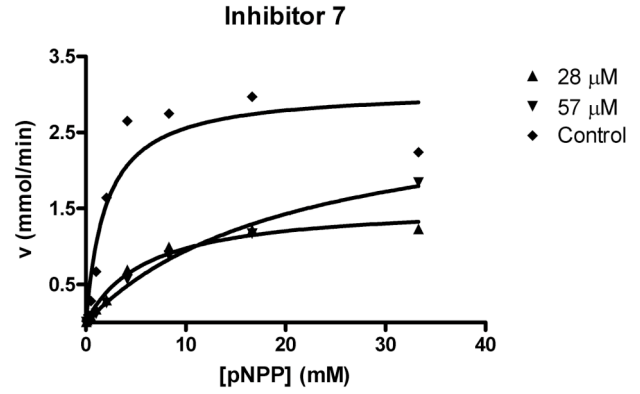
Inhibitor 7
v (mmol/min)
[pNPP] (mM)
28 μM
57 μM
Control

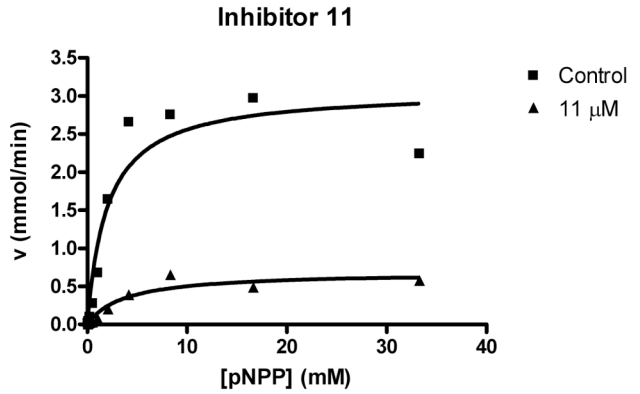
Inhibitor 11
v (mmol/min)
[pNPP] (mM)
Control
11 μM

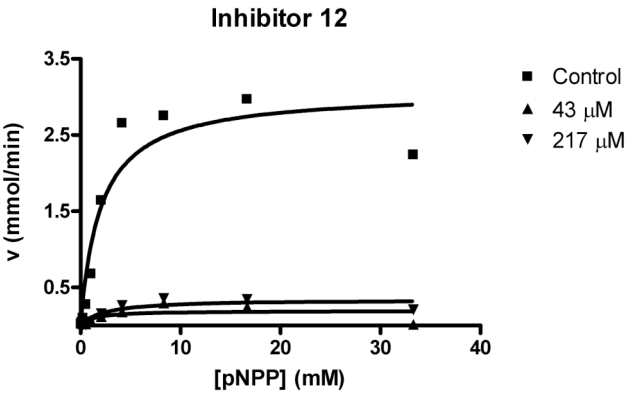
Inhibitor 12
v (mmol/min)
[pNPP] (mM)
Control
43 μM
217 μM

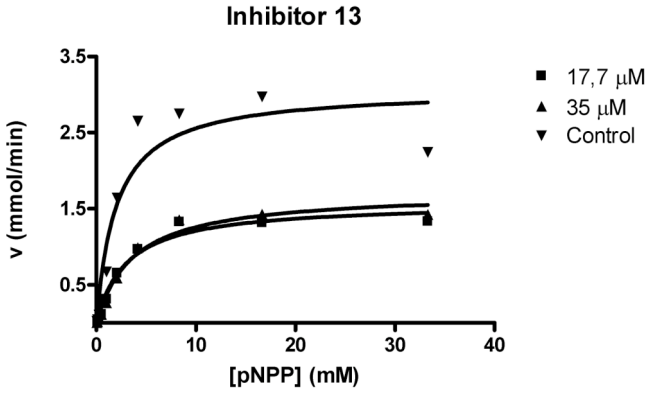
Inhibitor 13
v (mmol/min)
[pNPP] (mM)
17,7 μM
35 μM
Control

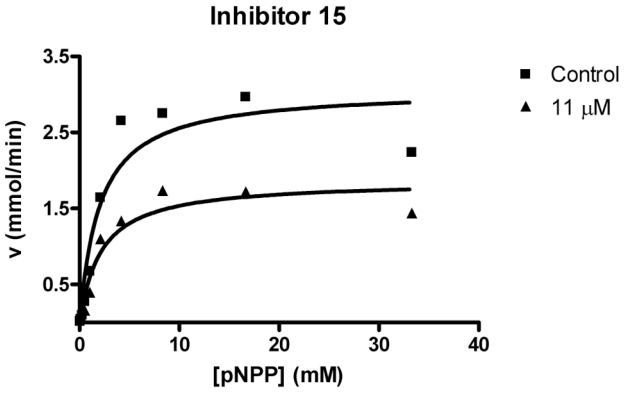
Inhibitor 15
v (mmol/min)
[pNPP] (mM)
Control
11 μM

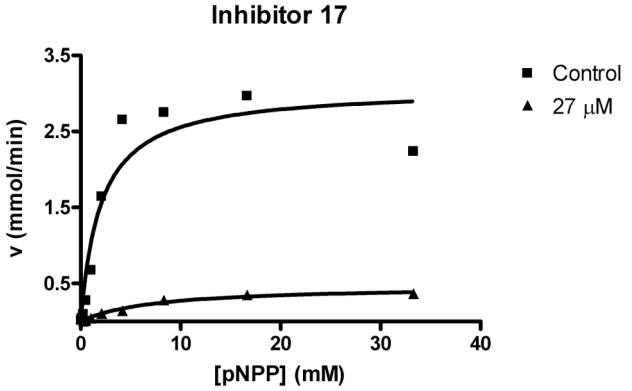
Inhibitor 17
v (mmol/min)
[pNPP] (mM)
Control
27 μM

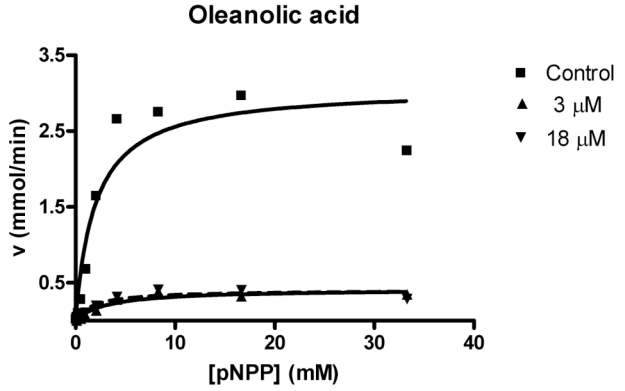
Oleanolic acid
v (mmol/min)
[pNPP] (mM)
Control
3 μM
18 μM

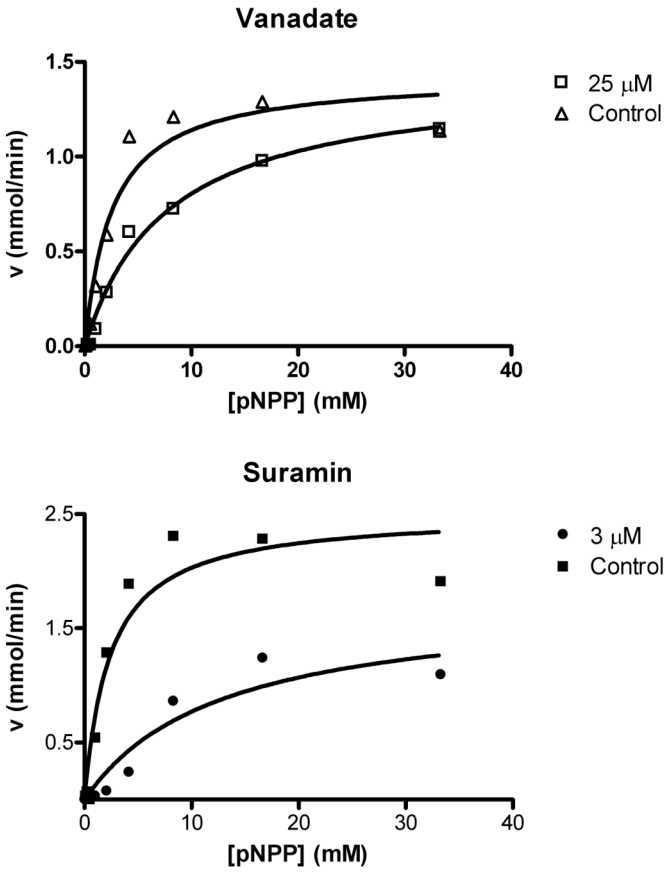

***Tb*PTP1 competition assays with the different PTP1B inhibitors.** The Michealis and Menten curves for the seven DDP inhibitors tested (In.5, 7, 11, 12, 13, 15 and 17), together with oleanolic acid, BZ3, vanadate and suramin are shown; the concentration of inhibitor used is shown in the right-hand side panel of each graph (control= *Tb*PTP1 alone). The gra phs were done using GrphPad Prism®, Version 4.

Appendix D

Solutions

Cell culture solutions:

PSG

3 mM NaH_2PO_4-$2H_2O$,
43.6 mM NaCl,
57 mM Na_2HPO_4
83 mM D-glucose, pH 7.8

Freezing mix

SDM-79 or HMI-9
14 % glycerol

DNA manipulation solutions:

TE

10 mM Tris-HCl pH 8.0,
1 mM EDTA

TAE

0.4 mM Tris-HCl,
0.1 mM EDTA, pH 7.7

Mini-scale DNA preparation:

Solution I

50 mM glucose,

25 mM Tris-HCl pH 8.0

10 mM EDTA

Solution II

0.2 N NaOH
1% SDS

Solution III

3 M KAc
40% of Glacial Acetic acid

Large-scale DNA preparation:

Solution P1

50 mM Tris-HCl, pH 8.0,
10 mM EDTA
100 μg/ml RNase A

Solution P2

200 mM NaOH
1% SDS

Solution P3

3 M KAc, pH 5.5

Solution QC

1 M NaCl,
50 mM MOPS pH 7.0
15% isopropanol

Elution Buffer

1.25 M NaCl,
50 mM Tris-HCl pH 8.5
15% isopropanol.

Northern blot solutions:

10X MOPS

40 mM 4-morpholinepropanesulfonic acid,
10 mM sodium acetate, pH 7.0
1 mM EDTA

RNA loading buffer

6 % formaldehyde,
30 % formamide,
1x MOPS,
10% glycerol
0.01% bromophenol blue

10X SSC

1.5 M NaCl,
0.15 M Tri Na Citrate

Hybridization buffer

5x SSC,
50% formamide,
0.02% SDS
2% blocking solution

Wash buffer

100 mM maleic acid,
150 mM NaCl, pH 7.4
0.3 % Tween 20

Maleic acid buffer

100 mM maleic acid,
150 mM NaCl, pH 7.4

Detection buffer

100 mM Tris-HCl pH 9.5
100 mM NaCl.

Western blot solutions:

TBS

140 mM NaCl
10 mM Tris-HCl, pH 7.4

PBS

137 mM NaCl,
3 mM KCl,
16 mM Na_2HPO_4,
3 mM KH_2PO_4, pH 7.6

Laemmli buffer

62.5 mM Tris-HCl, pH6.8,
2% SDS,
10% glycerol
traces of bromophenol blue

Running gel buffer

1.5M Tris-HCl, pH8.8,
0.4% SDS

Stacking gel buffer

0.5 M Tris-HCl pH 6.8,
0.4% SDS

Running buffer

25 mM Tris-HCl, pH 8.3,
192 mM Glycine,
0.1% SDS

Wet blotting buffer

2.5 mM Tris,
192 mM Glycine
20% methanol

Semi-dry blotting buffer

2.5 mM Tris,
15 mM Glycine,
0.02% SDS,
20% methanol

Ponceau

0.4 % of Ponceau S
3% tri-chloroacetic acid

Stripping solution

0.2 N NaOH
1% SDS

Immunoprecipitation buffer:

Lysis buffer

10 mM Tirs-HCl, pH 8.0,
0.05 mM EDTA
150 mM NaCl

Recombinant protein buffers:

His lysis buffer

20 mM Tris-HCl, pH 7.5-8.0,
250 mM NaCl,
1% Trition X-100,
1 mM β mercapthoethanol
5 mM imidazole

Wash 1

20 mM Tris-HCl, pH 8.0,
250 mM NaCl
5 mM imidazole

Wash 2

20 mM Tris-HCl, pH 8.0,
250 mM NaCl
20 mM imidazole

Elution 1

20 mM Tris-HCl, pH 8.0,
250 mM NaCl
250 mM imidazole

Elution 2

20 mM Tris-HCl, pH 8.0,
250 mM NaCl,
500 mM imidazole
1mM β mercapthoethanol

*Tb*PTP1 pNPP activity buffer

50 mM Tris,
50 mM Bis-Tris
100 mM NaAc, pH 5.5

PTP1B buffer

25 mM Hepes pH 7.2,
50 mM NaCl,
2.5 mM EDTA
BSA 0.01 mg/ml

Bibliography

Aboagye-Kwarteng T, O.-M.-Y. O. K., Lonsdale-Eccles J D (1991). "Phosphorylation differences among proteins of bloodstream developmental stages of Trypanosoma brucei brucei." *Biochem J* 275 (Pt 1): 7-14.

Acosta-Serrano, A., E. Vassella, M. Liniger, C. Kunz Renggli, R. Brun, I. Roditi and P. T. Englund (2001). "The surface coat of procyclic Trypanosoma brucei: programmed expression and proteolytic cleavage of procyclin in the tsetse fly." *Proc Natl Acad Sci U S A* 98(4): 1513-8.

Aguero, F., B. Al-Lazikani, M. Aslett, M. Berriman and F. S. Buckner (2008). "Genomic-scale prioritization of drug targets: the TDR Targets database." *Nat Rev Drug Discov* 7(11): 900-7.

Aguiar, R. C., Y. Yakushijin, S. Kharbanda, S. Tiwari, G. J. Freeman and M. A. Shipp (1999). "PTPROt: an alternatively spliced and developmentally regulated B-lymphoid phosphatase that promotes G0/G1 arrest." *Blood* 94(7): 2403-13.

Ahima, R. S., H. R. Patel, N. Takahashi, Y. Qi, S. M. Hileman and M. A. Zasloff (2002). "Appetite suppression and weight reduction by a centrally active aminosterol." *Diabetes* 51(7): 2099-104.

Alberts, B., A. Johnson, J. Lewis, M. Raff, K. Roberts and P. Walter (2002). The Biology of the Cell.Garland Science.

Albrecht, T., W. J. Almond, M. J. Alfa and G. G. Alton (1996). Medical Microbiology, The University of Texas Medical Branch at Galveston.

Allen, C. L., D. Goulding and M. C. Field (2003). "Clathrin-mediated endocytosis is essential in Trypanosoma brucei." *Embo J* 22(19): 4991-5002.

Alonso, A., J. Sasin, N. Bottini, I. Friedberg, A. Osterman, A. Godzik, T. Hunter, J. Dixon and T. Mustelin (2004). "Protein tyrosine phosphatases in the human genome." *Cell* 117(6): 699-711.

Andersen, J. N., O. H. Mortensen, G. H. Peters, P. G. Drake, L. F. Iversen, O. H. Olsen, P. G. Jansen, H. S. Andersen, N. K. Tonks and N. P. Moller (2001). "Structural and evolutionary relationships among protein tyrosine phosphatase domains." *Mol Cell Biol* 21(21): 7117-36.

Andrade, M. A. and P. Bork (1995). "HEAT repeats in the Huntington's disease protein." *Nat Genet* 11(2): 115-6.

Andrews, K. T., A. Walduck, M. J. Kelso, D. P. Fairlie, A. Saul and P. G. Parsons (2000). "Anti-malarial effect of histone deacetylation inhibitors and mammalian tumour cytodifferentiating agents." *Int J Parasitol* 30(6): 761-8.

Aoshiba, K., K. Yasuda, S. Yasui, J. Tamaoki and A. Nagai (2001). "Serine proteases increase oxidative stress in lung cells." *Am J Physiol Lung Cell Mol Physiol* 281(3): L556-64.

Aravind, L. and C. P. Ponting (1997). "The GAF domain: an evolutionary link between diverse phototransducing proteins." *Trends Biochem Sci* 22(12): 458-9.

Arnold, K., L. Bordoli, J. Kopp and T. Schwede (2006). "The SWISS-MODEL workspace: a web-based environment for protein structure homology modelling." *Bioinformatics* 22(2): 195-201.

Ashburn, T. T. and K. B. Thor (2004). "Drug repositioning: identifying and developing new uses for existing drugs." *Nat Rev Drug Discov* 3(8): 673-83.

Bacchi, C. J., H. C. Nathan, S. H. Hutner, P. P. McCann and A. Sjoerdsma (1980). "Polyamine metabolism: a potential therapeutic target in trypanosomes." *Science* 210(4467): 332-4.

Bae, Y. S., S. W. Kang, M. S. Seo, I. C. Baines, E. Tekle, P. B. Chock and S. G. Rhee (1997). "Epidermal growth factor (EGF)-induced generation of hydrogen peroxide. Role in EGF receptor-mediated tyrosine phosphorylation." *J Biol Chem* 272(1): 217-21.

Bakalara, N., A. Seyfang, T. Baltz and C. Davis (1995). "Trypanosoma brucei and Trypanosoma cruzi: life cycle-regulated protein tyrosine phosphatase activity." *Exp Parasitol* 81(3): 302-12.

Bandyopadhyay, D., A. Kusari, K. A. Kenner, F. Liu, J. Chernoff, T. A. Gustafson and J. Kusari (1997). "Protein-tyrosine phosphatase 1B complexes with the insulin receptor in vivo and is tyrosine-phosphorylated in the presence of insulin." *J Biol Chem* 272(3): 1639-45.

Bangs, J. D., D. M. Ransom, M. A. McDowell and E. M. Brouch (1997). "Expression of bloodstream variant surface glycoproteins in procyclic stage Trypanosoma brucei: role of GPI anchors in secretion." *Embo J* 16(14): 4285-94.

Barford D, Flint A J and Tonks NK (1994). "Crystal structure of human protein tyrosine phosphatase 1B." *Science* 263(5152): 1397-404.

Barquilla, A., J. L. Crespo and M. Navarro (2008). "Rapamycin inhibits trypanosome cell growth by preventing TOR complex 2 formation." *Proc Natl Acad Sci U S A* 105(38): 14579-84.

Barr, A. J., E. Ugochukwu, W. H. Lee, O. N. King, P. Filippakopoulos, I. Alfano, P. Savitsky, N. A. Burgess-Brown, S. Muller and S. Knapp (2009). "Large-scale structural analysis of the classical human protein tyrosine phosphatome." *Cell* 136(2): 352-63.

Barrett, M. P., D. W. Boykin, R. Brun and R. R. Tidwell (2007). "Human African trypanosomiasis: pharmacological re-engagement with a neglected disease." *Br J Pharmacol* 152(8): 1155-71.

Bass, K. E. and C. C. Wang (1991). "The in vitro differentiation of pleomorphic Trypanosoma brucei from bloodstream into procyclic form requires neither intermediary nor short-stumpy stage." *Mol Biochem Parasitol* 44(2): 261-70.

Basselin, M. and M. Robert-Gero (1998). "Alterations in membrane fluidity, lipid metabolism, mitochondrial activity, and lipophosphoglycan expression in pentamidine-resistant Leishmania." *Parasitol Res* 84(1): 78-83.

Bastin, P., T. H. MacRae, S. B. Francis, K. R. Matthews and K. Gull (1999). "Flagellar morphogenesis: protein targeting and assembly in the paraflagellar rod of trypanosomes." *Mol Cell Biol* 19(12): 8191-200.

Bastin, P., T. Sherwin and K. Gull (1998). "Paraflagellar rod is vital for trypanosome motility." *Nature* 391(6667): 548.

Benaim, G., C. Lopez-Estrano, R. Docampo and S. N. Moreno (1993). "A calmodulin-stimulated Ca2+ pump in plasma-membrane vesicles from Trypanosoma brucei; selective inhibition by pentamidine." *Biochem J* 296 (Pt 3): 759-63.

Berg, J. M., J. L. Tymoczko and L. Stryer (2002). Biochemistry. W.H. Freeman and Co. Chapter 8.

Berridge, M. J. (1993). "Inositol trisphosphate and calcium signalling." *Nature* 361(6410): 315-25.

Berriman, M., E. Ghedin, C. Hertz-Fowler, G. Blandin, H. Renauld, D. C. Bartholomeu, N. J. Lennard, E. Caler, N. E. Hamlin, etc., F. Opperdoes, B. G. Barrell, J. E. Donelson, N. Hall, C. M. Fraser, S. E. Melville and N. M. El-Sayed (2005). "The genome of the African trypanosome Trypanosoma brucei." *Science* 309(5733): 416-22.

Besteiro, S., M. P. Barrett, L. Riviere and F. Bringaud (2005). "Energy generation in insect stages of Trypanosoma brucei: metabolism in flux." *Trends Parasitol* 21(4): 185-91.

Besteiro, S., M. Biran, N. Biteau, V. Coustou, T. Baltz, P. Canioni and F. Bringaud (2002). "Succinate secreted by Trypanosoma brucei is produced by a novel and unique glycosomal enzyme, NADH-dependent fumarate reductase." *J Biol Chem* 277(41): 38001-12.

Bey, P., C. Danzin, V. Van Dorsselaer, P. Mamont, M. Jung and C. Tardif (1978). "Analogues of ornithine as inhibitors of ornithine decarboxylase. New deductions concerning the topography of the enzyme's active site." *J Med Chem* 21(1): 50-5.

Bienen, E. J., E. Hammadi and G. C. Hill (1980). "Initiation of trypanosome transformation from bloodstream trypomastigotes to procyclic trypomastigotes." *J Parasitol* 66(4): 680-2.

Black, S. J., C. N. Sendashonga, C. O'Brien, N. K. Borowy, M. Naessens, P. Webster and M. Murray (1985). "Regulation of parasitaemia in mice infected with Trypanosoma brucei." *Curr Top Microbiol Immunol* 117: 93-118.

Blanchetot, C., Chagnon M., Dube N., Halle M. and T. M. L. (2005). "Substrate-trapping techniques in the identification of cellular PTP targets." *Methods* 35(1): 44-53.

Blanchetot, C., L. G. Tertoolen and J. den Hertog (2002). "Regulation of receptor protein-tyrosine phosphatase alpha by oxidative stress." *Embo J* 21(4): 493-503.

Bleicher, K. H., H. J. Bohm, K. Muller and A. I. Alanine (2003). "Hit and lead generation: beyond high-throughput screening." *Nat Rev Drug Discov* 2(5): 369-78.

Blom, N., S. Gammeltoft and S. Brunak (1999). "Sequence and structure-based prediction of eukaryotic protein phosphorylation sites." *J Mol Biol* 294(5): 1351-62.

Bordoli, L., F. Kiefer, K. Arnold, P. Benkert, J. Battey and T. Schwede (2009). "Protein structure homology modeling using SWISS-MODEL workspace." *Nat Protoc* 4(1): 1-13.

Borst, P., P. J. Weijers and G. J. Brakenhoff (1982). "Analysis by electron microscopy of the variable segment in the maxi-circle of kinetoplast DNA from Trypanosoma brucei." *Biochim Biophys Acta* 699(3): 272-80.

Bosch, F. and L. Rosich (2008). "The contributions of Paul Ehrlich to pharmacology: a tribute on the occasion of the centenary of his Nobel Prize." *Pharmacology* 82(3): 171-9.

Bourdeau, A., N. Dube and M. L. Tremblay (2005). "Cytoplasmic protein tyrosine phosphatases, regulation and function: the roles of PTP1B and TC-PTP." *Curr Opin Cell Biol* 17(2): 203-9.

Branche, C., S. Ochaya, L. Aslund and B. Andersson (2006). "Comparative karyotyping as a tool for genome structure analysis of Trypanosoma cruzi." *Mol Biochem Parasitol* 147(1): 30-8.

Brenchley, R., H. Tariq, H. McElhinney, B. Szoor, J. Huxley-Jones, R. Stevens, K. Matthews and L. Tabernero (2007). "The TriTryp phosphatome: analysis of the protein phosphatase catalytic domains." *BMC Genomics* 8: 434.

Brown, R. C., D. A. Evans and K. Vickerman (1973). "Changes in oxidative metabolism and ultrastructure accompanying differentiation of the mitochondrion in Trypanosoma brucei." *Int J Parasitol* 3(5): 691-704.

Brown-Shimer, S., K. A. Johnson, D. E. Hill and A. M. Bruskin (1992). "Effect of protein tyrosine phosphatase 1B expression on transformation by the human neu oncogene." *Cancer Res* 52(2): 478-82.

Brun, R. and M. Schonenberger (1981). "Stimulating effect of citrate and cis-Aconitate on the transformation of Trypanosoma brucei bloodstream forms to procyclic forms in vitro." *Z Parasitenkd* 66(1): 17-24.

Bulow, R. and P. Overath (1985). "Synthesis of a hydrolase for the membrane-form variant surface glycoprotein is repressed during transformation of Trypanosoma brucei." *FEBS Lett* 187(1): 105-10.

Burgess, S. A., M. L. Walker, H. Sakakibara, P. J. Knight and K. Oiwa (2003). "Dynein structure and power stroke." *Nature* 421(6924): 715-8.

Burkard, G., C. M. Fragoso and I. Roditi (2007). "Highly efficient stable transformation of bloodstream forms of Trypanosoma brucei." *Mol Biochem Parasitol* 153(2): 220-3.

Caselli, A., R. Marzocchini, G. Camici, G. Manao, G. Moneti, G. Pieraccini and G. Ramponi (1998). "The inactivation mechanism of low molecular weight phosphotyrosine-protein phosphatase by H2O2." *J Biol Chem* 273(49): 32554-60.

Cavalli, A., F. Lizzi, S. Bongarzone, F. Belluti, L. Piazzi and M. L. Bolognesi (2009). "Complementary medicinal chemistry-driven strategies toward new antitrypanosomal and antileishmanial lead drug candidates." *FEMS Immunol Med Microbiol* 58(1): 51-60.

Chang, Y. C., S. Y. Lin, S. Y. Liang, K. T. Pan, C. C. Chou, C. H. Chen, C. L. Liao, K. H. Khoo and T. C. Meng (2008). "Tyrosine phosphoproteomics and identification of substrates of protein tyrosine phosphatase dPTP61F in Drosophila S2 cells by mass spectrometry-based substrate trapping strategy." *J Proteome Res* 7(3): 1055-66.

Chaudhuri, M., R. D. Ott and G. C. Hill (2006). "Trypanosome alternative oxidase: from molecule to function." *Trends Parasitol* 22(10): 484-91.

Chen, C. H., T. H. Cheng, H. Lin, N. L. Shih, Y. L. Chen, Y. S. Chen, C. F. Cheng, W. S. Lian, T. C. Meng, W. T. Chiu and J. J. Chen (2006). "Reactive oxygen species generation is involved in epidermal growth factor receptor transactivation through the transient oxidization of Src homology 2-containing tyrosine phosphatase in endothelin-1 signaling pathway in rat cardiac fibroblasts." *Mol Pharmacol* 69(4): 1347-55.

Chen, K., M. T. Kirber, H. Xiao, Y. Yang and J. F. Keaney, Jr. (2008). "Regulation of ROS signal transduction by NADPH oxidase 4 localization." *J Cell Biol* 181(7): 1129-39.

Chiarugi, P., G. Pani, E. Giannoni, L. Taddei, R. Colavitti, G. Raugei, M. Symons, S. Borrello, T. Galeotti and G. Ramponi (2003). "Reactive oxygen species as essential mediators of cell adhesion: the oxidative inhibition of a FAK tyrosine phosphatase is required for cell adhesion." *J Cell Biol* 161(5): 933-44.

Choi, J. H., H. S. Kim, S. H. Kim, Y. R. Yang, Y. S. Bae, J. S. Chang, H. M. Kwon, S. H. Ryu and P. G. Suh (2006). "Phospholipase Cgamma1 negatively regulates growth hormone signalling by forming a ternary complex with Jak2 and protein tyrosine phosphatase-1B." *Nat Cell Biol* 8(12): 1389-97.

Chothia, C. and A. M. Lesk (1986). "The relation between the divergence of sequence and structure in proteins." *Embo J* 5(4): 823-6.

Chou, S., B. C. Jensen, M. Parsons, T. Alber and C. Grundner (2010). "The Trypanosoma brucei life cycle switch TbPTP1 is structurally conserved and dephosphorylates the nucleolar protein, NOPP44/46." *J Biol Chem*.

Clarkson, A. B., Jr., E. J. Bienen, G. Pollakis and R. W. Grady (1989). "Respiration of bloodstream forms of the parasite Trypanosoma brucei brucei is dependent on a plant-like alternative oxidase." *J Biol Chem* 264(30): 17770-6.

Clayton, C. E. (2002). "Life without transcriptional control? From fly to man and back again." *Embo J* 21(8): 1881-8.

Cross, G. A. (1978). "Antigenic variation in trypanosomes." *Proc R Soc Lond B Biol Sci* 202(1146): 55-72.

Cross, G. A. (1984). "Release and purification of Trypanosoma brucei variant surface glycoprotein." *J Cell Biochem* 24(1): 79-90.

Cross, G. A. and J. C. Manning (1973). "Cultivation of Trypanosoma brucei sspp. in semi-defined and defined media." *Parasitology* 67(3): 315-31.

Czichos, J., C. Nonnengaesser and P. Overath (1986). "Trypanosoma brucei: cis-aconitate and temperature reduction as triggers of synchronous transformation of bloodstream to procyclic trypomastigotes in vitro." *Exp Parasitol* 62(2): 283-91.

Dadke, S., S. Cotteret, S. C. Yip, Z. M. Jaffer, F. Haj, A. Ivanov, F. Rauscher, 3rd, K. Shuai, T. Ng, B. G. Neel and J. Chernoff (2007). "Regulation of protein tyrosine phosphatase 1B by sumoylation." *Nat Cell Biol* 9(1): 80-5.

Dadke, S., A. Kusari and J. Kusari (2001). "Phosphorylation and activation of protein tyrosine phosphatase (PTP) 1B by insulin receptor." *Mol Cell Biochem* 221(1-2): 147-54.

Das, A., M. Gale, Jr., V. Carter and M. Parsons (1994). "The protein phosphatase inhibitor okadaic acid induces defects in cytokinesis and organellar genome segregation in Trypanosoma brucei." *J Cell Sci* 107 (Pt 12): 3477-83.

Das, A., J. H. Park, C. B. Hagen and M. Parsons (1998). "Distinct domains of a nucleolar protein mediate protein kinase binding, interaction with nucleic acids and nucleolar localization." *J Cell Sci* 111 (Pt 17): 2615-23.

Das, A., G. C. Peterson, S. B. Kanner, U. Frevert and M. Parsons (1996). "A major tyrosine-phosphorylated protein of Trypanosoma brucei is a nucleolar RNA-binding protein." *J Biol Chem* 271(26): 15675-81.

Das, B. P. and D. W. Boykin (1977). "Synthesis and antiprotozoal activity of 2,5-bis(4-guanylphenyl)furans." *J Med Chem* 20(4): 531-6.

De Koning, H. P. (2001). "Uptake of pentamidine in Trypanosoma brucei brucei is mediated by three distinct transporters: implications for cross-resistance with arsenicals." *Mol Pharmacol* 59(3): 586-92.

de Oliveira-Silva, F., E. de Morais-Teixeira and A. Rabello (2008). "Antileishmanial activity of azithromycin against Leishmania (Leishmania) amazonensis, Leishmania (Viannia) braziliensis, and Leishmania (Leishmania) chagasi." *Am J Trop Med Hyg* 78(5): 745-9.

Dean, S., R. Marchetti, K. Kirk and K. R. Matthews (2009). "A surface transporter family conveys the trypanosome differentiation signal." *Nature* 459(7244): 213-7.

den Hertog, J., A. Ostman and F. D. Bohmer (2008). "Protein tyrosine phosphatases: regulatory mechanisms." *Febs J* 275(5): 831-47.

Denise, H. and M. P. Barrett (2001). "Uptake and mode of action of drugs used against sleeping sickness." *Biochem Pharmacol* 61(1): 1-5.

Denu, J. M., D. L. Lohse, J. Vijayalakshmi, M. A. Saper and J. E. Dixon (1996). "Visualization of intermediate and transition-state structures in protein-tyrosine phosphatase catalysis." *Proc Natl Acad Sci U S A* 93(6): 2493-8.

Denu, J. M. and K. G. Tanner (1998). "Specific and reversible inactivation of protein tyrosine phosphatases by hydrogen peroxide: evidence for a sulfenic acid intermediate and implications for redox regulation." *Biochemistry* 37(16): 5633-42.

Dhanasekaran, N. and E. Premkumar Reddy (1998). "Signaling by dual specificity kinases." *Oncogene* 17(11 Reviews): 1447-55.

DNDi and P. A. S. Network (2009). Drug Screening for kinetoplastids Diseases.

Docampo, R. and S. N. Moreno (1986). "Free radical metabolism of antiparasitic agents." *Fed Proc* 45(10): 2471-6.

Dolan, M. T., C. G. Reid and H. P. Voorheis (1986). "Calcium ions initiate the selective depolymerization of the pellicular microtubules in bloodstream forms of Trypanosoma brucei." *J Cell Sci* 80: 123-40.

Dressel and Oesper (1961). "The discovery of Germanin by Oskar Dressel and Richard Kothe." *Journal of Chemical Education* 38: 620-621.

Duckert, P., S. Brunak and N. Blom (2004). "Prediction of proprotein convertase cleavage sites." *Protein Eng Des Sel* 17(1): 107-12.

Durieux, P. O., P. Schutz, R. Brun and P. Kohler (1991). "Alterations in Krebs cycle enzyme activities and carbohydrate catabolism in two strains of Trypanosoma brucei during in vitro differentiation of their bloodstream to procyclic stages." *Mol Biochem Parasitol* 45(1): 19-27.

Ekwanzala, M., J. Pepin, N. Khonde, S. Molisho, H. Bruneel and P. De Wals (1996). "In the heart of darkness: sleeping sickness in Zaire." *Lancet* 348(9039): 1427-30.

El-Sayed, N. M., P. Hegde, J. Quackenbush, S. E. Melville and J. E. Donelson (2000). "The African trypanosome genome." *Int J Parasitol* 30(4): 329-45.

Elchebly, M., P. Payette, E. Michaliszyn, W. Cromlish, S. Collins, A. L. Loy, D. Normandin, A. Cheng, J. Himms-Hagen, C. C. Chan, C. Ramachandran, M. J. Gresser, M. L. Tremblay and B. P. Kennedy (1999). "Increased insulin sensitivity and obesity resistance in mice lacking the protein tyrosine phosphatase-1B gene." *Science* 283(5407): 1544-8.

Ellis, D. S. and D. A. Evans (1977). "Passage of Trypanosoma brucei rhodesiense through the peritrophic membrane of Glossina morsitans morsitans." *Nature* 267(5614): 834-5.

Engstler, M. and M. Boshart (2004). "Cold shock and regulation of surface protein trafficking convey sensitization to inducers of stage differentiation in Trypanosoma brucei." *Genes Dev* 18(22): 2798-811.

Engstler, M., T. Pfohl, S. Herminghaus, M. Boshart, G. Wiegertjes, N. Heddergott and P. Overath (2007). "Hydrodynamic flow-mediated protein sorting on the cell surface of trypanosomes." *Cell* 131(3): 505-15.

Ersfeld, K. and K. Gull (1997). "Partitioning of large and minichromosomes in Trypanosoma brucei." *Science* 276(5312): 611-4.

Ersfeld, K., S. E. Melville and K. Gull (1999). "Nuclear and genome organization of Trypanosoma brucei." *Parasitol Today* 15(2): 58-63.

Fairbairn, H. and A. T. Culwick (1947). "The modification of Trypanosoma rhodesiense on prolonged syringe passage." *Ann Trop Med Parasitol* 41(1): 26-9.

Fairlamb, A. H. and I. B. Bowman (1977). "Trypanosoma brucei: suramin and other trypanocidal compounds' effects on sn-glycerol-3-phosphate oxidase." *Exp Parasitol* 43(2): 353-61.

Fairlamb, A. H., G. B. Henderson, C. J. Bacchi and A. Cerami (1987). "In vivo effects of difluoromethylornithine on trypanothione and polyamine levels in bloodstream forms of Trypanosoma brucei." *Mol Biochem Parasitol* 24(2): 185-91.

Fairlamb, A. H., G. B. Henderson and A. Cerami (1989). "Trypanothione is the primary target for arsenical drugs against African trypanosomes." *Proc Natl Acad Sci U S A* 86(8): 2607-11.

Falet, H., S. Pain and F. Rendu (1998). "Tyrosine unphosphorylated platelet SHP-1 is a substrate for calpain." *Biochem Biophys Res Commun* 252(1): 51-5.

FAO (1982). Training manual for tsetse control personnel. F. a. A. O. o. t. U. Nations. **volume 1**.

Fauman, E. B. and M. A. Saper (1996). "Structure and function of the protein tyrosine phosphatases." *Trends Biochem Sci* 21(11): 413-7.

Fedoroff, N. (2006). "Redox regulatory mechanisms in cellular stress responses." *Ann Bot* 98(2): 289-300.

Ferrante, A. and A. C. Allison (1983). "Alternative pathway activation of complement by African trypanosomes lacking a glycoprotein coat." *Parasite Immunol* 5(5): 491-8.

Fevre, E., K. Picozzi, J. Jannin, S. Welburn and I. Maudlin (2006a). "Human African Trypanosomiasis: epidemiology and control." *Advances in Parasitology* 61: 167-221.

Fevre, E. M., K. Picozzi, J. Jannin, S. C. Welburn and I. Maudlin (2006b). "Human African trypanosomiasis: Epidemiology and control." *Adv Parasitol* 61: 167-221.

Field, M. C. and M. Carrington (2009). "The trypanosome flagellar pocket." *Nat Rev Microbiol* 7(11): 775-86.

Figarella, K., N. L. Uzcategui, A. Beck, C. Schoenfeld, B. K. Kubata, F. Lang and M. Duszenko (2006). "Prostaglandin-induced programmed cell death in Trypanosoma brucei involves oxidative stress." *Cell Death Differ* 13(10): 1802-14.

Flint, A. J., M. F. Gebbink, B. R. Franza, Jr., D. E. Hill and N. K. Tonks (1993). "Multi-site phosphorylation of the protein tyrosine phosphatase, PTP1B: identification of cell cycle regulated and phorbol ester stimulated sites of phosphorylation." *Embo J* 12(5): 1937-46.

Flint, A. J., T. Tiganis, D. Barford and N. K. Tonks (1997). "Development of "substrate-trapping" mutants to identify physiological substrates of protein tyrosine phosphatases." *Proc Natl Acad Sci U S A* 94(5): 1680-5.

Frangioni, J. V., P. H. Beahm, V. Shifrin, C. A. Jost and B. G. Neel (1992). "The nontransmembrane tyrosine phosphatase PTP-1B localizes to the endoplasmic reticulum via its 35 amino acid C-terminal sequence." *Cell* 68(3): 545-60.

Frangioni, J. V., A. Oda, M. Smith, E. W. Salzman and B. G. Neel (1993). "Calpain-catalyzed cleavage and subcellular relocation of protein phosphotyrosine phosphatase 1B (PTP-1B) in human platelets." *Embo J* 12(12): 4843-56.

Frevert, U., F. Herzberg, E. Reinwald and H. J. Risse (1986). "Morphological changes in Trypanosoma congolense after proteolytic removal of the surface coat." *J Ultrastruct Mol Struct Res* 94(2): 140-8.

Friedheim, E. A. (1949). "Mel B in the treatment of human trypanosomiasis." *Am J Trop Med Hyg* 29(2): 173-80.

Gale, M., Jr., V. Carter and M. Parsons (1994). "Translational control mediates the developmental regulation of the Trypanosoma brucei Nrk protein kinase." *J Biol Chem* 269(50): 31659-65.

Garton, A. J., A. J. Flint and N. K. Tonks (1996). "Identification of p130(cas) as a substrate for the cytosolic protein tyrosine phosphatase PTP-PEST." *Mol Cell Biol* 16(11): 6408-18.

Gebbink, M. F., G. C. Zondag, G. M. Koningstein, E. Feiken, R. W. Wubbolts and W. H. Moolenaar (1995). "Cell surface expression of receptor protein tyrosine phosphatase RPTP mu is regulated by cell-cell contact." *J Cell Biol* 131(1): 251-60.

Geerts, S. and B. Gryseels (2001). "Anthelmintic resistance in human helminths: a review." *Trop Med Int Health* 6(11): 915-21.

Gibson, W. (2001). "Sex and evolution in trypanosomes." *Int J Parasitol* 31(5-6): 643-7.

Gordon, J. A. (1991). "Use of vanadate as protein-phosphotyrosine phosphatase inhibitor." *Methods Enzymol* 201: 477-82.

Gruszynski, A. E., A. DeMaster, N. M. Hooper and J. D. Bangs (2003). "Surface coat remodeling during differentiation of Trypanosoma brucei." *J Biol Chem* 278(27): 24665-72.

Guan, K. L. and J. E. Dixon (1991). "Evidence for protein-tyrosine-phosphatase catalysis proceeding via a cysteine-phosphate intermediate." *J Biol Chem* 266(26): 17026-30.

Haag, J., C. O'HUigin and P. Overath (1998). "The molecular phylogeny of trypanosomes: evidence for an early divergence of the Salivaria." *Mol Biochem Parasitol* 91(1): 37-49.

Haj, F. G., P. J. Verveer, A. Squire, B. G. Neel and P. I. Bastiaens (2002). "Imaging sites of receptor dephosphorylation by PTP1B on the surface of the endoplasmic reticulum." *Science* 295(5560): 1708-11.

Hall, B. S., C. Gabernet-Castello, A. Voak, D. Goulding, S. K. Natesan and M. C. Field (2006). "TbVps34, the trypanosome orthologue of Vps34, is required for Golgi complex segregation." *J Biol Chem* 281(37): 27600-12.

Hao, Z., I. Kasumba and S. Aksoy (2003). "Proventriculus (cardia) plays a crucial role in immunity in tsetse fly (Diptera: Glossinidiae)." *Insect Biochem Mol Biol* 33(11): 1155-64.

Hargrove, J. W. (2003). "Tsetse Eradication: Sufficiency, Necessity and Desirability. (Research Report, DFDI Animal Health Programme)."

Hart, D. T., P. Baudhuin, F. R. Opperdoes and C. de Duve (1987). "Biogenesis of the glycosome in Trypanosoma brucei: the synthesis, translocation and turnover of glycosomal polypeptides." *Embo J* 6(5): 1403-11.

Harvey, L., B. Arnold, Z. S. Lawrence, B. David and D. James (2000). Molecular Cell Biology. New York, W. H. Freeman.

Heffetz, D., W. J. Rutter and Y. Zick (1992). "The insulinomimetic agents H2O2 and vanadate stimulate tyrosine phosphorylation of potential target proteins for the insulin receptor kinase in intact cells." *Biochem J* 288 (Pt 2): 631-5.

Hemphill, A., T. Seebeck and D. Lawson (1991). "The Trypanosoma brucei cytoskeleton: ultrastructure and localization of microtubule-associated and spectrin-like proteins using quick-freeze, deep-etch, immunogold electron microscopy." *J Struct Biol* 107(3): 211-20.

Hertz-Fowler, C., K. Ersfeld and K. Gull (2001). "CAP5.5, a life-cycle-regulated, cytoskeleton-associated protein is a member of a novel family of calpain-related proteins in Trypanosoma brucei." *Mol Biochem Parasitol* 116(1): 25-34.

Hirumi, H. and K. Hirumi (1989). "Continuous cultivation of Trypanosoma brucei blood stream forms in a medium containing a low concentration of serum protein without feeder cell layers." *J Parasitol* 75(6): 985-9.

Hosokawa, N., T. Sasaki, S. Iemura, T. Natsume, T. Hara and N. Mizushima (2009). "Atg101, a novel mammalian autophagy protein interacting with Atg13." *Autophagy* 5(7): 973-9.

Hotez, P. J. and A. Kamath (2009). "Neglected tropical diseases in sub-saharan Africa: review of their prevalence, distribution, and disease burden." *PLoS Negl Trop Dis* 3(8): e412.

Hunt, M., R. Brun and P. Kohler (1994). "Studies on compounds promoting the in vitro transformation of Trypanosoma brucei from bloodstream to procyclic forms." *Parasitol Res* 80(7): 600-6.

Hunter, T. (1987). "A thousand and one protein kinases." *Cell* 50(6): 823-9.

Huyer, G., S. Liu, J. Kelly, J. Moffat, P. Payette, B. Kennedy, G. Tsaprailis, M. J. Gresser and C. Ramachandran (1997). "Mechanism of inhibition of protein-tyrosine phosphatases by vanadate and pervanadate." *J Biol Chem* 272(2): 843-51.

Imbuga, M. O., E. O. Osir and V. L. Labongo (1992). "Inhibitory effect of Trypanosoma brucei brucei on Glossina morsitans midgut trypsin in vitro." *Parasitol Res* 78(4): 273-6.

Ishiyama, A., K. Otoguro, M. Namatame, A. Nishihara, T. Furusawa, R. Masuma, K. Shiomi, Y. Takahashi, M. Ichimura, H. Yamada and S. Omura (2008). "In vitro and in vivo antitrypanosomal activitiy of two microbial metabolites, KS-505a and alazopeptin." *J Antibiot (Tokyo)* 61(10): 627-32.

Iten, M., H. Mett, A. Evans, J. C. Enyaru, R. Brun and R. Kaminsky (1997). "Alterations in ornithine decarboxylase characteristics account for tolerance of Trypanosoma brucei rhodesiense to D,L-alpha-difluoromethylornithine." *Antimicrob Agents Chemother* 41(9): 1922-5.

Jacob, L., B. Hoffmann, V. Stoven and J. P. Vert (2008). "Virtual screening of GPCRs: an in silico chemogenomics approach." *BMC Bioinformatics* 9: 363.

Jemc, J. and I. Rebay (2007). "The eyes absent family of phosphotyrosine phosphatases: properties and roles in developmental regulation of transcription." *Annu Rev Biochem* 76: 513-38.

Jenni, L., S. Marti, J. Schweizer, B. Betschart, R. W. Le Page, J. M. Wells, A. Tait, P. Paindavoine, E. Pays and M. Steinert (1986). "Hybrid formation between African trypanosomes during cyclical transmission." *Nature* 322(6075): 173-5.

Jensen, B. C., D. L. Brekken, A. C. Randall, C. T. Kifer and M. Parsons (2005). "Species specificity in ribosome biogenesis: a nonconserved phosphoprotein is required for formation of the large ribosomal subunit in Trypanosoma brucei." *Eukaryot Cell* 4(1): 30-5.

Jia, Z., D. Barford, A. J. Flint and N. K. Tonks (1995). "Structural basis for phosphotyrosine peptide recognition by protein tyrosine phosphatase 1B." *Science* 268(5218): 1754-8.

Johnson, P. J., J. M. Kooter and P. Borst (1987). "Inactivation of transcription by UV irradiation of T. brucei provides evidence for a multicistronic transcription unit including a VSG gene." *Cell* 51(2): 273-81.

Jones, C., S. Anderson, U. K. Singha and M. Chaudhuri (2008). "Protein phosphatase 5 is required for Hsp90 function during proteotoxic stresses in Trypanosoma brucei." *Parasitol Res* 102(5): 835-44.

Kabani, S., K. Fenn, A. Ross, A. Ivens, T. K. Smith, P. Ghazal and K. Matthews (2009). "Genome-wide expression profiling of in vivo-derived bloodstream parasite stages and dynamic analysis of mRNA alterations during synchronous differentiation in Trypanosoma brucei." *BMC Genomics* 10: 427.

Kaiser, D. and R. Losick (1993). "How and why bacteria talk to each other." *Cell* 73(5): 873-85.

Kaur, K. J. and L. Ruben (1994). "Protein translation elongation factor-1 alpha from Trypanosoma brucei binds calmodulin." *J Biol Chem* 269(37): 23045-50.

Kim, E., M. Niethammer, A. Rothschild, Y. N. Jan and M. Sheng (1995). "Clustering of Shaker-type K+ channels by interaction with a family of membrane-associated guanylate kinases." *Nature* 378(6552): 85-8.

Klayman, D. L. (1985). "Qinghaosu (artemisinin): an antimalarial drug from China." *Science* 228(4703): 1049-55.

Kobe, B., T. Gleichmann, J. Horne, I. G. Jennings, P. D. Scotney and T. Teh (1999). "Turn up the HEAT." *Structure* 7(5): R91-7.

Kobor, M. S., J. Archambault, W. Lester, F. C. Holstege, O. Gileadi, D. B. Jansma, E. G. Jennings, F. Kouyoumdjian, A. R. Davidson, R. A. Young and J. Greenblatt (1999). "An unusual eukaryotic protein phosphatase required for transcription by RNA polymerase II and CTD dephosphorylation in S. cerevisiae." *Mol Cell* 4(1): 55-62.

Kohl, L., D. Robinson and P. Bastin (2003). "Novel roles for the flagellum in cell morphogenesis and cytokinesis of trypanosomes." *Embo J* 22(20): 5336-46.

Kohl, L., T. Sherwin and K. Gull (1999). "Assembly of the paraflagellar rod and the flagellum attachment zone complex during the Trypanosoma brucei cell cycle." *J Eukaryot Microbiol* 46(2): 105-9.

Kontaridis, M. I., S. Eminaga, M. Fornaro, C. I. Zito, R. Sordella, J. Settleman and A. M. Bennett (2004). "SHP-2 positively regulates myogenesis by coupling to the Rho GTPase signaling pathway." *Mol Cell Biol* 24(12): 5340-52.

Krantz, I. D., J. McCallum, C. DeScipio, M. Kaur, L. A. Gillis, D. Yaeger, L. Jukofsky, N. Wasserman, A. Bottani, C. A. Morris, M. J. Nowaczyk, H. Toriello, M. J. Bamshad, J. C. Carey, E. Rappaport, S. Kawauchi, A. D. Lander, A. L. Calof, H. H. Li, M. Devoto and L. G.

Jackson (2004). "Cornelia de Lange syndrome is caused by mutations in NIPBL, the human homolog of Drosophila melanogaster Nipped-B." *Nat Genet* 36(6): 631-5.

Krauth-Siegel, R. L. and M. A. Comini (2008). "Redox control in trypanosomatids, parasitic protozoa with trypanothione-based thiol metabolism." *Biochim Biophys Acta* 1780(11): 1236-48.

Lacomble, S., S. Vaughan, C. Gadelha, M. K. Morphew, M. K. Shaw, J. R. McIntosh and K. Gull (2009). "Three-dimensional cellular architecture of the flagellar pocket and associated cytoskeleton in trypanosomes revealed by electron microscope tomography." *J Cell Sci* 122(Pt 8): 1081-90.

LaCount, D. J., S. Bruse, K. L. Hill and J. E. Donelson (2000). "Double-stranded RNA interference in Trypanosoma brucei using head-to-head promoters." *Mol Biochem Parasitol* 111(1): 67-76.

Laiping X, Zhang Y and Z. Z (2001). "Deisgn and Characterization of an Improved Potein Tyrosine Phosphatase Substrate-Trapping Mutant." *Biochemistry* 41(12): 4032-4039.

Laiping, X., Zhang Y and Z. Z (2001). "Deisgn and Characterization of an Improved Potein Tyrosine Phosphatase Substrate-Trapping Mutant." *Biochemistry* 41(12): 4032-4039.

LaMontagne, K. R., Jr., A. J. Flint, B. R. Franza, Jr., A. M. Pandergast and N. K. Tonks (1998a). "Protein tyrosine phosphatase 1B antagonizes signalling by oncoprotein tyrosine kinase p210 bcr-abl in vivo." *Mol Cell Biol* 18(5): 2965-75.

LaMontagne, K. R., Jr., G. Hannon and N. K. Tonks (1998b). "Protein tyrosine phosphatase PTP1B suppresses p210 bcr-abl-induced transformation of rat-1 fibroblasts and promotes differentiation of K562 cells." *Proc Natl Acad Sci U S A* 95(24): 14094-9.

Lanham, S. M. and D. G. Godfrey (1970). "Isolation of salivarian trypanosomes from man and other mammals using DEAE-cellulose." *Exp Parasitol* 28(3): 521-34.

Laxman, S., A. Riechers, M. Sadilek, F. Schwede and J. A. Beavo (2006). "Hydrolysis products of cAMP analogs cause transformation of Trypanosoma brucei from slender to stumpy-like forms." *Proc Natl Acad Sci U S A* 103(50): 19194-9.

Lee, H., L. Xie, Y. Luo, S. Y. Lee, D. S. Lawrence, X. B. Wang, F. Sotgia, M. P. Lisanti and Z. Y. Zhang (2006). "Identification of phosphocaveolin-1 as a novel protein tyrosine phosphatase 1B substrate." *Biochemistry* 45(1): 234-40.

Lessard, L., M. Stuible and M. L. Tremblay (2010). "The two faces of PTP1B in cancer." *Biochim Biophys Acta* 1804(3): 613-9.

Li, S. and J. E. Donelson (1995). "Inhibition of protein phosphatase 1 and 2A down-regulates beta-tubulin gene expression in Trypanosoma rhodesiense." *Biochem Biophys Res Commun* 212(3): 793-9.

Li, Z., X. Tu and C. C. Wang (2006). "Okadaic acid overcomes the blocked cell cycle caused by depleting Cdc2-related kinases in Trypanosoma brucei." *Exp Cell Res* 312(18): 3504-16.

Liao, S., T. Wang, K. Fan and X. Tu (2010). "The small ubiquitin-like modifier (SUMO) is essential in cell cycle regulation in Trypanosoma brucei." *Exp Cell Res* 316(5): 704-15.

Liu, F., M. A. Sells and J. Chernoff (1998). "Protein tyrosine phosphatase 1B negatively regulates integrin signaling." *Curr Biol* 8(3): 173-6.

Liu, J. (1995). "Pharmacology of oleanolic acid and ursolic acid." *J Ethnopharmacol* 49(2): 57-68.

Liu, W., K. Apagyi, L. McLeavy and K. Ersfeld (2010). "Expression and cellular localisation of calpain-like proteins in Trypanosoma brucei." *Mol Biochem Parasitol* 169(1): 20-6.

Lochhead, P. A., G. Sibbet, R. Kinstrie, T. Cleghon, M. Rylatt, D. K. Morrison and V. Cleghon (2003). "dDYRK2: a novel dual-specificity tyrosine-phosphorylation-regulated kinase in Drosophila." *Biochem J* 374(Pt 2): 381-91.

Lou, Y. W., Y. Y. Chen, S. F. Hsu, R. K. Chen, C. L. Lee, K. H. Khoo, N. K. Tonks and T. C. Meng (2008). "Redox regulation of the protein tyrosine phosphatase PTP1B in cancer cells." *Febs J* 275(1): 69-88.

Lourie, E. and W. Yorke (1937). "Studies in chemotherapy. XVI. The trypanocidal action of synthalin." *Ann Trop Med Parasitol* 31: 435-445.

Lundkvist, G. B., K. Kristensson and M. Bentivoglio (2004). "Why trypanosomes cause sleeping sickness." *Physiology (Bethesda)* 19: 198-206.

MacLeod, E. T., I. Maudlin, A. C. Darby and S. C. Welburn (2007). "Antioxidants promote establishment of trypanosome infections in tsetse." *Parasitology* 134(Pt 6): 827-31.

Mahadev, K., A. Zilbering, L. Zhu and B. J. Goldstein (2001). "Insulin-stimulated hydrogen peroxide reversibly inhibits protein-tyrosine phosphatase 1b in vivo and enhances the early insulin action cascade." *J Biol Chem* 276(24): 21938-42.

Mair, G., E. Ullu and C. Tschudi (2000). "Cotranscriptional cap 4 formation on the Trypanosoma brucei spliced leader RNA." *J Biol Chem* 275(37): 28994-9.

Makumi, J. N., C. Green and M. Baylis (1998). "Activity patterns in Glossina longipennis: a field study using different sampling methods." *Med Vet Entomol* 12(4): 399-406.

Matthews K R, E. J. R., Paterou A. (2004). "Molecular regulation of the life cycle of African trypanosomes." *Trends Parasitol* 20(1): 40-7.

Matthews, K. R. and K. Gull (1994). "Evidence for an interplay between cell cycle progression and the initiation of differentiation between life cycle forms of African trypanosomes." *J Cell Biol* 125(5): 1147-56.

Matthews, K. R., T. Sherwin and K. Gull (1995). "Mitochondrial genome repositioning during the differentiation of the African trypanosome between life cycle forms is microtubule mediated." *J Cell Sci* 108 (Pt 6): 2231-9.

McCain, D. F., L. Wu, P. Nickel, M. U. Kassack, A. Kreimeyer, A. Gagliardi, D. C. Collins and Z. Y. Zhang (2004). "Suramin derivatives as inhibitors and activators of protein-tyrosine phosphatases." *J Biol Chem* 279(15): 14713-25.

McElhinney, H. (2007). Functional analysis of Protein Tyrosine Phosphatases in *Trypanosoma brucei*. Faculty of Life Sciences Manchester, University of Manchester. **Doctor of Philosophy Thesis**.

McKean, P. G. (2003). "Coordination of cell cycle and cytokinesis in Trypanosoma brucei." *Curr Opin Microbiol* 6(6): 600-7.

Melville, S. E., V. Leech, C. S. Gerrard, A. Tait and J. M. Blackwell (1998). "The molecular karyotype of the megabase chromosomes of Trypanosoma brucei and the assignment of chromosome markers." *Mol Biochem Parasitol* 94(2): 155-73.

Meng, T. C., D. A. Buckley, S. Galic, T. Tiganis and N. K. Tonks (2004). "Regulation of insulin signaling through reversible oxidation of the protein-tyrosine phosphatases TC45 and PTP1B." *J Biol Chem* 279(36): 37716-25.

Meng, T. C., T. Fukada and N. K. Tonks (2002). "Reversible oxidation and inactivation of protein tyrosine phosphatases in vivo." *Mol Cell* 9(2): 387-99.

Meshnick, S. R., R. W. Grady, S. H. Blobstein and A. Cerami (1978). "Porphyrin-induced lysis of Trypanosoma brucei: a role for zinc." *J Pharmacol Exp Ther* 207(3): 1041-50.

Michels, P. A. (1989). "The glycosome of trypanosomes: properties and biogenesis of a microbody." *Exp Parasitol* 69(3): 310-5.

Midgley, I., K. Fitzpatrick, L. M. Taylor, T. L. Houchen, S. J. Henderson, S. J. Wright, Z. R. Cybulski, B. A. John, A. McBurney, D. W. Boykin and K. L. Trendler (2007). "Pharmacokinetics and metabolism of the prodrug DB289 (2,5-bis[4-(N-methoxyamidino)phenyl]furan monomaleate) in rat and monkey and its conversion to the antiprotozoal/antifungal drug DB75 (2,5-bis(4-guanylphenyl)furan dihydrochloride)." *Drug Metab Dispos* 35(6): 955-67.

Miezan, T. W., U. Bronner, F. Doua, P. Cattand and L. Rombo (1994). "Long-term exposure of Trypanosoma brucei gambiense to pentamidine in vitro." *Trans R Soc Trop Med Hyg* 88(3): 332-3.

Mills, E., H. P. Price, A. Johner, J. E. Emerson and D. F. Smith (2007). "Kinetoplastid PPEF phosphatases: dual acylated proteins expressed in the endomembrane system of Leishmania." *Mol Biochem Parasitol* 152(1): 22-34.

Moeslein, F. M., M. P. Myers and G. E. Landreth (1999). "The CLK family kinases, CLK1 and CLK2, phosphorylate and activate the tyrosine phosphatase, PTP-1B." *J Biol Chem* 274(38): 26697-704.

Montalibet, J., K. I. Skorey and B. P. Kennedy (2005). "Protein tyrosine phosphatase: enzymatic assays." *Methods* 35(1): 2-8.

Monteiro, H. P. and A. Stern (1996). "Redox modulation of tyrosine phosphorylation-dependent signal transduction pathways." *Free Radic Biol Med* 21(3): 323-33.

Motlusky, H. and A. Christopoulus (2003). Fitting Models to Biological Data using Linear and Nonlinear Regression. A practical Guide to Curve Fitting. San Diego, CA.

Mottram, J. C. and G. Smith (1995). "A family of trypanosome cdc2-related protein kinases." *Gene* 162(1): 147-52.

Mowatt, M. R., G. S. Wisdom and C. E. Clayton (1989). "Variation of tandem repeats in the developmentally regulated procyclic acidic repetitive proteins of Trypanosoma brucei." *Mol Cell Biol* 9(3): 1332-5.

Muller, I. B., D. Domenicali-Pfister, I. Roditi and E. Vassella (2002). "Stage-specific requirement of a mitogen-activated protein kinase by Trypanosoma brucei." *Mol Biol Cell* 13(11): 3787-99.

Mulumba, K. (2003). Socio-Economic and Cultural Factors in the Research and Control of Trypanosomiasis. PAAT TECHNICAL AND SCIENTIFIC SERIES 4. FAO. Rome, PAAT.

Murone, M., S. M. Luoh, D. Stone, W. Li, A. Gurney, M. Armanini, C. Grey, A. Rosenthal and F. J. de Sauvage (2000). "Gli regulation by the opposing activities of fused and suppressor of fused." *Nat Cell Biol* 2(5): 310-2.

Murray, C. (1994). "Quantifying the burden of disease: the technical basis for disability-adjusted life years." *Bulletin of the World Health Organization* 72: 429-445.

Myers, M. P., J. N. Andersen, A. Cheng, M. L. Tremblay, C. M. Horvath, J. P. Parisien, A. Salmeen, D. Barford and N. K. Tonks (2001). "TYK2 and JAK2 are substrates of protein-tyrosine phosphatase 1B." *J Biol Chem* 276(51): 47771-4.

Myhre, O., J. M. Andersen, H. Aarnes and F. Fonnum (2003). "Evaluation of the probes 2',7'-dichlorofluorescin diacetate, luminol, and lucigenin as indicators of reactive species formation." *Biochem Pharmacol* 65(10): 1575-82.

Myler, P. J., A. L. Allen, N. Agabian and K. Stuart (1985). "Antigenic variation in clones of Trypanosoma brucei grown in immune-deficient mice." *Infect Immun* 47(3): 684-90.

Nakaar, V., A. Gunzl, E. Ullu and C. Tschudi (1997). "Structure of the Trypanosoma brucei U6 snRNA gene promoter." *Mol Biochem Parasitol* 88(1-2): 13-23.

Nascimento, M., W. W. Zhang, A. Ghosh, D. R. Houston, A. M. Berghuis, M. Olivier and G. Matlashewski (2006). "Identification and characterization of a protein-tyrosine phosphatase in Leishmania: Involvement in virulence." *J Biol Chem* 281(47): 36257-68.

Nett, I. R., L. Davidson, D. Lamont and M. A. Ferguson (2009a). "Identification and specific localization of tyrosine-phosphorylated proteins in Trypanosoma brucei." *Eukaryot Cell* 8(4): 617-26.

Nett, I. R., D. M. Martin, D. Miranda-Saavedra, D. Lamont, J. D. Barber, A. Mehlert and M. A. Ferguson (2009b). "The phosphoproteome of bloodstream form Trypanosoma brucei, causative agent of African sleeping sickness." *Mol Cell Proteomics* 8(7): 1527-38.

Nolan, D. P., P. Reverlard and E. Pays (1994). "Overexpression and characterization of a gene for a Ca(2+)-ATPase of the endoplasmic reticulum in Trypanosoma brucei." *J Biol Chem* 269(42): 26045-51.

Nolan, D. P., S. Rolin, J. R. Rodriguez, J. Van Den Abbeele and E. Pays (2000). "Slender and stumpy bloodstream forms of Trypanosoma brucei display a differential response to extracellular acidic and proteolytic stress." *Eur J Biochem* 267(1): 18-27.

Nwagwu, M., D. M. Okenu, T. A. Olusi and R. I. Molokwu (1988). "Trypanosoma brucei releases proteases extracellularly." *Trans R Soc Trop Med Hyg* 82(4): 577.

Nwaka, S. and A. Hudson (2006). "Innovative lead discovery strategies for tropical diseases." *Nat Rev Drug Discov* 5(11): 941-55.

Obenauer, J. C., L. C. Cantley and M. B. Yaffe (2003). "Scansite 2.0: Proteome-wide prediction of cell signaling interactions using short sequence motifs." *Nucleic Acids Res* 31(13): 3635-41.

Oberholzer, M., G. Marti, M. Baresic, S. Kunz, A. Hemphill and T. Seebeck (2007). "The Trypanosoma brucei cAMP phosphodiesterases TbrPDEB1 and TbrPDEB2: flagellar enzymes that are essential for parasite virulence." *Faseb J* 21(3): 720-31.

Ogbadoyi, E. O., D. R. Robinson and K. Gull (2003). "A high-order trans-membrane structural linkage is responsible for mitochondrial genome positioning and segregation by flagellar basal bodies in trypanosomes." *Mol Biol Cell* 14(5): 1769-79.

Opperdoes, F. R., P. Baudhuin, I. Coppens, C. De Roe, S. W. Edwards, P. J. Weijers and O. Misset (1984). "Purification, morphometric analysis, and characterization of the glycosomes (microbodies) of the protozoan hemoflagellate Trypanosoma brucei." *J Cell Biol* 98(4): 1178-84.

Opperdoes, F. R., P. Borst and H. Spits (1977). "Particle-bound enzymes in the bloodstream form of Trypanosoma brucei." *Eur J Biochem* 76(1): 21-8.

Overath, P., M. Chaudhri, D. Steverding and K. Ziegelbauer (1994). "Invariant surface proteins in bloodstream forms of Trypanosoma brucei." *Parasitol Today* 10(2): 53-8.

Overath, P., J. Czichos and C. Haas (1986). "The effect of citrate/cis-aconitate on oxidative metabolism during transformation of Trypanosoma brucei." *Eur J Biochem* 160(1): 175-82.

Overath, P. and M. Engstler (2004). "Endocytosis, membrane recycling and sorting of GPI-anchored proteins: Trypanosoma brucei as a model system." *Mol Microbiol* 53(3): 735-44.

Paindavoine, P., S. Rolin, S. Van Assel, M. Geuskens, J. C. Jauniaux, C. Dinsart, G. Huet and E. Pays (1992). "A gene from the variant surface glycoprotein expression site encodes one of several transmembrane adenylate cyclases located on the flagellum of Trypanosoma brucei." *Mol Cell Biol* 12(3): 1218-25.

Park, J. H., D. L. Brekken, A. C. Randall and M. Parsons (2002). "Molecular cloning of Trypanosoma brucei CK2 catalytic subunits: the alpha isoform is nucleolar and phosphorylates the nucleolar protein Nopp44/46." *Mol Biochem Parasitol* 119(1): 97-106.

Parsons, M. (2004). "Glycosomes: parasites and the divergence of peroxisomal purpose." *Mol Microbiol* 53(3): 717-24.

Parsons, M. (2005). "Comparative analysis of the kinome of the three pathogenic trypanosomatids:Leishmania major, Trypanosoma brucei and Trypanosoma cruzi." *BMC Genomics* 6(127).

Parsons, M., J. A. Ledbetter, G. L. Schieven, A. E. Nel and S. B. Kanner (1994). "Developmental regulation of pp44/46, tyrosine-phosphorylated proteins associated with tyrosine/serine kinase activity in Trypanosoma brucei." *Mol Biochem Parasitol* 63(1): 69-78.

Parsons, M. and L. Ruben (2000). "Pathways involved in environmental sensing in trypanosomatids." *Parasitol Today* 16(2): 56-62.

Parsons, M., Valentine M, Deans J, Schieven GL and L. JA (1990). "Distinct patterns of tyrosine phosphorylation during the life cycle of Trypanosoma brucei." *Molecular and Biochemical Parasitology*(45): 241-248.

Parsons M, V. M., Deans J, Schieven GL, Ledbetter JA (1991). "Distinct patterns of tyrosine phosphorylation during the life cycle of Trypanosoma brucei." *Mol Biochem Parasitol* 45(2): 241-8.

Parsons, M., E. A. Worthey, P. N. Ward and J. C. Mottram (2005). "Comparative analysis of the kinomes of three pathogenic trypanosomatids: Leishmania major, Trypanosoma brucei and Trypanosoma cruzi." *BMC Genomics* 6: 127.

Pays, E., J. Hanocq-Quertier, F. Hanocq, S. Van Assel, D. Nolan and S. Rolin (1993). "Abrupt RNA changes precede the first cell division during the differentiation of Trypanosoma brucei bloodstream forms into procyclic forms in vitro." *Mol Biochem Parasitol* 61(1): 107-14.

Pei, D., J. Wang and C. T. Walsh (1996). "Differential functions of the two Src homology 2 domains in protein tyrosine phosphatase SH-PTP1." *Proc Natl Acad Sci U S A* 93(3): 1141-5.

Pepin, J., F. Milord, B. Mpia, F. Meurice, L. Ethier, D. DeGroof and H. Bruneel (1989). "An open clinical trial of nifurtimox for arseno-resistant Trypanosoma brucei gambiense sleeping sickness in central Zaire." *Trans R Soc Trop Med Hyg* 83(4): 514-7.

Persson, C., T. Sjoblom, A. Groen, K. Kappert, U. Engstrom, U. Hellman, C. H. Heldin, J. den Hertog and A. Ostman (2004). "Preferential oxidation of the second phosphatase domain of receptor-like PTP-alpha revealed by an antibody against oxidized protein tyrosine phosphatases." *Proc Natl Acad Sci U S A* 101(7): 1886-91.

Pitt, G. S., N. Milona, J. Borleis, K. C. Lin, R. R. Reed and P. N. Devreotes (1992). "Structurally distinct and stage-specific adenylyl cyclase genes play different roles in Dictyostelium development." *Cell* 69(2): 305-15.

Priotto, G., C. Fogg, M. Balasegaram, O. Erphas, A. Louga, F. Checchi, S. Ghabri and P. Piola (2006). "Three drug combinations for late-stage Trypanosoma brucei gambiense sleeping sickness: a randomized clinical trial in Uganda." *PLoS Clin Trials* 1(8): e39.

Priotto, G., S. Kasparian, W. Mutombo, D. Ngouama, S. Ghorashian, U. Arnold, S. Ghabri, E. Baudin, V. Buard, S. Kazadi-Kyanza, M. Ilunga, W. Mutangala, G. Pohlig, C. Schmid, U. Karunakara, E. Torreele and V. Kande (2009). "Nifurtimox-eflornithine combination therapy for second-stage African Trypanosoma brucei gambiense trypanosomiasis: a multicentre, randomised, phase III, non-inferiority trial." *Lancet* 374(9683): 56-64.

Puius YA, Zhao Y, Sullivan M, Lawrence DS, Almo SC and Z. ZY (1997). "Identification of a second aryl phosphate-binding site in proten-tyrosine phosphatase 1B: A paradigm for inhibitor design." *Proc.Natl.Acad.Sci.USA* 94(25): 13420-5.

Puius, Y. A., Zhao Y, Sullivan M, Lawrence DS, Almo SC and Z. ZY (1997). "Identification of a second aryl phosphate-binding site in proten-tyrosine phosphatase 1B: A paradigm for inhibitor design." *Proc.Natl.Acad.Sci.USA* 94(25): 13420-5.

Raether, W. and H. Seidenath (1983). "The activity of fexinidazole (HOE 239) against experimental infections with Trypanosoma cruzi, trichomonads and Entamoeba histolytica." *Ann Trop Med Parasitol* 77(1): 13-26.

Rajendrakumar, G. V., V. Radha and G. Swarup (1993). "Stabilization of a protein-tyrosine phosphatase mRNA upon mitogenic stimulation of T-lymphocytes." *Biochim Biophys Acta* 1216(2): 205-12.

Ravichandran, L. V., H. Chen, Y. Li and M. J. Quon (2001). "Phosphorylation of PTP1B at Ser(50) by Akt impairs its ability to dephosphorylate the insulin receptor." *Mol Endocrinol* 15(10): 1768-80.

Rayasam, G. V., V. K. Tulasi, R. Sodhi, J. A. Davis and A. Ray (2009). "Glycogen synthase kinase 3: more than a namesake." *Br J Pharmacol* 156(6): 885-98.

Raz, B., M. Iten, Y. Grether-Buhler, R. Kaminsky and R. Brun (1997). "The Alamar Blue assay to determine drug sensitivity of African trypanosomes (T.b. rhodesiense and T.b. gambiense) in vitro." *Acta Trop* 68(2): 139-47.

Reed, J., V. Kinzel, B. E. Kemp, H. C. Cheng and D. A. Walsh (1985). "Circular dichroic evidence for an ordered sequence of ligand/binding site interactions in the catalytic reaction of the cAMP-dependent protein kinase." *Biochemistry* 24(12): 2967-73.

Ren, J., X. Gao, C. Jin, M. Zhu, X. Wang, A. Shaw, L. Wen, X. Yao and Y. Xue (2009). "Systematic study of protein sumoylation: Development of a site-specific predictor of SUMOsp 2.0." *Proteomics* 9(12): 3409-3412.

Reuner, B., E. Vassella, B. Yutzy and M. Boshart (1997). "Cell density triggers slender to stumpy differentiation of Trypanosoma brucei bloodstream forms in culture." *Mol Biochem Parasitol* 90(1): 269-80.

Rhoads, A. R. and F. Friedberg (1997). "Sequence motifs for calmodulin recognition." *Faseb J* 11(5): 331-40.

Ridgley, E. L., Z. H. Xiong and L. Ruben (1999). "Reactive oxygen species activate a Ca2+-dependent cell death pathway in the unicellular organism Trypanosoma brucei brucei." *Biochem J* 340 (Pt 1): 33-40.

Robinson, D. R., T. Sherwin, A. Ploubidou, E. H. Byard and K. Gull (1995). "Microtubule polarity and dynamics in the control of organelle positioning, segregation, and cytokinesis in the trypanosome cell cycle." *J Cell Biol* 128(6): 1163-72.

Roditi, I., M. Carrington and M. Turner (1987). "Expression of a polypeptide containing a dipeptide repeat is confined to the insect stage of Trypanosoma brucei." *Nature* 325(6101): 272-4.

Roditi, I., H. Schwarz, T. W. Pearson, R. P. Beecroft, M. K. Liu, J. P. Richardson, H. J. Buhring, J. Pleiss, R. Bulow, R. O. Williams and et al. (1989). "Procyclin gene expression and loss of the variant surface glycoprotein during differentiation of Trypanosoma brucei." *J Cell Biol* 108(2): 737-46.

Rogers, D. J. (2000). "Satellites, space, time and the African trypanosomiases." *Adv Parasitol* 47: 129-71.

Rolin, S., J. Hancocq-Quertier, F. Paturiaux-Hanocq, D. P. Nolan and E. Pays (1998). "Mild acid stress as a differentiation trigger in Trypanosoma brucei." *Mol Biochem Parasitol* 93(2): 251-62.

Rolin, S., J. Hanocq-Quertier, F. Paturiaux-Hanocq, D. Nolan, D. Salmon, H. Webb, M. Carrington, P. Voorheis and E. Pays (1996). "Simultaneous but independent activation of adenylate cyclase and glycosylphosphatidylinositol-phospholipase C under stress conditions in Trypanosoma brucei." *J Biol Chem* 271(18): 10844-52.

Rolin, S., P. Paindavoine, J. Hanocq-Quertier, F. Hanocq, Y. Claes, D. Le Ray, P. Overath and E. Pays (1993). "Transient adenylate cyclase activation accompanies differentiation of Trypanosoma brucei from bloodstream to procyclic forms." *Mol Biochem Parasitol* 61(1): 115-25.

Ross, S. H., Y. Lindsay, S. T. Safrany, O. Lorenzo, F. Villa, R. Toth, M. J. Clague, C. P. Downes and N. R. Leslie (2007). "Differential redox regulation within the PTP superfamily." *Cell Signal* 19(7): 1521-30.

Ruben, L., N. Haghighat and A. Campbell (1990). "Cyclical differentiation of Trypanosoma brucei involves changes in the cellular complement of calmodulin-binding proteins." *Exp Parasitol* 70(2): 144-53.

Ruben, L. and C. L. Patton (1987). "Calmodulin from Trypanosoma brucei: immunological analysis and genomic organization." *Methods Enzymol* 139: 262-76.

Rudenko, G., D. Bishop, K. Gottesdiener and L. H. Van der Ploeg (1989). "Alpha-amanitin resistant transcription of protein coding genes in insect and bloodstream form Trypanosoma brucei." *Embo J* 8(13): 4259-63.

Ruepp, S., A. Furger, U. Kurath, C. K. Renggli, A. Hemphill, R. Brun and I. Roditi (1997). "Survival of Trypanosoma brucei in the tsetse fly is enhanced by the expression of specific forms of procyclin." *J Cell Biol* 137(6): 1369-79.

Salem, M. M. and K. A. Werbovetz (2006). "Isoflavonoids and other compounds from Psorothamnus arborescens with antiprotozoal activities." *J Nat Prod* 69(1): 43-9.

Salmeen, A., J. N. Andersen, M. P. Myers, T. C. Meng, J. A. Hinks, N. K. Tonks and D. Barford (2003). "Redox regulation of protein tyrosine phosphatase 1B involves a sulphenyl-amide intermediate." *Nature* 423(6941): 769-73.

Salmeen, A., J. N. Andersen, M. P. Myers, N. K. Tonks and B. D (2000). "Molecular basis for the dephosphorylation of the activation segment of the insulin receptor by protein tyrosine phosphatase 1B." *Mol Cell* 6(6): 1401-12.

Sarmiento, M., Puius YA, Vetter SW, Keng YF, Wu L, Zhao Y, Lawrence DS, Almo SC and Z. ZY (2000). "Structural Basis of Plasticity in Protein Tyrosine Phosphatase 1B Substrate Recognition." *Biochemistry* 39(28): 8171-9

.

Sarmiento, M., Y. Zhao, S. J. Gordon and Z. Y. Zhang (1998). "Molecular basis for substrate specificity of protein-tyrosine phosphatase 1B." *J Biol Chem* 273(41): 26368-74.

Sbicego, S., E. Vassella, U. Kurath, B. Blum and I. Roditi (1999). "The use of transgenic Trypanosoma brucei to identify compounds inducing the differentiation of bloodstream forms to procyclic forms." *Mol Biochem Parasitol* 104(2): 311-22.

Schnaufer, A., G. D. Clark-Walker, A. G. Steinberg and K. Stuart (2005). "The F1-ATP synthase complex in bloodstream stage trypanosomes has an unusual and essential function." *Embo J* 24(23): 4029-40.

Seebeck T, G. K., Kunz S, Schaub R, Shalaby T, Zoraghi R (2001). "cAMP signalling in Trypanosoma brucei." *Int J Parasitol* 31(5-6): 491-8.

Sell, S. M. and D. Reese (1999). "Insulin-inducible changes in the relative ratio of PTP1B splice variants." *Mol Genet Metab* 66(3): 189-92.

Semenov, A., J. E. Olson and P. J. Rosenthal (1998). "Antimalarial synergy of cysteine and aspartic protease inhibitors." *Antimicrob Agents Chemother* 42(9): 2254-8.

Shalaby, T., M. Liniger and T. Seebeck (2001). "The regulatory subunit of a cGMP-regulated protein kinase A of Trypanosoma brucei." *Eur J Biochem* 268(23): 6197-206.

Shapiro, S. Z., J. Naessens, B. Liesegang, S. K. Moloo and J. Magondu (1984). "Analysis by flow cytometry of DNA synthesis during the life cycle of African trypanosomes." *Acta Trop* 41(4): 313-23.

Sharma, P., R. Chakraborty, L. Wang, B. Min, M. L. Tremblay, T. Kawahara, J. D. Lambeth and S. J. Haque (2008a). "Redox regulation of interleukin-4 signaling." *Immunity* 29(4): 551-64.

Sharma, R., L. Peacock, E. Gluenz, K. Gull, W. Gibson and M. Carrington (2008b). "Asymmetric cell division as a route to reduction in cell length and change in cell morphology in trypanosomes." *Protist* 159(1): 137-51.

Sherwin, T. and K. Gull (1989). "The cell division cycle of Trypanosoma brucei brucei: timing of event markers and cytoskeletal modulations." *Philos Trans R Soc Lond B Biol Sci* 323(1218): 573-88.

Shifrin, V. I. and B. G. Neel (1993). "Growth factor-inducible alternative splicing of nontransmembrane phosphotyrosine phosphatase PTP-1B pre-mRNA." *J Biol Chem* 268(34): 25376-84.

Shiu, S. H. and A. B. Bleecker (2001). "Plant receptor-like kinase gene family: diversity, function, and signaling." *Sci STKE* 2001(113): re22.

Siegel, T. N., D. R. Hekstra, X. Wang, S. Dewell and G. A. Cross (2010). "Genome-wide analysis of mRNA abundance in two life-cycle stages of Trypanosoma brucei and identification of splicing and polyadenylation sites." *Nucleic Acids Res*.

Siman, R., J. C. Noszek and C. Kegerise (1989). "Calpain I activation is specifically related to excitatory amino acid induction of hippocampal damage." *J Neurosci* 9(5): 1579-90.

Simpson, A. G., J. R. Stevens and J. Lukes (2006). "The evolution and diversity of kinetoplastid flagellates." *Trends Parasitol* 22(4): 168-74.

Soeiro, M. N., E. M. De Souza, C. E. Stephens and D. W. Boykin (2005). "Aromatic diamidines as antiparasitic agents." *Expert Opin Investig Drugs* 14(8): 957-72.

Souza, A. V., J. H. Petretski, M. Demasi, E. J. Bechara and P. L. Oliveira (1997). "Urate protects a blood-sucking insect against hemin-induced oxidative stress." *Free Radic Biol Med* 22(1-2): 209-14.

Steele, J. C., D. C. Warhurst, G. C. Kirby and M. S. Simmonds (1999). "In vitro and in vivo evaluation of betulinic acid as an antimalarial." *Phytother Res* 13(2): 115-9.

Steverding, D. (2010). "The development of drugs for treatment of sleeping sickness: a historical review." *Parasit Vectors* 3(1): 15.

Subramanya, S., C. F. Hardin, D. Steverding and K. Mensa-Wilmot (2009). "Glycosylphosphatidylinositol-specific phospholipase C regulates transferrin endocytosis in the African trypanosome." *Biochem J* 417(3): 685-94.

Sun, J. P., A. A. Fedorov, S. Y. Lee, X. L. Guo, K. Shen, D. S. Lawrence, S. C. Almo and Z. Y. Zhang (2003). "Crystal structure of PTP1B complexed with a potent and selective bidentate inhibitor." *J Biol Chem* 278(14): 12406-14.

Swarup, G., S. Cohen and D. L. Garbers (1982). "Inhibition of membrane phosphotyrosyl-protein phosphatase activity by vanadate." *Biochem Biophys Res Commun* 107(3): 1104-9.

Szoor, B. (2010). "Trypanosomatid protein phosphatases." *Mol Biochem Parasitol* 173(2): 53-63.

Szoor B, Wilson J, McElhinney H, Tabernero L and M. K. R (2006). "Protein tyrosine phosphatase TbPTP1: a molecular switch controlling life cycle differentiation in trypanosomes." *JBC* 175(2): 293-303.

Szoor, B., I. Ruberto, R. Burchmore and K. Matthews (2010). ""A novel phosphatase cascade regulates differentiation in Trypanosoma brucei via a glycosomal signaling pathway."." *Genes and Develpment* 24(12): 1306-16.

Szoor, B., J. Wilson, H. McElhinney, L. Tabernero and K. R. Matthews (2006). "Protein tyrosine phosphatase TbPTP1: A molecular switch controlling life cycle differentiation in trypanosomes." *J Cell Biol* 175(2): 293-303.

Tachado, S. D. and L. Schofield (1994). "Glycosylphosphatidylinositol toxin of Trypanosoma brucei regulates IL-1 alpha and TNF-alpha expression in macrophages by protein tyrosine kinase mediated signal transduction." *Biochem Biophys Res Commun* 205(2): 984-91.

Tait, A., A. Macleod, A. Tweedie, D. Masiga and C. M. Turner (2007). "Genetic exchange in Trypanosoma brucei: evidence for mating prior to metacyclic stage development." *Mol Biochem Parasitol* 151(1): 133-6.

Tait, A. and C. M. Turner (1990). "Genetic exchange in Trypanosoma brucei." *Parasitol Today* 6(3): 70-5.

Tait, A., C. M. Turner, R. W. Le Page and J. M. Wells (1989). "Genetic evidence that metacyclic forms of Trypanosoma brucei are diploid." *Mol Biochem Parasitol* 37(2): 247-55.

Takahashi, N., Y. Qi, H. R. Patel and R. S. Ahima (2004). "A novel aminosterol reverses diabetes and fatty liver disease in obese mice." *J Hepatol* 41(3): 391-8.

Tao, J., C. C. Malbon and H. Y. Wang (2001). "Insulin stimulates tyrosine phosphorylation and inactivation of protein-tyrosine phosphatase 1B in vivo." *J Biol Chem* 276(31): 29520-5.

Tasker, M., J. Wilson, M. Sarkar, E. Hendriks and K. Matthews (2000). "A novel selection regime for differentiation defects demonstrates an essential role for the stumpy form in the life cycle of the African trypanosome." *Mol Biol Cell* 11(5): 1905-17.

TDRnews (2001). New lease of life for resurrection drug. Issue n°64.

Tetley, L. and K. Vickerman (1985). "Differentiation in Trypanosoma brucei: host-parasite cell junctions and their persistence during acquisition of the variable antigen coat." *J Cell Sci* 74: 1-19.

Therond, P., G. Alves, B. Limbourg-Bouchon, H. Tricoire, E. Guillemet, J. Brissard-Zahraoui, C. Lamour-Isnard and D. Busson (1996). "Functional domains of fused, a serine-threonine kinase required for signaling in Drosophila." *Genetics* 142(4): 1181-98.

Thomas, W. (1905). "The experimental treatment of trypanosomiasis in animals." *Proc Roy Soc Ser B* 76: 589-591.

Thompson, J. D., D. G. Higgins and T. J. Gibson (1994). "CLUSTAL W: improving the sensitivity of progressive multiple sequence alignment through sequence weighting, position-specific gap penalties and weight matrix choice." *Nucleic Acids Res* 22(22): 4673-80.

Tielens, A. G. and J. J. Van Hellemond (1998). "Differences in energy metabolism between trypanosomatidae." *Parasitol Today* 14(7): 265-72.

Tomlinson, S., F. Vandekerckhove, U. Frevert and V. Nussenzweig (1995). "The induction of Trypanosoma cruzi trypomastigote to amastigote transformation by low pH." *Parasitology* 110 (Pt 5): 547-54.

Tonks, N. K. (2003). "PTP1B: from the sidelines to the front lines!" *FEBS Lett* 546(1): 140-8.

Tonks, N. K. (2005). "Redox redux: revisiting PTPs and the control of cell signaling." *Cell* 121(5): 667-70.

Tonks, N. K. (2006). "Protein tyrosine phosphatases: from genes, to function, to disease." *Nat Rev Mol Cell Biol* 7(11): 833-46.

Tonks, N. K., M. F. Cicirelli, C. D. Diltz, E. G. Krebs and E. H. Fischer (1990). "Effect of microinjection of a low-Mr human placenta protein tyrosine phosphatase on induction of meiotic cell division in Xenopus oocytes." *Mol Cell Biol* 10(2): 458-63.

Tonks, N. K., C. D. Diltz and E. H. Fischer (1988). "Characterization of the major protein-tyrosine-phosphatases of human placenta." *J Biol Chem* 263(14): 6731-7.

Torr, S. J., J. W. Hargrove and G. A. Vale (2005). "Towards a rational policy for dealing with tsetse." *Trends Parasitol* 21(11): 537-41.

Trouiller, P., E. Torreele, P. Olliaro, N. White, S. Foster, D. Wirth and B. Pecoul (2001). "Drugs for neglected diseases: a failure of the market and a public health failure?" *Trop Med Int Health* 6(11): 945-51.

Tsuda, A., W. H. Witola, S. Konnai, K. Ohashi and M. Onuma (2006). "The effect of TAO expression on PCD-like phenomenon development and drug resistance in Trypanosoma brucei." *Parasitol Int* 55(2): 135-42.

Turner, C. M., J. D. Barry and K. Vickerman (1988). "Loss of variable antigen during transformation of Trypanosoma brucei rhodesiense from bloodstream to procyclic forms in the tsetse fly." *Parasitol Res* 74(6): 507-11.

Ullu, E., K. R. Matthews and C. Tschudi (1993). "Temporal order of RNA-processing reactions in trypanosomes: rapid trans splicing precedes polyadenylation of newly synthesized tubulin transcripts." *Mol Cell Biol* 13(1): 720-5.

Ulm, R., K. Ichimura, T. Mizoguchi, S. C. Peck, T. Zhu, X. Wang, K. Shinozaki and J. Paszkowski (2002). "Distinct regulation of salinity and genotoxic stress responses by Arabidopsis MAP kinase phosphatase 1." *Embo J* 21(23): 6483-93.

Urwyler, S., E. Studer, C. K. Renggli and I. Roditi (2007). "A family of stage-specific alanine-rich proteins on the surface of epimastigote forms of Trypanosoma brucei." *Mol Microbiol* 63(1): 218-28.

Van Den Abbeele, J., Y. Claes, D. van Bockstaele, D. Le Ray and M. Coosemans (1999). "Trypanosoma brucei spp. development in the tsetse fly: characterization of the post-mesocyclic stages in the foregut and proboscis." *Parasitology* 118 (Pt 5): 469-78.

Van den Bossche, H. (1978). "Chemotherapy of parasite infections." *Nature* 273(5664): 626-30.

Van der Ploeg, L. H., A. W. Cornelissen, J. D. Barry and P. Borst (1984). "Chromosomes of kinetoplastida." *Embo J* 3(13): 3109-15.

Van Hellemond, J. J., F. R. Opperdoes and A. G. Tielens (1998). "Trypanosomatidae produce acetate via a mitochondrial acetate:succinate CoA transferase." *Proc Natl Acad Sci U S A* 95(6): 3036-41.

van Montfort, R. L., M. Congreve, D. Tisi, R. Carr and H. Jhoti (2003). "Oxidation state of the active-site cysteine in protein tyrosine phosphatase 1B." *Nature* 423(6941): 773-7.

Van Nieuwenhove, S., P. J. Schechter, J. Declercq, G. Bone, J. Burke and A. Sjoerdsma (1985). "Treatment of gambiense sleeping sickness in the Sudan with oral DFMO (DL-alpha-difluoromethylornithine), an inhibitor of ornithine decarboxylase; first field trial." *Trans R Soc Trop Med Hyg* 79(5): 692-8.

Van Schaftingen, E., F. R. Opperdoes and H. G. Hers (1987). "Effects of various metabolic conditions and of the trivalent arsenical melarsen oxide on the intracellular levels of fructose 2,6-

bisphosphate and of glycolytic intermediates in Trypanosoma brucei." *Eur J Biochem* 166(3): 653-61.

van Weelden, S. W., B. Fast, A. Vogt, P. van der Meer, J. Saas, J. J. van Hellemond, A. G. Tielens and M. Boshart (2003). "Procyclic Trypanosoma brucei do not use Krebs cycle activity for energy generation." *J Biol Chem* 278(15): 12854-63.

Vassella, E., J. V. Den Abbeele, P. Butikofer, C. K. Renggli, A. Furger, R. Brun and I. Roditi (2000). "A major surface glycoprotein of trypanosoma brucei is expressed transiently during development and can be regulated post-transcriptionally by glycerol or hypoxia." *Genes Dev* 14(5): 615-26.

Vassella, E., M. Oberle, S. Urwyler, C. K. Renggli, E. Studer, A. Hemphill, C. Fragoso, P. Butikofer, R. Brun and I. Roditi (2009). "Major surface glycoproteins of insect forms of Trypanosoma brucei are not essential for cyclical transmission by tsetse." *PLoS One* 4(2): e4493.

Vassella, E., B. Reuner, B. Yutzy and M. Boshart (1997). "Differentiation of African trypanosomes is controlled by a density sensing mechanism which signals cell cycle arrest via the cAMP pathway." *J Cell Sci* 110 (Pt 21): 2661-71.

Vaughan, S. and K. Gull (2003). "The trypanosome flagellum." *J Cell Sci* 116(Pt 5): 757-9.

Vetter, S. W., Y. F. Keng, D. S. Lawrence and Z. Y. Zhang (2000). "Assessment of protein-tyrosine phosphatase 1B substrate specificity using "inverse alanine scanning"." *J Biol Chem* 275(4): 2265-8.

Vickerman, K. (1965). "Polymorphism and mitochondrial activity in sleeping sickness trypanosomes." *Nature* 208(5012): 762-6.

Vickerman, K. (1978). "Antigenic variation in trypanosomes." *Nature* 273(5664): 613-7.

Vickerman, K. (1985). "Developmental cycles and biology of pathogenic trypanosomes." *Br Med Bull* 41(2): 105-14.

Vickerman, K., L. Tetley, K. A. Hendry and C. M. Turner (1988). "Biology of African trypanosomes in the tsetse fly." *Biol Cell* 64(2): 109-19.

Vintonyak, V. V., A. P. Antonchick, D. Rauh and H. Waldmann (2009). "The therapeutic potential of phosphatase inhibitors." *Curr Opin Chem Biol* 13(3): 272-83.

Vuori, K. (1998). "Integrin signaling: tyrosine phosphorylation events in focal adhesions." *J Membr Biol* 165(3): 191-9.

Walchli, S., X. Espanel, A. Harrenga, M. Rossi, G. Cesareni and R. Hooft van Huijsduijnen (2004). "Probing protein-tyrosine phosphatase substrate specificity using a phosphotyrosine-containing phage library." *J Biol Chem* 279(1): 311-8.

Webster, P. and D. G. Russell (1993). "The flagellar pocket of trypanosomatids." *Parasitol Today* 9(6): 201-6.

Webster, P., D. C. Russo and S. J. Black (1990). "The interaction of Trypanosoma brucei with antibodies to variant surface glycoproteins." *J Cell Sci* 96 (Pt 2): 249-55.

Weibrecht, I., S. A. Bohmer, M. Dagnell, K. Kappert, A. Ostman and F. D. Bohmer (2007). "Oxidation sensitivity of the catalytic cysteine of the protein-tyrosine phosphatases SHP-1 and SHP-2." *Free Radic Biol Med* 43(1): 100-10.

Welburn, S. C., E. M. Fevre, P. G. Coleman, M. Odiit and I. Maudlin (2001). "Sleeping sickness: a tale of two diseases." *Trends Parasitol* 17(1): 19-24.

Welburn, S. C., I. Maudlin and P. P. Simarro (2009). "Controlling sleeping sickness - a review." *Parasitology* 136(14): 1943-9.

Wheeler-Alm, E. and S. Z. Shapiro (1992). "Evidence of tyrosine kinase activity in the protozoan parasite Trypanosoma brucei." *J Protozool* 39(3): 413-6.

WHO (1998). "Control and Surveillance of African Trypanosomiasis." *WHO Technical Report Series* 881.

WHO (2006a). "Human African Trypanosomiasis: epidemiological update. ." *Weekly epidemiological records* 81(8): 71-80.

WHO. (2006b). "Obesity and Overweight." Fact sheet N°311 September 2006. http://www.who.int/mediacentre/factsheets/fs311/en/index.html.

WHO. (2010). "Human African trypanososmiasis: number of new cases drop to historically low levels in 50 years." http://www.who.int/neglected_diseases/integrated_media/integrated_media_hat_june_2010/en/index.html.

Wierenga, R. K., B. Swinkels, P. A. Michels, K. Osinga, O. Misset, J. Van Beeumen, W. C. Gibson, J. P. Postma, P. Borst, F. R. Opperdoes and et al. (1987). "Common elements on the surface of glycolytic enzymes from Trypanosoma brucei may serve as topogenic signals for import into glycosomes." *Embo J* 6(1): 215-21.

Wiesmann, C., K. J. Barr, J. Kung, J. Zhu, D. A. Erlanson, W. Shen, B. J. Fahr, M. Zhong, L. Taylor, M. Randal, R. S. McDowell and S. K. Hansen (2004). "Allosteric inhibition of protein tyrosine phosphatase 1B." *Nat Struct Mol Biol* 11(8): 730-7.

Wilkinson, K. A. and J. M. Henley (2010). "Mechanisms, regulation and consequences of protein SUMOylation." *Biochem J* 428(2): 133-45.

Wirtz, E., S. Leal, C. Ochatt and G. A. Cross (1999). "A tightly regulated inducible expression system for conditional gene knock-outs and dominant-negative genetics in Trypanosoma brucei." *Mol Biochem Parasitol* 99(1): 89-101.

Wolstencroft, K., P. Lord, L. Tabernero, A. Brass and R. Stevens (2006). "Protein classification using ontology classification." *Bioinformatics* 22(14): e530-8.

Woodford-Thomas, T. A., J. D. Rhodes and J. E. Dixon (1992). "Expression of a protein tyrosine phosphatase in normal and v-src-transformed mouse 3T3 fibroblasts." *J Cell Biol* 117(2): 401-14.

Woodward, R. and K. Gull (1990). "Timing of nuclear and kinetoplast DNA replication and early morphological events in the cell cycle of Trypanosoma brucei." *J Cell Sci* 95 (Pt 1): 49-57.

Wrobel, J., J. Sredy, C. Moxham, A. Dietrich, Z. Li, D. R. Sawicki, L. Seestaller, L. Wu, A. Katz, D. Sullivan, C. Tio and Z. Y. Zhang (1999). "PTP1B inhibition and antihyperglycemic activity in the ob/ob mouse model of novel 11-arylbenzo[b]naphtho[2,3-d]furans and 11-arylbenzo[b]naphtho[2,3-d]thiophenes." *J Med Chem* 42(17): 3199-202.

Wu, Y., J. Deford, R. Benjamin, M. G. Lee and L. Ruben (1994). "The gene family of EF-hand calcium-binding proteins from the flagellum of Trypanosoma brucei." *Biochem J* 304 (Pt 3): 833-41.

www.dndi.org.

www.genedb.org.

Xue, Y., F. Zhou, M. Zhu, K. Ahmed, G. Chen and X. Yao (2005). "GPS: a comprehensive www server for phosphorylation sites prediction." *Nucleic Acids Res* 33(Web Server issue): W184-7.

Yabu, Y. and T. Takayanagi (1988). "Trypsin-stimulated transformation of Trypanosoma brucei gambiense bloodstream forms to procyclic forms in vitro." *Parasitol Res* 74(6): 501-6.

Zasloff, M., J. I. Williams, Q. Chen, M. Anderson, T. Maeder, K. Holroyd, S. Jones, W. Kinney, K. Cheshire and M. McLane (2001). "A spermine-coupled cholesterol metabolite from the shark with potent appetite suppressant and antidiabetic properties." *Int J Obes Relat Metab Disord* 25(5): 689-97.

Zhang, S. and Z. Y. Zhang (2007). "PTP1B as a drug target: recent developments in PTP1B inhibitor discovery." *Drug Discov Today* 12(9-10): 373-81.

Zhang, Y. N., W. Zhang, D. Hong, L. Shi, Q. Shen, J. Y. Li, J. Li and L. H. Hu (2008). "Oleanolic acid and its derivatives: new inhibitor of protein tyrosine phosphatase 1B with cellular activities." *Bioorg Med Chem* 16(18): 8697-705.

Zhang, Z. Y. and J. E. Dixon (1993). "Active site labeling of the Yersinia protein tyrosine phosphatase: the determination of the pKa of the active site cysteine and the function of the conserved histidine 402." *Biochemistry* 32(36): 9340-5.

Ziegelbauer, K., M. Quinten, H. Schwarz, T. W. Pearson and P. Overath (1990). "Synchronous differentiation of Trypanosoma brucei from bloodstream to procyclic forms in vitro." *Eur J Biochem* 192(2): 373-8.

Zilberstein, D., N. Blumenfeld, V. Liveanu, A. Gepstein and C. L. Jaffe (1991). "Growth at acidic pH induces an amastigote stage-specific protein in Leishmania promastigotes." *Mol Biochem Parasitol* 45(1): 175-8.

Zweygarth, E. and R. Kaminsky (1991). "Evaluation of DL-alpha-difluoromethylornithine against susceptible and drug-resistant Trypanosoma brucei brucei." *Acta Trop* 48(3): 223-32.

A novel phosphatase cascade regulates differentiation in *Trypanosoma brucei* via a glycosomal signaling pathway

Balázs Szöor, Irene Ruberto, Richard Burchmore, et al.

Genes Dev. 2010 24: 1306-1316
Access the most recent version at doi:10.1101/gad.570310

A novel phosphatase cascade regulates differentiation in *Trypanosoma brucei* via a glycosomal signaling pathway

Balázs Szöőr,[1,4] Irene Ruberto,[1] Richard Burchmore,[2] and Keith R. Matthews[1,3]

[1]Centre for Immunity, Infection, and Evolution, Institute of Immunology and Infection Research, School of Biological Sciences, University of Edinburgh, Edinburgh EH9 3JT; United Kingdom; [2]Sir Henry Wellcome Proteomics Facility, University of Glasgow G12 8QQ, United Kingdom

In the mammalian bloodstream, the sleeping sickness parasite *Trypanosoma brucei* is held poised for transmission by the activity of a tyrosine phosphatase, *Tb*PTP1. This prevents differentiation of the transmissible "stumpy forms" until entry into the tsetse fly, whereupon *Tb*PTP1 is inactivated and major changes in parasite physiology are initiated to allow colonization of the arthropod vector. Using a substrate-trapping approach, we identified the downstream step in this developmental signaling pathway as a DxDxT phosphatase, *Tb*PIP39, which is activated upon tyrosine phosphorylation, and hence is negatively regulated by *Tb*PTP1. In vitro, *Tb*PIP39 promotes the activity of *Tb*PTP1, thereby reinforcing its own repression, this being alleviated by the trypanosome differentiation triggers citrate and *cis*-aconitate, generating a potentially bistable regulatory switch. Supporting a role in signal transduction, *Tb*PIP39 becomes rapidly tyrosine-phosphorylated during differentiation, and RNAi-mediated transcript ablation in stumpy forms inhibits parasite development. Interestingly, *Tb*PIP39 localizes in glycosomes, peroxisome-like organelles that compartmentalize the trypanosome glycolytic reactions among other enzymatic activities. Our results invoke a phosphatase signaling cascade in which the developmental signal is trafficked to a unique metabolic organelle in the parasite: the glycosome. This is the first characterized environmental signaling pathway targeted directly to a peroxisome-like organelle in any eukaryotic cell.

[*Keywords*: Glycosome; peroxisome; signal transduction; phosphatase; *Trypanosoma brucei*; differentiation]

Supplemental material is available at http://www.genesdev.org.

Received November 26, 2009; revised version accepted April 22, 2010.

Developmental events in eukaryotic cells are often driven by a transmembrane signaling event, this being transduced via phosphorylation/dephosphorylation of signaling proteins to generate a cellular response. Such signaling events are particularly important in unicellular eukaryotes, which are required to react to external stimuli, either as part of an adaptive response to a changing environment, or through triggered developmental responses intrinsic to their normal life cycle progression. An excellent model for such developmentally regulated responses is the African trypanosome,*Trypanosoma brucei* (Fenn and Matthews 2007). These are important disease organisms of sub-Saharan Africa, where they generate significant problems for public health and economic welfare (Barrett et al. 2003). Furthermore, as highly diverged and evolutionarily ancient organisms (Sogin et al. 1986), they have provided an important paradigm for organelle evolution and function in the eukaryotic cell (Hannaert et al. 2003; He et al. 2004, 2005; Broadhead et al. 2006; He 2007), exemplified by their use of extensive RNA editing for mitochondrial transcripts (Stuart et al. 2005), and by their possession of unusual peroxisome-like organelles, glycosomes (Opperdoes 1987). These compartmentalize the trypanosome glycolytic enzymes, which in other eukaryotes are cytosolic, thereby avoiding the lethal consequences of the "turbo design" of glycolysis (Teusink et al. 1998; Bakker et al. 2000). Glycosomes also contain enzymes required for ether lipid biosynthesis, the β oxidation of fatty acids, as well as several additional activities (Michels et al. 2006; Opperdoes and Szikora 2006), although their precise enzymatic composition and number is regulated during the trypanosome life cycle (Michels et al. 2006).

The life cycle regulation of organellar function is a central component of the developmental biology of the trypanosome, which entails extensive cellular remodeling during passage from the mammalian blood to the midgut of the tsetse fly, the parasite's vector (Matthews 2005). These differentiation events are triggered by exposure

Corresponding authors.
[3]E-MAIL keith.matthews@ed.ac.uk; FAX 44-131-651-3670.
[4]E-MAIL Balazs.Szoor@ed.ac.uk; FAX 44-131-651-3670.
Article is online at http://www.genesdev.org/cgi/doi/10.1101/gad.570310. Freely available online through the *Genes & Development* Open Access option.

of bloodstream parasites to citrate/*cis*-aconitate (CCA) (Czichos et al. 1986; Engstler and Boshart 2004). This signal is transduced via a family of surface transporters, PAD proteins (Dean et al. 2009), with signal recognition being promoted by temperature reduction to 20°C—conditions encountered upon uptake by feeding tsetse flies (Engstler and Boshart 2004). PAD proteins are expressed on the cell surface of stumpy forms, the stage of the bloodstream parasite population adapted for transmission to tsetse flies. Importantly, stumpy forms are held ready for this developmental change by the action of a tyrosine phosphatase, *Tb*PTP1 (Szöőr et al. 2006), until differentiation is triggered. Thus, the activity of *Tb*PTP1 prevents stumpy forms from initiating differentiation and, when this enzyme is inactivated after exposure to either CCA or chemical inhibitors of PTPs, the cells differentiate from bloodstream to procyclic forms (Szöőr et al. 2006). This places *Tb*PTP1 at the head of an intracellular signaling pathway whose components are completely unknown.

Here we exploited a tyrosine phosphatase substrate selection strategy to identify the downstream step in the differentiation signaling pathway. This has identified a glycosomally targeted DxDxT family Ser/Thr phosphatase, invoking the presence of a phosphatase signaling cascade directing developmental regulation in trypanosomes. Our findings provide the first evidence of developmentally regulated signal transduction via the glycosome, and link the external differentiation stimulus through this signaling pathway to control of the trypanosome life cycle.

Results

Tb*PTP1 substrate is a novel DxDxT phosphatase,* Tb*PIP39*

To identify potential substrates of *Tb*PTP1, we exploited the ability to generate mutant PTP enzymes, which bind but do not release substrates (Blanchetot et al. 2005). Specifically, His-tagged *Tb*PTP1 was generated in which residue 199, the catalytic aspartic acid in the predicted WPD loop (Szöőr et al. 2006), was mutated to alanine. This "substrate-trapping" mutant (*Tb*PTP1-D199A) was bound to a His trap chelating column, and was used to select interacting proteins and substrates of *Tb*PTP1 from stumpy cell lysates. Mass spectrometry reproducibly identified a selected protein encoded by a gene on chromosome 9, *Tb*09.160.4460, this being almost identical (339 out of 343 amino acids) to that encoded by its immediately downstream gene (*Tb*09.160.4480), invoking a gene duplication event. *Tb*09.160.4460 encodes a protein with a predicted molecular mass of 39 kDa, this being named *Tb*PIP39 (*Tb*PTP1-interacting protein, 39 kDa). The *Tb*PIP39 gene is well conserved in those kinetoplastids that have been subject to genome sequence analysis, although in *Trypanosoma cruzi*, *Trypanosoma vivax*, and *Leishmania major*, it has not undergone gene duplication (Supplemental Fig. 1).

To confirm the interaction between *Tb*PTP1 and *Tb*PIP39, an antibody was raised to *Tb*PIP39 and used to probe the eluate from stumpy cell lysates incubated with either His-tagged *Tb*PTP1D199A or wild-type *Tb*PTP1. Figure 1A demonstrates that the binding of *Tb*PIP39 to the substrate-trapping *Tb*PTP-D199A was much more effective than to the wild-type protein (Fig. 1A, lanes 2,3). To validate this interaction in vivo, transgenic bloodstream forms were generated ectopically expressing wild-type *Tb*PTP1 or *Tb*PTP1-D199A proteins, each with a C-terminal Ty1 epitope tag (Bastin et al. 1996). Since *Tb*PIP39 expression is induced during differentiation (see later), cells were treated with *cis*-aconitate for 24 h, and Ty1-specific antibody was used to immunoprecipitate *Tb*PTP1. This revealed coimmunoprecipitation of *Tb*PIP39 with the *Tb*PTP-D199A substrate-trapping mutant, selection being blocked in the presence of a synthetic peptide comprising the Ty1 epitope (Fig. 1B, cf. lanes 3 and 5). Matching the in vitro pull-down assay, *Tb*PIP39 was selected less efficiently with wild-type *Tb*PTP1 (Fig. 1B, cf. lanes 5 and 10), supportive of the interaction being stabilized by the substrate-trapping mutation. Confirming

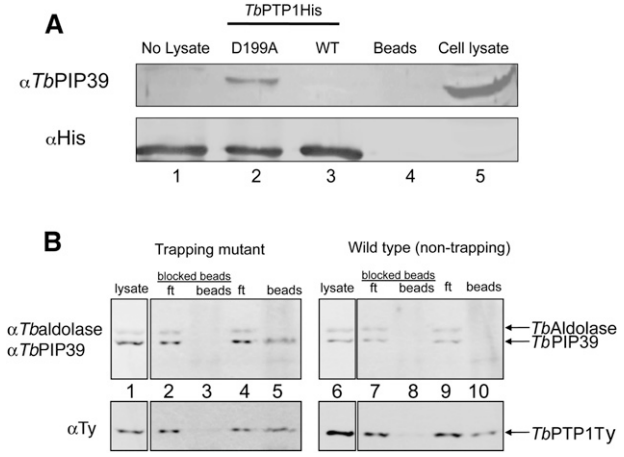

Figure 1. *Tb*PTP1 interacts with *Tb*PIP39 in vitro and in vivo. (*A*) Substrate-trapping selection of *Tb*PIP39 by *Tb*PTP1. Wild-type (WT) or substrate-trapping recombinant *Tb*PTP1 (D199A) was expressed as a His-tagged fusion protein and then bound to a His trap chelating column. Lysate from 5×10^8 stumpy cells was then passed over the column in order to select interacting proteins. Bound material was eluted from the beads and reacted with either antibody specific for the His tag (detecting the *Tb*PTP1 ligand), or *Tb*PIP39. *Tb*PIP39 was preferentially selected by the D199A *Tb*PTP1 substrate-trapping mutant. (*B*) Wild-type or D199A *Tb*PTP1-Ty was expressed in cultured bloodstream form *T. brucei*, which were then induced to differentiate to procyclic forms for 24 h by the addition of 6 mM *cis*-aconitate. Immunoprecipitation was then performed using the TY-1 epitope-specific antibody, which had been incubated either with ("blocked beads") or without a peptide sequence recognized by the antibody. Input cell lysate, flow-through (ft), or precipitated material (beads) from each immunoprecipitation, either with or without blocking, was then reacted with the Ty1-specific antibody (to detect the ectopically expressed *Tb*PTP1 or D199A *Tb*PTP1) or antibodies detecting *Tb*PIP39 or aldolase (as a negative control). The D199A-trapping mutant of *Tb*PTP1 preferentially selected *Tb*PIP39, whereas aldolase was not selected.

specificity, an unrelated protein, aldolase, was not coselected by immunoprecipitation of the substrate-trapping or wild-type *Tb*PTP1 (Fig. 1B).

Examination of the sequence of *Tb*PIP39 and its orthologous sequences in related kinetoplastids revealed the presence of a conserved predicted tyrosine phosphorylation site (Y278) toward the C terminus (Supplemental Fig. 1A). Although the trypanosome genome encodes no tyrosine-specific kinases (Parsons et al. 2005), a group-based phosphorylation scoring analysis (Xue et al. 2005) predicted that the Y278 residue could be phosphorylated effectively in vitro by the human Gardner-Rasheed feline sarcoma viral (v-fgr) oncogene homolog FGR kinase. Confirming this, incubating recombinant *Tb*PIP39 with FGR kinase rapidly generated tyrosine-phosphorylated *Tb*PIP39 (Fig. 2A, left panel), whereas mutation of Y278 to phenylalanine (Y278F) in *Tb*PIP39 prevented tyrosine phosphorylation under the same conditions (Fig. 2A, right panel). Tyrosine-phosphorylated *Tb*PIP39 was then incubated with either wild-type *Tb*PTP1, or a catalytically dead mutant of *Tb*PTP1 in which the active site cysteine was mutated to serine (C229S). Figure 2B demonstrates that *Tb*PIP39 was effectively dephosphorylated by wild-type *Tb*PTP1, but not by the inactive C229S mutant, establishing that *Tb*PIP39 not only interacted with substrate-trapping *Tb*PTP1 in cell lysates, but that it could form a *Tb*PTP1 substrate.

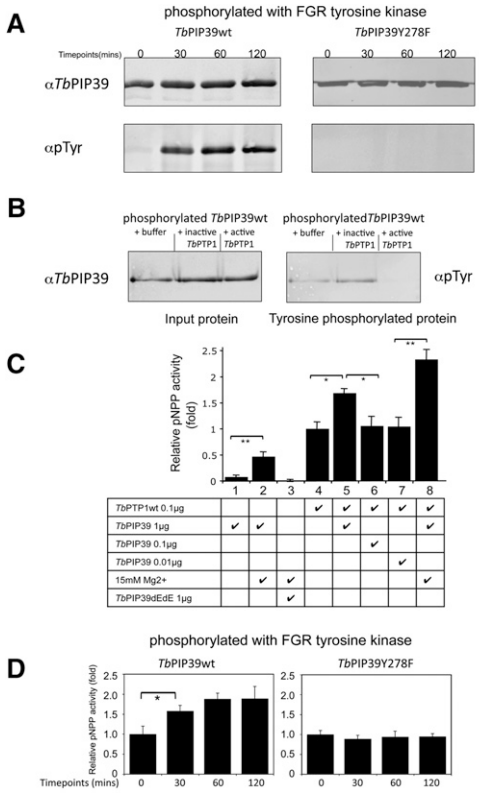

Figure 2. *Tb*PIP39 is a phosphatase with regulatory interaction with *Tb*PTP1. (*A*). Recombinant *Tb*PIP39 was incubated with FGR kinase to generate a tyrosine-phosphorylated form over the course of 120 min. Tyrosine phosphorylation of the recombinant protein was detected using the phophotyrosine-specific antibody 4G10 (α-pTyr; Millipore). The *right* panel shows the same analysis using a mutant form of *Tb*PIP39 in which the predicted tyrosine phosphorylation site Y278 is mutated to phenylalanine (F278). In this case, α-pTyr reactivity is lost. (*B*) Tyrosine-phosphorylated *Tb*PIP39 is a substrate of *Tb*PTP1. *Tb*PIP39 was incubated with FGR kinase to generate tyrosine-phosphorylated protein, this being detected with the 4G10 antibody (α-pTyr). Upon incubation with wild-type *Tb*PTP1, tyrosine phosphorylation of *Tb*PIP39 is lost. In contrast, when incubated with either buffer alone or a catalytically dead (C229S) *Tb*PTP1 mutant, *Tb*PIP39 remains phosphorylated. (*C*) Activity against pNPP of recombinant *Tb*PIP39 in the absence (column 1) or presence (column 2) of Mg^{2+}. Column 3 shows the same assay as in column 2, using a dEdE mutant of *Tb*PIP39. Columns 4–7 show the activity against pNPP of *Tb*PTP1 alone (column 4) or in the presence of 1 µg (column 5), 0.1 µg (column 6), or 0.01 µg of *Tb*PIP39. No Mg^{2+} was included in the reactions in columns 4–7, preventing *Tb*PIP39 activity. Statistical analyses used a general linear model. (*) $P < 0.05$; (**) $P < 0.001$. (*D*) Activity against pNPP of recombinant *Tb*PIP39 as it becomes tyrosine-phosphorylated by FGR kinase. With increasing phosphorylation, the activity increases. (*Right* graphs) In *Tb*PIP39-Y278F, no enhanced activity is observed, demonstrating that tyrosine phosphorylation on Y278 is responsible for *Tb*PIP39 regulation. The input recombinant proteins are those depicted in *A*. Statistical analyses used a general linear model. (*) $P < 0.05$.

Regulatory interactions between Tb*PTP1 and* Tb*PIP39*

The protein sequence of *Tb*PIP39 suggested that it was a member of an unusual class of serine/threonine phosphatases, with a characteristic DxDx (T/V) motif toward the N terminus of the predicted catalytic domain (Supplemental Fig. 1A). This family of proteins comprises FCP1/SCP1, responsible for the dephosphorylation of the eukaryotic C-terminal domain of RNA polymerase II (Kamenski et al. 2004), as well as several stress response phosphatases, typified by the yeast haloacid dehalogenase-type phosphatases PSR1/PSR2 (Siniossoglou et al. 2000) and a phosphatase required in nuclear membrane biogenesis, Dullard (Kim et al. 2007). The catalytic activity of this group of phosphatases depends on magnesium ions, requiring the integrity of the DxDxT motif as the intermediate phosphoryl acceptor (Collet et al. 1998). Consistent with this, the activity of recombinant *Tb*PIP39 against the artificial phosphatase substrate pNPP was enhanced dramatically ($P < 0.001$) in the presence of 15 mM Mg^{2+} (Fig. 2C, columns 1,2). Moreover, when residues 55D and 57D were each mutated to glutamic acid (*Tb*PIP39dEdE), no catalytic activity could be detected under the same conditions (Fig. 2C, column 3).

To investigate the possibility that the tyrosine phosphorylation status of *Tb*PIP39 might modulate its activity, the activity of *Tb*PIP39 against pNPP was assayed at time points after incubation with FGR kinase to generate the tyrosine-phosphorylated form (Fig. 2D). As a control, the nonphosphorylable *Tb*PIP39 mutant (Y278F) was incubated under the same conditions. *Tb*PIP39 activity was progressively enhanced with increasing phosphorylation, while the nonphosphorylatable mutant showed no enhanced activity above its baseline activity. This confirmed that the activity of *Tb*PIP39 was enhanced upon

the phosphorylation of Y278, this site being the target of *Tb*PTP1 activity (Fig. 2B).

As well as *Tb*PTP1 regulating *Tb*PIP39 activity, we also found evidence that *Tb*PIP39 could reciprocally influence the activity of *Tb*PTP1. Thus, although 1 μg of *Tb*PIP39 showed negligible activity against pNPP in the absence of magnesium (Fig. 2C, column 1), when it was incubated together with 0.1 μg of *Tb*PTP1, the overall activity of the combined phosphatase enzymes was significantly greater than the activity of 0.1 μg of *Tb*PTP1 alone (Fig. 2C, cf. columns 1,4,5). Confirming that this was due to the activity of *Tb*PTP1, the same analysis using the inactive D199A mutant of *Tb*PTP1 generated no increase in phosphatase activity (Supplemental Fig. 2). This demonstrated that a positive interaction existed between *Tb*PTP1 and *Tb*PIP39, such that *Tb*PIP39 promoted the activity of *Tb*PTP1 when in significant molar excess.

In a final assay of the interaction between *Tb*PIP39 and *Tb*PTP1, we investigated the effect on their respective phosphatase activities of incubation with citrate, which acts as a trypanosome differentiation trigger. This was prompted by the structural analysis of the DxDxT class phosphatase SCP1, which exhibits a citrate-binding pocket (Kamenski et al. 2004), the required residues for which are conserved in *Tb*PIP39 (Supplemental Fig. 1A). Therefore, we investigated the ability of citrate and the structurally related differentiation trigger *cis*-aconitate to moderate the activity of either *Tb*PIP39 or *Tb*PTP1, or the two phosphatases in combination (Supplemental Fig. 3A,B, columns 5–8). This demonstrated that both metabolites produced a concentration-dependent reduction of the enhanced phosphatase activity of *Tb*PTP1/*Tb*PIP39 when combined. Eliminating the possibility that divalent cation chelation was responsible for this, citrate or *cis*-aconitate had no effect on either *Tb*PIP39 or *Tb*PTP1 alone (Supplemental Fig. 3A,B, columns 1–4,9–12).

Combined, these experiments demonstrated that *Tb*PIP39 showed less activity when nonphosphorylated; i.e., as the product of *Tb*PTP1 activity, whereas *Tb*PIP39 could activate *Tb*PTP1. Moreover, we found that this regulatory interaction between *Tb*PTP1 and *Tb*PIP39 was abolished by citrate and *cis*-aconitate, both of which act as trypanosome differentiation stimuli.

Life cycle regulation and glycosomal location of Tb*PIP39*

*Tb*PTP1 acts in stumpy forms to prevent the parasites undergoing spontaneous differentiation to procyclic forms (Szöőr et al. 2006). To investigate whether its substrate, *Tb*PIP39, was present at the same life cycle stage, the RNA and protein expression of *Tb*PIP39 was investigated in bloodstream slender, bloodstream stumpy, and cultured procyclic forms of *T. brucei*. Although the mRNA for *Tb*PIP39 was abundant in all life cycle stages (albeit enriched in bloodstream stumpy forms) (Fig. 3A), *Tb*PIP39 protein was barely detectable in slender forms, but was expressed in stumpy and elevated during differentiation and in procyclic forms (Fig. 3B; Supplemental Fig. 4A), demonstrating regulation at the level of protein synthesis or turnover. Interestingly, the migration of the *Tb*PIP39 protein was altered between stumpy and procyclic forms (Fig. 3B), there being a slightly higher-molecular-weight form in the latter. This was expected to represent the phosphorylated form of *Tb*PIP39. To establish the tyrosine phosphorylation status of *Tb*PIP39 during differentiation,

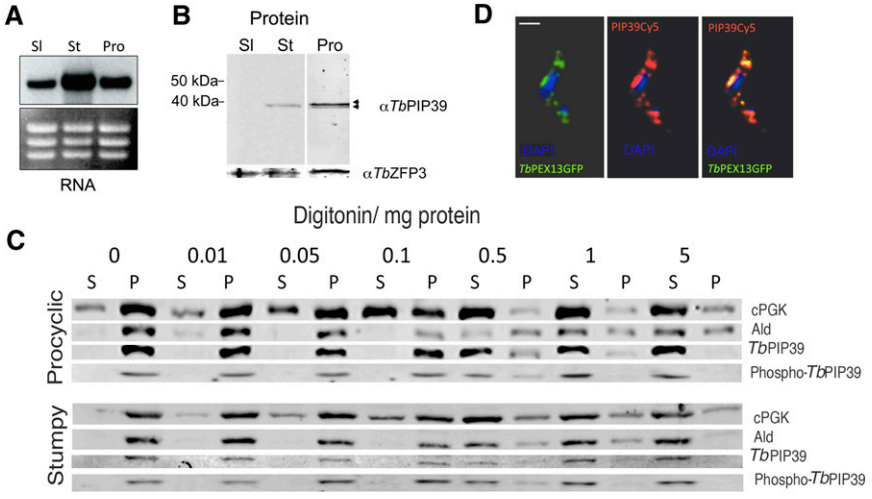

Figure 3. *Tb*PIP39 is a procyclic-enriched glycosomal phosphoprotein. (*A*) Northern blot of *Tb*PIP39 expression in bloodstream slender (Sl), bloodstream stumpy (St), or cultured procyclic (Pro) forms. The *bottom* panel shows the ethidium bromide-stained rRNA, indicating loading. (*B*) Western blot of *Tb*PIP39 in bloodstream slender (Sl), bloodstream stumpy (St), or cultured procyclic (Pro) forms. In stumpy forms, a lower-molecular-weight form is observed, whereas in procyclic forms, a higher-molecular-weight form predominates (arrowheads). The constitutively expressed protein *Tb*ZFP3 (Paterou et al. 2006) is included as a loading control. An empty intervening lane between the stumpy and procyclic form samples has been removed for clarity. (*C*) Digitonin fractionation of procyclic and stumpy form cells reacted with an antibody specific for *Tb*PIP39, *Tb*PIP39 (phospho-Y278), a glycosomal protein (aldolase), or a cytosolic protein (cytosolic PGK). Exposures have been adjusted to best reveal the distribution between fractions for each protein and are not equivalent between the distinct profiles. In each case, the digitonin concentration is shown with the cell extract being separated into either soluble or pelleted (organellar) fractions. *Tb*PIP39 cofractionates with glycosomal aldolase. A quantitative analysis of the fractionation of procyclic forms is shown in Supplemental Figure 6. (*D*) Localization of *Tb*PIP39 (red) with an N-terminal GFP fusion of the glycosomal protein *Tb*PEX13 (green). The two proteins colocalize precisely. DNA of the cells was counterstained using DAPI (blue). Bar, 5 μm.

an anti-peptide tyrosine phospho-specific antibody directed to Y278 of *Tb*PIP39 (ELD HWR TDE Y*TK C) was generated. This revealed enhanced phosphorylation of *Tb*PIP39 within 120 min of exposure to *cis*-aconitate or the tyrosine phosphatase inhibitor BZ3 (Supplemental Fig. 4B). Moreover, reactivity of the phospho-specific antibody was lost upon treatment of procyclic cell extracts with *Tb*PTP1 (Supplemental Fig. 5B C), establishing Y278 as the tyrosine phosphorylation site of *Tb*PIP39 in vivo and the target of *Tb*PTP1. The expression of *Tb*PIP39 was also elevated in stumpy forms exposed to 20°C (Supplemental Fig. 4C)—conditions that sensitize trypanosomes to the differentiation stimuli CCA (Engstler and Boshart 2004), and elevate the expression and surface distribution of PAD2, one member of the protein family responsible for conveying the CCA differentiation signal (Dean et al. 2009). Hence, the developmental expression, thermal regulation, and predicted phosphorylation profile of *Tb*PIP39 matched expectations for a *Tb*PTP1 substrate involved in the differentiation control pathway.

When the cellular location of *Tb*PIP39 was investigated by immunofluorescence, a punctate staining was detected, similar to that of trypanosome glycosomal proteins. This was supported by the analysis of the *Tb*PIP39 protein sequence, which exhibited a predicted C-terminal peroxisomal location signal (PTS1) (−SRL) (Supplemental Fig. 1A; Opperdoes and Szikora 2006), and the detection of *Tb*PIP39 in purified procyclic form glycosomes by proteomic analysis (Colasante et al. 2006). Nonetheless, to verify that *Tb*PIP39 associated with the glycosomes, we assessed the fractionation of the protein under a digitonin detergent titration. This demonstrated that *Tb*PIP39 cofractionated with a glycosomal marker protein (aldolase) in both procyclic and stumpy forms, this profile being shared with the phosphorylated form of *Tb*PIP39 detected using the Y278 phospho-specific antibody (Fig. 3C; Supplemental Fig. 6B). Confirming its association with glycosomes, *Tb*PIP39 colocalized with GFP in a transgenic procyclic line expressing an N-terminal GFP fusion of *Tb*PEX13, a glycosomal import protein (Fig. 3D; Verplaetse et al. 2009; the plasmid was a kind gift of P. Michels, Brussels). Hence, by sequence prediction, biochemical and cellular fractionation, and colocalization studies, *Tb*PIP39 was identified as a glycosome-associated protein.

Tb*PIP39 RNAi inhibits differentiation of bloodstream forms*

To investigate whether *Tb*PIP39 was a component of the differentiation signaling pathway, its mRNA was ablated by tetracycline-regulated RNAi. To assay early differentiation events in a biologically relevant context, it was important to assay stumpy cells capable of synchronous differentiation to procyclic forms. Thus, the *T. brucei* AnTat1.1 90:13 pleomorphic line was transfected with the stem–loop RNAi vector pALC14 containing opposing fragments of the *Tb*PIP39 gene. A transfectant line was then grown for 6 d in mice provided either without (−DOX) or with (+DOX) 200 μg/mL doxycyline in their drinking water to induce transcript ablation, and hence prevent *Tb*PIP39 protein expression in developing stumpy forms. Although *Tb*PIP39 was ~85% depleted in the +DOX parasites (Fig. 4A), no reproducible difference between the progression of the parasitaemia for the uninduced (−DOX) or induced (+DOX) parasites was observed; moreover, both samples generated highly enriched stumpy form populations within 6 d (Supplemental Fig. 7). This demonstrated that *Tb*PIP39 was not required for stumpy formation or viability. The stumpy forms were then harvested and incubated for 16 h at either 37°C or 20°C, the latter sensitizing the parasites to physiological levels of CCA (i.e., ~0.1 mM) (Engstler and Boshart 2004; Dean et al. 2009). Both the +DOX and −DOX populations were then exposed to 0 mM, 0.1 mM, or 6 mM *cis*-aconitate in vitro and assayed for their expression of the differentiation marker EP procyclin after 4 and 24 h to detect effects on the initiation of

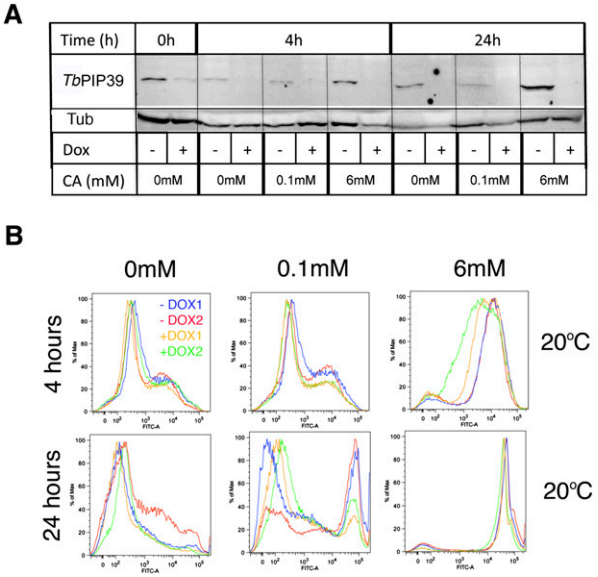

Figure 4. *Tb*PIP39 depletion in stumpy forms inhibits differentiation. (*A*) Western blots of *Tb*PIP39 from samples derived from *Tb*PIP39-RNAi cells either induced (+Dox) or uninduced (−Dox) with doxycycline. Samples were incubated overnight at 20°C, and then proteins were isolated 0 h, 4 h, or 24 h after exposure to 0 mM, 0.1 mM, or 6 mM *cis*-aconitate. The *bottom* panels represent analysis of the same samples using an antibody against α-tubulin as a loading control. (*B*) Flow cytometry traces of EP procyclin expression in four independent stumpy cell populations either induced (+Dox, orange and green traces) or not (−Dox, blue and red traces) to ablate *Tb*PIP39 by RNAi. Individual stumpy cell samples were derived from day 6 infections of mice either with or without doxycyline in their drinking water. Samples were incubated at 20°C before the addition of *cis*-aconitate, and flow cytometry was carried out either 4 h or 24 h later. The induced populations showed reduced differentiation at 0.1 mM (4 h and 24 h); at 6 mM, differentiation was efficient in all populations (likely enabled by the remaining ~15% *Tb*PIP39 in the RNAi line), although it was delayed in the induced samples. Flow cytometry traces from this experiment with cells incubated at 37°C are available in Supplemental Figure 8.

differentiation. Although the extent of *Tb*PIP39 depletion and the overall kinetics of EP procyclin expression in different experiments varied, perhaps reflecting the amount of remaining enzyme following RNAi (~15%), the *Tb*PIP39-depleted parasites showed reduced differentiation with 0.1 mM *cis*-aconitate (mean, 58% reduction; range, 52%–67% reduction at 24 h) (Fig. 4B), this effect being consistent in five out of five experiments, whereas at 6 mM *cis*-aconitate, an effect of *Tb*PIP39 depletion was observed in only two out of five experiments. Hence, the depletion of *Tb*PIP39 reduced the differentiation of stumpy forms, with a reduction of sensitivity to physiological levels of CCA. Being detected in uniform populations of cells before the onset of outgrowth as procyclic forms, we conclude that *Tb*PIP39 acts as a positive signaling component operating downstream from, and negatively regulated by, *Tb*PTP1.

To confirm that the differentiation signaling response required the glycosomal location of *Tb*PIP39, we investigated the ability of mutants with a deleted or an epitope tag-blocked C-terminal PTS1 signal to rescue the *Tb*PIP39 RNAi-mediated differentiation phenotype. To achieve this, monomorphic bloodstream forms capable of *Tb*PIP39 RNAi (Supplemental Fig. 9) were engineered to express recoded synthetic genes that would be immune to RNAi, but encode proteins of the same amino sequence as endogenous *Tb*PIP39 (Supplemental Fig. 10A,B). Initially, the monomorphic *Tb*PIP39 RNAi line was stimulated to differentiate with *cis*-aconitate, demonstrating reduced procyclin expression over 48 h when RNAi was induced with tetracycline (Fig. 5A). When a wild-type recoded *Tb*PIP39 copy was coexpressed in the same line, however, differentiation was fully restored, supporting rescue of the phenotype (Fig. 5B). In contrast, the expression of *Tb*PIP39ΔSRL or *Tb*PIP39-C terminal Ty, both of which were cytosolic by digitonin fractionation (Supplemental Fig. 10C), failed to rescue the differentiation phenotype (Fig. 5C,D), as did a catalytically inactive (*Tb*PIP39dEdE) *Tb*PIP39 mutant (Fig. 5E). These observations support the glycosomal location and activity of *Tb*PIP39 being important for differentiation signaling.

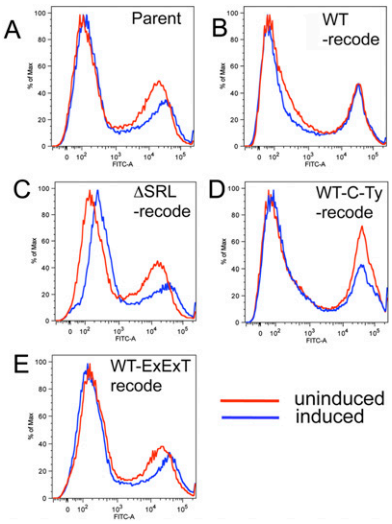

Figure 5. An intact glycosomal targeting signal is required for *Tb*PIP39-dependent differentiation. (*A*) *T. brucei* single-marker bloodstream forms were transfected with the *Tb*PIP39 RNAi construct used in Figure 4. The resulting transfectant cell line was then induced (blue) or not induced (red) to ablate *Tb*PIP39 by incubation with 1 μg/mL tetracycline for 2 d. The RNAi-depleted cells and the uninduced controls were then stimulated to differentiate to procyclic forms by the addition of 6 mM *cis*-aconitate and the expression of the differentiation marker EP procyclin monitored by flow cytometry. Depletion of *Tb*PIP39 resulted in reduced differentiation efficiency at 48 h after exposure to *cis*-aconitate. (*B*) The same cell line as in *A* was transfected with pHD451 expressing an intact recoded synthetic *Tb*PIP39 gene, expressed under tetracycline regulation. Cells were grown with tetracycline for 2 d, allowing silencing of the endogenous *Tb*PIP39 transcript and expression of the recoded gene. Differentiation was then monitored for EP procyclin expression 48 h after exposure to 6 mM *cis*-aconitate using flow cytometry. The differentiation phenotype was fully rescued. (*C*) As in *B*, but the recoded synthetic gene product lacked the ΔSRL glycosomal targeting signal and redistributed to the cytosolic fraction (Supplemental Fig. 10C). In this case, the differentiation defect was not rescued. (*D*) As in *B*, but the recoded synthetic gene product contained a Ty1 epitope tag after the ΔSRL glycosomal targeting signal. As with the truncated mutant, the protein was redistributed to the cytosolic fraction (Supplemental Fig. 10C) and the differentiation defect was not rescued. (*E*) As in *B*, but the recoded synthetic gene product was mutated for the DxDxT motif (to ExExT) to prevent catalytic activity. No rescue of the differentiation defect was observed.

Discussion

We demonstrated previously that the tyrosine phosphatase *Tb*PTP1 acts as a "molecular brake" that prevents differentiation of bloodstreams stumpy forms in the mammalian bloodstream (Szöőr et al. 2006). In this study, we identify a downstream substrate of *Tb*PTP1 as a second phosphatase, *Tb*PIP39. *Tb*PIP39 is shown to be a developmentally regulated magnesium-dependent phosphatase whose activity is modulated by tyrosine phosphorylation. Moreover, we show that *Tb*PIP39 contributes to the efficient differentiation to procyclic forms, thereby invoking the existence of a phosphatase signaling cascade regulating trypanosome development. Supporting this, we show regulatory cross-talk between *Tb*PIP39 and *Tb*PTP1 in vitro, this being abolished by the differentiation regulators citrate and *cis*-aconitate. Finally, we demonstrate that *Tb*PIP39 is glycosomal, identifying this molecule as a new marker for distinguishing bloodstream from procyclic form glycosomes, and the first example of a signaling molecule targeted to this fundamental metabolic organelle in trypanosomes. To our knowledge, this is the first well-characterized signaling pathway targeted directly to a peroxisomal-type organelle in any eukaryotic cell.

*Tb*PIP39 was identified as an unusual type of Ser/Thr phosphatase, a DxDxT phosphatase. This is an emerging family of phosphatases, and one of a group of such phosphatases encoded in kinetoplastid genomes (14, 13, and 13 members, in *T.brucei*, *T.cruzi*, and *L. major*, respectively)

(Brenchley et al. 2007), but the only representative possessing a predicted PTS1. Consistent with expectations for this class of molecules (Selengut and Levine 2000; Ndubuisil et al. 2002), *Tb*PIP39 showed magnesium-dependent activity, with its activity being abolished by mutation of the predicted magnesium-coordinating aspartate residues in the DxDxT phosphoryl acceptor motif (Collet et al. 1998). Interestingly, however, when *Tb*PIP39 was coincubated with *Tb*PTP1, the overall phosphatase activity of the combined enzymes was elevated over their predicted additive values. Since the effect was observed with inactive *Tb*PIP39 (i.e., in the absence of magnesium) and was not recapitulated when *Tb*PIP39 was incubated with a catalytically dead C229S mutant of *Tb*PTP1, we assign the enhanced phosphatase activity of *Tb*PTP1/*Tb*PIP39 to an activation of *Tb*PTP1. While being potentially muted by the relatively high levels of citrate in the *Escherichia coli* expression system (~5 mM), we observed that the activation of recombinant *Tb*PTP1 required a 10-fold excess of its substrate, *Tb*PIP39, in vitro. In vivo, the physiological interactions between the proteins could be enhanced significantly by their relative context or the presence of associated proteins in the cell, but nonetheless *Tb*PIP39 is in considerable excess of *Tb*PTP1 in stumpy forms (Supplemental Fig. 4D). Hence, *Tb*PIP39 is predicted to promote its own dephosphorylation by activating *Tb*PTP1. Given our finding that the Y278-phosphorylated form of *Tb*PIP39 shows greater phosphatase activity than its unphosphorylated form, these observations combine to generate a feedback loop whereby *Tb*PIP39 reinforces its own dephosphorylation, and hence repression, by activating *Tb*PTP1.

Although *Tb*PTP1 was found to be a cytosolic/cytoskeletally associated protein (Szöőr et al. 2006), its substrate, *Tb*PIP39, was found to be glycosomally associated. This apparent paradox can be resolved by considering the maturation of proteins as they are trafficked to peroxisome-related organelles, such as glycosomes. Such proteins are initially translated in the cytosol and then folded. The peroxisomal targeting signal is then recognized, and the protein is translocated to the peroxisome membrane where it is imported via peroxins to the lumen. This passage through the cytosol, from synthesis to import, has been measured to take from 5 to 60 min (McNew and Goodman 1994; Terlecky et al. 2001), providing ample opportunity for *Tb*PIP39 to be phosphorylated or dephosphorylated prior to glycosome targeting.

Based on our experiments, we propose a new model for the early steps in trypanosome differentiation (Fig. 6). In stumpy forms, *Tb*PIP39 would be synthesized, but held relatively inactive through its dephosphorylation by *Tb*PTP1, this being reinforced by the enhanced activity of *Tb*PTP1 generated by its substrate when in excess. When trafficked to the glycosome, dephosphorylated, inactive *Tb*PIP39 would not stimulate differentiation. When entering the tsetse, however, temperature reduction to 20°C would facilitate CCA transport into the cell via PAD expression (Dean et al. 2009). If matching our in vitro observations, this would prevent the feedback activation of *Tb*PTP1 by *Tb*PIP39, although CCA may also inhibit *Tb*PTP1 indirectly through other unknown mechanisms. Combined with the enhanced expression of *Tb*PIP39 at low temperature, this would increase the level of phosphorylated *Tb*PIP39, which, upon entry to the glycosome, would promote differentiation.

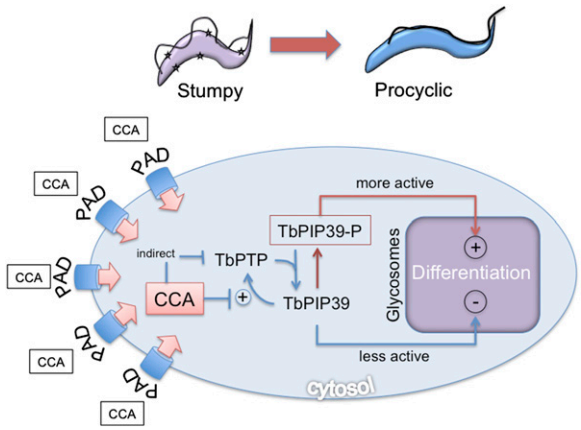

Figure 6. A model depicting the regulatory interactions between *Tb*PTP1 and *Tb*PIP39 when exposed to the differentiation triggers citrate or *cis*-aconitate. The CCA signal is conveyed by PAD proteins expressed on the surface of stumpy forms. This inhibits the activation of *Tb*PTP1 by *Tb*PIP39, although *Tb*PTP1 may also be inactivated indirectly. Upon the inactivation of *Tb*PTP1, phosphorylated *Tb*PIP39 predominates, this being generated by an unidentified protein kinase. *Tb*PIP39, activated by phosphorylation, is directed toward the glycosomes by its C-terminal PTS1 signal, and therein promotes a differentiation response.

The proposed pathway is reminiscent of cell fate decision pathways in other eukaryotes, whereby phosphorylation–dephosphorylation events coordinate a transition from one stable state to another—a so-called bistable switch (Pomerening et al. 2003; Ingolia and Murray 2007). In this case, the activation of *Tb*PTP1 by *Tb*PIP39 would repress differentiation by enhancing the dephosphorylation of *Tb*PIP39, whereas exposure to CCA would alleviate this repression, favor *Tb*PIP39 phosphorylation, and so stimulate differentiation. Importantly, the sequestration of phosphorylated *Tb*PIP39 in the glycosomal compartment would protect it from further *Tb*PTP1 activity, rendering its activation irreversible. Although metabolic regulation via phosphorylation represents an obvious point of downstream control (Christofk et al. 2008) and is a known regulator of differentiation events (Milne et al. 1998; Morris et al. 2002), glycosomes are predicted to comprise >200 distinct proteins (Colasante et al. 2006; Opperdoes and Szikora 2006) associated with ether lipid biosynthesis, the β oxidation of fatty acids, purine salvage, pyrimidine biosynthesis, gluconeogenesis, and isoprenoid biosynthesis, in addition to glycolysis. Several identified DxDxT phosphatases, including Dullard, a regulator of mammalian nuclear membrane biogenesis, exhibit lipid phosphatase activity (Kim et al. 2007; Reddy et al. 2008), suggesting that these enzymes may have the potential to regulate second messenger signaling pathways. Hence, any one, or several, of the trypanosome

glycosomal activities may be regulated by *Tb*PIP39 with consequences independent of, or indirectly linked to (Chambers et al. 2008), metabolism.

The existence of signaling pathways directed to peroxisome-like organelles, and specifically glycosomes, has been proposed previously (Albert et al. 2005; Michels and Rigden 2006). Our experiments establish that such a pathway exists, comprising a phosphatase signaling cascade that drives an early step in cell type differentiation in African trypanosomes. Moreover, the bistable regulation of this pathway by the physiological conditions encountered during stumpy form transmission suggests a new elegance to trypanosome developmental control, linked to the biology of their key metabolic organelle, the glycosome.

Materials and methods

Parasite growth and transfection

Bloodstream form and procyclic form trypanosomes were cultured in vitro in HMI-9 medium (Hirumi and Hirumi 1984) or SDM-79 medium (Brun and Schonenberger 1979), respectively.

Culturing, differentiation, pleomorphic trasnfection, and cold-shock assays of parasites were performed as described in Dean et al. (2009) using the *T. brucei* AnTat1.1 90:13 cell line (Engstler and Boshart 2004), transfectants being generated using an AMAXA nucleofector protocol (T-cell nucleofection buffer, program X001) and selected using 0.5 mg mL^{-1} puromycin. Stumpy-enriched populations were obtained by DEAE cellulose purification (Lanham 1968) of parasites 6–7 d after infection into cyclophosphamide-treated mice.

For ectopic expression, *T. brucei* Lister 427 bloodstream forms were used, these being engineered previously to express the tetracycline repressor protein (Wirtz et al. 1999), enabling regulated gene expression of wild-type or substrate-trapping forms of *Tb*PTP1 (Szöőr et al. 2006). Established, cultured procyclic forms were *T. brucei* Lister 427.

A transgenic procyclic line expressing an N-terminal GFP fusion of PEX13, a glycosomal import protein, was created by transfection of a previously characterized expression plasmid kindly provided by Paul Michels (Université Catholique de Louvain, Brussels) (Verplaetse et al. 2009).

DNA cloning

The *Tb*PIP39 coding region was amplified using *Tb*PIP39-specific primers Primer 1 (see Table 1) and Primer 2, and was integrated into the pGEX4T1 (GE Heathcare Lifesciences) protein expression vector for recombinant protein production. Primer 3 and Primer 4 (see Table 1) were used to insert *Tb*PIP39 into the pHD451 trypanosome ectopic expression vector (Biebinger et al. 1997). The pGEX4T1*Tb*PIP39 construct was used as a template for site-directed mutagenesis in order to mutate *Tb*PIP39 Tyr 278 to phenylalanine (abbreviated Y278F *Tb*PIP39). This was carried out using a commercial site-directed mutagenesis kit (Stratagene) using the mutagenesis primers Primer 5 and Primer 6 (see Table 1). Recoded synthetic genes (Supplemental Fig. 10) were synthesized by Geneart (http://www.geneart.com), recloned into pHD451, and transfected into monomorphic cells already containing the pALC14*Tb*PIP39 RNAi plasmid as a stable integrant.

Generation of Tb*PIP39 RNAi cell line*

The *Tb*PIP39 reading frame was amplified from genomic DNA by PCR using Primer 7 and Primer 8 (Table 1), and was integrated into the HindIII–XbaI and XhoI–NdeI cloning sites of pALC14 (Pusnik et al. 2007) to generate the pALC14*Tb*PIP39 RNAi plasmid.

Antibody production

Polyclonal antibody was produced in rabbits against full-length recombinant *Tb*PIP39 by Eurogentec; an anti-peptide phospho-278Y*Tb*PIP39 antibody was raised in rabbits against the sequence N-ELDHWRTDE-[phospho]Y-TKC-C from the amino acid sequence at position 269–281 in *Tb*PIP39 (Eurogentec). The resulting antibody was affinity-purified against the phosphorylated peptide immunogen, and was counterselected against the nonphosphorylated peptide to maximize specificity.

Substrate trapping with Tb*PTP1D199A*

The production and purification of the substrate-trapping mutant of *Tb*PTP1 (*Tb*PTP1D199A) was described in Szoor et al. (2006). Purified His-*Tb*PTP1D199A was mixed with His chelating Ni-NTA Agarose beads (Qiagen) for 30 min at 4°C. The beads were then collected by centrifugation and washed three times with ice-cold His purification lysis buffer (20 mM Tris, 250 mM NaCl, 1% Triton-X, 1 mM β mercaptoethanol, 5 mM Imidazole at pH 7.5–8) supplemented with complete, and EDTA-free protease inhibitor cocktail (Roche).

Approximately 5×10^8 DEAE-purified *T. brucei* stumpy cells were harvested by centrifugation, and the cell pellet was frozen in liquid nitrogen. Cells were then lysed in the presence of 150 mM PTP1B inhibitor BZ3 (Calbiochem) by addition of 500 μL of His purification lysis buffer supplemented with complete, and EDTA-free protease inhibitor cocktail (Roche). The extract was lysed by two freeze/thaw cycles at −80°C, centrifuged for 20 min at 4°C in a microfuge, and then sonicated for 3 min in a water bath. Quantification of cellular protein was performed by the Bradford method following the manufacturer's instructions.

Table 1. *Oligonucleotides used in the study*

Oligonucleotide name	Sequence
Primer 1 (BamHI Fwd)	5′-TATGGATCCATGGTGAGGACGACACGCTTTTC-3′
Primer 2 (XhoI Rev)	5′-ATACTCGAGCTAAAGTCTTGAAGGAGTGTGTC-3′
Primer 3 (HindIII Fwd)	5′-TATAAGCTTATGGTGAGGACACGCTTTTC-3′
Primer 4 (BamHI Rev)	5′-ATAGGATCCCTAAAGTCTTGAAGGAGTGTGTC-3′
Primer 5 (Y278F Fwd)	5′-CCATTGGCGTACGGATGAGTTCACAAAGTGTGACGACTTTCG-3′
Primer 6 (Y278F Rev)	5′-CGAAAGTCGTCACACTTTGTGAACTCATCCGTACGCCAATGG-3′
Primer 7 (HindIIIBamHIFwd)	5′-ATAAAGCTTGGATCCGTGAGGACGACACGCTTTTCACG-3′
Primer 8 (XhoINdeI Rev)	5′-TGCCATATGCTCGAGGGGAGTTGTAACACCTGCACCTCC-3′

Approximately 0.5 mg of fresh cell extract was incubated for 1.5 h on ice with 20–30 μL of Ni-NTA beads coated with His-tagged protein; nonspecific interactions were removed by washing the beads three times with 1 mL of 20 mM Tris, 250 mM NaCl, and 20 mM imidazole (pH: 8.0), and the bound proteins were eluted by addition of SDS-PAGE sample buffer.

Mass spectrometry

Eluate from substrate-trapping columns was separated by SDS-PAGE, and Coomassie Blue-stained bands were excised and washed in 100 mM ammonium bicarbonate with shaking for 1 h at room temperature, followed by a second wash in 50% acetonitrile/100 mM ammonium bicarbonate. Proteins were reduced with 3 mM DTT in 100 mM ammonium bicarbonate for 30 min at 60°C, followed by alkylation with 10 mM iodoacetamide for 30 min in the dark at room temperature. The gel pieces were washed with 50% acetonitrile/100 mM ammonium bicarbonate, shaking for 1 h at room temperature, and then were dehydrated by incubation with 0.1 mL of acetonitrile for 10 min at room temperature. All liquid was removed and gel pieces were dried to completion under vacuum, then rehydrated with a sufficient volume of trypsin (Promega sequencing grade, 2 mg/mL in 25 mM ammonium bicarbonate) to cover the gel pieces. Digestion was performed overnight at 37°C, the gel pieces washed for 10 min with 0.02 mL of 1% formic acid, and then 0.02 mL acetonitrile was added. After 10 min of incubation, all liquid was transferred to a fresh tube, and the tryptic peptides were dried to completion.

Tryptic peptides were solubilized in 0.5% formic acid and 2% acetonitrile, and were fractionated on a nanoflow HPLC system (Famos/Switchos/Ultimate, LC Packings) before being analyzed by electrospray ionization (ESI) mass spectrometry on a Q-STAR Pulsar i hybrid MS/MS System. Peptide separation was performed on a Pepmap C18 reversed-phase column (LC Packings) using a 5%–85% v/v acetonitrile gradient (in 0.5% v/v formic acid) run over 45 min. The flow rate was maintained at 0.2 μL per minute. Mass spectrometric analysis was performed using a 3-sec survey MS scan, followed by up to four MS/MS analyses of the most abundant peptides (3 sec per peak) in Information-Dependent Acquisition (IDA) mode, choosing 2+ to 4+ ions above threshold of 30 counts, with dynamic exclusion for 120 sec.

Mass spectrometry data was analyzed using Applied Biosystems Analyst QS (version 1.1) software and the automated Matrix Science Mascot Daemon server (version 2.1.06). Protein identifications were assigned using the Mascot search engine, with carbamidomethylation of cysteines and variable methionine oxidation being allowed. An MS tolerance of 1.2 Da for MS and 0.4 Da for MS/MS analysis was used. Searches were performed against the *T. brucei* genome database (version 3) obtained from the Wellcome Trust Sanger Institute and maintained on a local Mascot server.

Digitonin permeabilization assay

Approximately 5×10^8 procyclic forms were collected to perform digitonin permeabilization. The cell suspension was diluted to ~1 mg of total protein per milliliter, and increasing amounts of digitonin (0.01–5 mg/mg total protein) were used in digitonin assays according to Ferella et al. (2008).

Immunoprecipitation

Transgenic bloodstream form cell lines in which either wild-type *Tb*PTP1 or *Tb*PTP1-D199A proteins were expressed ectopically with a C-terminal Ty1 epitope tag sequence (Szöőr et al. 2006) were treated with 6 mM *cis*-aconitate for 24 h. Immunoprecipitation was carried out using 1×10^8 to 5×10^8 cells as described in Paterou et al. (2006).

Western and Northern blotting

Western blotting and Northern blotting was performed as described in Tasker et al. (2000). For Western blotting, primary antibodies were diluted 1:1000 and secondary antibodies were diluted 1:5000. Proteins were detected using the LI-COR Odyssey system for quantification against a tubulin or loading control as described in Dean et al. (2009). For Northern blots, a digoxygenin-labeled *Tb*PIP39-specific riboprobe (Roche) was used, hybridization being detected using CDP-star as a reaction substrate.

Phosphatase and kinase activity assays

Phosphatase activity was measured by monitoring the *Tb*PIP39-catalyzed and *Tb*PTP1-catalyzed (0.01–1 μg) hydrolysis of pNPP to *p*-nitrophenol (Szöőr et al. 2006). Phosphorylation of recombinant *Tb*PIP39 by FGR kinase was performed according to the manufacturer's instructions (Calbiochem). The reaction, containing purified *Tb*PIP39 (5 μg), was initiated with the addition of FGR kinase, and samples were taken at time points after incubation (0, 30, 60, 90, 120, 240 min) at 30°C for Western blots. After the 240-min time point, the remainder of the phosphorylation mixture was loaded on a GSTrap HP column (GE Healthcare Life Sciences) to remove the GST-tagged FGR kinase. After collection of the flow-through from the column containing the phosphorylated *Tb*PIP39, the sample was concentrated on Vivaspin 2 columns with a 10-kDa-molecular-weight cutoff (Sartorius AG) before use in the in vitro *Tb*PTP1 phosphatase assay.

In vitro Tb*PTP1 phosphatase assay*

To monitor phosphatase activity of phosphorylated *TbPIP39*, the concentrated phosphorylated *Tb*PIP39 was treated with either 1 μg of active wild-type *Tb*PTP1 or the same amount of inactive C229S *Tb*PTP1 mutant in a 100-μL phosphatase assay (50 mM Tris, 50 mM Bis Tris, 100 mM Na acetate, 1mM DTT at pH 5.5). The phosphatase reaction was started with the addition of *Tb*PTP1, and, after 30 min of incubation at 37°C, 20-μL samples were removed for Western blot.

Flow cytometry and immunofluorescence

Differentiating cells (2×10^6 to 5×10^6) were harvested and fixed in 2% formaldehyde/0.05% glutaraldehyde for a minimum of 1 h at 4°C. Antibody staining was executed according to Dean et al. (2009). Flow cytometry analysis was performed using the BD LSRII Flow cytometer (Becton Dickenson), and flow cytometry data was analyzed using FlowJO 8.8.6 software (Tree Star, Inc.) with unstained cells; cells stained with only the secondary antibody provided negative controls. For immunofluorescence, air-dried smears of parasites were prepared and fixed in methanol for at least 30 min at −20°C. Cells were rehydrated in PBS for 30 min before labeling, as described in Dean et al. (2009).

Image acquisition equipment and settings

Phase-contrast and immunofluorescence microscopy images (Supplemental Fig. 7A) were captured on a Zeiss Axioskop2 (Carl Zeiss Microimaging) with a Prior Lumen 200 light source using a QImaging Retiga 2000RCCD camera; objectives were either Plan Neofluar ×63 (1.25 NA) or Plan Neofluar ×100 (1.30 NA).

Images were captured via QImage (QImaging). Confocal imaging (Fig. 3D) used a Leica SP5 confocal laser scanning microscope, using ×63 oil immersion objective (NA = 1.4), with 4.2 zoom. The green channel was imaged using a 488-nm argon laser, and the red channel was imaged using a 543-nm helium/neon laser. The final image was acquired using Volocity Software (Improvision Ltd.) version 4.4.

Acknowledgments

We thank Achim Schnaufer for comments on the manuscript and for suggesting the use of recoded synthetic genes, Paul Michels for *Tb*PEX13-GFP construct, and Michael Boshart and Markus Engstler for the gift of the *T. brucei* AnTat1.1 90:13 line. We also thank Martin Waterfall for assistance with FACS analysis. This work was supported by grants from the Wellcome Trust, the BBSRC (for the provision of confocal facilities), and by a Strategic Award from the Wellcome Trust for the Centre for Immunity, Infection, and Evolution.

References

Albert MA, Haanstra JR, Hannaert V, Van Roy J, Opperdoes FR, Bakker BM, Michels PA. 2005. Experimental and in silico analyses of glycolytic flux control in bloodstream form *Trypanosoma brucei*. *J Biol Chem* **280:** 28306–28315.

Bakker BM, Mensonides FI, Teusink B, van Hoek P, Michels PA, Westerhoff HV. 2000. Compartmentation protects trypanosomes from the dangerous design of glycolysis. *Proc Natl Acad Sci* **97:** 2087–2092.

Barrett MP, Burchmore RJ, Stich A, Lazzari JO, Frasch AC, Cazzulo JJ, Krishna S. 2003. The trypanosomiases. *Lancet* **362:** 1469–1480.

Bastin P, Bagherzadeh Z, Matthews KR, Gull K. 1996. A novel epitope tag system to study protein targeting and organelle biogenesis in *Trypanosoma brucei*. *Mol Biochem Parasitol* **77:** 235–239.

Biebinger S, Wirtz LE, Lorenz P, Clayton C. 1997. Vectors for inducible expression of toxic gene products in bloodstream and procyclic *Trypanosoma brucei*. *Mol Biochem Parasitol* **85:** 99–112.

Blanchetot C, Chagnon M, Dubé N, Hallé M, Tremblay ML. 2005. Substrate-trapping techniques in the identification of cellular PTP targets. *Methods* **35:** 44–53.

Brenchley R, Tariq H, McElhinney H, Szoor B, Huxley-Jones J, Stevens R, Matthews K, Tabernero L. 2007. The TriTryp phosphatome: Analysis of the protein phosphatase catalytic domains. *BMC Genomics* **8:** 434. doi: 10.1186/1471-2164-8-434.

Broadhead R, Dawe HR, Farr H, Griffiths S, Hart SR, Portman N, Shaw MK, Ginger ML, Gaskell SJ, McKean PG, et al. 2006. Flagellar motility is required for the viability of the bloodstream trypanosome. *Nature* **440:** 224–227.

Brun R, Schonenberger. 1979. Cultivation and *in vitro* cloning or procyclic culture forms of *Trypanosoma brucei* in a semi-defined medium. Short communication. *Acta Trop* **36:** 289–292.

Chambers JW, Kearns MT, Morris MT, Morris JC. 2008. Assembly of heterohexameric trypanosome hexokinases reveals that hexokinase 2 is a regulable enzyme. *J Biol Chem* **283:** 14963–14970.

Christofk HR, Vander Heiden MG, Wu N, Asara JM, Cantley LC. 2008. Pyruvate kinase M2 is a phosphotyrosine-binding protein. *Nature* **452:** 181–186.

Colasante C, Ellis M, Ruppert T, Voncken F. 2006. Comparative proteomics of glycosomes from bloodstream form and procyclic culture form *Trypanosoma brucei brucei*. *Proteomics* **6:** 3275–3293.

Collet JF, Stroobant V, Pirard M, Delpierre G, Van Schaftingen E. 1998. A new class of phosphotransferases phosphorylated on an aspartate residue in an amino-terminal DXDX (T/V) motif. *J Biol Chem* **273:** 14107–14112.

Czichos J, Nonnengaesser C, Overath P. 1986. *Trypanosoma brucei*: *Cis*-aconitate and temperature reduction as triggers of synchronous transformation of bloodstream to procyclic trypomastigotes in vitro. *Exp Parasitol* **62:** 283–291.

Dean SD, Marchetti R, Kirk K, Matthews K. 2009. A surface transporter family conveys the trypanosome differentiation signal. *Nature* **459:** 213–217.

Engstler M, Boshart M. 2004. Cold shock and regulation of surface protein trafficking convey sensitization to inducers of stage differentiation in *Trypanosoma brucei*. *Genes Dev* **18:** 2798–2811.

Fenn K, Matthews KR. 2007. The cell biology of *Trypanosoma brucei* differentiation. *Curr Opin Microbiol* **10:** 539–546.

Ferella M, Li ZH, Andersson B, Docampo R. 2008. Farnesyl diphosphate synthase localizes to the cytoplasm of *Trypanosoma cruzi* and *T. brucei*. *Exp Parasitol* **119:** 308–312.

Hannaert V, Saavedra E, Duffieux F, Szikora JP, Rigden DJ, Michels PA, Opperdoes FR. 2003. Plant-like traits associated with metabolism of *Trypanosoma* parasites. *Proc Natl Acad Sci* **100:** 1067–1071.

He CY. 2007. Golgi biogenesis in simple eukaryotes. *Cell Microbiol* **9:** 566–572.

He CY, Ho HH, Malsam J, Chalouni C, West CM, Ullu E, Toomre D, Warren G. 2004. Golgi duplication in *Trypanosoma brucei*. *J Cell Biol* **165:** 313–321.

He CY, Pypaert M, Warren G. 2005. Golgi duplication in *Trypanosoma brucei* requires Centrin2. *Science* **310:** 1196–1198.

Hirumi H, Hirumi K. 1984. Continuous cultivation of animal-infective bloodstream forms of an East African *Trypanosoma* congolense stock. *Ann Trop Med Parasitol* **78:** 327–330.

Ingolia NT, Murray AW. 2007. Positive-feedback loops as a flexible biological module. *Curr Biol* **17:** 668–677.

Kamenski T, Heilmeier S, Meinhart A, Cramer P. 2004. Structure and mechanism of RNA polymerase II CTD phosphatases. *Mol Cell* **15:** 399–407.

Kim Y, Gentry MS, Harris TE, Wiley SE, Lawrence JC Jr, Dixon JE. 2007. A conserved phosphatase cascade that regulates nuclear membrane biogenesis. *Proc Natl Acad Sci* **104:** 6596–6601.

Lanham SM. 1968. Separation of trypanosomes from the blood of infected rats and mice by anion-exchangers. *Nature* **218:** 1273–1274.

Matthews KR. 2005. The developmental cell biology of *Trypanosoma brucei*. *J Cell Sci* **118:** 283–290.

McNew JA, Goodman JM. 1994. An oligomeric protein is imported into peroxisomes *in vivo*. *J Cell Biol* **127:** 1245–1257.

Michels PA, Rigden DJ. 2006. Evolutionary analysis of fructose 2,6-bisphosphate metabolism. *IUBMB Life* **58:** 133–141.

Michels PA, Bringaud F, Herman M, Hannaert V. 2006. Metabolic functions of glycosomes in *Trypanosoma*tids. *Biochim Biophys Acta* **1763:** 1463–1477.

Milne KG, Prescott AR, Ferguson MA. 1998. Transformation of monomorphic *Trypanosoma brucei* bloodstream form trypomastigotes into procyclic forms at 37 degrees C by removing glucose from the culture medium. *Mol Biochem Parasitol* **94:** 99–112.

Morris JC, Wang Z, Drew ME, Englund PT. 2002. Glycolysis modulates trypanosome glycoprotein expression as revealed by an RNAi library. *EMBO J* **21:** 4429–4438.

Ndubuisil MI, Kwok BH, Vervoort J, Koh BD, Elofsson M, Crews CM. 2002. Characterization of a novel mammalian phosphatase having sequence similarity to *Schizosaccharomyces pombe* PHO2 and *Saccharomyces cerevisiae* PHO13. *Biochemistry* **41:** 7841–7848.

Opperdoes FR. 1987. Compartmentation of carbohydrate metabolism in trypanosomes. *Annu Rev Microbiol* **41:** 127–151.

Opperdoes FR, Szikora JP. 2006. In silico prediction of the glycosomal enzymes of *Leishmania major* and trypanosomes. *Mol Biochem Parasitol* **147:** 193–206.

Parsons M, Worthey EA, Ward PN, Mottram JC. 2005. Comparative analysis of the kinomes of three pathogenic *Trypanosoma*tids: *Leishmania major, Trypanosoma brucei* and *Trypanosoma cruzi*. *BMC Genomics* **6:** 127. doi: 10.1186/1471-2164-6-127.

Paterou A, Walrad P, Craddy P, Fenn K, Matthews K. 2006. Identification and stage-specific association with the translational apparatus of *Tb*ZFP3, a ccch protein that promotes trypanosome life cycle development. *J Biol Chem* **281:** 39002–39013.

Pomerening JR, Sontag ED, Ferrell JE Jr. 2003. Building a cell cycle oscillator: Hysteresis and bistability in the activation of Cdc2. *Nat Cell Biol* **5:** 346–351.

Pusnik M, Small I, Read LK, Fabbro T, Schneider A. 2007. Pentatricopeptide repeat proteins in *Trypanosoma brucei* function in mitochondrial ribosomes. *Mol Cell Biol* **27:** 6876–6888.

Reddy VS, Singh AK, Rajasekharan R. 2008. The *Saccharomyces cerevisiae* PHM8 gene encodes a soluble magnesium-dependent lysophosphatidic acid phosphatase. *J Biol Chem* **283:** 8846–8854.

Selengut JD, Levine RL. 2000. MDP-1: A novel eukaryotic magnesium-dependent phosphatase. *Biochemistry* **39:** 8315–8324.

Siniossoglou S, Hurt EC, Pelham HR. 2000. Psr1p/Psr2p, two plasma membrane phosphatases with an essential DXDX (T/V) motif required for sodium stress response in yeast. *J Biol Chem* **275:** 19352–19360.

Sogin ML, Elwood HJ, Gunderson JH. 1986. Evolutionary diversity of eukaryotic small-subunit rRNA genes. *Proc Natl Acad Sci* **83:** 1383–1387.

Stuart KD, Schnaufer A, Ernst NL, Panigrahi AK. 2005. Complex management: RNA editing in trypanosomes. *Trends Biochem Sci* **30:** 97–105.

Szöőr B, Wilson J, McElhinney H, Tabernero L, Matthews KR. 2006. Protein tyrosine phosphatase *Tb*PTP1: A molecular switch controlling life cycle differentiation in trypanosomes. *J Cell Biol* **175:** 293–303.

Tasker M, Wilson J, Sarkar M, Hendriks E, Matthews K. 2000. A novel selection regime for differentiation defects demonstrates an essential role for the stumpy form in the life cycle of the African trypanosome. *Mol Biol Cell* **11:** 1905–1917.

Terlecky SR, Legakis JE, Hueni SE, Subramani S. 2001. Quantitative analysis of peroxisomal protein import *in vitro*. *Exp Cell Res* **263:** 98–106.

Teusink B, Walsh MC, van Dam K, Westerhoff HV. 1998. The danger of metabolic pathways with turbo design. *Trends Biochem Sci* **23:** 162–169.

Verplaetse E, Rigden DJ, Michels PA. 2009. Identification, characterization and essentiality of the unusual peroxin 13 from *Trypanosoma brucei*. *Biochim Biophys Acta* **1793:** 516–527.

Wirtz E, Leal S, Ochatt C, Cross GA. 1999. A tightly regulated inducible expression system for conditional gene knock-outs and dominant-negative genetics in *Trypanosoma brucei*. *Mol Biochem Parasitol* **99:** 89–101.

Xue Y, Zhou F, Zhu M, Ahmed K, Chen G, Yao X. 2005. GPS: A comprehensive www server for phosphorylation sites prediction. *Nucleic Acids Res* **33:** W184–W187. doi: 10.1093/nar/gki393.